Behavioural and neuronal correlates of visual saliency in mouse

Gioia De Franceschi

Thesis submitted in fulfilment of the requirements for the degree of

Doctor of Philosophy

Department of Experimental Psychology

University College London

Declaration

I, Gioia De Franceschi, confirm that the work presented in this thesis is my own. Where information has been derived from other sources, I confirm that this has been indicated in the thesis.

Gioia De Franceschi

_____

Some of the results described in this thesis have been published or presented at scientific conferences:

De Franceschi G., Vivattanasarn T., Saleem A.B. and Solomon S. (2016), Vision guides selection of freeze or flight defence strategies in mice. *Current Biology,* 26(16): 2150-2154.

De Franceschi G., Solomon S. (2016), Contextual modulation of receptive fields in superior colliculus of awake mouse. *Applied Vision Association Christmas Meeting,* UCL, UK.

De Franceschi G., Vivattanasarn T., Saleem A.B. and Solomon S. (2016), Freeze or flight: vision guides choice of defence strategies in mice. *46th Annual Meeting of the Society of Neuroscience,* San Diego, USA.

De Franceschi G. and Solomon S. (2015), Spatial, temporal and contrast sensitivities of suppressive surrounds in mouse superior colliculus. *UCL Neuroscience symposium*, UK.

De Franceschi G. and Solomon S. (2015), Neurons in the superior colliculus of mouse are sensitive to spatial and temporal visual context. *British Neuroscience Association Festival of Neuroscience*, Edinburgh, UK.

De Franceschi G. and Solomon S (2014). Spatiotemporal properties of suppressive surrounds in mouse superficial superior colliculus. *Applied Vision Association Christmas Meeting*, UCL, UK.

Acknowledgments

There are no words to describe how grateful I am to Sam Solomon, who has been the finest supervisor I could have hoped for. He has guided me through the PhD being a mentor always worth listening to, giving me constant support and advice, and providing the push I needed to go beyond my limits and achieve what I would not have achieved alone. Thank you.

Thanks to the European Community Marie Curie Scheme and to the UCL Impact Award for the economic support during the PhD.

The IBN, my second home during the PhD, has been an ideal place where to work. I want to thank Kate Jeffery, Dan Bendor, Hugo Spiers, Sam Solomon and Aman Saleem for creating and maintaining such a wonderful work environment.

I thank all the current and former members of the IBN who have shared this journey with me. Giulio Casali, Ankur Perry, Shaz Rathore and Neel Dhruv have made my transition to the UK as easy as it could be, making me feel at home since the very beginning. I want to thank Neil Garret, Zita Eva Patai, Han Cheng, William de Cothi, James Cooke, Efthymia Mika Diamanti, Catherine Perrodin, Risto Jamul, Amir-Homayoun Javadi, Pierre-Yves Jacob, James Street, Soraya Dunn, Eleonore Duvelle, Roddy Grieves, Sophie Reneaudineau, Aman Saleem, Hector Page, Ningyu Zhang, Tomaso Muzzu, Tipok Ohm Vivattanasarn, Amalia Papanikolaou and Marta Huelin for being marvellous colleagues. I particularly want to thank those with whom I spent a lot of time outside UCL, you have become precious friends.

A special thanks to Paul Sapin and Martin Wilkinson, who were always there to help me unwind having fun or just relaxing.

Heartfelt thanks to my family for their support and understanding throughout the PhD, and for being there whenever I need.

Most importantly I thank Matteo Tripodi, my shield and sword, who has been by my side since I met him being a constant source of encouragement, comfort and reward.

Abstract

While early parts of the brain's sensory pathways convey signals about the entire environment, animal behaviour is usually devoted to one or just a few potential objects of interest at any given time. Objects that are more salient (more distinct) are usually prioritised, particularly if they are potential threats, but how and where salience is represented in the brain is not known. Here I examine how salience may be constructed in the visual pathways of mice. To highlight the importance of vision in mice I first show that vision can guide the selection of distinct defence behaviours in response to potential threats - freeze and flight. I then characterise potential neural mechanisms for salience, by making recordings from neurons in the superficial layers of the mouse superior colliculus, an area important in orienting behaviour towards- or away from objects and likely to be part of the salience circuit. I show that many of these neurons are sensitive to visual discontinuities in both the spatial and the temporal domain, and that this sensitivity is more pronounced in awake animals than in anesthetized animals. These results suggest that neurons in the mouse superior colliculus can highlight parts of the environment that are distinct from the spatial and temporal context that they are embedded in, and thus may help in directing animal behaviour with respect to salient objects.

Impact statement

The brain allows animals, including humans, to sense what is happening in the outside world, and to adapt their behaviour to it. This adaptive behaviour is important for normal function and understanding how we and other animals interact with the environment is therefore a fundamental question in brain science. This thesis contributes to our knowledge of adaptive behaviours by describing two fundamental discoveries. First, I show how mice use vision to avoid potential threats, and show that different behaviours (freeze or flight) are evoked by different visual stimuli. This opens the way to understanding the sensory-motor transformations and cognitive processes involved in a simple and evolutionarily conserved behaviour, that is likely to be rely on the pathways that organise many of our daily activities, including risk assessment and anxiety. Second, I show some of the neural signals that are likely to be important in making visual objects perceptually salient. Normal behaviour revolves around one or a few (salient) stimuli at any one time, and indeed many brain disorders are characterised by inability to concentrate on one or a few objects at a time. I investigated neural signals in the mouse superior colliculus, a brain area that is important for orienting behaviours towards –or away from - salient objects. I show the presence of two complementary processes – in space and time – for highlighting objects that are novel, or different from their surroundings. These processes seem to be co-expressed in individual neurons, suggesting a dedicated pathway for making objects salient. These might be good targets for future work and understanding salience, and disorders in it.

Table of Contents

List of figures

Chapter 1

Chapter 2

Chapter 3

Chapter 4

List of abbreviations

AI adaptation index

AL anterolateral visual area

AN anesthetized

AW awake

CA^+ calcium

CRF classical receptive field

DAPI 4',6-diamidino-2-phenylindole

dLGN dorsal lateral geniculate nucleus

DOE difference-of-exponentials

DOG difference-of-Gaussians

DSI direction selectivity index

DS-RGC directionally selective retinal ganglion cells

GABA *gamma*-Aminobutyric acid

GAD glutamate decarboxylase

gDSI global direction selectivity index

gOSI global orientation selectivity index

HD high definition

ICF ipsilateral cuneiform projection

ISI inter-spike interval

LED local edge detector

LGN lateral geniculate nucleus

LM lateromedial visual area

LP lateral posterior nucleus of the thalamus

LS lateral suprasylvian area

MT middle temporal area

nCRF non-classical receptive field

NF narrow field neurons

OSI orientation selectivity index

OT optic tectum

PBg parabigeminal nucleus

PBS phosphate buffered saline

PCA principal component analysis

PDB predorsal bundle

PM posteromedial visual area

PSTH post stimulus time histogram

Pul pulvinar

PV parvalbumin-positive interneurons

RF receptive field

RGC retinal ganglion cell

SAI stratum album intermediale

SC superior colliculus

SGI stratum griseum intermediale

SGS stratum griseum superficiale

SI suppression index

SIAI adaptation index of nCRF suppression

SO stratum opticum/optic layer

sSC superficial superior colliculus

STP superior polysensory area

V1 primary visual cortex

vLGN ventral lateral geniculate nucleus

WF wide field neurons

WTA winner take all

ZO stratum zonale

ξ speed tuning index

Chapter 1
Introduction

1.1 OVERVIEW

The flexibility of animals' behaviour in response to a constantly changing environment is stunning. Despite the widely variable sizes and shapes of central nervous systems across species, the essential functional pillars are the same across the animal kingdom: to sense what's out there, and to act accordingly. Trying to understand how we and other animals interact with the environment is a fundamental question in neuroscience to which we haven't yet been able to give an answer. In this work, I hope to provide some understanding of how the brain enables the interaction with the outside world.

The brain is constantly receiving a huge amount of sensory information, but behaviour usually depends on the most salient elements in the environment. This implies that the central nervous system filters incoming information, devoting its computational power to a subset of potential objects of interest at any given time. The ability to select what stimuli are worth focus is essential for survival. For prey species for example, not attending to a predator when it appears may easily result in death. The brain is therefore likely to assess the sensory information

it receives based on its salience, prioritizing the analysis of the most conspicuous or important stimuli. But how and where in the brain salience is encoded is not known.

In the following I investigate potential neural mechanisms for constructing salience in the mouse, focusing on the superior colliculus (SC), which in this species is the major target of retinal projections (Ellis et al., 2016). The SC, homologue of the optic tectum (OT) in non-mammalian vertebrates, is an evolutionarily ancient midbrain structure that receives signals from multiple senses, integrates them and helps guide behaviours. The SC has been shown in several species to play a critical role in detecting salient stimuli and orienting to or away from them. The SC is composed of multiple topographically organized layers, switching from visual to multisensory to motor as a function of depth. The SC is also densely linked with much of the rest of the brain. The superficial layers not only receive massive retinotopic input from retina and primary visual cortex, but also send outputs to the key visual nuclei of the thalamus, which in turn convey signals to cortical visual areas and other behaviourally important structures such as the amygdala. Deeper layers receive, in addition to visual, somatosensory and auditory information, inputs from the cerebellum, the basal ganglia, and from sensory, motor and association cortical areas. Deep layers also project to the brainstem, the spinal cord and the reticular formation in the medulla (May, 2006). As a key node in this intricate network, the SC is likely to be critically involved in the complex dynamics between cortical and subcortical brain regions.

The mouse is becoming an increasingly popular animal model in which to study brain function, connections and development. The advantages are manifold: they have a simpler brain compared to primates, they are easily accessible and simple to maintain. Additionally, the mouse is an attractive model system because of the availability of powerful experimental techniques allowing for example to record the activity of many neurons at the same time (e.g. two-photon imaging) or to finely target the manipulation of neural subpopulations and circuits (e.g. combining viral and optogenetic approaches). The techniques available in mice are unparalleled, making this species a key model for the study of brain function.

Despite having very poor vision relative to humans, lacking a foveal region (Carter-Dawson and LaVail, 1979) and having an acuity of only 0.55 cycles/degree (Prusky and Douglas, 2004), the mouse visual system is endowed with most of the features that have been described in

traditional animal models of vision – cat and primate (Niell and Stryker, 2008; Huberman and Niell, 2011). The field of visual neuroscience has therefore recently seen a surge of research in mouse, focusing in particular on the retina (eg. Zhang et al., 2012; Kim and Kerschensteiner, 2017) and primary visual cortex (Niell and Stryker, 2008; Gao et al., 2010; Andermann et al., 2011; Ayaz et al., 2013; Vaiceliunaite et al., 2013), but now expanding into both higher visual cortical areas (eg. Andermann et al., 2011; Tohmi et al., 2014), and the many subcortical targets of the retina (eg. Abrahamson and Moore, 2001; Piscopo et al., 2013; Dhande et al., 2015; Durand et al., 2016; Martersteck et al., 2017).

In this introductory chapter my objective is to familiarize the reader with the knowledge necessary to understand the foundations on which this thesis is built. I first describe what visual saliency is, why it is important, and outline the dominant model of visual saliency, pinpointing the superior colliculus as an area crucial for representation of salience. I then describe neural mechanisms that are suitable for highlighting salience in space and time, respectively 'non-classical' receptive fields and adaptation. The second part of the chapter focuses on the superior colliculus and illustrates its anatomy, connections and behavioural role, describing how visual receptive fields are characterized and what we currently know about the functional properties of visual neurons in the superior colliculus.

1.2 SALIENCE

The focus of this thesis is how brains allow animals to respond appropriately to sensory stimuli. Through evolution, organisms have adapted to the environment to increase their chances of surviving and reproducing. Species have evolved physical features that enable them to thrive in specific habitats, and behaviours that further enhance their likelihood of surviving. One of the most fascinating results of these evolutionary processes is the animals' ability to dynamically adjust their behaviour depending on context. Understanding how the brain receives sensory information and uses it to choose the appropriate behaviour is a central question in neuroscience, but we are still far from understanding how the brain performs this complex set of processes.

The amount of information that reaches our senses is enormous. One way to prevent sensory overload is to identify and select the most important stimuli in the environment, and devote detailed processing to them (Itti et al., 1998). The process of selecting the most relevant stimuli is often referred to as selective attention or orienting, and can be further subdivided into "bottom-up" and "top-down". Top-down mechanisms arise in cognitive processes that can weigh factors such as the current situation, previous experience, or will. These mechanisms are likely to be mediated by higher-level brain areas thought important in sophisticated cognitive processes, which have expanded through evolution. By contrast, bottom-up selection is faster, likely to be supported by evolutionarily ancient pathways, depends on the basic features of the stimuli and is thought to be implemented early in the sensory pathways. In these cases the saliency of an external object is often determined by the difference between its properties and those of its surroundings, for example a vertical bar is salient among horizontal bars but not among other vertical bars. This thesis will focus on bottom-up processes and in particular on suitable neural mechanisms for constructing saliency. I will concentrate on the visual pathways, where saliency has been most explored.

In the following I will introduce a dominant model for visual salience that is based on the anatomy and function of visual circuits, and illustrate how known neurophysiological mechanisms of visual processing may put into effect the different stages of the model. I will then address the question of where in the brain a master saliency map may be established, suggesting the superior colliculus as a suitable region.

1.2.1 Visual saliency maps

How bottom-up, stimulus-driven salience is supported by the brain is the subject of continuing and intensive research (Borji and Itti, 2013). The first computational model of salience to be based on neuronal architecture is that proposed by Koch and Ullman (Koch and Ullman, 1985), an exemplar and reference point for subsequent work (Li et al., 2013). The model introduces the concept of saliency maps to describe how the brain may perform bottom-up selection of the most conspicuous object in a visual scene. Koch and Ullman's model (Koch and Ullman, 1985) is organised into several stages, and it is useful to consider these in turn (Fig. 1.1).

The first stage of Koch and Ullman's model was motivated by the then emerging evidence for modular visual analysis (eg. Livingstone and Hubel, 1988b) and by evidence of competitive spatial interactions in cortical visual areas (eg. Allman et al., 1985a). This stage consists of parallel filter banks each selective to different visual features and tiling the visual field. The early visual system is proposed to generate a topographic map for each of several simple features of the visual scene, such as colour, orientation, or direction of motion. Within each feature map, the relative strength of activation (saliency) of a particular location is given by how different the activation in that region is from its local surroundings. The second step implements a linear combination of these feature maps into a master saliency map, in which saliency is feature

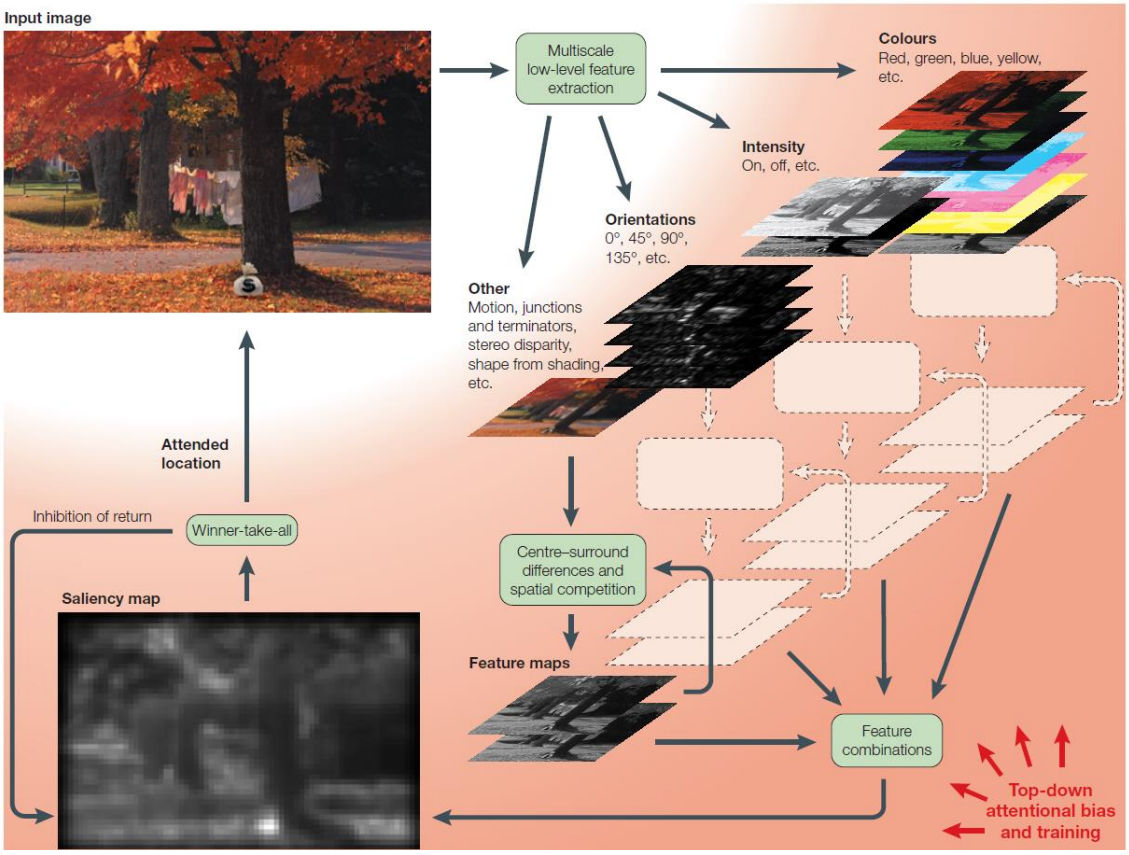

Figure 1.1. Schematic of visual saliency model. The input visual image is decomposed in several feature specific maps (sensitive to orientation, colour, intensity, etc.), and in each feature map the most salient location is identified through center-surround differences and spatial competition. The feature maps are then linearly combined in a master saliency map, identifying the most conspicuous location across features. A winner take all network finds that location and directs attention towards it. Inhibition of return allows the next most salient location to be selected. Modified from Itti and Koch (2001).

independent. In the master saliency map the most conspicuous stimulus is represented by the unit with highest firing rate. The third stage involves a winner-take-all (WTA) network, which scans the master saliency map to detect the most conspicuous location, towards which attention will be deployed. In order for the selection process to move from one location to another the model implements a long-lasting inhibition of the unit detected by the WTA network, whose saliency value decreases allowing the WTA network to select the next most salient location. This results in attentional shifts from one position to another as a function of decreasing saliency. In extended versions of the model, the master saliency map is integrated with top-down signals encoding behavioural relevance, to construct a priority map from which the stimulus deserving attention is selected.

The power of this model of saliency, and subsequent implementations, is that it rests on basic known properties of visual representations in the brain. (1) The retinotopic organization of visual areas preserves information about stimulus location, and cells in the early visual pathway are usually tuned to one or a few visual features (Hubel and Wiesel, 1959; Livingstone and Hubel, 1988a), providing the substrate for constructing feature-selective saliency maps. (2) In addition to their classical receptive field (CRF), the visual space region from which firing activity can be elicited, most neurons show presence of a larger *non-classical receptive field* (nCRF) able to modulate the response of the CRF and make neurons sensitive to spatial context (Fig. 1.2). The effect of non-classical surrounds on the CRF is usually suppressive, and suppression is generally stronger if the surround features match those over the CRF (Malach et al., 1993; Sillito et al., 1995; Girman and Lund, 2007). The result is that the nCRF highlights portions of the visual field that are dissimilar from their surrounding, a key requirement for building feature-specific conspicuity maps. (3) Neural responses can adjust depending on stimulus history through adaptation, which decreases the firing activity of cells in case of repeated uniform stimulation (Kohn, 2007). Adaptation makes neurons sensitive to stimulus changes over time, allowing them to encode novelty. Similar to surround suppression, which acts in the spatial domain, adaptation is a suitable mechanism for saliency detection in the temporal domain.

1.2.2 Visual saliency in space and time: neural mechanisms

Sensory neurons face the daunting task of encoding stimuli that are variable over space and time. Two major processes allow sensory systems to deal with this issue. The first is adaptation, which allows neurons to adjust their response properties depending on what they have been previously exposed to. The second is the nCRF, which allows response properties to adjust depending on what is present in a portion of visual space larger than the classical receptive field. The nCRF and adaptation make sensory encoding strongly dependent on spatial- and temporal context. The more a stimulus is distinct from its context, and thus the more it is salient, the weaker adaptation and nCRFs will be. Indeed, spatial and temporal context have a similar effect on perception and neural activity (Schwartz et al., 2007).

Adaptation. Adaptation refers to those neural mechanisms that adjust the firing rate of neurons depending on the temporal context in which a stimulus is embedded in (reviewed in Solomon and Kohn, 2014). Through adaptation, neurons become sensitive to the history of the sensory environment and their sensitivity is adjusted based on the statistical properties of the visual field over the recent past. Adaptation allows neurons to integrate sensory information over different timescales, from milliseconds to minutes or hours. This is consistent with the fact that environmental changes can also happen slowly or very rapidly, and suggests the existense of multiple neural mechanisms subserving adaptation at different timescales. Fast adaptation occurs in the order of a hew hundreds of milliseconds, while slow adaptation needs seconds or minutes to take place. Whether different mechanisms subserve these different timescales, or whether the functional impact of adaptation depends on timescale, remain unknown, and the precise functional role of adapation has yet to be conclusively determined (Baccus and Meister, 2002; Kohn, 2007; Solomon and Kohn, 2014).

Non-classical receptive fields. The most studied nCRFs, suppressive surrounds, are unable to drive neuronal activity when stimulated alone but can modulate the response to signals presented in the CRF when the CRF and nCRF are stimulated together, usually by suppressing the output of the CRF. nCRFs are likely to be a mechanism for contrast gain controls (Shapley

and Victor, 1978; Bonin et al., 2005), adjusting the neuronal responses depending on the average contrast over a portion of visual space that is wider than the CRF.

Perceptual work in humans shows that the perceived contrast of a target stimulus strongly depends on the relative contrast of the surroundings, and perceived contrast decreases with increasing surround contrast (Chubb et al., 1989; Cannon and Fullenkamp, 1991; Yu et al., 2001). Surrounds with lower contrast than the target can also be facilitatory, increasing perceived contrast (Cannon and Fullenkamp, 1991; Xing and Heeger, 2001). In electrophysiological recordings from several species including cat, primate and mouse, the spiking activity of visual neurons is usually suppressed by stimuli presented in the surround in a contrast dependent manner, such that the higher the surround contrast, the larger the suppression (DeAngelis et al., 1994; Levitt and Lund, 1997; Solomon et al., 2006). The contrast over the surround also affects the extent of spatial summation area of the CRF: increased surround contrast leads to decreases in preferred stimulus size (Sceniak et al., 1999; Solomon et al., 2006).

Spatial discontinuities between regions of the visual field can stem from differences in contrast and other visual features, such as spatial frequency, temporal frequency or motion direction. Spatial frequency modulates the perceptual effect of context in human subjects

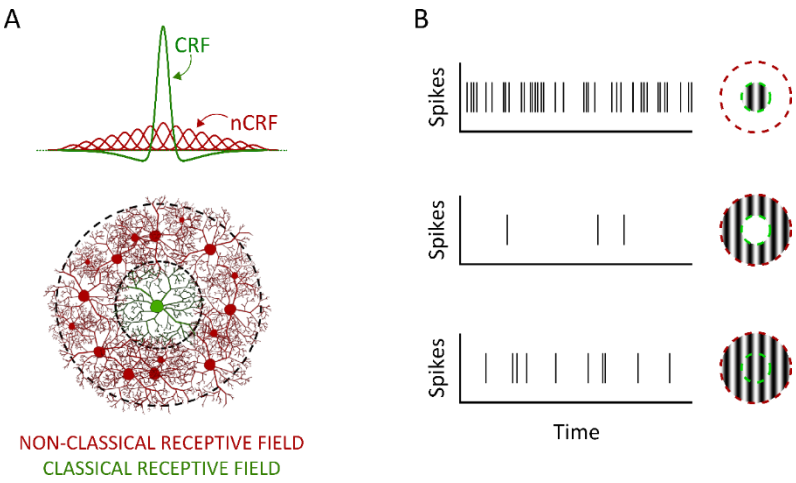

Figure 1.2. Non-classical receptive fields. *A*. Schematic of classical (green) and non-classical (red) receptive fields. The CRF is embedded in a larger nCRF, pooling information from neurons with neighbouring receptive fields. ***B***. Schematic of a neuron's responses. Each vertical line represents the occurrence of an action potential over time. The activity of the neuron is strongly increased when a stimulus is presented just over the CRF (top), it does not change when just the nCRF is stimulated (middle), and is suppressed compared to (top) when both the CRF and the nCRF are simultaneously stimulated (bottom).

(Chubb et al., 1989; Cannon and Fullenkamp, 1991; Petrov et al., 2005; Serrano-Pedraza et al., 2012), such that contextual effects are stronger when the spatial frequency used in the surround matches the one of the target stimulus. Analogous dependence has been found in neural recordings from primary visual cortex (DeAngelis et al., 1994; Li and Li, 1994). Contextual suppressive effects have been shown to be dependent on the relative orientation over the CRF and nCRF in both psychophysical measurements (Xing and Heeger, 2001; Petrov et al., 2005) and at the neuronal level (DeAngelis et al., 1994; Sillito et al., 1995; Levitt and Lund, 1997; Sengpiel et al., 1997; Cavanaugh et al., 2002b; Muller et al., 2003; Ozeki et al., 2004; Girman and Lund, 2007; Ozeki et al., 2009; Shushruth et al., 2013; Self et al., 2014). Suppression appears stronger when the orientation over the nCRF coincides with the orientation of the stimulus presented in the CRF, suggesting the presence of mutual dependencies between classical and non-classical receptive fields (Cavanaugh et al., 2002b).

In summary, adaptation and nCRFs are mechanisms through which the neuronal activity in response to stimuli can be modulated depending on the temporal and spatial context. By influencing the firing rate of neurons based on the statistics of the environment over time and space, these mechanisms shape sensory encoding and are likely to promote the detection of stimuli that are novel or different from the surroundings, and therefore salient.

1.2.3 The superior colliculus as the master saliency map

What area in the brain represents the master saliency map? An area representing saliency needs to fulfil several criteria. First, it needs to preserve spatial information to allow the localization of salient stimuli. Second, it should signal stimulus-intrinsic salience rather than its relevance for a goal (Fecteau and Munoz, 2006), and it should be able to detect saliency independently of specific features. Third, it should guide spatial attention, such that perturbations result in impaired salience. Many areas of the brain have been suggested to constitute the master saliency map (Koch and Ullman, 1985; Robinson and Petersen, 1992; Kustov and Robinson, 1996; Li, 2002;Mazer and Gallant, 2003; Gottlieb, 2007; Knudsen, 2011; Krauzlis et al., 2013; Dutta and Gutfreund, 2014) but most of the proposed areas do not fulfil all criteria. For example V1 has been proposed to constitute a saliency map (Li, 2002), but neural-

based evidence of feature-agnostic maps in V1 is lacking (Veale et al., 2017). V1 seems to rather implement a feature map: the pattern of gaze allocation in free-viewing macaques with lesioned V1 is impaired towards salient stimuli in the orientation domain, while saliency of other domains (e.g. movement or colour) is unchanged (Yoshida et al., 2012a). This supports the hypothesis that V1 is not the master saliency map but a feature map specific for orientation, and potentially other stimulus dimensions.

The superior colliculus is a good candidate for the master saliency map (Fecteau and Munoz, 2006; White and Munoz, 2011; Veale et al., 2017). It is organized retinotopically, it is sensitive to low-level visual features, and its neurons show presence of nCRFs that may allow spatial competition between stimuli. It receives information from many visual areas and sends projections not only to brain structures involved in motor control of orienting behaviours, but also to areas implicated in spatial selective attention. Finally, lesioning the superior colliculus leads to spatial attention deficits while electrical stimulation results in facilitation of object selection and orienting movements (Butter et al., 1978; Carello and Krauzlis, 2004; McPeek and Keller, 2004; McPeek, 2008). The superior colliculus therefore fulfils the criteria for a master saliency map.

The superior colliculus (or its homologue in non-mammalian vertebrates, the optic tectum) has been causally implicated in the selection of the most conspicuous stimulus in several species (Dean and Redgrave, 1984; Carello and Krauzlis, 2004; Muller et al., 2005; Cavanaugh et al., 2006; Mysore et al., 2010; 2011; Knudsen et al., 2017). Additionally, monkeys with unilateral ablation of V1 are still attracted by salient visual stimuli during free viewing of complex natural visual scenes (Yoshida et al., 2012a). Neurons in the superficial superior colliculus have also been shown to encode a form of saliency map during the free viewing of naturalistic videos (White et al., 2017a), while the intermediate and deep layers lack the signatures of visual saliency and encode a priority map which is important for selecting the target and generating orienting movements towards it. It has been proposed that the saliency map emerged in the superior colliculus/optic tectum in lower vertebrates and through evolution moved to primary visual cortex in primates (Zhaoping, 2016), although recent work shows in monkey that visual saliency emerges in superficial SC earlier than in V1 (White et al., 2017b). It is likely that the superficial

layers of the superior colliculus inform deeper layers about exogenous, stimulus-inherent visual saliency, while deep layers integrate this information with endogenous, top-down signals coming from cortical areas and choose the next locus of attention (White et al., 2017b). Thus, despite the substantial role of the neocortex in vision in higher mammals, the superior colliculus is likely to play a major role in salience.

1.3 THE SUPERIOR COLLICULUS

In mammals, visual information is transmitted from the retina to the brain through two major pathways. The retino-geniculo-cortical pathway transfers visual information from the retina to the dorsal lateral geniculate nucleus of the thalamus (LGN), which in turn transmits signals to primary visual cortex (V1). This pathway has evolved more recently and is mainly devoted to image-forming vision. The retinocollicular pathway brings information from the retina to the superior colliculus (SC), is evolutionarily ancient and is the primary target of retinal projections in rodents (Fig. 1.3).

The superior colliculus receives sensory information, analyses it and organises output motor commands, and can thus be seen as a microcosm of the brain as a whole (King, 2004). Its main role is to guide the position of the head and eyes towards interesting stimuli or away from threatening ones (May, 2006). In addition to the descending projections which direct sensory structures towards a target, the SC can also influence sensory processing through ascending connections. Even if mammals, being endowed with neocortex, rely less than other vertebrates on this region for sensory-motor integration, it remains an important structure for orienting behaviours (May, 2006).

In the following I first describe the anatomy of the superior colliculus and (some of) its connections, both within the SC and with the rest of the brain. Given the high quantity of feedforward, feedback and reciprocal connections between the SC and the rest of the brain, I will focus on those that I consider important in the framework of this thesis: connections with the retina, visual thalamus, visual cortical areas, select subcortical structures, and connections within the superior colliculus itself. I then review current knowledge about the role of the SC in

approach and defensive responses highlighting, when available, information about the anatomical structures and cell types involved in such behaviours. I finally briefly describe how the properties of visual neurons are usually investigated and review what is known about the functional visual properties of neurons in the superficial superior colliculus.

The superior colliculus has been extensively studied in a variety of species, from rodents to primates, and the available literature spans decades. Information about specific aspects of this area is therefore often sparse, being available for just a subset of animals, or difficult to compare

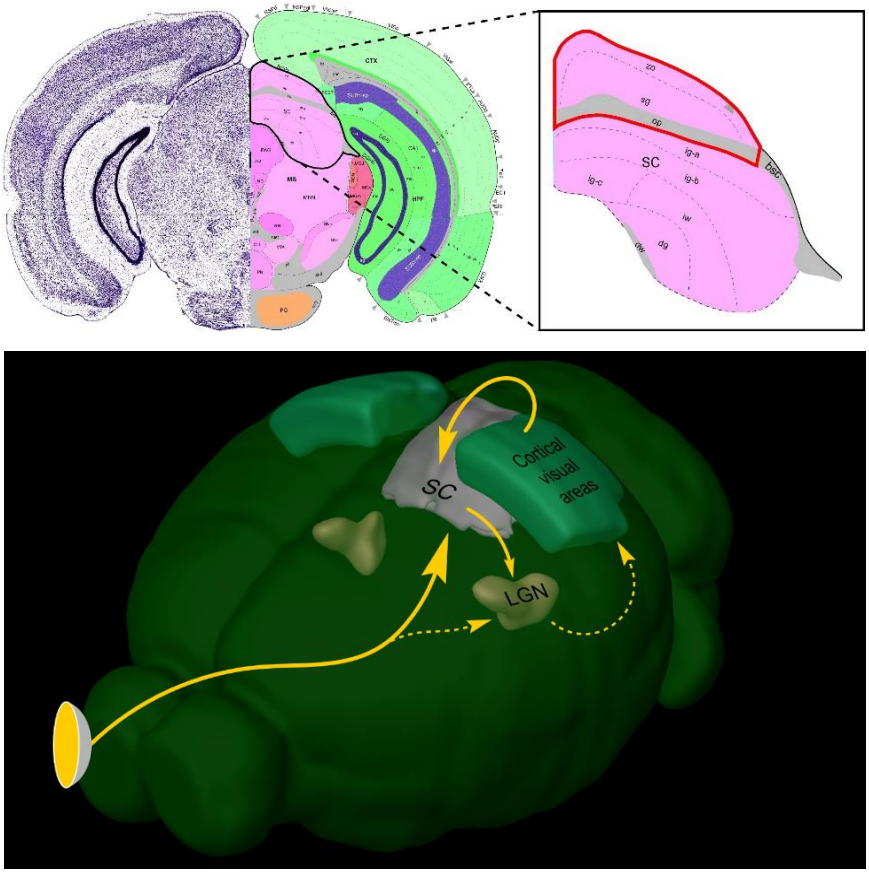

Figure 1.3. The mouse superior colliculus. *Top*. Left: Coronal section of a Nissl stained mouse brain (left) through the superior colliculus, and schematic of the relative areas (right). The black solid line highlights the superior colliculus. Right: enlarged version of the SC. The red solid line highlights the superficial layers. Modified from the Allen Institute Reference Mouse Brain Atlas (http://mouse.brainmap.org/experiment/thumbnails/100142143?image_type=atlas). *Bottom*. In mouse, the major pathway originating from the retina is sent to the superficial superior colliculus (pink). A minor proportion of retinal projections is sent to the LGN (brown), that in turn sends visual information to visual cortex (green). The SC sends projections to the LGN, and visual cortex sends feedback to the SC. Modified from Allen Institute Brain Explorer 2 (http://mouse.brain-map.org/static/brainexplorer).

due to the use of different experimental techniques. It is also important to note that the superior colliculus is an evolutionarily ancient structure that has adapted depending on the specific biology of each species (e.g. their main guiding sense). It is therefore critically important to remember that despite the presence of shared features, the role(s) of the superior colliculus are likely to have components that are species-specific. In the description of the anatomy and connections of the SC I focus on a particular topic at a time (e.g. a specific connection) and summarise the available information across species. When outlining the functional properties of visual neurons in SC, I instead organize the literature in species-specific subsections.

1.3.1 Anatomy of the superior colliculus

Laminar structure. The superior colliculus is a laminated structure located on the midbrain roof (Fig. 1.3). Based on anatomical, electrophysiological and behavioural studies it has been subdivided into different layers, the number of which varies across species. Generically, the SC consists of seven layers functionally divided into superficial and deep layers. The superficial layers consist of the stratum zonale (ZO), stratum griesum superficiale (SGS) and stratum opticum (SO), while the deep layers comprise stratum griseum intermediale (SGI), stratum album intermediale (SAI), stratum griseum profundum (SGP) and stratum album profundum (SAP) (Fig. 1.4) (Wurtz and Albano, 1980; May, 2006).

At the most basic level, the SC is formed of a superficial part, mainly visual, and of deeper layers involved in the analysis of other sensory modalities and multisensory inputs and the generation of a motor output. The superficial layers of SC (layers ZO, SGS, SO) are mostly dedicated to sensory visual stimuli. The dorsalmost stratum zonale is thin and almost cell free. Ventral to it, the superficial gray layer (SGS) is constituted of many small cells and in some species has been further subdivided into sublaminae. The optic layer (SO) consists of some cells but mainly of fibers, among which are the axons arriving from the retina. The deeper layers of SC are characterized by the presence of cells responding to visual stimuli or other sensory modalities (somatosensory, auditory), some of which are sensitive to more than one modality. In addition to sensory cells, motor output neurons are found (Drager and Hubel, 1976; May,

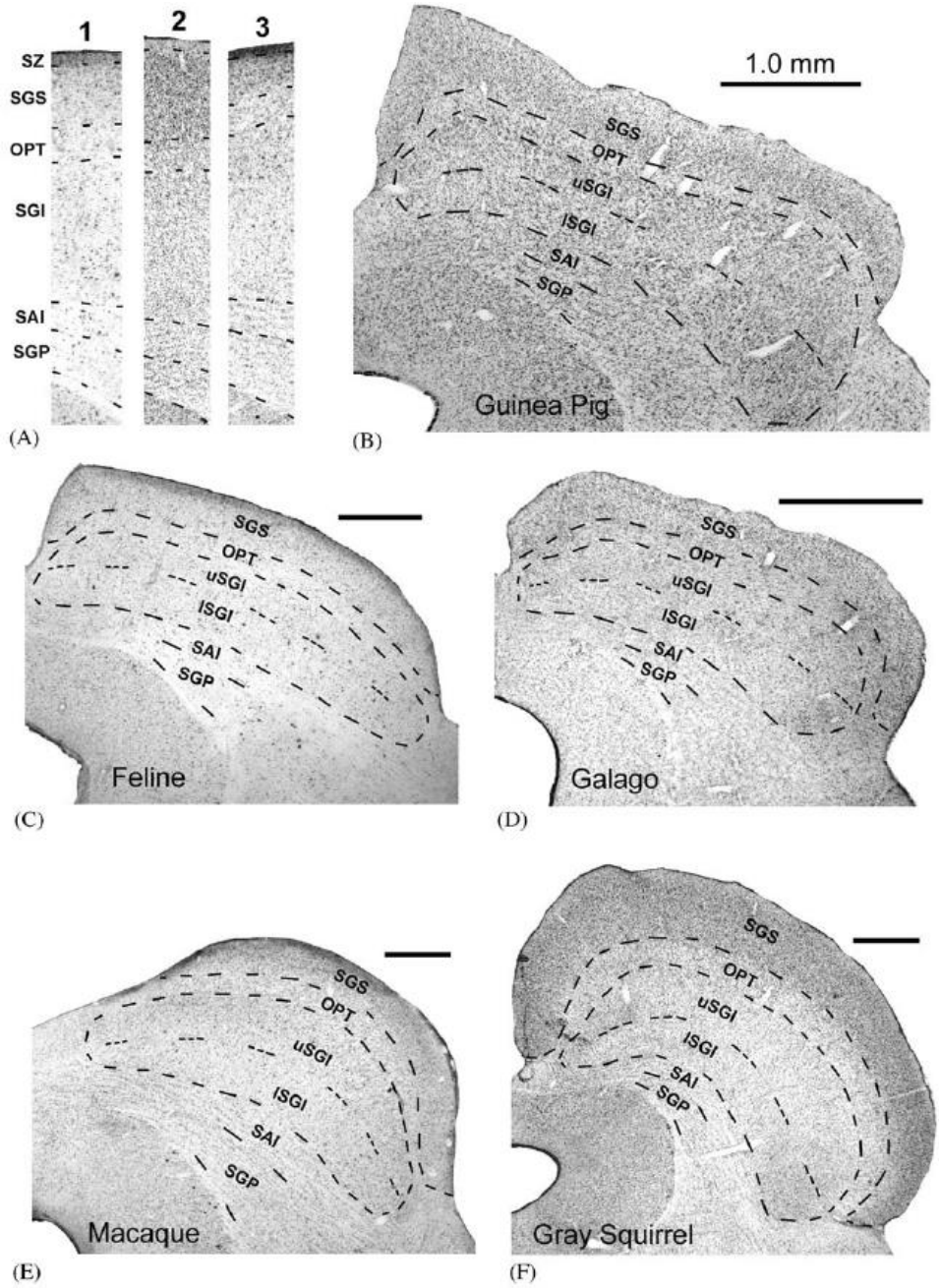

Figure 1.4. Laminar structure of the SC. **A.** 1) Cat, 2) squirrel and 3) M. Fascicularis vertical slice through the SC, highlighting the proportional thickness of the layers in different species. The slices were scaled to the same hight. **B**. Cresyl violet stained coronal sections of the superior colliculus in five different species, showing the conserved laminar structure. All scale bars are 1 mm. SGS: stratum griesum superficiale. OPT: stratum opticum. uSGI: upper stratum griseum intermediale. lSGI: lower stratum griseum intermediale. SAI: stratum album intermediale. SGP: stratum griseum profundum. Modified from May (2006).

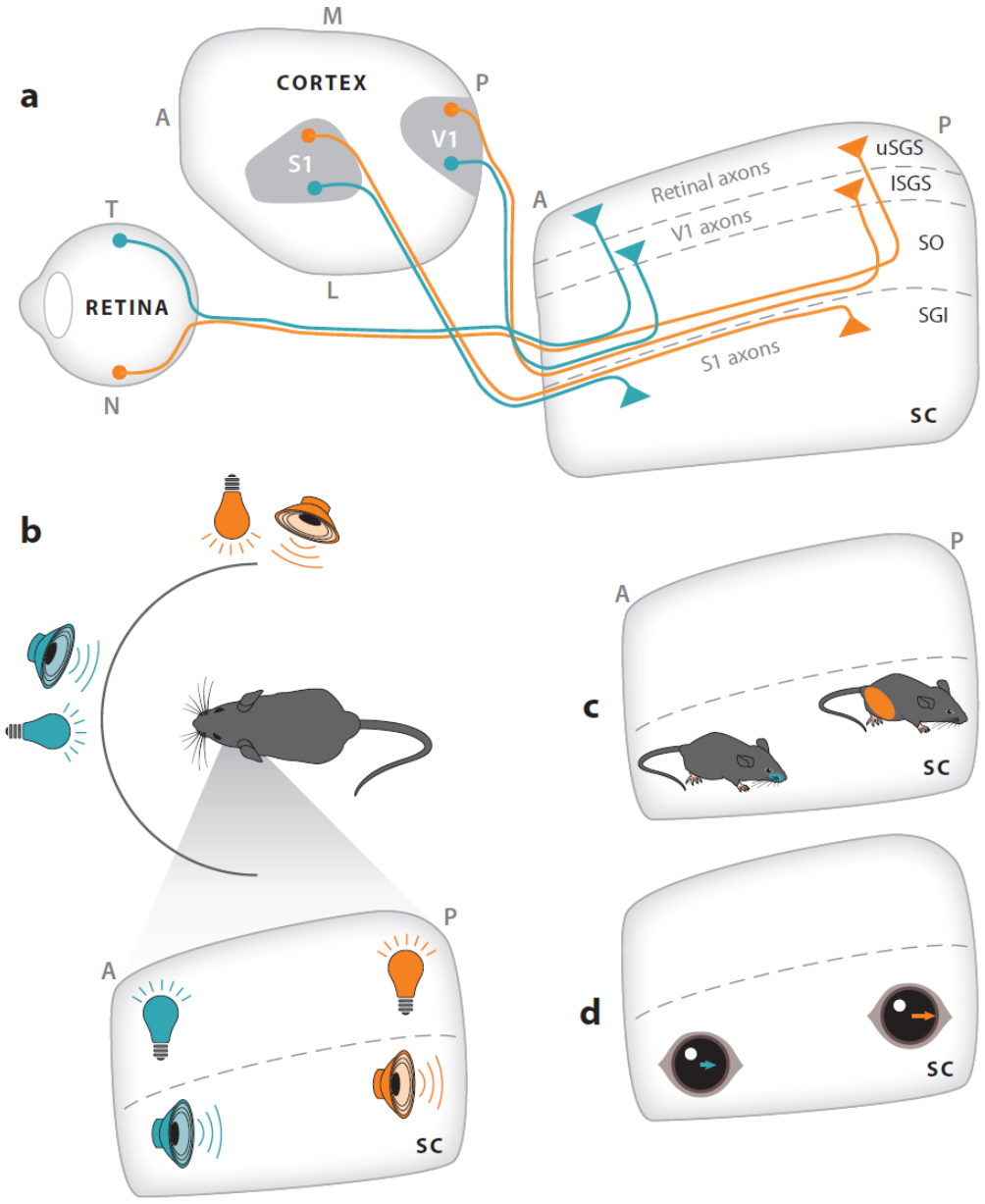

Figure 1.5. Topographical alignment of multiple maps in the superior colliculus. ***A.*** Schematic showing the laminated superior colliculus and inputs coming from the retina, primary visual cortex (V1) and somatosensory cortex (S1). The projections are topographically aligned. Abbreviations: N, nasal; T, temporal; A, anterior; P, posterior; L, lateral; M, medial; uSGS, upper stratum griseum superficiale; lSGS, lower stratum griseum superficiale; SO, stratum opticum; SGI, stratum griseum intermediale. ***B***. The topographical input alignment results in visual, auditory, or somatosensory neurons having similarly localized receptive fields (as indicated by the same color) being vertically aligned in the superior colliculus. ***D***. Consistent with the sensory map, stimulation of the anterior deep SC results in small eye movements while stimulation of the posterior part results in larger shifts in eye position. Modified from Cang and Feldheim (2013).

2006). The intermediate gray layer is composed of different types of multipolar neurons and rostrocaudally running fibers. The intermediate white layer is formed by dorsomedial to ventrolateral fibers. The deep gray is a cellular layer, while the deep white layer is constituted by fibers adjoining the periacqueductal grey.

Neurons sensitive to different sensory modalities are positioned in the laminar structure of the SC such that they are often precisely aligned: the topography of the visual superficial layers is retinotopic, and the position of sensory cells in deeper layers is approximately aligned with that map of visual space. Given this anatomical registration, the receptive fields of sensory neurons located in different layers (hence, responsive to different sensory modalities) but in the same rostro-caudal and medio-lateral position are often overlapping (Fig. 1.5). The prominence of inputs coming from sensory systems other than vision depends on the relative importance of each modality and is therefore species-specific. For example, somatosensation is important for rodents and SC intermediate layers receive strong input from the whiskers (Drager and Hubel,

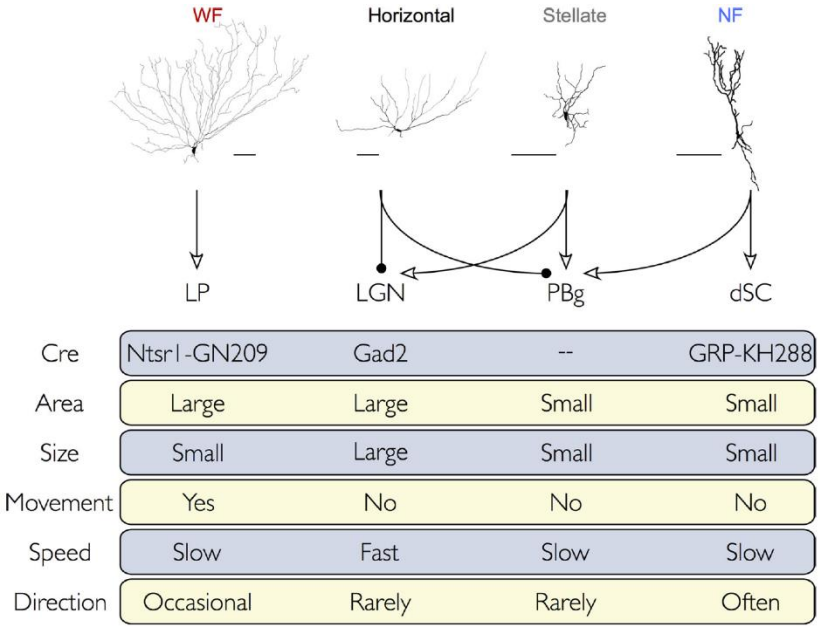

Figure 1.6. sSC neuronal types. Summary of sSC cell types, their output areas, genetic markers, and visual preferences. Arrows indicate excitatory, glutamatergic projections. Filled circles indicate inhibitory, GABAergic projections. The row labeled Area refers to receptive field size, Size refers to preferred stimulus (spot) size, Movement corresponds to whether a cell prefers moving over stationary spots, Speed refers to preferred speed of moving spots, and Direction indicates how often direction-selective responses were observed in each cell type. Scale bar, 100um. Modified from Gale and Murphy (2014).

1976); audition is important in cats, and indeed auditory inputs in their intermediate SC are predominant; in monkeys, which are highly visual animals, the intermediate layers mainly receive visual inputs (Wallace and Stein, 1996).

Cell types. The superficial layers of the rodent SC include four main classes of neurons displaying characteristic visual properties and axonal projections: horizontal, wide field (WF), narrow field (NF) and stellate cells (Fig. 1.6). Horizontal cells are GABAergic interneurons with dendrites spreading over a large area in the horizontal plane, prefer large stationary or swiftly moving stimuli and project to the LGN and the parabigeminal nucleus (PBg). Wide field cells are vertically oriented with dendrites extending diagonally and spanning a large portion of the SC surface, prefer small stimuli, are sensitive to movement and send bilateral glutamatergic axons to the lateral posterior nucleus of the thalamus (LP). Narrow field neurons are also glutamatergic and display narrow vertical arborization in the SGS, prefer small stimuli, tend to be directional selective, and project to the PBg and to the intermediate SC. Finally, stellate cells are characterized by unoriented dendrites, have a small receptive fields responding to small stimuli, and send projections to LGN and PBg (Endo et al., 2003; May, 2006; Gale and Murphy, 2014).

1.3.2 Connections

The superior colliculus is highly interconnected with other brain regions. The patterns of input to and output from the SC are complex, and many of them have not yet been clarified. A complete description of SC connections is beyond the scope of this work and the reader is directed to relevant reviews (e.g. May, 2006; Comoli et al., 2012; Oh et al., 2014; Savage et al., 2017). Here I focus on major projections to and from the SC that are likely to be important for salience detection and orienting behaviours.

Retina. The retinotectal pathway primarily projects to the superficial layers of SC (Fig. 1.7) (May, 2006; Morin and Studholme, 2014). The main retinal input is sent to SGS, some connections transmit to SO, and there are a few projections to SGI. The extent of binocular overlap in different species influences the ratio of controlateral and ipsilateral projections. Animals with high binocular overlap show a complex organization where ipsi- and contralateral

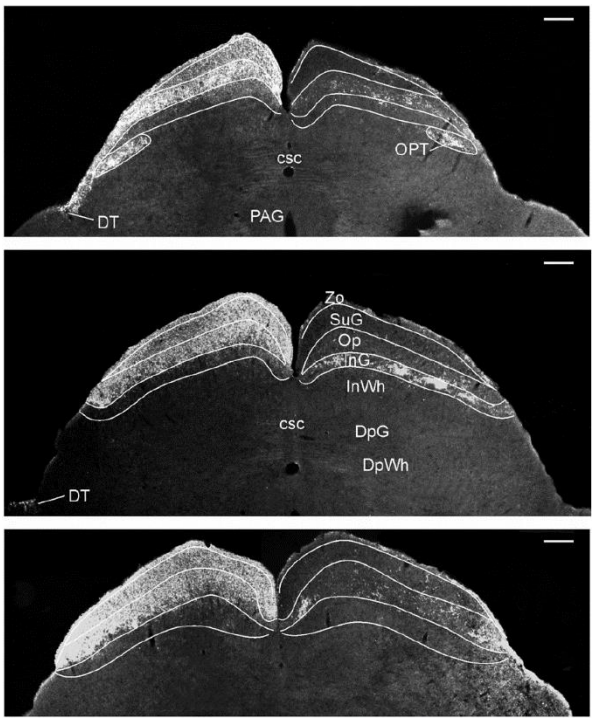

Figure 1.7. Retinotectal projections. Darkfield photomicrographs of the mouse superior colliculus (slices are 60 µm apart) showing innervation from the controlateral (left) and ipsitateral (right) retina after intraocular injection of cholera toxin β-subunit. The controlateral retina mainly projects to ZO, SGS (here named SuG), and SO (here named Op). Ipsilateral retinocollicular terminals form discrete patches in SO and SGI (here named InG). Modified from Morin and Studholme (2014).

projections are present in both sides of SC, while in animals with a low level of binocular overlap (e.g. rodents) the retina projects primarily to the contralateral SC. Nevertheless, even in rodents a small fraction of retinal axons project ipsilaterally, arising in the lower temporal retina and targeting the SGS, SO and SGI (Fig. 1.7).

There is a great deal of variability among species in the proportion of retinal ganglion cells connecting with SC, which can be partially predicted by the importance of the visual sensory modality to the species. At least ~90% of RGCs project to SC in mouse (Ellis et al., 2016), 50% in cat (Wassle and Illing, 1980) and just 10% in monkeys (Perry and Cowey, 1984). Conversely, ca. 40% of RGCs project to the dLGN in rat (Martin, 1986), and 90% in primate (Spear et al., 1996). Thus, in mammals with high visual acuity the retinogeniculate pathway is more prominent, perhaps to the detriment of retinotectal connections. The RGC types that project to the SC is

well established in some species. In cat the main population of RGC conveying information to the SC are the slow conducting, phasic, small gamma cells (W-type), terminating in the uppermost sSC lamina, and the fast conducting, large alpha cells (Y-type), terminating in the stratum opticum and the stratum griseum intermediale (Hoffmann, 1973; Fukuda and Stone, 1974; Wassle and Illing, 1980; Rowe and Palmer, 1995). A small number of beta cells (X-type) have also been found to project to SC. In primates, retinal inputs to SC primarily arise in cells analogous to cat's Y-type and W-type RGCs (M and K cells) (Crook et al., 2008).

In rodents and lagomorphs most RGCs and most RGC types project to the SC (Chalupa and Thompson, 1980; Vaney et al., 1981; Linden and Perry, 1983; Hofbauer and Drager, 1985; Ellis et al., 2016). In mouse, most retinogeniculate projecting retinal ganglion cells also project to SC, while the SC selectively receives inputs from a number of RGCs that avoid the LGN (Ellis et al., 2016). Mouse RGCs projecting to the SC display transient responses and prefer small stimuli (Ellis et al., 2016). A few genetically identified RGC types have been shown to send axons to the mouse superior colliculus: W3 RGCs, a likely homologue of rabbit local-edge-detector cells (LED) (Levick, 1967), which are characterized by small ON-OFF receptive fields and strong lateral inhibition (Kim et al., 2010; Zhang et al., 2012); OFF J-RGCs and ON-OFF BD-RGSc, strongly directional and also suppressed by large stimuli (Kim et al., 2010).

Cortex. Many cortical areas project to SC, including areas 17, 18, 19, 20a and 20b, 21a and 21b, many areas adjoining the sylvian gyrus, area MT in primates, portions of the superior temporal sulcus, dorsomedial, medial and posterior parietal areas (Harting et al., 1992; May, 2006). Interestingly, visual cortico-collicular projections from extrastriate cortex show topographic organisation, such that the further the source area is from area V1, the deeper their axons terminate in the SC, supporting the involvement of deeper SC neurons in progressively more complex analysis (Fig. 1.8. cat: Graybiel, 1978; Harting et al., 1992). In all species cortico-collicular projections mainly originate from layer V, with some axons originating from layer VI in V1 (macaque: Lock et al., 2003; cat: Kawamura and Konno, 1979; rat: Sefton et al., 1981). The main target of both retinal and cortical terminals are collicular dendrites. Although retinal and cortical synapses can occasionally be found on the very same dendrite,

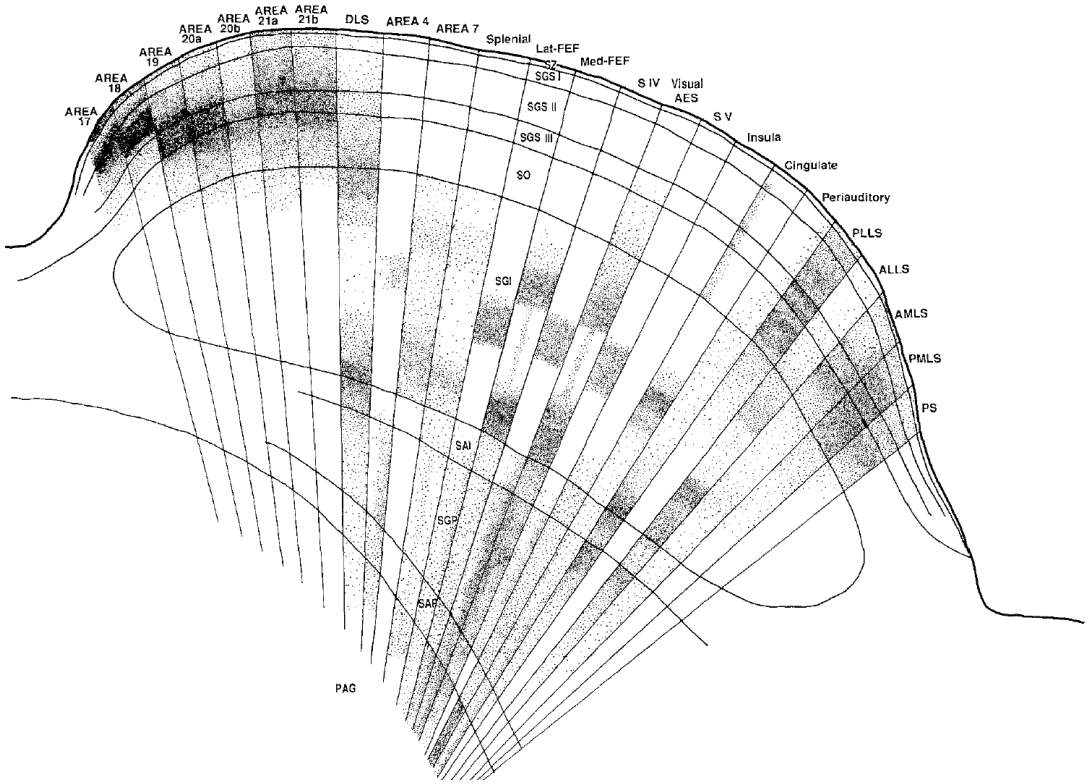

Figure 1.8. Cortico-collicular projections. Summary diagram displaying the laminar and sublaminar distribution of cortical terminals in the superior colliculus of the cat. Abbreviations: DLS: dorsal lateral suprasylvian area; Lat-FEF: lateral frontal eye field area; Med-FEF: medial frontal eye field area; S IV: fourth somatosensory cortical area; S V: fifth somatosensory cortical area; PLLS: posterolateral lateral suprasylvian area; ALLS: anterolateral lateral suprasylvian area; AMLS: anterolateral medial suprasylvian area; PMLS: posteromedial lateral suprasylvian area; PS: posterior suprasylvian area. PAG: periacqueductal grey. Modified from Harting et al. (1992).

sometimes divided by a glial cell, they “give rather the impression of avoiding each other” (rabbit: Hofbauer and Hollander, 1986).

In mouse, V1 inputs have been shown to influence the gain of SC responses without clearly affecting their tuning (Wang et al., 2010; Zhao et al., 2014). In turn, SC disruption in mouse has been shown to shape the velocity tuning properties of higher cortical visual areas (lateromedial, anterolateral, anteromedial and rostrolateral areas), while it has no effect on V1 velocity preferences (Tohmi et al., 2014).

Damage to the SC also affects the tuning properties of extrastriate cortical areas in cat. Electrophysiological recordings from the lateral suprasylvian area (LS, putative area MT

homologue in cat) after SC inhibition suggested a facilitatory role during visually evoked potentials in response to fast moving stimuli (Ogino and Ohtsuka, 2000). SC removal also showed an increase in response to stationary flashes of light and to slow-moving stimuli, and a different spatial distribution of surround suppression in area LS neurons. Specifically, surround inhibition was asymetrically stronger along one RF axis and very weak or absent along the orthogonal one, bringing orientation selectivity in cells displaying these changes (Smith and Spear, 1979).

In primates cortical visual processing splits in two parallel streams, the dorsal and the ventral. The dorsal stream, also referred to as the "where pathway", has a crucial role in orienting movements with respect to objects, while the ventral stream -the "what pathway"- is thought to be devoted to visual object recognition (Ungerleider and Haxby, 1994). Whether there are similarly distinct processing streams in the rodent extrastriate cortex is still debated, but in rodents dorsal cortical areas are particularly sensitive to visual motion and ventral areas are particularly sensitive to visual patterns and object identity (Andermann et al., 2011; Marshel et al., 2011; Wang et al., 2012; Juavinett and Callaway, 2015; Vermaercke et al., 2015; Tafazoli et al., 2017). Interestingly, dorsal cortical visual areas have been shown to primarily project to the superficial layers of SC, while parietal areas mainly contact deeper layers (mouse: Wang and Burkhalter, 2013). This differential targeting of cortico-collicular inputs to the SC is consistent with SC superficial and deep layers having distinct roles: superficial SC neurons are likely to be more important for detecting and localizing stimuli, while deeper layers are more likely to be involved in the initiation of orienting movements. The functional localization of cortico-collicular projections suggests that the more recently evolved neocortex has developed to work in concert with the ancient SC.

Intra- and interlaminar connections. Axons in the SGS exhibit short collaterals projecting in the vicinity of the dendritic field, but some intrinsic neurons can connect to distant regions of SC, and these neurons are thought to be involved in the inhibitory effect of remote visual stimuli on the visual responses of SC (cat: Rizzolatti et al., 1974) or the generation of saccade signals (in those animals that show goal directed saccades). Other authors have suggested the presence of intrinsic excitatory circuits in the intermediate gray layer and their role in the presaccadic

command bursts (tree shrew: Pettit et al., 1999). Investigations of superficial lateral connections *in vitro* have shown that they induce non-linear proximal facilitation and distal inhibition, mechanisms that may be suitable for saliency detection (mouse: Phongphanphanee et al., 2014). Interlaminar connections are also present in the SC of many species, connecting the visual laminae in a cascade fashion from the superficial to the deep layers (tree shrew: Hall and Lee, 1993). The different layers make synaptic contacts with the deeper ones in an approximately columnar fashion, projecting to neurons with similar location in the topographic maps. Superficial axons can also terminate in deep laminae and contact tectoreticulospinal projection neurons (ferret: Doubell et al., 2003). Coordinating sensory inputs and motor commands, these connections may be an anatomical substrate of the sensorimotor integration occurring in the SC.

Subcortical structures. The SC is reciprocally connected with the pretectum, which is also involved in directing eye movements. Afferent inputs originating from the pretectum have been shown to be GABAergic, and to target GABA-negative dendrites in SGS (cat: Baldauf et al., 2003). The role of this tectal pathway is still unknown. The parabigeminal nucleus (PBg), a satellite nucleus of SC, receives bilateral input from - and sends cholinergic bilateral output back to - SC superficial layers in an ordered topographic fashion (cat: Graybiel, 1978; Sherk, 1979; rat: Taylor et al., 1986; mouse: Mufson et al., 1986), as well as to the LGN (tree shrew: Fitzpatrick et al., 1988) and to the amygdala (mouse: Shang et al., 2015). PBg cholinergic neurons are thought to modulate the activity of colliculo-thalamic SGS neurons reducing their excitability via intracollicular GABAergic interneurons, a mechanism suggested to amplify SGS projection neuron responses to subsequent novel stimuli through activation of low threshold Ca^{2+} channels (rat: Lee et al., 2001). Additionally, it has been shown that parvalbumin positive (PV^{+}) neurons projecting to PBg in the superficial SC are glutamatergic, appear selective for looming stimuli (expanding black disks), and trigger avoidance behaviours (mouse: Shang et al., 2015). The SC also sends direct ipsilateral terminals to the substantia nigra pars compacta (SNc), contacting both dopaminergic and non-dopaminergic neurons. Dopaminergic neurons in the SNc respond

to unexpected biologically relevant stimuli, and SNc short latency visual responses are abolished by ipsilateral lesion of the SC and increased by SC stimulation (rat: Comoli et al., 2003).

Visual thalamus. The tectogeniculate pathway, projecting to the dorsal lateral geniculate nucleus (dLGN), has been studied in several mammals (Harting et al., 1991). This pathway originates in small SGS neurons which are close to the layers that are innervated by retinal W-cells (Harting et al., 1991). The area of the dLGN receiving tectogeniculate projections is also a target of W-like RGCs: in primates, the koniocellular layers in the LGN are the only targets of colliculogeniculate inputs and have therefore been suggested to collaborate with the SC in generating visually guided behaviours such as saccades. Koniocellular layers in dLGN contain neurons projecting to extrastiate cortical areas, suggesting the presence of a colliculo-geniculo-cortical pathway likely to support some visual behaviours in the event of lacking or damaged V1 (Harting et al., 1991; Hendry and Reid, 2000). In rodents, tectogeniculate neurons project to the dorsolateral shell, which mainly encodes direction and motion information (mouse: Bickford et al., 2015). Reciprocal connections are also present between SC and ventral lateral geniculate nucleus (vLGN) (Harrington, 1997; monkey: Benevento and Fallon, 1975; cat: Edwards et al., 1974; tree shrew: Conley and Friederich-Ecsy, 1993; rat: Cosenza and Moore, 1984). SGS sends input primarily to the vLGN layer adjoining the optic tract, and the terminals' topography resembles the W-like distribution seen in dLGN. The vLGN also sends projections to the SC, and vLGN cells have been suggested to represent the main thalamic input to the superior colliculus, at least in rat (Matute and Streit, 1985).

Neurons in the superficial SC also project to the pulvinar/lateral posterior complex (Pul/LP) (mouse: Wei et al., 2015; Zhou et al., 2017; cat: Graham, 1977; monkey: Stepniewska et al., 2000), a structure suggested to be important in visual attention. In primate the pulvinar has powerful control over gating visual responses in V1 (Purushothaman et al., 2012), and it relays collicular inputs to dorsal stream areas in primates and cats (Kaas and Lyon, 2007). In mouse, the tectopulvinar pathway only includes glutamatergic projections originating from wide field cells. The tectorecipient portions of the pulvinar, interconnected in loops with cortex, striatum and amygdala (Amg), are likely to be part of a network coordinating the transformation of

perceptual information into action during ongoing movement (Zhou et al., 2017). In particular, the pathway connecting the superior colliculus to the LP and the LP to the amygdala has been shown to induce fear responses and to be important in the generation of visually triggered defensive behaviours (Wei et al., 2015).

1.3.3 Behavioural role of the superior colliculus

Activity in the superior colliculus has been shown to be important in selecting a conspicuous stimulus among similar, competing ones. In this section I provide an overview of what is currently known about the involvement of the superior colliculus in the detection of salient stimuli and in orienting behaviours in different species.

The activity of collicular neurons is thought to reflect both bottom-up and top-down attentional biases for visual stimuli (Fecteau et al., 2004; Krauzlis et al., 2013). SC lesions in primates usually have very slight or negligible effects on the neuronal properties of different cortical areas, such as a weak reduction in RF sizes and strength of visual response in the superior polysensory area (STP) or a slight increase in visual responses in area MT neurons. In addition, while ablation of V1 influences properties of downstream cortical areas, it does not usually lead to a complete loss of visual responsiveness, and the concurrent ablation of SC and striate cortex often abolishes residual visual responsiveness. This suggests that the SC is not strictly necessary for higher cortical areas to function, but can contribute to visual responses when V1 is absent (Bruce et al., 1986; Rodman et al., 1990).

Role of SC in approach behaviours

In primates, where eye movements are used to bring images of objects onto the high-acuity foveal region, the SC has a prominent role in generating saccadic eye movements. The firing rate of neurons in intermediate and deeper layers of the SC is associated with saccade targets, such that the response to a visual stimulus is increased when its location is the end point of a saccade (Goldberg and Wurtz, 1972b; McPeek and Keller, 2002). Lesions of the SC in monkeys produce persistent impairment in peripheral localization of briefly presented stimuli (Butter et al., 1978). Unilateral ablation of the superior colliculus has minimal influences on the initiation and the

accuracy of saccades directed to targets, but larger lesions including pretectum and posterior-medial thalamus seriously impair saccade accuracy (Albano and Wurtz, 1982). SC lesions also increase the latency and speed of saccadic responses (Wurtz and Goldberg, 1972; Mohler and Wurtz, 1977). In presence of competing stimuli, inactivation studies have shown that saccade target selection is profoundly impaired if the cue stimulus is presented in the visual field portion represented by the affected part of the SC, leading to increased saccades towards distractors (McPeek and Keller, 2004; McPeek, 2008). The disruption is not due to motor or visual deficits (McPeek and Keller, 2004), and has also been observed in the absence of explicit orienting movements (Lovejoy and Krauzlis, 2010). Microstimulation of the SC in primates increases the probability of selecting a target presented in the portion of the visual field corresponding to the stimulated site (Carello and Krauzlis, 2004), and brings about a decrease in reaction time and an increase in performance consistent with a shift of attention to that location (Cavanaugh and Wurtz, 2004). The SC has been shown to be involved not only in saccadic target selection but also in target pursuit (Krauzlis and Dill, 2002; Nummela and Krauzlis, 2010). Stimulation of the SC has been shown to induce gaze shifts that are accompanied by head movements with strong stimulation (Freedman et al., 1996). The monkey SC is therefore mainly involved in directing eye movements.

In cat the superior colliculus is not only involved in gaze, but also in head and body movement. Electrical microstimulation induces foveation towards the portion of visual field corresponding to the RF of the stimulated neurons that are similar to behavioural saccades towards novel stimuli (Harris, 1980), or in head turning (Schaefer, 1970). Unilateral superior colliculus lesions result in visual neglect in the contralateral hemifield, in particular when competing distractors are present, hyper-responsiveness to ipsilateral stimuli, and motor deficits such as repetitive circling movement towards the ipsilateral side of the lesion. Bilateral lesions cause impaired visual pursuit and localization of stationary stimuli (Sprague and Meikle, 1965). Compared to monkey, the SC in cat has a larger role influencing not only saccades, but also head and body movements.

In rodents, which lack a fovea or area centralis and where saccadic eye movements are therefore less important, the SC is mainly involved in head and body movements. Lesions of the

superficial layers in tree shrews (a highly visual rodent) leads to visual discrimination deficit, while a larger lesion affecting also the deep layers and part of the pretectum results in supplementary decline in the ability to orient to objects (Casagrande and Diamond, 1974). In hamsters, the SC has been shown to be essential to approach a dark and stationary target using vision as guiding sense, and the deficit has been suggested to be due to visuomotor integration impairment (Carman and Schneider, 1992). Similarly, hamsters with lesioned SC fail to approach sunflower seeds (Schneider, 1969; Dean and Redgrave, 1984). In rat, ablation of the SC leads to absence of orienting responses towards stimuli appearing in peripheral regions of the visual space but leaves intact their ability to perform other visually guided tasks (Goodale and Murison, 1975; Goodale et al., 1978), while electrical stimulation causes circling behaviour similar to what has been observed in cats (Tehovnik, 1989). The SC in rodents is involved in the generation of whole body movements, and is therefore likely to have a much larger influence on animals' behaviour compared to monkey.

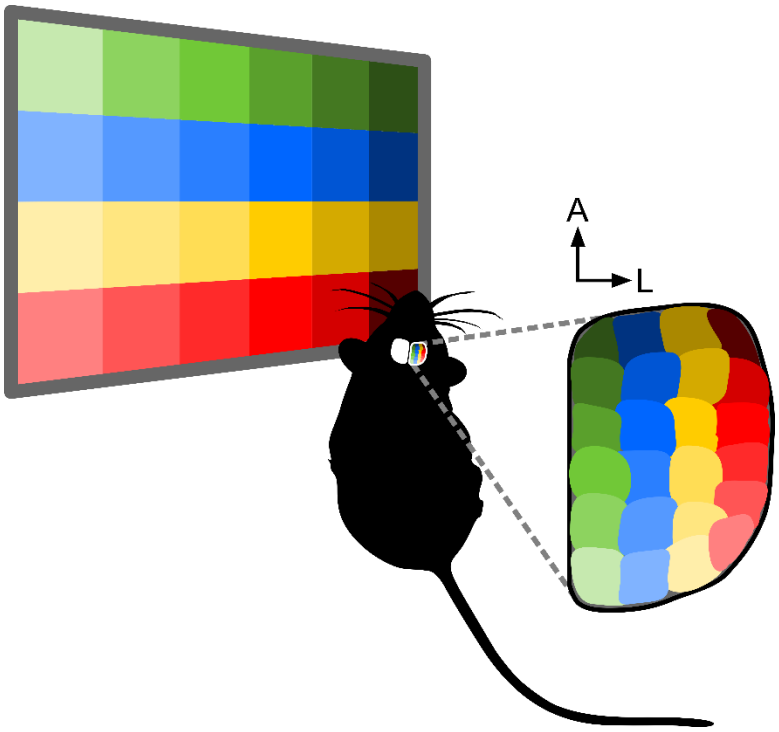

Figure 1.9. SC retinotopy. In rodents, the sSC is retinotopically organized with the medial SC representing the upper visual field, the lateral SC representing the lower visual field, the anterior SC representing the nasal and the posterior SC the temporal visual field.

Role of SC in defence behaviours

In addition to its role in approach behaviours, at least in rodents the superior colliculus is important for defensive behaviours such as freeze and flight (Dean et al., 1989). When a salient visual stimulus is detected, it might indeed be attractive like in the case of food, or aversive, as in the case of a predator or an object on collision course. In both cases animals should initiate behaviours, of opposite nature: food should generate approach, while danger should initiate avoidance or escape responses. For rodents, food is usually found on the ground while predators come from the ground and sky. The topographical organization of the rodent SC is such that the medial SC represents the upper visual field and the lateral SC the lower, while moving rostro-caudally the receptive fields shift from nasal to temporal (Fig. 1.9) (Drager and Hubel, 1976). Remarkably, the medial and lateral subregions of the SC have been shown to receive different inputs and project through different descending pathways (Fig. 1.10) (Comoli et al., 2012; Savage et al., 2017). These pathways seem to be ideal for generating appropriate approach and defensive behaviours (Sahibzada et al., 1986; Ellard and Goodale, 1988; Dean et al., 1989; Westby et al., 1990; Comoli et al., 2012; Savage et al., 2017).

Afferent signals to the medial and lateral SC are largely non-overlapping, with a majority of structures selectively projecting to the medial SC. The two major output pathways are the contralateral tecto-reticular-spinal projection (predorsal bundle, PDB) and the ipsilateral cuneiform projection (ICF). The PDB arises from intermediate SC layers and contains neurons that primarily respond to somatosensory vibrissae stimulation or small moving visual stimuli located in the lower frontal and lateral visual field (at least in anesthetized animals), implying a role in approach behaviour. The ICF, innervating various regions among which the parabigeminal nucleus, caudal pontine nuclei and the ponto-medullary reticular formation, originates from rostromedial SC regions, and is primarily responsive to visual stimuli in the upper visual field (particularly looming stimuli) implying a role in avoidance and escape behaviours.

Consistent with a role of the ICF in avoidance behaviour, it has recently been shown that in mouse SC glutamatergic PV^+ neurons that contact cells in the parabigeminal nucleus are activated by looming stimuli, and elicit avoidance behaviours (Shang et al., 2015). In addition, optogenetic activation of a subset of medial glutamatergic neurons expressing CaMKIIa, located

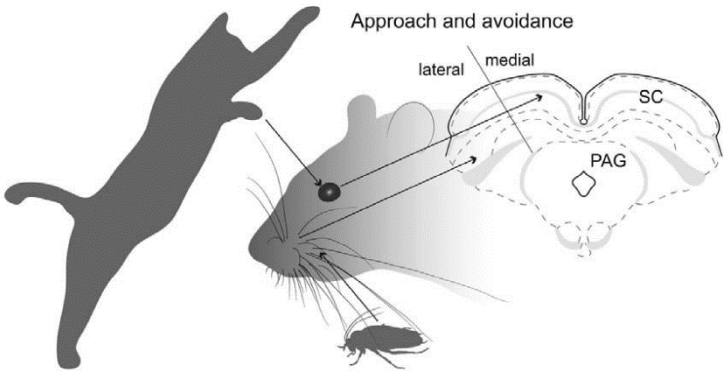

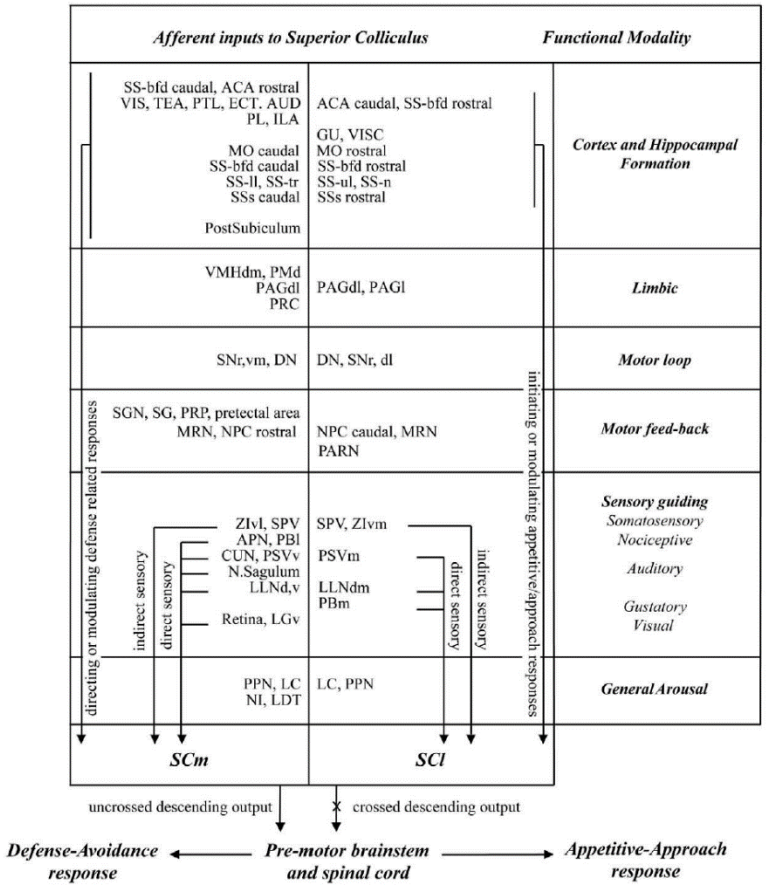

Figure 1.10. Functional anatomy of the SC. *Top:* Schematic displaying that predators coming from the upper visual field is detected from the medial SC, and promotes defence responses. Whisker related somatosensory stimuli in the lower field, associated with preys, are detected in the lateral SC and promote approaching behaviours. *Bottom:* Summary of inputs and outputs from and to the medial (left) and lateral (right) regions of the SC, associated with defence and approach behaviours, respectively. Modified from Comoli et al. (2012).

between the stratum opticum and the intermediate grey layer, is sufficient to induce freezing behaviour. These neurons belong to a di-synaptic pathway rapidly (6-26 ms) transferring information from the SC to the amygdala via a LP relay (Wei et al., 2015).

Progressively stronger electrical stimulation of deep regions in the rat SC induce gradual changes in the type of aversive responses from arousal, to freezing, to flight (Brandao et al., 1994). This is intriguingly consistent with the Predatory Imminence Theory which hypothesizes that the selection of the appropriate aversive response depends on the distance from the predator in space or time, such that with increasing predator proximity the behaviour of a prey switches from arousal, to freezing, to flight, to attack (Fanselow, 1994; Eilam, 2005). The superior colliculus might therefore be the brain structure where sensory signals informative about threat imminence are integrated for selection of the appropriate defensive behaviour.

1.3.4 Functional properties of visual cells in the superficial superior colliculus

The superior colliculus is important for orienting behaviours in many species, transforming sensory information in order to select salient stimuli and generate appropriate motor responses. To understand how the superior colliculus implements such mechanisms, it is essential to understand how sensory information is encoded and transformed in this area. This section describes how visual receptive fields are usually characterized, and then reviews the current knowledge about visual receptive field properties in the superior colliculus. I then describe non-classical receptive fields and review the available literature about nCRFs in the superior colliculus.

Characterization of visual receptive fields.

The information carried by visual pathways is dependent on the functional properties of the constituent neurons. In each species, the specific sensitivities to different properties of the stimuli have been shaped by evolution and ecology - for example many animals have developed magnetoreception to aid orientation (Clites and Pierce, 2017), and others including rodents have developed photoreceptors able to detect light in the ultraviolet range (Tovee, 1995). As wings

are used to fly and fins to swim, the description of the anatomical and functional properties of visual neurons is essential for understanding what vision is used for, and how.

Sensory neurons generally respond to stimuli presented over a circumscribed portion of the sensory epithelium, providing the so-called classical receptive field (CRF). For a visual neuron, the CRF is usually defined as the portion of the retina (or equivalently, visual space) where an appropriate stimulus can change the spiking activity of the neuron. In the following I briefly describe the CRF of visual neurons, concentrating on retinal ganglion cells (RGCs), the first processing stage in which action potentials are generated.

The basic unit of description of the CRF of visual neurons is whether they primarily respond to increments in luminance (ON cells), to decrements in luminance (OFF cells), or to both (ON-OFF). Many RGCs are characterized by circular, concentric and spatially overlapping subfields that have opposite effects on the firing activity of the neuron, generating an antagonistic centre-surround receptive field structure. Both ON centre/OFF surround and OFF centre/ON surround types are found. In modern work, sensitivity of RGCs and subsequent neurons to visual stimuli is generally characterised by their response to luminance contrast: the more a neuron is responsive to low contrasts (i.e. the lower its contrast threshold), the higher its contrast sensitivity. At suprathreshold contrasts different neurons can show varied response – in some, response increases linearly with contrast while in others it starts to saturate.

The second basic descriptor of a receptive field is the linearity of spatial summation. Depending on the linearity of spatial summation RGCs are classified as linear (or X-like) and non-linear (or Y-like) (Enroth-Cugell and Robson, 1966; Hochstein and Shapley, 1976b). Similar distinctions between linear (simple-like) and non-linear (complex-like) spatial summation has been made in neurons of visual cortex (Movshon et al., 1978; Skottun et al., 1991). A simple description of linearity is as follows. When stimulated with a drifting sinusoidal grating of optimal spatial frequency, the luminance over a neuron's receptive field changes over time in a sinusoidal fashion. The response of linear neurons is strongly modulated at the temporal frequency of the grating, while non-linear cells respond with an elevation of the mean firing rate that is only weakly modulated at the grating temporal frequency. In the model of retinal Y-cell receptive fields proposed by Shapley and Hochstein, this is because retinal Y-cells' receptive

fields include multiple spatially overlapping subunits and the output of each subunit is rectified before summation within the receptive field. Similarly, cortical complex cells can be thought of as the summation of rectified subunits, like those found in cortical simple cells.

The third basic descriptor is receptive field size. The sensitivity of a receptive field falls off with increasing distance from its centre, and this distribution of sensitivity can be well captured by a Gaussian function (Rodieck, 1965). For a linear neuron, this Gaussian provides a sufficient descriptor of the receptive field in space, and dictates how the neuron will respond to arbitrary patterns. So for example, the size of the Gaussian limits how fine a sinusoidal pattern can be used to drive the neuron – smaller Gaussians also respond to finer patterns (higher spatial frequencies). Both the centre and surround of the CRF can be described by Gaussian functions, and the response of a neuron to different spatial frequencies is well described by a difference-of-Gaussians where the center Gaussian, due to its smaller size, is sensitive to higher spatial frequencies than the surround (Fig. 1.11) (Enroth-Cugell and Robson, 1966; Croner and Kaplan, 1995).

The fourth basic descriptor is the temporal response of a neuron. This can be measured in many ways: for static stimuli the time course of response can be used to describe neurons as transient or sustained and the latency of response can be used to describe neurons as brisk or

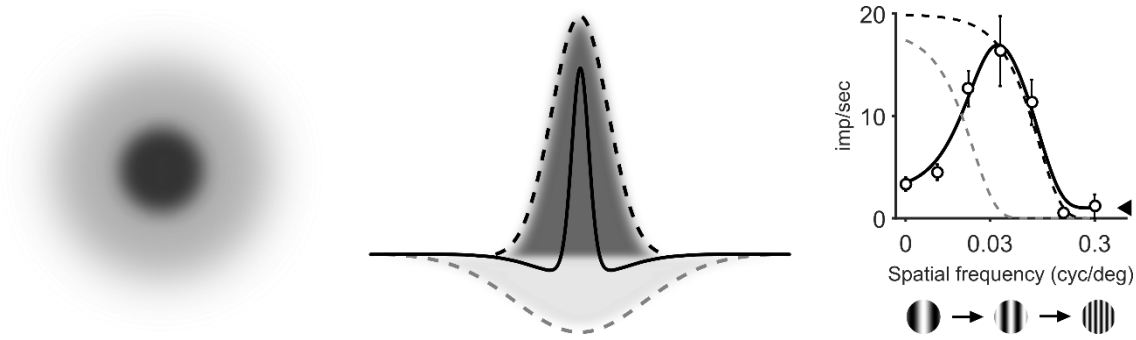

Figure 1.11. Analytic description of classical receptive field. The sensitivity of the classical receptive field is the sum of concentric and antagonistic subregions. *Left, middle*: the receptive field center (black areas and black dashed curve) and surround (grey areas and grey dashed curve) can be modelled as Gaussians. *Right:* responses to gratings of varying spatial frequency can be predicted by a difference-of-Gaussians equation. Circles indicate responses of an example neuron in the SC. Black dashed line depicts best fitting centre mechanism. Grey dashed line depicts best fitting surround mechanism. Black solid line depicts difference between centre and surround mechanism.

sluggish. As the spatial frequency tuning of a visual neuron depends on how the cell integrates luminance over space, so the temporal frequency tuning of a visual neuron reflects how quickly CRFs can integrate changes in luminance over time. I note that a moving object can be decomposed into different spatial frequencies which move at the same speed, and therefore different temporal frequencies. Similarly, two objects of identical temporal frequency but different spatial frequency will have different speeds, because the speed of an object depends on the ratio between its temporal frequency and spatial frequency. Some visual neurons are sensitive to temporal frequency and their temporal frequency tuning depends little on spatial frequency. In neurons that are sensitive to speed, the temporal frequency tuning depends on spatial frequency (Priebe et al., 2003; Andermann et al., 2011; Gale and Murphy, 2014).

The fifth basic descriptor is whether neurons are selective for direction or orientation of motion of moving stimulus. The selectivity of visual neurons for movement direction and orientation has been extensively studied, and is thought to be a feature of visual processing essential for interacting with the environment. The computations that support direction and orientation selectivity remain, however, unclear. One proposed model for direction selectivity suggests a precise spatial organization of input synapses with differential response latencies, that only allows the postsynaptic neuron to optimally integrate excitatory currents if the stimulus moves in a particular direction (Reichardt, 1987). Similarly, orientation selectivity in the cat retina has been suggested to originate from RGCs presenting asymmetric dendritic arborisation (Leventhal and Schall, 1983), while in cat primary visual cortex V1 neurons have been proposed to receive excitatory input from LGN cells with spatially offset, circular receptive fields aligned along a particular axis (Hubel and Wiesel, 1962). [Note though that orientation selectivity is already found in the LGN of rodents (Piscopo et al., 2013; Scholl et al., 2013) and marmosets (Cheong et al., 2013), and that the mechanisms underlying cortical orientation selectivity may differ among species]. The study of motion detection is a very active field in visual neuroscience, and we are just starting to find neural correlates for some of the suggested models (Yonehara and Roska, 2013).

Receptive field properties in the superficial superior colliculus.

Surprisingly, previous studies have generally focused on the deep layers of SC and the integration of sensory and motor information, while the visual computations performed by the superficial layers have been less investigated, especially in rodent (Girman and Lund, 2007). This trend has recently reversed. In the following I will first describe the receptive field properties of neurons in the superficial SC of monkey and cats and then focus on rodents.

Monkey. Monkey superficial SC neurons are transiently responsive to stationary flashing spots of light and respond usually both to the onset and the offset of the stimulus. Moving spots are always able to induce responses. RF sizes in monkey superior colliculus can be as small as 0.75° diameter near the fovea and generally increase with distance from the fovea, reaching 17° at 40° eccentricity. Despite the possibility of finding very large RF far from the fovea, receptive fields as small as 4° can be found throughout the SC, indicating a fine-grained representation of the visual space. Interestingly, it has recently been shown that, in monkey, SC neurons representing the upper visual field are tuned for higher spatial frequencies and respond faster and more strongly than cells with RF in the lower visual field (Hafed and Chen, 2016). Neurons are not highly selective for stimulus velocity. Strikingly dissimilar to cat and mouse is the fact that in monkey superior colliculus direction selective neurons are rare (Schiller and Koerner, 1971; Cynader and Berman, 1972; Davidson and Bender, 1991). The main effect of cortical ablation is seen in the deep layers, where the visual responses disappear (Schiller et al., 1974).

Cat. In cat, most SC cells respond to both the onset and the offset of stimuli with a low proportion of cells (3-10%) displaying solely ON or OFF responses. Receptive field sizes are widely variable, with values ranging between 1-2° to more than 50°. As in monkey, RF size increases with the distance from the area centralis. Direction selectivity is prominent in cat SC: directionally selective cells have been suggested to be at least two thirds of the population, and often more than that (McIlwain and Buser, 1968; Sterling and Wickelgren, 1969; Rosenquist and Palmer, 1971; Pinter and Harris, 1981). Since lesioning area 17 leads to reduced proportion of directional cells, the directionality of neurons in cat SC seems to be depentent on cortical input. Cat SC neurons prefer spatial frequencies around 0.1-0.3 cyc/deg (Bisti and Sireteanu, 1976; Pinter and Harris, 1981; Waleszczyk et al., 2007; Markus et al., 2009), temporal frequencies

around 6 cyc/sec (Waleszczyk et al., 2007; Markus et al., 2009), and the contrast threshold is higher than in other parts of the visual stream (Bisti and Sireteanu, 1976). Liu et al. (2011) showed the presence of looming-sensitive neurons in cat SC. These cells represented about 33% of the recorded population, and were further subdivided into *eta* and *rho* classes based on the firing pattern in response to approaching stimuli. *Rho* cells response continuously increased until object collision, while for *eta* cells the firing rate peak depended on the diameter/velocity ratio of the looming objects, and occurred some time before collision. Like other SC cells, their RF generally comprises a classical excitatory center and a large suppressive surround. Lesions of primary visual cortex dramatically reduces binocular convergence and increases the spontaneous firing rate and sensitivity to stationary stimuli, while the neuronal spatial summation properties are spared (Sterling and Wickelgren, 1970; Rosenquist and Palmer, 1971; Bisti and Sireteanu, 1976).

Mouse. In mouse, the great majority of the cells shows ON-OFF responses, and less than 10% respond only to luminance increases or decreases. The magnitude of ON and OFF responses, their spatial distribution and their size are generally similar, indicating overlapped ON and OFF subfields. Receptive fields are generally small, about 5° in radius, for both $GAD2^+$ and $GAD2^-$ neurons (Drager and Hubel, 1975; Wang et al., 2010; Inayat et al., 2015), with responses peaking for the majority of cells at stimuli of 6-10° in radius (Wang et al., 2010). When stimulated with moving sinusoidal gratings of different orientations, SC neurons display a broad spectrum of responses. In Wang et al. (2010) almost 40% of the recorded cells showed orientation selectivity, of which half had high direction selectivity, while another 40% were insensitive to direction. Directional selectivity has been shown to be stronger in WF and NF cells compared to stellate and horizontal neurons (Gale and Murphy, 2014). Directional selectivity is particularly pronounced in the uppermost SC and decreases with depth (Inayat et al., 2015). Directional selectivity in the SC appears to be inherited from the retina, and then linearly amplified by intracollicular circuits connecting similarly tuned neurons (Shi et al., 2017). In contrast to the salt-and-pepper orientation preference found in rodent primary visual cortex and similarly to V1 in other mammals (Hubel and Wiesel, 1974; 1979; Blasdel and Salama, 1986; Van Hooser et al., 2005; Yacoub et al., 2008; Kaschube et al., 2010; Yoshida et al., 2012b), cells in the superior

colliculus seem to be organized into orientation columns (Feinberg and Meister, 2015; Ahmadlou and Heimel, 2015). Despite this, in the most superficial SC lamina neurons preferring similar directions have not been found to spatially cluster (Inayat et al., 2015); future experiments will be needed to clarify the disagreement between studies. The preferred spatial frequencies range between 0.02 and 0.16 cyc/deg, with most cells preferring intermediate values. Horizontal cells prefer lower spatial frequencies compared to WF, NF and stellate neurons (Wang et al., 2010; Gale and Murphy, 2014). Most (74%) units are reported to have non-linear responses to a drifting sinusoidal grating of optimal spatial frequency (Wang et al., 2010). WF, NF and stellate cells are more sensitive to speed than horizontal cells and respond best to grating velocities up to ~100 deg/sec (Gale and Murphy, 2014). Cells in the mouse SC respond robustly and in a speed-dependent fashion to looming stimuli (Zhao et al., 2014).

V1 removal influences the preferred spatial frequency of mouse SC cells, increasing it towards 0.16 or even 0.31 cycles/degree. Given the preference of V1 neurons for lower spatial frequencies (around 0.02-0.07 cyc/deg, Wang et al., 2010; Andermann et al., 2011; Durand et al., 2016), V1 probably acts to dampen SC responses at high spatial frequencies, for reasons that remain unclear. The absence of cortical inputs from V1 also increases the direction selectivity of SC neurons while orientation selectivity is unaffected (Wang et al., 2010; Shi et al., 2017). Cortical ablation also results in weaker spatial overlap between ON and OFF subfields, despite a similar proportion of linear cells and percentages of ON, OFF, and ON-OFF neurons. Receptive field size and evoked rate are similar in presence or absence of V1, while the spontaneous firing rate increases after cortical lesioning (Wang et al., 2010). Finally, V1 exerts a modulatory effect on SC responses to looming stimuli, dramatically decreasing the gain but sparing the tuning properties (Zhao et al., 2014).

Non-classical receptive field properties in the superficial superior colliculus.

As discussed above (Section 1.2.2), the activity of visual neurons does not simply depend on signals within the CRF. Instead, cells integrate information over a larger portion of visual space known as the non-classical receptive field (nCRF), unable to drive the cell when stimulated on its own but able to modulate the activity of the CRF when they are stimulated together. The

nCRF can be modelled as an additional Gaussian that envelopes the CRF and acts on it in a divisive fashion (Fig. 1.12). The presence of a nCRF can be revealed by the spatial summation profile of neurons: when stimulated with gratings of increasing size, the response of a neuron increases because more of the CRF is stimulated. As the grating extends beyond the CRF, the response decreases due to nCRF suppression. In order to disentangle the contributions of classical receptive field surround inhibition (sensitive to lower spatial frequency than the centre) and of nCRF suppression, gratings beyond the spatial resolution of the classical receptive field surround should be used. The sensitivity and selectivity of nCRF can be probed by using a central stimulus over the CRF surrounded by a larger annular grating recruiting the nCRF, an approach that allows to independently adjust the properties of the visual stimuli over CRF and nCRF.

nCRFs have been demonstrated in the SC of many species. In monkey SC, surround suppression is selective for direction and speed, so that the firing rate is more suppressed when the visual properties of the stimulus over the nCRF match those over the CRF. The selectivity for relative motion between the RF and the background is independent of absolute orientation or velocity for both the RF and the background. Relative motion selective surround suppression is particularly present in the lower portion of the superficial layers, where 90% of neurons display this property, while in upper layers the proportion is about 45% (Schiller and Koerner, 1971;

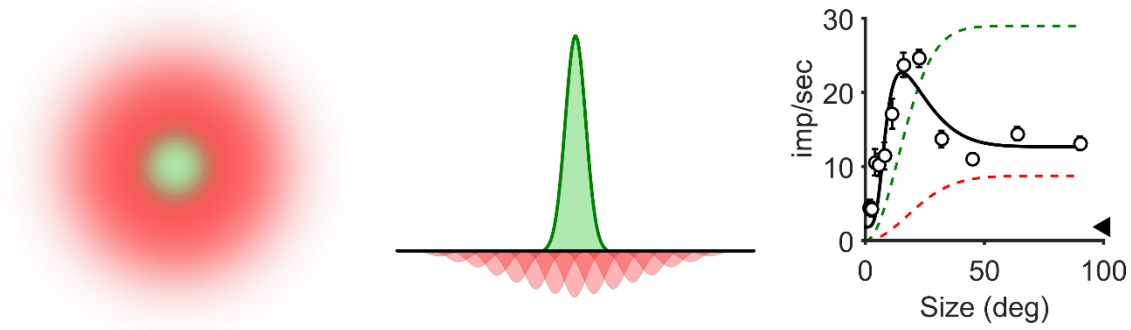

Figure 1.12. Analytic description of non-classical receptive field. The classical receptive field (green) is embedded in and can be modulated by the non-classical receptive field (red), which summates over a region larger than the CRF. Both CRF and nCRF can be modelled as Gaussians (middle). *Right*: responses to gratings increasing in size can be predicted by a ratio-of-Gaussians model. Circles indicate responses of an example neuron in the SC. Green dashed line depicts best fitting CRF mechanism. Red dashed line depicts best fitting nCRF mechanism. Black solid line depicts ratio between centre and surround mechanism.

Cynader and Berman, 1972; Goldberg and Wurtz, 1972a; Marrocco and Li, 1977; Moors and Vendrik, 1979; Wurtz and Albano, 1980; Davidson and Bender, 1991).

In cat, 50-90% of cells show surround suppression in response to large moving stimuli, but are less effective with stationary stimuli (McIlwain and Buser, 1968; Sterling and Wickelgren, 1969; Pinter and Harris, 1981). Whether surround suppression is sensitive to relative direction between a central and peripheral stimulus is less clear (McIlwain and Buser, 1968; Sterling and Wickelgren, 1969).

In mouse, surround suppression is evident in most SC neurons, with responses to drifting gratings generally peaking around 8° radius and then decreasing in response to larger stimuli (Wang et al., 2010). Responses to presentation of two small moving spots (one passing through the RF and the second at varying distances from the first) are suppressed in wide field and narrow field cells when the distance between the spots is ≥ 10°, while the response of horizontal and stellate neurons is unchanged (Gale and Murphy, 2014). A recent study suggests that the responses of both GABAergic and non-GABAergic interneurons are affected by surround suppression (Kasai and Isa, 2016), but since that work used light patches of different sizes on a dark background it is not clear if the measured reduction in response to large stimuli was due to surround suppression or to inhibition from the CRF surround. Light and dark patches have also been used to show that in wide field cells suppression is partly implemented by horizontal cells (Gale and Murphy, 2016), but again it is not clear how much of the decrease in response to large stimuli was due to inhibition from the CRF surround rather than nCRF suppression. The use of a random checkerboard stimulus, in which an optimally sized patch was moved across the receptive field and against a moving background, has shown that in wide field cells suppression is stronger when the speed and direction of the background are similar to those of the patch, suggesting that nCRF suppression may be selective for the direction and speed of the stimulus over the CRF (Gale and Murphy, 2016). Similarly, in rat SC nCRFs have been shown to be selective for the orientation and direction of a grating relative to that presented over the CRF (Girman and Lund, 2007).

1.4 OUTLINE OF THE THESIS

In this thesis I first demonstrate the importance of vision for mice by showing that they use visual information for selecting between distinct defensive behaviours, freeze and flight (Chapter 2). In order to shed light on how mice detect salient visual stimuli, I then characterize the visual properties of neurons in the main visual hub of the mouse brain, the superior colliculus, using electrophysiological recordings (Chapter 3). Finally, I investigate potential neural correlates of salience representations in the superior colliculus (Chapter 4).

Chapter 2 describes behavioural experiments showing that mice can use visual cues to select between alternative defensive behaviours, freeze and flight. I demonstrate that the simple use of two distinct visual stimuli can trigger opposite aversive behaviours, proving that mice use vision for decisions that may have a great impact on their survival.

Chapter 3 characterizes the visual properties of receptive fields in the mouse superior colliculus, using extracellular electrophysiological recordings from single-units in anesthetized and awake animals. I further show how eye movements can influence the responses of neurons in SC of awake animals.

Chapter 4 investigates potential neural correlates of salience in mouse superior colliculus, both non-classical receptive fields and adaptation. Using extracellular recordings, I first confirm the presence of non-classical receptive fields in this area, then investigate their functional properties. I describe a fast form of adaptation in the SC, and compare the strength of non-classical receptive fields and adaptation mechanisms in individual neurons.

Chapter 2

Behavioural correlates of visual saliency in mouse

2.1 INTRODUCTION

The mouse has become the most popular experimental model in biological sciences. To study mouse visual function, a number of behavioural paradigms have been developed. Visual thresholds have been measured taking advantage of the optomotor response (Prusky et al., 2004), or by training mice to detect changes in luminance (Naarendorp et al., 2010), spatial frequency (Prusky et al., 2000; Wong and Brown, 2006), orientation (Wong and Brown, 2006; Andermann et al., 2010) or contrast (Busse et al., 2011). Despite this, we still know little about their natural visual behaviours.

What visual patterns might a mouse naturally find salient? In prey species such as mice, avoidance of predators is key to survival and drives instinctual behaviours like freeze or flight (Tinbergen, 1951; LeDoux, 2012). Both behaviours help avoiding capture, but have opposite underlying escape strategies. From an ethological point of view, the advantage of fleeing is to distance the prey from the predator at the cost of increasing its visibility. Conversely, freezing

raises the probability of eluding the predator's attention, yet is not the best strategy if the prey has already been targeted as it will become an easy catch. Sensory signals guide the selection of appropriate behaviour (Dean et al., 1989), and for aerial predators only vision provides useful information. Surprisingly, there is no evidence that vision can guide the selection of escape strategies. Fleeing behaviour can be readily triggered by a rapidly looming overhead stimulus (Yilmaz and Meister, 2013). Freezing behaviour, however, has previously been induced by real predators or their odours (Blanchard, 1997). Here I discover that a small moving disk, simulating the sweep of a predator cruising overhead, is sufficient to induce freezing response in mice. Looming and sweeping therefore provide visual triggers for opposing flight and freeze behaviours, providing evidence that mice innately make behavioural choices based on vision alone.

2.2 METHODS

All procedures were conducted in accordance with the UK Animals Scientific Procedures Act (1986). Experiments were performed at University College London under personal and project licenses released by the Home Office following appropriate ethics review.

2.2.1 Environment & Visual Stimulation

The behavioural arena was a 48 cm wide x 35 cm deep x 30 cm high box. An opaque triangular refuge 20 cm wide x 12 cm high was positioned in one corner (Fig. 2.2c). Visual stimuli were generated using the freely available software Expo (P. Lennie) and presented on a calibrated LCD monitor displaying a grey screen (48 cm x 27 cm, mean luminance 30-40 candela/m2, refresh rate 60 Hz, Asus) that filled most of the open top of the arena. Mouse movements were video-recorded with a camera (DMK 22BUC03, Imaging Source, sampling rate 60 Hz; except in cohort 'a', described below, where it was a Creative HD USB, sampling rate 30 Hz; this cohort was excluded from latency calculations), fitted with a wide-angle lens and positioned over the arena. Frames were acquired continuously in Matlab (Mathworks, Natick, MA) and temporally aligned to visual stimulus by simultaneously acquiring (via a Labjack U6, sample rate 1 kHz) the response of a photodiode to synchronous visual stimuli presented in a corner of the monitor that was

obscured from the animal. The 'loom' stimulus was a 1 cm (thus a visual angle of diameter 2° when directly over the animal) black disk rapidly widening to 25.5 cm (50°) in 250 ms, and remaining on the screen at this size for an additional 500 ms. The standard 'sweep' stimulus was a 2.5 cm (5°) black disk that appeared at a corner of the monitor and then translated smoothly to the diagonally opposite corner over 4 seconds (21°/s). In some experiments the same black disc instead moved across the monitor in 16 s (5°/s), 2 s (42°/s), or 1 s (84°/s), or was a white disc of the same size and moving at the standard speed (21°/s). The 'sweep + loom' stimulus was also a 2.5 cm black disk, that appeared on the short edge of the monitor and translated along the midline for 2.6 s, by which time it had traversed 32 cm from the starting edge of the monitor. The disk then expanded (loom) to 25.5 cm either from the same position, or on the other side of the monitor (16 cm from the starting edge).

2.2.2 Testing

Prior to the first trial, animals were allowed to habituate to the arena for 15 minutes; in subsequent trials, the habituation period was 5 minutes. After habituation, a visual stimulus was triggered when the animal's location was approximately under the centre of the monitor. One trial was conducted each day, except in one cohort of animals ('a', defined below) where the loom stimulus followed the sweep stimulus by at least 1 minute.

2.2.3 Cohorts

A total of 65 adult mice were housed under 12:12 light/dark cycle and tested during the dark period (Table 2.1). Cohort 'a' (Fig. 2.2g,h) consisted of 8 male adult wild-type mice (C57BL/6, aged 13 - 18 weeks), and was tested once for the sweep stimulus, and then 6 times for the loom. Cohort 'a' was then tested once for the loom in the absence of a nest, and twice for the loom in the presence of two nests. Cohort 'b' (Fig. 2.2g,h) consisted of 10 male adult wild-type mice (C57BL/6, aged 11 -12 weeks), that were tested 4 times for the sweep stimulus (the first encounter is indicated by 'b1', subsequent encounters are indicated by 'b2') and then 3 times for the loom stimulus. Cohort 'c' (Fig. 2.2g, Fig. 2.5c) consisted of 18 adult wild-type mice (C57BL/6, 4 female, aged 8 -10 weeks), tested 4 (8 animals) or 5 (10 animals) times for the sweep

+ loom stimulus. Ten of the animals were also tested 2 times for the loom stimulus. In the sweep + loom trials, the looming disk expanded from either the final position of the sweep (cohort 'c2') or from an alternative location of the sweep trajectory (cohort 'c1') (Fig. 2.5c). Cohort 'd' (Fig. 2.2h) consisted of 19 mice housed and tested in a different facility, and included animals of different ages and genetic profile. 11 animals were adult male Gad2Cre on C57BL/6 background (aged 6-42 weeks), 6 were adult wild-type mice (C57BL/6, aged 8 weeks with an exception of 43 weeks), 2 were of other genetic profiles on C57BL/6 background (aged 7-9 weeks). Subdividing this cohort in animals aged 13 weeks or less (n=14), more than 28 weeks (n = 5), or Gad2Cre genetic profile (n = 11) showed no differences in freezing probability after the sweep stimulus (78.6%, 78.6% and 81.8% respectively). Cohort 'e' was 10 male adult wild-type mice (C57BL/6, aged 7-8 weeks), that were tested with black sweep stimuli of different speeds (5, 21, 42 and 84 o/s), and a white sweep stimulus of speed 21 o/s, in 6 sessions. The order of stimuli was randomised for each mouse.

COHORT	N° OF ANIMALS	SEX	AGE (WEEKS)	STRAIN	TEST
a	8	males	13-18	C57BL/6	1x sweep 21°/s 6x loom with nest 1x loom w/o nest 2x loom with two nests
b	10	males	11-12	C57BL/6	4x sweep 21°/s 3x loom with nest
c	18	14 males 4 females	8-10	C57BL/6	4x sweep 21°/s + loom (8 mice) 5x sweep 21°/s + loom (10 mice) 2x loom with nest (10 mice)
d	19	data not recorded	6-43	6 C57BL/6 11 Gad2Cre 2 Other	1x sweep 21°/s
e	10	male	7-8	C57BL/6	5x sweep (1x 5°/s, 2x 21°/s, 1x 42°/s, 1x 84°/s) 1x white sweep

Table 2.1. Summary of animal cohorts. For each cohort of animals used, the table reports the number of mice, their sex, age during the experiments, strain and visual stimulus tested throughout sessions.

2.2.4 Analysis

The position of the animal during the experiment was extracted from video recordings using custom software in the Matlab environment. Manual thresholds were set to identify pixels over the mouse in each video, and the centre-of-mass of these pixels was used to define mouse position on each frame (Fig. 2.1). The wide-angle and oblique orientation of the camera lens introduces barrel and projective distortions in the image. I estimated this distortion by calculating the requisite polynomial transformation matrix from daily calibration images using the function *cp2tform* in Matlab. The inverse of this matrix was used to transform positional estimates from image space to arena space, using the function *tforminv*. Transformed positions were accurate to within 1.5 mm. Inspection of responses to loom stimulus suggested that flights could be defined as periods of time during which the mouse speed was higher than 40 cm/s and the animal returned to the refuge within 1 second following the onset of this movement. Freezes were defined as periods of time during which the speed decreased to less than 2 cm/s for at least 0.5 seconds. Average speed across trials was calculated as the geometric mean and the s.e.m. of the geometric mean. For baseline measurements, I analyzed activity prior to presentation of visual stimulus. I analyzed 4s video sequences that were triggered on the animal moving away from the walls and towards the centre of the arena. Latency of flights was defined as the time from the onset of a stimulus to the time at which movement speed had increased by 20cm/s above that at stimulus onset (response on 1 loom trial did not reach this criterion). Latency was not clearly correlated with movement speed at time of loom onset (r = -0.02, p =

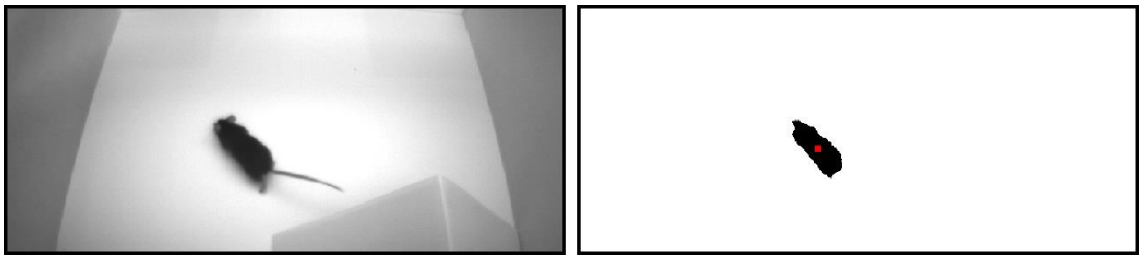

Figure 2.1. Video analysis. Example frame showing how the mouse position was extracted. *Left:* original frame. *Right:* thresholded frame. Black indicates pixels above threshold and classified as belonging to the mouse. Red dot indicates center of mass of the black pixels, from which the mouse position was estimated.

0.82, n = 94). For display purposes, I filtered the speed traces with a moving average filter of width 83 ms.

2.3 RESULTS

2.3.1 Visual patterns that elicit different freeze and flight behaviour

For a foraging mouse, a rapidly expanding overhead stimulus suggests the approach of a predator that has detected it. To avoid capture, rodents typically flee to an available refuge (Wallace et al., 2013; Yilmaz and Meister, 2013). But what if the potential predator is instead cruising overhead, as if unaware of the mouse? Flight or sudden movement would raise the risk of being detected, whereas freezing may promote survival. Here, I characterised the behaviour of mice during such distal threats.

I first confirmed that mice flee an imminent, looming threat (Fig. 2.2a). To do this I placed a mouse in a rectangular arena with an opaque refuge in one corner (Fig. 2.2c). A computer monitor placed on top of the arena displayed a blank grey screen. After habituating the mouse to the arena for 15 minutes, I triggered a visual stimulus when the mouse passed near the centre of the arena. The 'loom' stimulus was a black disk rapidly widening to 50 degrees of visual angle in 250 ms (Fig. 2.2a). As expected, presentation of this stimulus reliably caused mice to flee to the refuge (Fig. 2.2d-m; Movie 2.1). To quantify this behaviour I defined flight as epochs where

Figure 2.2. Visual stimulus dependence of freeze and flight behaviours in mouse. ***A-B.*** Schematics of visual stimuli. The loom stimulus expanded from 1 to 25.5 cm (2°–50°) in 250 ms and persisted for 500 ms. The sweep stimulus was a 2.5 cm (5°) diameter black disk translating across the monitor at an angular speed of ca. 21 °/s for 4 s. ***C.*** Schematic of the experimental arena. A computer monitor was placed on top of the arena. An opaque triangular refuge was provided in a corner. A camera video recorded the movements of the mouse. ***D-F.*** *Top:* images of the natural logarithm of movement speed in each trial (one trial per row). Red indicates low speed; green indicates high speed; black indicates speeds close to the mean across animals; white indicates times when the animal was in the refuge. *Bottom:* mean (±1 SEM) movement speed of mice across trials. Traces are clipped after flight home. Horizontal dashed lines indicate mean±1 SEM of movement speed in absence of visual stimuli, as shown in *F* (''BASELINE''). ***G-I***. Ethograms. Movement speed was used to classify flight and freeze behaviours. Flights were defined as epochs where speed was greater than 40 cm/s, and return to refuge within 1 s. Freezes were defined as epochs in which speed decreased to less than 2 cm/s for at least 0.5 s. The vertical line indicates onset of the stimulus. The horizontal lines subdivide different cohorts of animals (see Section 2.2.3). ***J-L.*** Instantaneous probability of freeze and flight. The probability of observing a flight (green) or a freeze (red) at each time point. The dotted line indicates the onset of the stimulus. ***M-O.*** Cumulative probability of having observed a flight (green) or freeze (red) response over time. See also Movie 2.1.

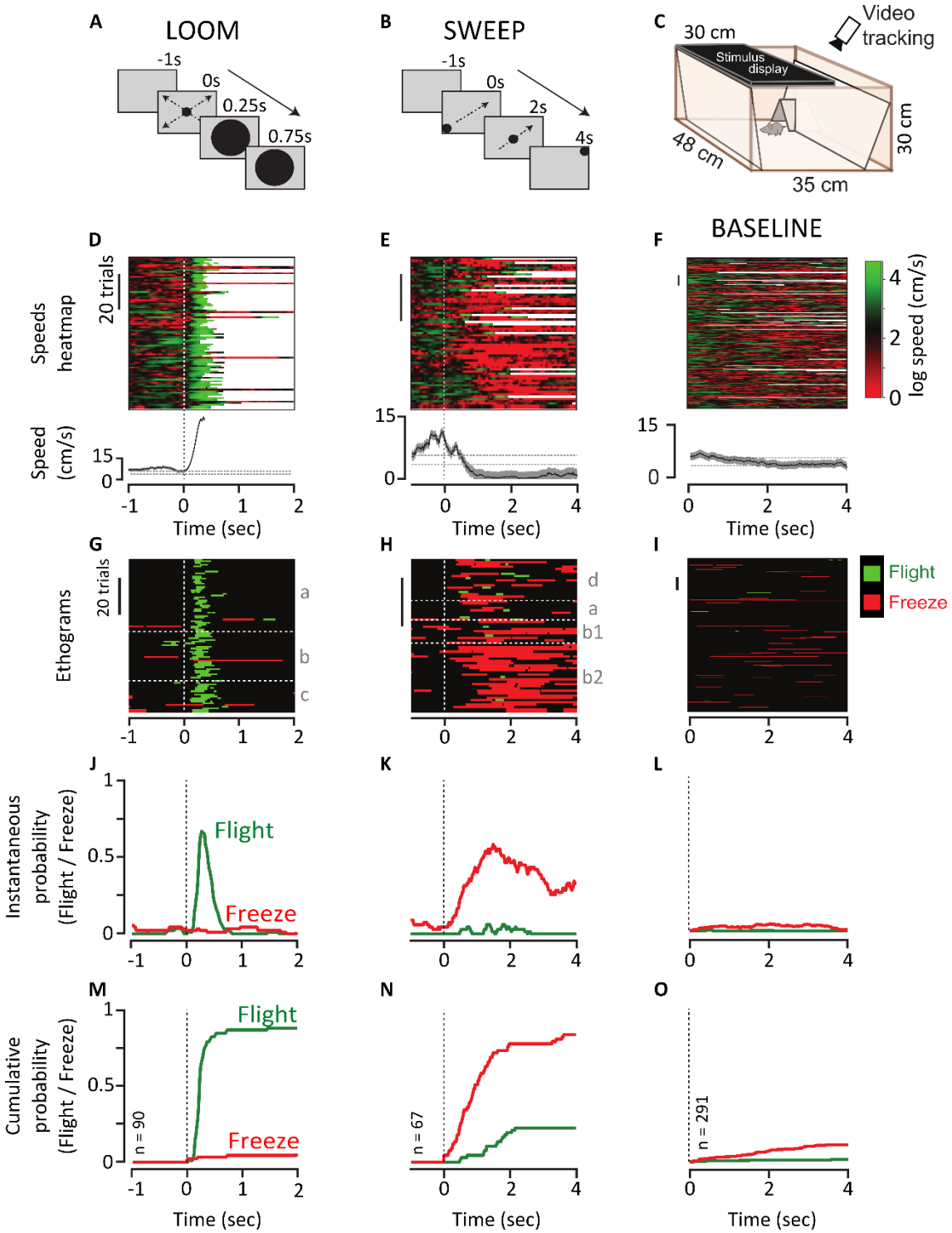
A
LOOM
-1s
0s
0.25s
0.75s
B
SWEEP
-1s
0s
2s
4s
C
30 cm
Video tracking
Stimulus display
48 cm
30 cm
35 cm
D
E
F
BASELINE
Speeds heatmap
20 trials
Speed (cm/s)
log speed (cm/s)
Time (sec)
G
H
I
Ethograms
20 trials
a
b
c
d
b1
b2
Flight
Freeze
J
K
L
Instantaneous probability (Flight / Freeze)
Flight
Freeze
M
N
O
Cumulative probability (Flight / Freeze)
n = 90
n = 67
n = 291
Time (sec)

the mouse returned to the refuge at speeds exceeding 40 cm/s (Fig. 2.2g). Flight was observed in 87.8% of loom presentations (79/90 trials in 28 mice; Fig. 2.2m).

I found an opposing response to a distal threat. The 'sweep' stimulus was a small black disk that appeared at a corner of the monitor and moved smoothly across it for 4 seconds (Fig. 2.2b). The stimulus emulates a 2m wide predator, flying 25m above the animal at 34 km/hr – a visual speed of 21 °/s to a mouse underneath it. The movement speed of the mice substantially decreased during the sweep stimulus (Fig. 2.2e,h; Movie 2.1), and included epochs of complete immobility. These data were obtained from animals that had only ever been exposed to the sweep stimulus. As a quantitative measure of freezing I identified epochs in which mouse speed was less than 2 cm/s for at least 0.5 s. Freezing was observed in 83.6% of the sweep presentations (56/67 trials in 38 mice, Fig. 2.2n). By contrast, flight occurred in 22.4% of trials (15/67 trials) - in 9 of these, the animal froze before fleeing. Freezing behaviour was similar for white and black sweep stimuli (Fig. 2.3).

Mice sometimes pause while foraging, or return to the refuge, even in the absence of a real threat. To estimate the frequency of these stimulus-independent behaviours I analyzed the last 5 minutes of the habituation period (before any visual stimulus), analysing only those epochs

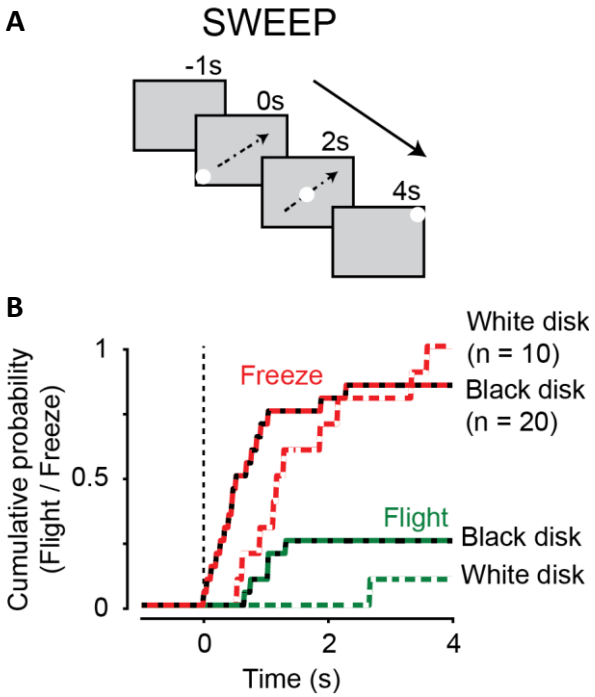

Figure 2.3. Responses to white sweep stimulus. ***A.*** Schematic of white sweep visual stimulus. The sweep stimulus was a 2.5 cm (5°) diameter white disc translating across the monitor at an angular speed of ca. 21 °/s for 4 s. ***B.*** The cumulative probability of having observed a flight (green-white) or freeze (red-white) response over time for a white sweep stimulus (10 trials in 10 animals). The cumulative probabilities of responses to a black sweep stimulus for the same cohort of animals are also shown (flight: green-black; freeze: red-black; 20 trials in 10 animals; replotted from Fig. 2.4b).

where the animal approached the centre of the arena, and applying the same criteria used above (Fig. 2.2f,i). I found that the 'chance' probability of freeze was 0.13, and of flight was 0.01. The stimulus-induced effects I observed above were much greater than this ($p < 10^{-10}$ for both freeze and flight, Binomial test).

2.3.2 Biasing behaviour towards freeze or flight

The speed of a distal threat might influence the behavioural response and we therefore asked if mice are sensitive to the speed of the sweep. In a new cohort of 10 mice we presented sweeps of varying speed (5, 21, 42 or 84°/s). The standard sweep speed (21°/s, Fig. 2.4b,f) produced responses similar to that in the cohorts described above. Slower speeds (5°/sec, Fig. 2.4a,e) led to robust freezing behaviour (Movie 2.2), occasionally with long-latency flight. Faster sweep stimuli (42°/s; Fig. 2.4c,g) led to freezing behaviour, with increased probability of flight. During presentation of the fastest sweep (84°/s; Fig. 2.4d,h), however, we observed a strikingly different pattern of responses: mice showed rapid flight behaviour (latency 705 ± 163 ms, mean ± s.e.m.; median = 549 ms; n = 9 flights in 10 trials), reaching movement speeds similar to those evoked by loom stimuli (Fig. 2.4k). The latency to flight is longer than those evoked by loom stimuli (218 ± 16 ms, median = 199 ms; n = 41/47), and pattern of movements around flight onset was quite different: fast sweeps were associated with a brief reduction in movement speed before flight commenced, but looms were not (Fig. 2.4k; Movie 2.2).

Does freezing behaviour impede subsequent flight, and thereby account for the different flight latencies for loom and fast-sweep stimuli? To assess this we presented the sweep stimulus and then the loom stimulus in succession (Fig. 2.5a), using new cohorts of mice. Using the trials where mice remained in the arena until the onset of the loom stimulus (65/82 trials), we were able to estimate the effect of a preceding sweep stimulus on probability and latency to flight. The probability of flight to the looming stimulus (53/65 trials, 81.5%; Fig. 2.5b,c) was similar to that in absence of a preceding sweep stimulus. Latency to flight after onset of loom stimulus was 250 ± 33 (median = 159 ms; n = 53), not significantly different to that observed in absence of a preceding sweep stimulus. This implies that engaging one motor action (freezing) does not interfere with activation of another (flight).

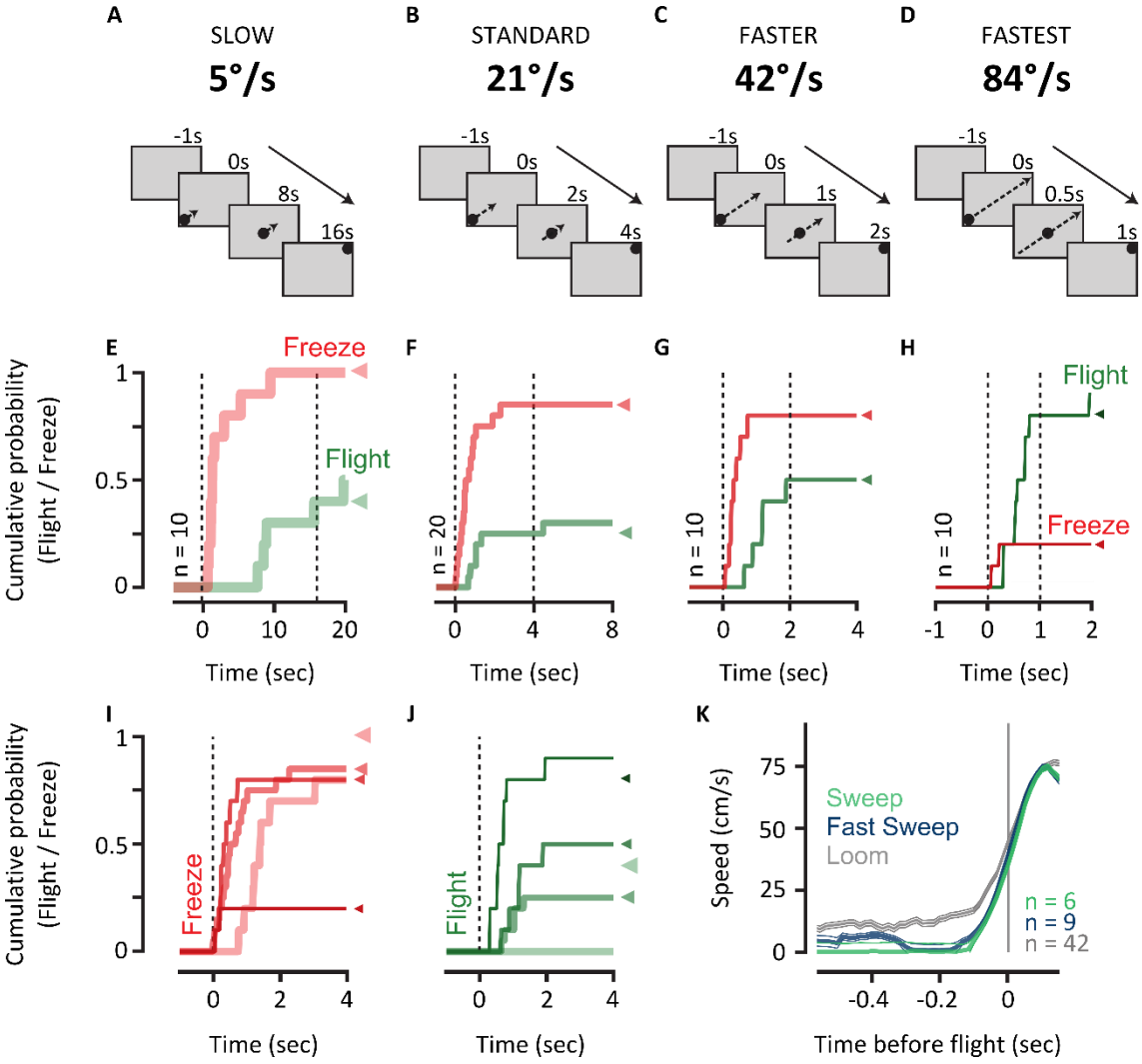

Figure 2.42. Dependence of freeze and flight behaviours on stimulus speed. ***A-D.*** Schematics of visual stimuli. The sweep stimulus was a 2.5 cm (5°) diameter black disk translating across the monitor at an angular speed of ca. 5 °/s for 16 s (*A*), 21 °/s for 4 s (*B*), 42 °/s for 2 s (*C*), or 84 °/s for 1 s (*D*). ***E-H.*** Cumulative probability of having observed a flight (green) or freeze (red) response during presentation of black sweep stimuli of varying speed. Vertical dashed lines indicate the start and end of the stimulus from the monitor. Triangles indicate probability at stimulus end. Duration of stimulus presentation depends on stimulus speed. ***I.*** Cumulative probability of observing a freeze response at each speed (5, 21, 42, and 84 °/s), over the first 4 s of stimulus presentation. Thickness of the line indicates stimulus speed, as in *E-H*, with thickest lines showing slowest speed. Triangles replotted from *E-H* show probability at stimulus end. Vertical dashed line indicates start of stimulus. ***J.*** Same as (*I*), but for flight response. ***K.*** Mean (±1 SEM) of movement speed around the time of flight responses during presentation of standard sweep (21 °/s, n = 6 flights from 20 trials), fast sweep (84 °/s, n = 9/10), or loom stimulus (n = 42/47). Speed traces were aligned to the time at which movement speed exceeded 20 cm/s of the speed at stimulus start (vertical line). See also Movie 2.2.

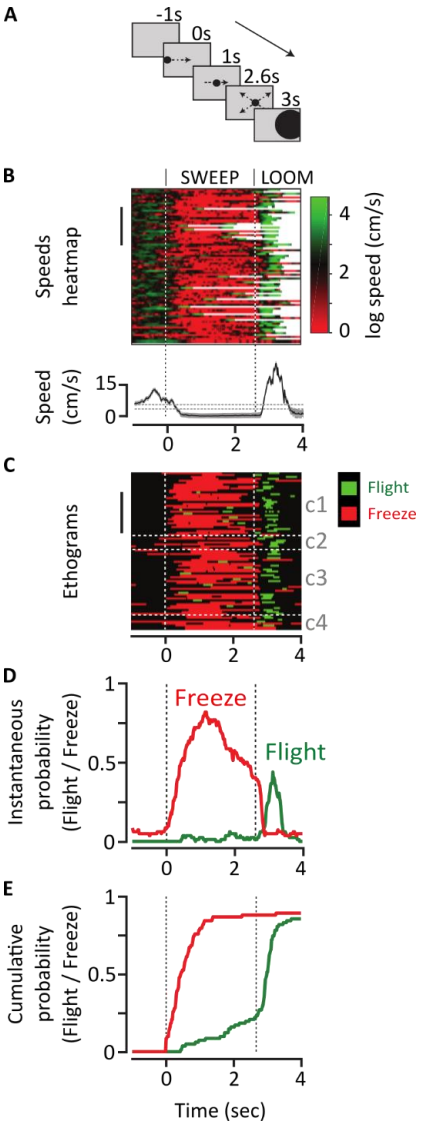

Figure 2.5. Behavioural responses to combinations of sweep and loom stimuli. ***A.*** Schematic of visual stimulus. The standard sweep stimulus (21 °/s) was presented for 2.6 s and was immediately followed by a loom stimulus. ***B.*** *Top:* images of the natural logarithm of movement speed in each trial (one trial per row). Red indicates low speed; green indicates high speed; black indicates speeds close to the mean across animals; and white indicates times when the animal was in the refuge. *Bottom:* mean (±1 SEM) movement speed of mice across trials. Horizontal dashed lines indicate mean ± 1 SEM of movement speed in absence of visual stimuli, as in Figure 2.2. ***C.*** Ethograms. Movement speed was used to classify flight and freeze behaviours as in Figure 2.2. The vertical line indicates onset of the sweep and of the loom stimuli. The horizontal lines subdivide different cohorts of animals (see Section 2.2.3). ***D.*** Instantaneous probability of freeze and flight. The probability of observing a flight (green) or a freeze (red) at each time point. The dotted lines indicate the onset of the sweep and of the loom stimuli. ***E.*** Cumulative probability of having observed a flight (green) or freeze (red) response over time. See also Movie 2.1.

2.3.3 Spatial learning in flight behaviour

When mice run, where do they run? To investigate this, I compared the target location of loom induced flights in the presence of one nest, two nests, or no nest. As is implicit above, when only one nest is present, most mice run to it (79/90 mice, 87.8%) (Fig. 2.2d). In previous work, presentation of a loom stimulus to mice in an open arena - in the absence of a place of refuge - elicited freeze behaviour (Wei et al., 2015). However, in those experiments mice would not be able to learn a location that might provide refuge, and the absence of flight behaviour might reflect the absence of any spatial representation (any 'place to go'). In 8 animals, I presented one loom stimulus per day for 6 days, always with a single nest present in the standard location. On the next day I removed the nest before placing the mouse in the arena, so that there was no place of refuge, and then presented the loom stimulus. All these animals (8/8, 100%) still showed flight-like behaviour in the absence of a nest - and ran towards the location where the nest used to be (Fig. 2.6). Analysis of flight latency showed that in the

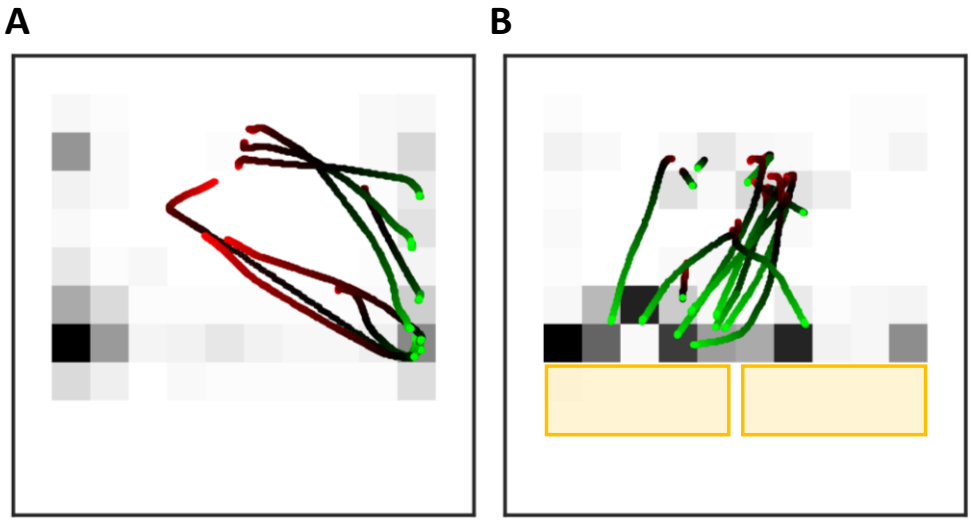

Figure 2.6. Spatial learning in flight behaviour. Background: average occupancy map of the arena across mice in the period preceding the loom stimulus. Black indicates highest occupancy rate, white the lowest occupancy rate. Traces: Each trace represents the path of one mouse in the 1 sec after the loom onset. Each path is red at the loom onset, and green either at 1 sec after the loom onset or when the animal enters a nest, whichever earlier. Yellow boxes indicate approximate position of the nests. **A.** Flight path in response to loom in the absence of a nest (n = 8). In previous loom presentations, the nest was positioned in bottom-right of the arena. **B.** Flight path in response to loom in the presence of two nests (n = 16). The original test is the one in bottom right of the arena, the new nest is in bottom-left.

absence of a refuge mice took longer to initiate flight behaviour (Fig. 2.7, 314 ± 98 ms, mean ± s.e.m.; median = 325 ms; n = 8). This suggests that the physical presence of a refuge might help mice to initiate and execute flight behaviour, but a spatial memory of its location is sufficient to guide orienting.

I therefore asked if flight destination (in the absence of a nest) reflected a place preference. To test this idea, I measured the preferred location in the arena (the occupancy rate) before the onset of the loom (Fig. 2.6) in each condition. As expected, when a nest was present, mice spent most of the time around it. When the nest was absent, however, mice showed no clear preference for its previous location. Thus, flight destination does not simply reflect a learned place preference.

When more than one potential refuge is available, a mouse must choose which to run to. The question that arises is, which refuge do they choose? Mice may seek refuge in the location they were most recently in, the closest refuge, or one that does not lie in the path of the potential predator. In 8 animals I presented one loom stimulus per day for 6 days, then tested their responses with no nest, and then added a second, identical refuge next to the one that was in the standard location. In this case, most mice flew towards the new nest (Fig. 2.6). They did not run to the closest nest, nor did they appear to take into account the location of the potential predator (which was always in the same central location). Analysis of flight latency showed faster initiation of flight behaviour (156 ± 65 ms, mean ± s.e.m.; median = 0.15 ms; n = 16).

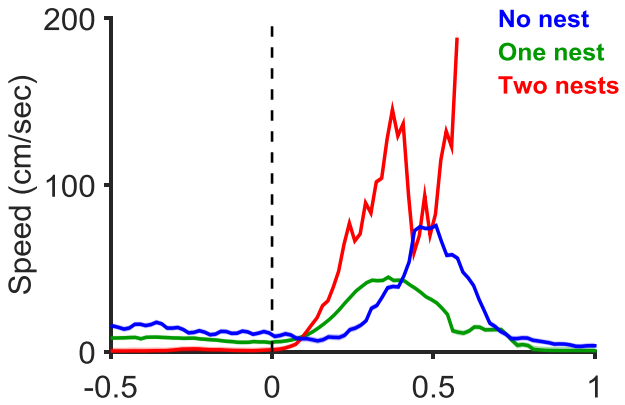

Figure 2.7. Dependence of flight latency on nest availability. Average speed across mice around onset of loom stimulus (dashed line) in absence of a nest (blue line, n = 8), and in presence of one (green, n = 95. Replotted from Fig. 2.2d) or two nests (red line, n = 16).

When the second nest was introduced in the environment, mice spent most of the time around the unfamiliar refuge (Fig. 2.6), consistent with a preference for novelty that has been extensively described in rodents (Wilz and Bolton, 1971; Bevins and Besheer, 2006; Ennaceur, 2010). This implies that mice developed and memorized a spatial representation of the arena. When a loom was presented, mice mainly ran towards this novel refuge, suggesting that flight behaviour is flexible and depends on the environmental context.

2.4 DISCUSSION

Our results reveal that mice naturally select between possible defensive behaviours based on vision alone. To our knowledge this is the first evidence that variation in a single sensory modality is sufficient to select between opposing freeze and flight behaviours, and a clear demonstration of the utility of vision for mice. Previous attempts to influence the choice of freeze and flight behaviours (Blanchard, 1997; Eilam, 2005) have had to rely on presenting real predators (Blanchard, 1997), which inherently produce multisensory cues, or changing the availability of refuge (Wei et al., 2015).

The different defensive behaviours might be mediated by distinct visual pathways. Specialised circuits for loom-induced flight emerge early in visual processing in many species (King et al., 1999; Gabbiani et al., 2002; Oliva et al., 2007; Card and Dickinson, 2008; de Vries and Clandinin, 2012), potentially as early as the retina (Yilmaz and Meister, 2013). A key region involved in defensive responses to visual stimuli is likely to be the superior colliculus (SC) (Dean and Redgrave, 1984; Sahibzada et al., 1986; Dean et al., 1989; Comoli et al., 2012; Savage et al., 2017). A looming visual stimulus will activate most visual receptive fields and many neurons in the SC are activated by loom stimuli. There is some evidence, including in humans, that looming stimuli may be particularly effective, though how this selectivity may arise is not clear (Westby et al., 1990; Billington et al., 2011; Liu et al., 2011; Zhao et al., 2014). Recent work shows that a subpopulation of parvalbumin positive, glutamatergic neurons in the superficial SC is responsive to looming visual stimuli, although the stimulus selectivity of these neurons was not studied in detail. Activation of these neurons is sufficient to trigger flight responses (Shang et al., 2015). The sweep induced behaviours that I observe might also be mediated by specialised subcortical

pathways. For example, recent work shows a class of neurons in the mouse superior colliculus ('widefield cells'), which respond to small moving stimuli over a large region of the visual field (Gale and Murphy, 2014). Activation of a subset of glutamatergic neurons in the SC can induce freezing behaviour (Wei et al., 2015), though their stimulus selectivity is not clear.

It is well known that electrical stimulation of the medial portion of rat SC triggers defensive behaviours including freeze and flight, and that the behaviour depends on the strength of stimulation (Brandao et al., 1994). Similarly, pharmacological disinhibition of the SC has been shown to elicit dose-dependent defensive behaviours (in primates as well as rodents), ranging from cowering, vocalization, escape behaviours and attack (DesJardin et al., 2013). These observations suggest a role of SC in defence responses that is conserved among mammals. Cortical contributions to defensive behaviours are also likely, as visual cortical projections to superior colliculus in mouse both modulate visual responsiveness (Zhao et al., 2014) and help drive temporary arrest behaviours (Liang et al., 2015).

Flight behaviour can be rapid and reproducible following loom stimuli. However, our observations and those of others (Ellard, 1996; Vale et al., 2017) suggest that flight is not a simple reflex. First, animals run directly to refuge, even when that flight requires turning (Fig. 2.6). Second, flight is less likely when the refuge is unavailable in naïve mice (Wei et al., 2015). This response flexibility is inconsistent with the usual idea of a reflex as a set of consistent motor responses to an adequate stimulus. Third, I observed flight responses to sweep stimuli of variable latency (Fig. 2.2e,h), and latency to loom-induced flight increased in absence of a nest and decreased in the presence of two nests (Fig. 2.7). If flight were a simple reflex, latency should be fixed and independent of context.

The loom stimulus emulates an approaching predator, which represents an imminent threat. On the other hand, the sweep stimulus emulates a predator scouting for preys, which represents a potential danger. The different behaviours I observe (flight, and freeze) are consistent with Predator Imminence Theory (Fanselow, 1994; Eilam, 2005), which hypothesises that the selection of the appropriate defensive response is influenced by the relative distance between the prey and the predator. As the predator moves closer, preys switch strategy from arousal, to freezing, to flight, and finally to fight. I found that flight behaviour can be initiated even whilst

freezing during presentation of a sweep stimulus. In the framework of the Predator Imminence Theory the switch in strategy may reflect assessment that the potential predator was getting closer, and suggests that during freezing behaviour mice are engaged in sustained assessment of their defence strategies, allowing deliberation and selection of an optimal strategy.

Which defensive behaviour is chosen depends on refuge availability (Yilmaz and Meister, 2013; Wei et al., 2015) - in mice that have not been able to learn a place of refuge, a looming stimulus over an open field induces freezing (Wei et al., 2015). I demonstrate that when a refuge is unavailable the choice between freeze and flight also depends on previous experience: mice exposed to looms in the presence of a nest still display flight towards the former nest location after its removal. Recent work has made similar observations (Vale et al., 2017), and suggests that mice retain a spatial representation of safety in the arena, developed during preceding trials in which a nest was present.

After introducing a new nest in the arena, mice preferably stayed around the new rather than the old refuge. It is well established that mice and other rodents explore novel objects for longer periods than familiar ones, a behaviour thought to reflect the development of memory representations (Bevins and Besheer, 2006; Ennaceur, 2010). I found that loom usually induced flight to the new shelter location, indicating a dynamic adjustment of defence strategies apt to cope with a changing spatial environment. Similarly, recent work shows that the remembered location of refuge can be rapidly updated (Vale et al., 2017). The reason for the high likelihood of flight towards the new nest could be at least twofold. In one scenario, when multiple safe places are available, mice prefer to run to the one they have recently visited the most. Alternatively, the spatial map of the environment might encode safety. In such a framework, the novel nature of the new nest might have increased its value in the spatial safety map.

In summary, I have shown that by taking into account the distance of the predator, its trajectory and velocity, as well as the availability of refuge and its location (Ydenberg and Dill, 1986; Cooper, 1997; Stankowich and Blumstein, 2005; Oliva et al., 2007; Hemmi and Tomsic, 2012), the engagement of defensive behaviours is more nuanced and dynamic than previously thought, and is not easily described as a reflexive response. Our observations also demonstrate a simple way to drive opposing avoidance behaviours through easily controlled visual stimuli.

Combined with the availability of genetic tools in mice, this new framework may help better understand how this selection is made, as well as the visual processing (Huberman and Niell, 2011) and sensorimotor integration that supports these decisions.

Chapter 3

Functional properties of visual neurons in superior colliculus of mouse

3.1 INTRODUCTION

The superior colliculus is a midbrain structure thought important for the detection of visual stimuli and for orienting behaviours towards or away from them. The superficial layers, namely stratum zonale (SZ), stratum griseum intermediale (SGS) and stratum opticum (SO), receive visual information from the retina and the cortex and are retinotopically organized - in mouse, 85-90% of the retinal projections are sent to the superior colliculus (Ellis et al., 2016). Despite being the most important visual area in this species, and a prominent model in developmental work (Huberman et al., 2008a; Cang and Feldheim, 2013), most functional investigations of visual processing in mouse have concentrated on the dorsal lateral geniculate nucleus (LGN) of the thalamus (Piscopo et al., 2013; Durand et al., 2016; Tang et al., 2016), and its major target, the primary visual cortex (Gao et al., 2010; Niell and Stryker, 2010; Andermann et al., 2011; Ayaz et al., 2013; Vaiceliunaite et al., 2013; Durand et al., 2016).

Previous work, primarily in anesthetized animals, has shown that visual neurons in SC of mouse generally prefer small stimuli, have spatially overlapping ON and OFF subfields, and show

non-linear responses (Drager and Hubel, 1975; Wang et al., 2010; Gale and Murphy, 2014; Ito et al., 2017). Almost half of the population is sensitive to orientation or direction of movement, with selectivity most pronounced in the uppermost layers and probably inherited from the retina (Wang et al., 2010; Gale and Murphy, 2014; Feinberg and Meister, 2015; Inayat et al., 2015; Durand et al., 2016; Ito et al., 2017; Shi et al., 2017). While recent work has moved towards understanding specific visual computations that might be performed in the SC (eg. detection of looming stimuli: Zhao et al., 2014), we lack basic knowledge of visual properties in the mouse superior colliculus, especially in awake animals. In LGN, lateral posterior nucleus of the thalamus and primary visual cortex, anaesthesia reduces the responsivity of neurons and makes their responses more sluggish (Vaiceliunaite et al., 2013; Durand et al., 2016). It is not clear if anaesthesia has similar impact on the visual pathways through SC.

Here, I made extracellular recordings from single-units in the superficial SC in both anesthetized and awake mice. I provide a description of visual properties that allows a direct comparison with other visual areas and between awake and anesthetized brain states. This survey will assist future studies aimed at understanding the development of the visual system and the functional role of the superior colliculus during visual processing *per se* and in the context of visually-guided behaviours.

3.2 METHODS

All procedures were conducted in accordance with the UK Animals Scientific Procedures Act (1986). Experiments were performed at University College London under personal and project licenses released by the Home Office following appropriate ethics review.

3.2.1 Preparation

Recordings from anesthetized animals. Recordings were obtained from 21 adult C57BL/6 mice (Charles River Laboratories). Initial anaesthesia was induced through an induction chamber, with 3% Isoflurane in O_2. Surgical anaesthesia was induced by intraperitoneal injection of a mixture of 80 mg/kg ketamine and 6 mg/kg xylazine in 0.9% NaCl saline solution. Post-surgical anaesthesia was maintained by a first intraperitoneal injection of 0.1-0.2 ml of 10% w/v

urethane in saline solution, and topped up with 0.05-0.15ml injections as needed. Depth of anaesthesia was monitored by breathing rate and absence of pinch-withdrawal reflex, and body temperature was maintained near 37°C via heating blanket. During surgery lubricant ophthalmic ointment (Refresh Lacri-Lube) was applied on both eyes. The cortical surface was exposed through a craniotomy (8-10 mm^2) performed over the right hemisphere and the brain was protected from dehydration by a layer of agarose (2% in 0.9% NaCl saline solution).

Extracellular recordings were made using quartz/platinum-tungsten single electrodes (impedance 4-5 MΩ, Thomas Recordings, Giessen, Germany) or tetrodes (impedance 0.5-0.8 MΩ, Thomas Recordings), lowered into the brain using a micromanipulator (Thomas Recordings Minimatrix). The analogue signal was amplified and filtered (0.3-10 kHz; Thomas Recordings), digitised (MoTU 828mkII, MOTU, Cambridge, USA) and acquired at 22.05 or 44.1 kHz using Expo/OpenGL (P. Lennie, Rochester, NY) on a Power Mac G5 computer. Single-unit activity was initially identified on-line by principal component analysis of amplified voltage signals to guide subsequent visual stimulation.

Electrodes were vertically inserted through the cortex 3.6 mm posterior to bregma, and 1.1 mm lateral from the midline suture. If additional penetrations were made in the same animal, the electrode was inserted at a distance of 100-300 µm from the previous recording site. The electrode was slowly advanced through the cortex for 800 µm, and the SC surface (located at about 1.3 mm in depth) was functionally identified by the characteristic multi-unit response modulation locked to the 3-4 Hz modulation frequency of large and uniformly flickering achromatic stimulus. The typical duration of a recording session was 4-6 hours. At the end of the experiment, animals were euthanized by sodium pentobarbital overdose (Pentoject, Animalcare) and death was confirmed by cervical dislocation.

Acute recordings from awake animals. Recordings were obtained from 6 adult C57BL/6 mice (Charles River Laboratories). Initial anaesthesia was induced through an induction chamber with 3% Isoflurane in O_2, and a preoperative analgesic was injected subcutaneously (Carprieve, Norbrook, 5 mg/kg). Surgical anaesthesia was maintained with 1-1.5% isoflurane in O_2. Depth of anaesthesia was monitored by breathing rate and absence of pinch-withdrawal reflex, and body temperature was maintained near 37°C via heating blanket. During surgery lubricant ophthalmic

ointment (Refresh Lacri-Lube) was applied on both eyes.

The cortical surface was exposed through a craniotomy (8-10 mm^2) performed over the superior colliculus in left hemisphere (3.5-3.7 mm posterior to bregma, 0.7-1.1 mm lateral from the midline suture) and the brain was covered with a layer of Kwik-Cast Sealant (WPI). A ground screw was implanted ~1mm anterior to bregma and lateral from the midline suture, in the hemisphere opposite to the craniotomy, and a custom-built metal head post was fixed on the skull using dental cement (Super-Bond C&B, Sun Medical). Animals recovered from surgery for at least one week, and were habituated to head-fixation (1 session per day, 5 minutes duration on the first day and then progressively increased). Once the animal was habituated to spending at least 75 min in head-restraint (6-12 sessions of habituation), recording commenced (one recording session per day for 4-10 days). During recording sessions, Kwik-Cast Sealant was removed to expose the cortical surface and replaced with artificial cerebrospinal fluid (Bio-techne Ltd, UK). At the end of each session the artificial cerebrospinal fluid was removed, the craniotomy covered with Kwik-Cast Sealant (WPI) and the animal was returned to its home cage.

Extracellular recordings were made using quartz/platinum-tungsten single electrodes (impedance 4-5 MΩ, Thomas Recordings) or tetrodes (impedance 0.5-0.8 MΩ, Thomas Recordings) as described above. Typical duration of a recording session was 90-120 minutes. In a subset of animals, after the last recording we coated the electrode with Vybrant® DiI cell-labeling solution (Invitrogen, Oregon, USA), a lipophilic membrane stain that diffuses laterally to stain the cells, weakly fluorescent until incorporated into membranes. At the end of the experiments, animals were transcardially perfused for histological reconstruction (see below. Fig. 3.1).

Chronic recordings from awake animals. Recordings were obtained from 2 adult C57BL/6 mice (Charles River Laboratories). Initial anaesthesia was induced through an induction chamber with 3% Isoflurane in O_2, and preoperative analgesic was injected subcutaneously (Carprieve, 5 mg/kg). Surgical anaesthesia was maintained with 1-1.5% Isoflurane in O_2. Depth of anaesthesia was monitored by breathing rate and absence of pinch-withdrawal reflex, and body temperature

was maintained at 37°C via heating blanket. During surgery lubricant ophthalmic ointment (Refresh Lacri-Lube) was applied on both eyes to prevent dehydration.

The cortical surface was exposed through a craniotomy (8-10 mm^2) performed over the superior colliculus in left hemisphere (3.6 mm posterior to bregma, 0.8 mm lateral from the midline suture). A ground screw was implanted ca. 1mm anterior to bregma and lateral from the midline suture, in the hemisphere opposite to the craniotomy, and a custom-built metal head post was also implanted. After removal of the *dura mater*, a custom built 16-channel microdrive (Axona Ltd, UK) was implanted so that electrodes were at a depth of ca. 700 µm. Each drive consisted four tetrodes, each formed by four 12.5 µm diameter tungsten wires (impedance 0.15-0.6 MΩ). The analogue signal was amplified and filtered (0.36-7 kHz), digitised and acquired at 48 kHz (dacqUSB; Axona Ltd, UK). One channel on each tetrode was also used to acquire the local field potential (0-500 Hz; sampling rate 1 kHz).

Animals recovered from surgery for at least one week. They were then habituated to the head-restraint (1 session per day, 8-12 sessions, 5 minutes long during the first day and then progressively prolonged). Tetrodes were then lowered slowly over several days, until characteristic multi-unit response modulation locked to a large and flickering uniform achromatic stimulus was found. The coarse location of the receptive fields was first manually identified and subsequently refined by recording the responses to black and white small squares flashed at a grid of positions over the monitor (see below for further details about receptive field analysis). Typical duration of a recording session was 90-120 minutes. Tetrodes were lowered ~65µm per session until visual responses could not be detected any more. After the last recording, animals were transcardially perfused for histological reconstruction (see below).

Eye movements. During recording in awake animals, I continuously imaged eye movements using an infrared camera (DMK 22BUC03, ImagingSource; 30 Hz) and a zoom lens (M3514-MP, Computar). Camera images were acquired in Matlab, and aligned to the visual stimulus presentation via the output of a photodiode that monitored a small corner of the stimulus monitor that was not visible to the animal. Eye position was estimated on-line using custom Matlab software to track the pupil as the centre of a fitted ellipse. For subsequent analysis I calculated the average pupil position over each stimulus trial as the average of the tracked

positions during the stimulus presentation. I removed blinks by calculating the area of the fitted ellipse and removing any points that exceeded a threshold of choice (3 standard deviations above the median). The removed values were replaced using nearest neighbour interpolation. Removal of trials in which a blink was present did not result in considerable changes of the responses, and did not change any of the results reported here. The angular eye movements were calculated as:

$$\theta_x = \frac{180}{\pi \times \arcsin(dx \times \frac{C_{res}}{r})} \quad \textit{(Eq. 3.1)}$$

$$\theta_y = \frac{180}{\pi \times \arcsin(dy \times \frac{C_{res}}{r})} \quad \textit{(Eq. 3.2)}$$

where θ_x and θ_y are the angular eye movements in azimuth and elevation, *r* is the radius of the mouse eye (1.25 mm, Sakatani and Isa, 2004), C_{res} is the camera resolution in mm/pixel and *dx, dy* reflect the difference between the tracked pupil center and the average pupil center across all the pupil positions recorded during the presentation of a stimulus set.

Histology. At the end of the experiment, animals were transcardially perfused with phosphate-buffered saline (PBS) 0.1 M followed by 4% paraformaldehyde. The brain was removed from the skull and kept in 4% paraformaldehyde for 24h at 4°C, followed by immersion in cryoprotective solution (15% w/v sucrose in PBS 0.1 M, then 30% w/v sucrose in PBS 0.1 M) for at least 48h each at 4 °C. Finally, the brain was sectioned in 30-50 µm thick coronal slices in a cryostat (Leica, CM1850 UV). In case of chronic implants, the slices were Nissl stained and photographed using bright-field settings (Leica, DMi8). In case of DiI electrode coating, slices were stained with DAPI (Fig. 3.1).

Spike sorting. For analyses, single-units were identified off-line using Plexon Offline Sorter software (Version 3.3.2) or KlustaSuite (Rossant et al., 2016). Single-units were identified by manual inspection of spike shape, auto- and cross-correlograms and clustering in the principal component analysis (PCA) space. To check for isolation quality, I calculated the proportion of inter-spike interval (ISI) violations for each cell, in response to stimuli of varying spatial

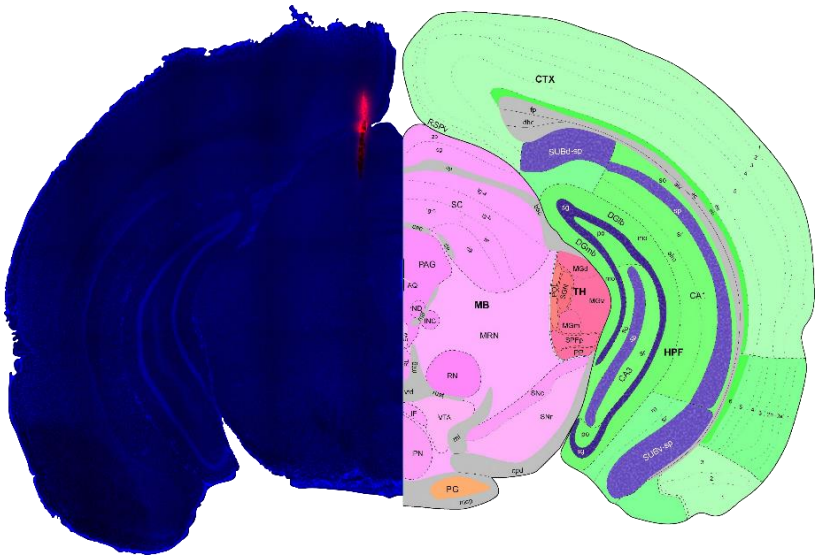

Figure 3.1. Example recording site. DAPI-stained coronal section at bregma -3.38 mm. On the left, the red trace shows the track left by a DiI coated electrode, inserted in the brain immediately after conclusion of the last acute recording in an awake mouse, and positioned as close as possible to the site of the last recording. On the right is shown the relative section from the Allen Brain Atlas.

frequency. I first classified as violations ISIs < 0.5 ms, and found that none of the isolated single units exceeded a threshold of 2% ISI violations on the total ISIs. When violations were classified as ISIs < 1 ms, the threshold of 2% ISI violations was reached by 14/227 (6.2%) neurons in awake animals, and 21/97 (21.7%) in anesthetized animals. Given the high proportion of neurons displaying more than 2% of ISI violations in anesthetized animals, I investigated their response linearity (see below for details. Section 3.2.3, *Linearity of spatial summation in response to drifting gratings*). Given that multiunit activity pools responses from multiple neurons, it is unlikely to display linear responses. Most of the neurons with more than 2% ISI violations (16/21, 76.2%) had an F1/F0 ratio >1, ergo linear responses. It is therefore unlikely that those neurons were multi-units. Exclusion of the putative multi-units did not change the major results, and I have therefore retained these units in my analyses.

3.2.2 Visual stimuli

Visual stimuli were generated using Expo (P. Lennie, Rochester, NY) and presented on a calibrated LCD monitor (Anesthetized animals: Asus, 48 cm x 27 cm, mean luminance 30–40 candela/m^2, refresh rate 60 Hz; Awake animals: Iyama ProLite EE1890SD, mean luminance 35-

45 candela/m^2, refresh rate 60 Hz) displaying a mean grey screen, positioned 20 cm away from the animals' eye. The monitors were gamma-corrected by measuring separately the luminance of the red, green and blue elements for an uncalibrated screen with a photometer (Konica Minolta, Chroma meter CS-100A), and calculating for each the best-fitting exponential. The inverse of measured exponent was then used to correct the output of the video card for the relevant element, and linearization confirmed. I first hand-mapped the receptive field position and adjusted the monitor location to centre the receptive field on the monitor using a flexible arm. Tilt was applied as appropriate to keep the monitor approximately normal to the eye. In those cases where the receptive field location was difficult to determine, I positioned the stimuli where I had maximal activity in response to small flashing squares (see below). Unless specified, stimuli lasted for 2 s with an interstimulus interval of 0.5 s and were of the maximal contrast I could present. Each set of stimuli included a blank condition (during which the screen was held at the mean luminance) from which spontaneous firing rates were estimated. Each set of stimuli was presented in pseudorandom order for 4-10 repetitions.

Sparse noise. Uniformly black or white squares flashed sequentially for 0.2 s in pseudorandom sequence over a 9x9 grid. I used either 10° squares with 5° spacing (spanning 50°x50° of visual space, for all experiments in anesthetized animals and a subset of awake animals) or 15° squares with 7.5° spacing (spanning 75°x75° of visual space, for all experiments in awake animals). For a subset of cells recorded in awake animals I compared receptive field

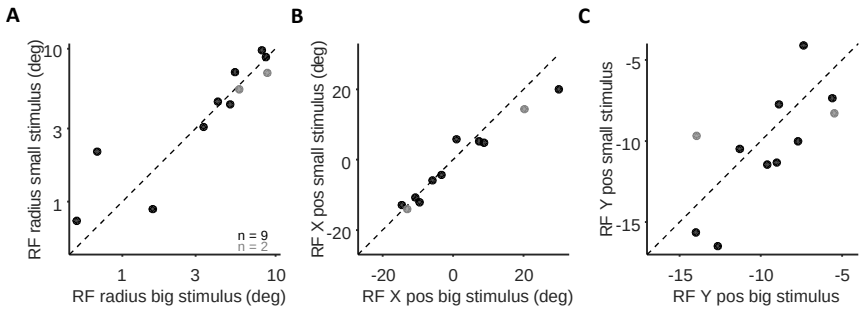

Figure 3.2. Neurons respond similarly to sparse noise using small and big stimuli. Comparison between estimates of receptive field radius (*A*), horizontal position (*B*) and vertical position (*C*) for single cells in which we measured responses to both flashing squares of 15° (x-axis) and 7.5° (y-axis). Black and grey points indicate black (n = 9) and white (n = 2) stimuli, respectively. Radius and position were estimated from a two-dimensional Gaussian fit of the response. I considered only neurons in which the fit explained at least 60% of the variance in the data. See also Fig. 3.4a.

estimates using both stimuli, and found similar results (Fig. 3.2, but see also Section 3.2.3, *Receptive field position and size from sparse noise*, and Fig. 3.4a).

Size tuning for uniform fields. Uniform black or white circular patches, diameter 2° to 90° in logarithmic steps, were flashed for 0.5 s with an interstimulus interval of 0.5 s.

Counterphase gratings. Large circular patches (diameter 80°-90°) of contrast-reversing sinusoidal gratings near the preferred spatial frequency and orientation of target units, counterphasing at 1 to 5 Hz. Responses were measured at each of 8 spatial phases (22.5° steps).

Drifting gratings. Large circular patches of drifting sinusoidal grating (diameter 80°-90°) varying in contrast, orientation/direction, spatial frequency or temporal frequency. When a large grating so strongly reduced the activity that response was not measurable, I decreased the size of the stimulus to be the largest size from which a clear response could be obtained. I measured contrast sensitivity using gratings of 4-6 contrasts (0.25, 0.5, 0.75, 1 or 0.17, 0.33, 0.5, 0.67, 0.83, 1). I measured direction and orientation selectivity using gratings of 12 different directions (30° steps). I measured spatial frequency tuning using gratings of 7 or 12 spatial frequencies (0, 0.005, 0.0085, 0.0144, 0.0245, 0.0416, 0.0707, 0.1201, 0.2040, 0.3466, 0.5887, 1 or 0, 0.0094, 0.0187, 0.0375, 0.075, 0.15, 0.3 cyc/°). I measured temporal frequency tuning using gratings of 6 or 7 temporal frequencies (0.4688, 0.9375, 1.8751, 3.7502, 7.5, 15 or 0.5, 1, 2, 4, 7.5, 12, 15 cyc/sec). I measured speed tuning using a matrix of 7 spatial frequencies (0, 0.0094, 0.0187, 0.0375, 0.075, 0.15, 0.3 cyc/deg), and 6 temporal frequencies (0.4688, 0.9375, 1.8751, 3.7502, 7.5, 15 cyc/ sec), and each of the 2 directions at the vertical orientation.

3.2.3 Data analysis

All offline analysis was performed using Matlab (MathWorks, Natick, MA, USA). Peristimulus time histograms (PSTHs, bin width 0.01 s) were constructed for each trial (or across trials - see below) and subjected to Fourier analysis. I always extracted the mean firing rate (F0), and the modulation amplitude of response at the stimulus temporal frequency (first harmonic; F1); in some cases I also analyzed the response at the second harmonic (F2). Using the responses to

the grating stimulus of optimal spatial frequency obtained during the spatial frequency tuning experiments, cells were classified as 'non-linear' if the stimulus-evoked change in F0 exceeded the change in F1, and 'linear' otherwise (Skottun et al., 1991). For further analysis, I used the F0 response for non-linear cells and the F1 response for linear cells. When the spatial frequency tuning was not available, I used the F0 for all analyses. Unless stated, I refer to responses as stimulus evoked activity, which is the difference between the F0 or F1 measured for any given stimulus, and that measured during presentation of blank screen of the same duration (spontaneous firing rate). The optimal parameters for each model fitting were estimated using the Matlab function *lsqcurvefit*. Statistical tests are specified in the text. Unless stated, error bars indicate ± 1 S.E.M.

Response latency. Latency was calculated from responses to the sparse noise stimulus. For each cell, I measured latency for all positions in which the trial-averaged mean responses exceeded the mean maintained rate by at least 1 s.d. of that rate (anesthetized recordings) or 2 s.d. (awake recordings). For each position, action potentials were folded into a PSTH (bin width 0.01 s). I then extracted the first two consecutive bins in which the firing activity of the PSTH exceeded the mean maintained rate by at least 2.5 s.d. of that rate, and a linear regression was calculated from the first bin to the bin of the initial response peak. The regression line was back-extrapolated to the maintained rate, and latency was defined as the intersection time (Fig. 3.3) (Pietersen et al., 2014). Each latency extrapolation was manually checked. In cases where the automated procedure clearly failed, a regression line was manually drawn to fit the rising phase of the PSTH, and the latency was re-extrapolated as described above.

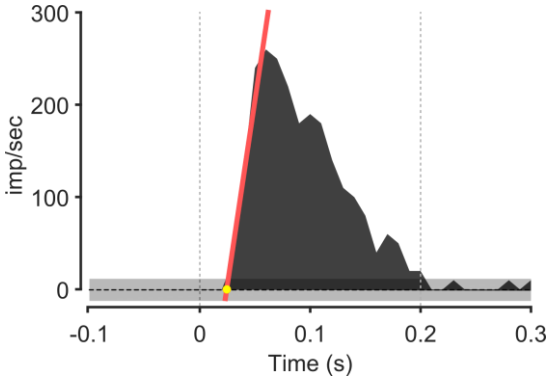

Figure 3.3. Response latency extrapolation. Representative example PSTH in response to a flashed square of the sparse noise stimulus. Dashed horizontal line indicates maintained discharge rate. Shaded grey area indicates maintained discharge rate ± 2.5 s.d. Vertical dashed lines indicate onset and offset of the stimulus. Red line depicts regression line fit. Yellow dot depicts extrapolated latency (0.0247 ms).

Receptive field position and size from sparse noise. The trial-averaged mean response to black (OFF) or white (ON) stimuli was fit with a two-dimensional Gaussian:

$$R(x,y) = K\pi r^2 e^{-(\pi r)^2} \qquad \textit{(Eq. 3.3)}$$

where *K* is the gain and *r* the size of the Gaussian. Because the stimulus size is larger than the grid spacing, I generated a receptive field for each combination of parameters at a resolution of 1 degree, and convolved these receptive fields with simulated visual stimuli rendered at the same spatial resolution. The result of the convolution was used as the estimated response of the receptive field for each stimulus. The fitting programme found the best predictions of the model by minimising the square error between the predictions and the observed responses. For cells in which the model fit explained at least 60% of the variance, I defined receptive field size of each subfield as the estimated *r*, from which the area was also calculated, and the position as the Gaussian centre (Fig. 3.4a).

Receptive field size from patches. The trial-averaged mean response to black (OFF) or white (ON) circular stimuli of varying size was fit with a two-dimensional difference-of-Gaussians model (Rodieck, 1965; Enroth-Cugell and Robson, 1966). I assumed that both the center and surround could be described by concentric and circular two-dimensional Gaussians. The activity of the centre (*Le*) to a patch of diameter *d* is proportional to the integrated volume of a Gaussian:

$$L_e(d) = \frac{2}{\sqrt{\pi}} \int_0^d e^{-(x/r_e)^2} dx \qquad \textit{(Eq. 3.4)}$$

where r_e is the width of the centre Gaussian. A similar expression can be derived for the larger surround (*Li*). I assume that the surround has subtractive influence on the activity of the centre such that response is:

$$R(d) = K_e L_e(d) - K_i L_i(d) \qquad \textit{(Eq. 3.5)}$$

where K_e and K_i are respectively the centre and surround gains. I estimated the preferred size from the model fit as the smallest size reaching 95% of the maximal response (Fig. 3.4b).

Spatial frequency tuning. I also characterised spatial frequency tuning-curves with a difference-of-Gaussians model (DOG) (Enroth-Cugell and Robson, 1966; Croner and Kaplan, 1995):

$$R(sf) = K_c \pi {r_c}^2 e^{-(\pi r_c sf)^2} - K_s \pi {r_s}^2 e^{-(\pi r_s sf)^2} \quad \textit{(Eq. 3.6)}$$

where s*f* is the spatial frequency, K_c and r_c are respectively gain and size of the center Gaussian, and K_s and r_s are the gain and the size for the surround Gaussian. The DOG model describes the center and the surround sensitivities as antagonistic Gaussians with size corresponding to the radius at which the Gaussians sensitivity has fallen to 1/*e* of the peak. I fit the spatial frequency tuning curves with Equation 3.6 with four free parameters: K_c, r_c, K_s and r_s. I constrained the parameters to be positive, and the surround size to be larger than the center (Fig. 3.4c). I calculated the spatial frequency resolution of each neurons as the characteristic frequency, fc = 1/π r_c.

Temporal frequency tuning. I characterised temporal frequency tuning curves with a difference-of-exponentials function (Derrington and Lennie, 1984):

$$R(tf) = S_1 e^{-k_1 tf} - S_2 e^{-k_2 tf} \quad \textit{(Eq. 3.7)}$$

where S_1 and S_2 are scale factors and K_1 and K_2 the time constants of the mechanisms (Fig. 3.4d).

Linearity of spatial summation in response to drifting gratings. When stimulated with a drifting sinusoidal grating of optimal spatial frequency, the activity of units showing nearly linear summation within receptive fields is strongly modulated at the temporal frequency of the stimulus (F1, amplitude of response at the stimulus first harmonic). In these cells, the amplitude of the F1 response is therefore larger than the F0. Non-linear cells instead respond with an increased average firing rate (F0) that is only weakly modulated. The amplitude of the F0 response is therefore larger than the F1. To classify the cells as linear or non-linear, I followed the procedure described in Skottun et al. (1991). I used the data obtained from spatial frequency tuning experiments to calculate the F1/F0 ratio at the preferred spatial frequency. Cells with a ratio smaller than 1 were classified as non-linear (or complex-like), while cells showing a ratio

larger than one were defined as linear (or simple-like). For plotting purposes I constrained F1/F0 ratios larger than 3 to be equal to 3.

Linearity of spatial summation in response to contrast-reversing gratings. In response to contrast-reversing gratings, non-linear cells show responses that are modulated at double the frequency of the stimulus (F2) at all phases (Hochstein and Shapley, 1976a). In contrast, the response of linear cells is modulated at the stimulus frequency (F1) and depends on spatial phase, displaying a marked decrease in response amplitude at the grating phase symmetrically stimulating the CRF ('null phase'). I calculated the mean F2 and the peak F1 across phases, and classified cells as linear if the F1 was larger than the F1 (F1/F2 ratio ≥1). Cells with F1/F2 ratio <1 were instead classified as non-linear.

Speed tuning. I characterised the tuning curves for speed by averaging the responses to combination of spatial- and temporal frequencies that produced similar speeds (Fig. 3.4e,f). I then quantified the degree of "speed tuning" by fitting a two-dimensional Gaussian in which the preferred temporal frequency could depend on the spatial frequency used for the stimulus (Priebe et al., 2003; Andermann et al., 2011; Gale and Murphy, 2014):

$$R\ (sf, tf) = A\ \times exp\left(\frac{-(log_2 sf\ -\ log_2 sf_{pref})^2}{2{\sigma_{sf}}^2}\right) \times\ exp\left(\frac{-(log_2 tf\ -\ log_2 tf_p(sf))^2}{2{\sigma_{tf}}^2}\right) \qquad \textit{(Eq. 3.8)}$$

where $R_{(sf,tf)}$ is the average response to each combination of spatial and temporal frequencies, A is the maximum response across stimuli, sf_{pref} is the preferred spatial frequency, tf_0 is the overall preferred temporal frequency, and $tf_p(sf)$ is the preferred temporal frequency at each spatial frequency. The degree of dependency of preferred temporal frequency on spatial frequency was captured by:

$$log_2 tf_p(sf) = \xi\ (log_2 sf\ -\ log_2 sf_0) +\ log_2 tf_0 \qquad \textit{(Eq. 3.9)}$$

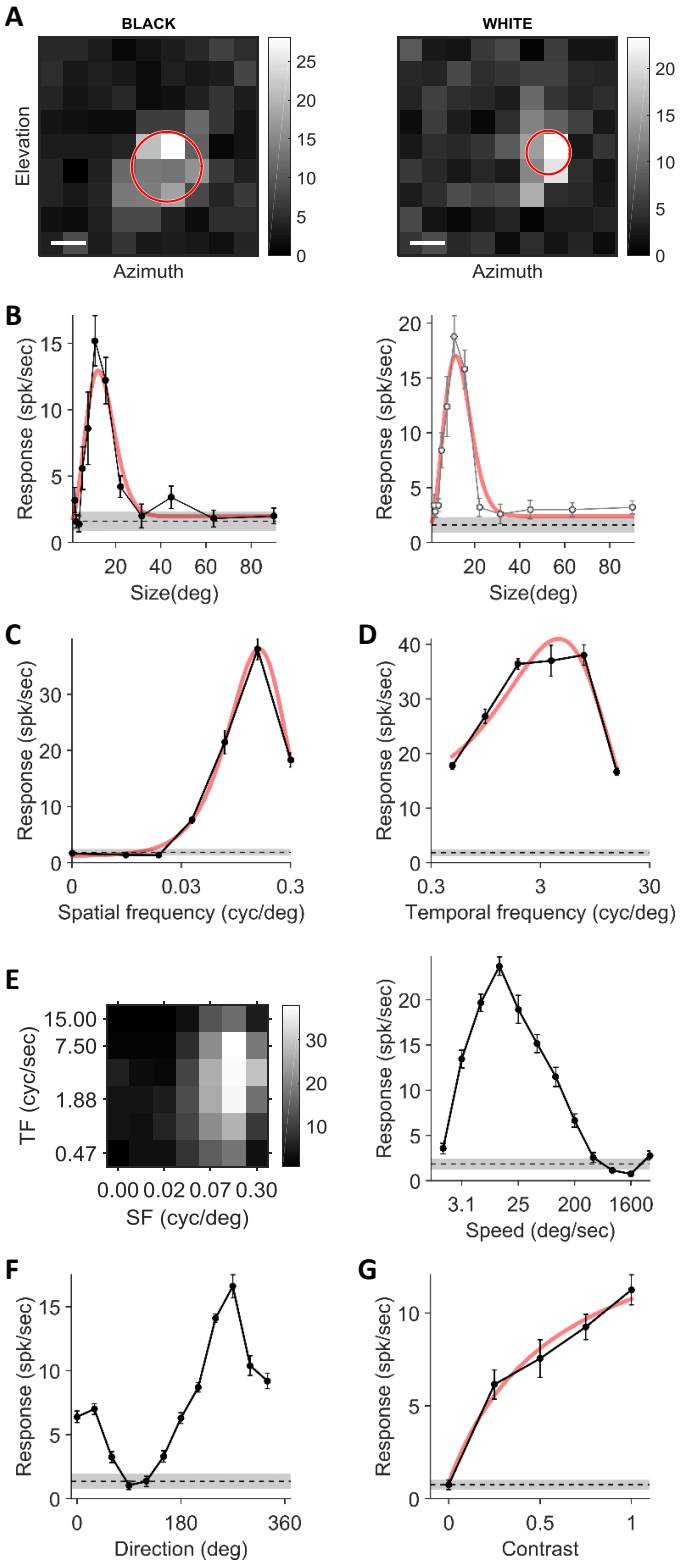
A
BLACK
WHITE
Elevation
Azimuth
Azimuth
B
Response (spk/sec)
Size(deg)
Response (spk/sec)
Size(deg)
C
Response (spk/sec)
Spatial frequency (cyc/deg)
D
Response (spk/sec)
Temporal frequency (cyc/deg)
E
TF (cyc/sec)
15.00
7.50
1.88
0.47
0.00 0.02 0.07 0.30
SF (cyc/deg)
Response (spk/sec)
3.1 25 200 1600
Speed (deg/sec)
F
Response (spk/sec)
Direction (deg)
G
Response (spk/sec)
Contrast

Figure 3.4. Responses to all tested visual stimuli for an example cell, mumc004_20160705Spk6. Dashed black lines and grey shaded areas indicate spontaneous activity ± s.e.m. ***A.*** Responses to sparse noise stimulus. Trial-averaged responses to each stimulus location for black (left) and white (right) flashed squares. The grey scale represents response magnitude (spk/sec). Red lines depict the two-dimensional Gaussian fit of the response. ***B***. Responses to patches increasing in size. *Left*: responses to black patches. *Right*: responses to white patches. ***C***. Responses to drifting gratings varying in spatial frequency. Red line depicts the difference-of-Gaussian fit of the response. ***D***. Responses to drifting gratings varying in temporal frequency. Red line depicts the difference-of-exponential fit of the response. ***E***. Responses to drifting gratings varying in spatial and temporal frequency. *Left.* Matrix of responses to different combinations of spatial and temporal frequencies. Grey scale represents response magnitude (spk/sec). *Right.* Speed tuning curve of responses to drifting gratings of different spatial and temporal frequency, derived from (*Left)* by averaging responses to combinations of spatial and temporal frequency of similar speeds. ***F***. Responses to drifting gratings varying in direction. ***G***. Responses to drifting gratings varying in contrast. Red lines depicts the Naka-Rushton function fit of the response.

where ξ, the speed tuning index, represents the relationship between the preferred temporal frequency at each stimulus spatial frequency (the function is linear with respect to log spatial frequency). The speed tuning index ξ is therefore 1 when preferred temporal frequency and stimulus spatial frequency are proportional, such that the neuron is selective for a particular speed rather than the spatial or temporal frequency components of the stimulus. I estimated the speed tuning index just for responses where the variance explained by the fit was ≥ 60%.

Direction and orientation tuning. I used two indices to quantify the direction and orientation selectivity - a direction/orientation selectivity index (DSI/OSI), and a global direction/orientation selectivity index (gDSI/gOSI). The global selectivity index (gDSI for direction and gOSI for orientation) is a better overall descriptor of selectivity (Mazurek et al., 2014). The selectivity indices (DSI/OSI) are used for comparison with previous studies (Wang et al., 2010; Inayat et al., 2015). The DSI is:

$$DSI = \frac{R_{pref} - R_{opp}}{R_{pref} + R_{opp}} \qquad \textit{(Eq. 3.10)}$$

where R_{pref} is the cell maximal response at the direction ϑ_{pref} and R_{opp} is the response at the direction opposite to preferred, $\theta_{pref} + \pi$. Similarly, the OSI is:

$$OSI = \frac{R'_{pref} - R_{orth}}{R'_{pref} + R_{orth}} \qquad \textit{(Eq. 3.11)}$$

where R'_{pref} is the mean of R_{pref} and R_{opp}, and R_{orth} is the mean response to the two directions orthogonal to θ_{pref}. I calculated gDSI as the vector sum of responses normalized by the scalar sum of responses:

$$gDSI = \frac{\sum R_\theta e^{i\theta}}{\sum R_\theta} \quad \textit{(Eq. 3.12)}$$

and the gOSI as:

$$gOSI = \frac{\sum R_\theta e^{i2\theta}}{\sum R_\theta} \quad \textit{(Eq. 3.13)}$$

where R_θ is the response to a grating of θ orientation. I defined the preferred direction or orientation as the angle of the vector sum of responses.

Contrast sensitivity. I characterised the contrast-response functions using a Naka-Rushton function:

$$R(C) = \frac{R_{max} \times C^p}{{C_{50}}^p + C^p} \quad \textit{(Eq. 3.14)}$$

where R is the neuronal response given a Michelson stimulus contrast (C), R_{max} is the saturating response amplitude, C_{50} is the contrast at half of the saturating response amplitude, and p is an exponent (Fig. 3.4g). I constrained the exponent to be between 1 and 4.

3.2.4 Inclusion criteria

I considered neurons visually responsive if their maximal response was at least 1.4 spk/sec, and exceeded the mean maintained rate by at least 1.25 s.d. of that rate (anesthetized recordings) or 1.5 s.d. (awake recordings). In awake animals, where I often recorded from multiple units simultaneously, I included additional selection criteria: in experiments using large gratings to test basic response properties (e.g. direction, spatial and temporal frequency, contrast) I required that the position of the estimated RF (obtained from the sparse noise stimulus) was within 30° of the stimulus centre.

3.3 RESULTS

I made extracellular recordings from a total of 471 neurons in the superficial layers of superior colliculus (sSC) in awake mice, and 109 neurons from these layers in anesthetized mice. Of these, 325 neurons in awake and 104 neurons in anesthetized mice were visually responsive (displayed significant response to at least one of the presented visual stimuli) and were included in the subsequent analysis (see also Methods, Section 3.2.3). Most neurons were recorded from the retinorecipient superficial layers of the SC: SZ, SGS and SO (Fig. 3.5a,b). The receptive fields of the neurons I recorded from spanned a large portion of visual space in both awake (Fig. 3.5c) and anesthetized (Fig. 3.5d) animals.

In the following, I first compare the spontaneous and evoked firing rates of neurons in the superficial SC in the awake and anesthetized state. I then describe responses to stimuli of

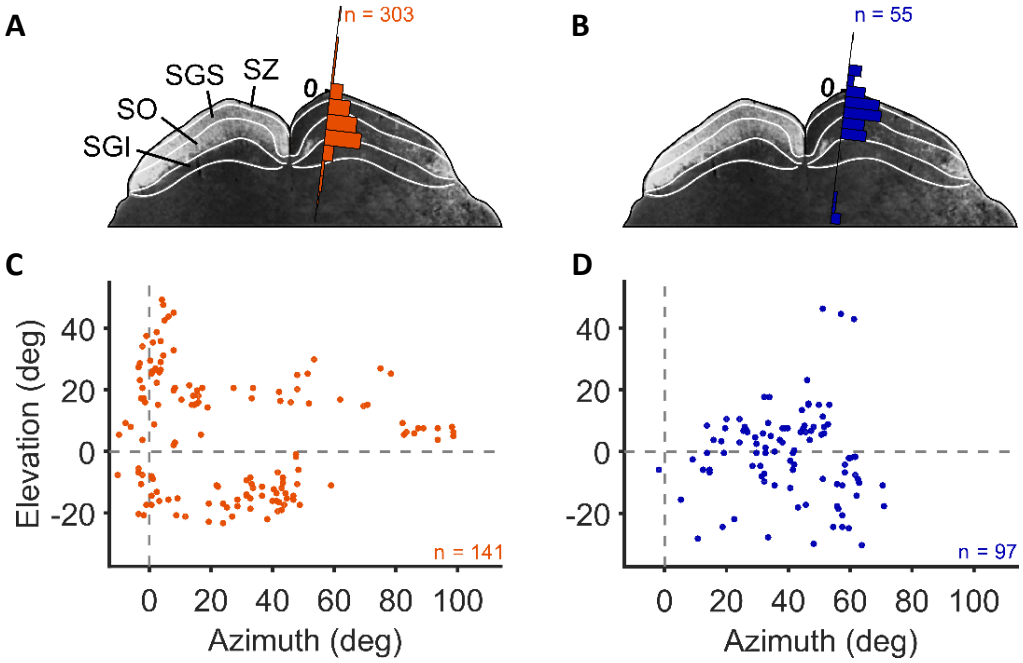

Figure 3.5. Collicular depth and receptive field position. ***A-B.*** Histograms of available estimated recording depths of neurons recorded in awake (*A,* n = 303) and anesthetized (*B,* n = 55) animals, with 0 indicating surface of the SC. Histograms have been appropriately scaled and overlaid to darkfield photomicrographs showing retinal innervation onto the superficial layers of the SC (modified from Morin and Studholme, 2014). ***C-D.*** Receptive field position of neurons estimated from sparse noise stimulus and adjusted for monitor position with respect to the eye in awake (*C*, n = 141) and anesthetized (D, *n = 97*) animals. Dashed lines indicate horizontal and vertical meridian. For graphic purposes, I randomly added a ±0-4° jitter to the receptive field positions.

different polarity, characterize spatial receptive field properties, and illustrate sensitivity to gratings of varying spatial frequency, temporal frequency, speed, direction, orientation and contrast.

I will show that neurons in mouse SC display highly sensitive, spatially confined RF, prefer black stimuli but respond to both black and white stimuli, have fast temporal integration, can encode direction and orientation of motion, and that anaesthesia mainly affects their sensitivity and temporal integration properties.

3.3.1 Spontaneous and evoked firing rates

Different brain areas as well as distinct neuronal subpopulations display characteristic firing rate patterns, that can also depend on brain state. I found that anaesthesia had pronounced effects on the spontaneous and evoked spiking activity of neurons in sSC. The average spontaneous firing rate was 0.8 imp/sec (s.d. 1.2) in anesthetized animals and 2.6 imp/sec (s.d. 4) in awake animals (Fig. 3.6a; $p < 10^{-7}$, Wilcoxon rank sum test). Evoked activity was also dependent on brain state: response to a large drifting sinusoidal grating of optimal spatial frequency was 12.7 imp/sec (s.d. 12.5) in anesthetized animals and 29.3 imp/sec (s.d. 34.4) in awake animals (Fig 3.6b; $p < 10^{-5}$, Wilcoxon rank sum test). Anaesthesia therefore reduces both the background and the evoked firing rate of SC neurons, and is likely to have a profound effect on the integration of visual information.

Figure 3.6. Firing rate properties in awake and anesthetized brain states. Orange: awake (AW). Blue: anesthetized (AN). ***A.*** Histogram of spontaneous firing rate of neurons in awake and anesthetized animals. Arrow heads indicate mean spontaneous firing rate (AW: 2.6 imp/sec; median 1 imp/sec; s.d. 4 imp/s. AN: 0.8 imp/sec; median 0.2 imp/sec; s.d. 1.2 imp/sec). ***B.*** Histogram of firing rate in response to a large drifting sinusoidal grating of optimal spatial frequency. Arrow heads indicate mean (AW: 29.3 imp/sec; median 18.8 imp/sec; s.d. 34.4 imp/s. AN: 12.7 imp/sec; median 8.6 imp/sec; s.d. 12.5 imp/sec). ***C.*** Average response latency to white (ON) or black (OFF) sparse noise stimulus in awake and anesthetized animals. Horizontal black bars indicate median (AW-ON: 45 ms, μ: 54 ms, s.d. 34 ms. AW-OFF: 45 ms, μ: 49 ms, s.d. 27 ms. AN-ON: 147 ms, μ: 147 ms, s.d. 27 ms. AN-OFF: 136 ms, μ: 134 ms, s.d. 22 ms.). ***D-E.*** Cumulative distribution of average response latencies shown in *C*. Solid line: latency of OFF responses. Dashed line: latency of ON responses. ***F-G.*** Population average PSTH in response to a black (coloured) or white (white) circular patch of optimal size in awake (*F*, n=46) and anesthetized (*G*, n=68) animals. Dashed lines indicate stimulus offset. ***H.*** Normalized versions of average PSTHs in response to black patches shown in *F-G*, and aligned to peak. Dashed lines indicate stimulus offset for awake (orange) and anesthetized (blue) animals.

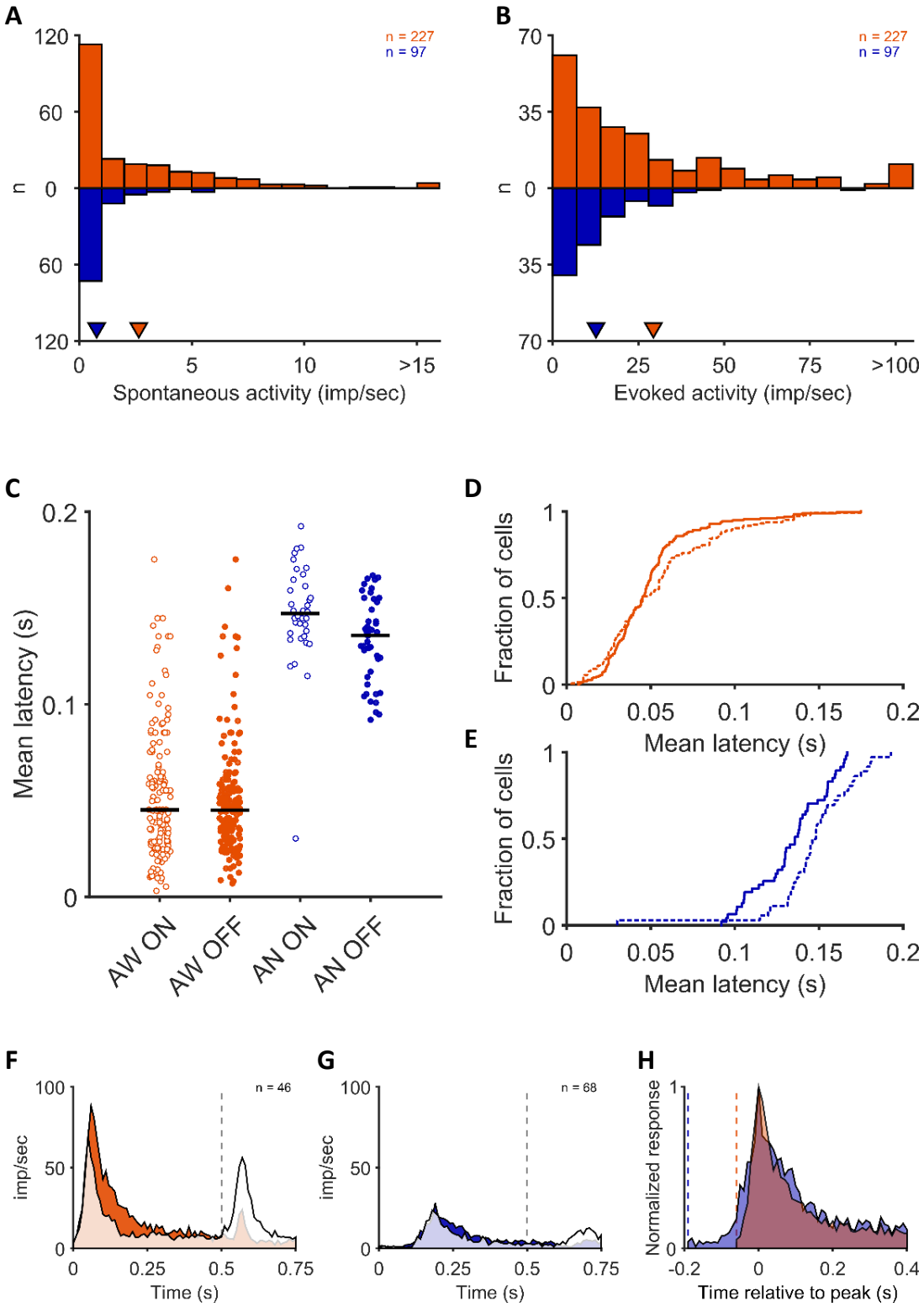
A
n = 227
n = 97
n
120
60
0
60
120
0
5
10
>15
Spontaneous activity (imp/sec)
B
n = 227
n = 97
n
70
35
0
35
70
0
25
50
75
>100
Evoked activity (imp/sec)
C
Mean latency (s)
0.2
0.1
0
AW ON
AW OFF
AN ON
AN OFF
D
Fraction of cells
1
0.5
0
0
0.05
0.1
0.15
0.2
Mean latency (s)
E
Fraction of cells
1
0.5
0
0
0.05
0.1
0.15
0.2
Mean latency (s)
F
n = 46
imp/sec
100
50
0
0
0.25
0.5
0.75
Time (s)
G
n = 68
imp/sec
100
50
0
0
0.25
0.5
0.75
Time (s)
H
Normalized response
1
0
-0.2
0
0.2
0.4
Time relative to peak (s)

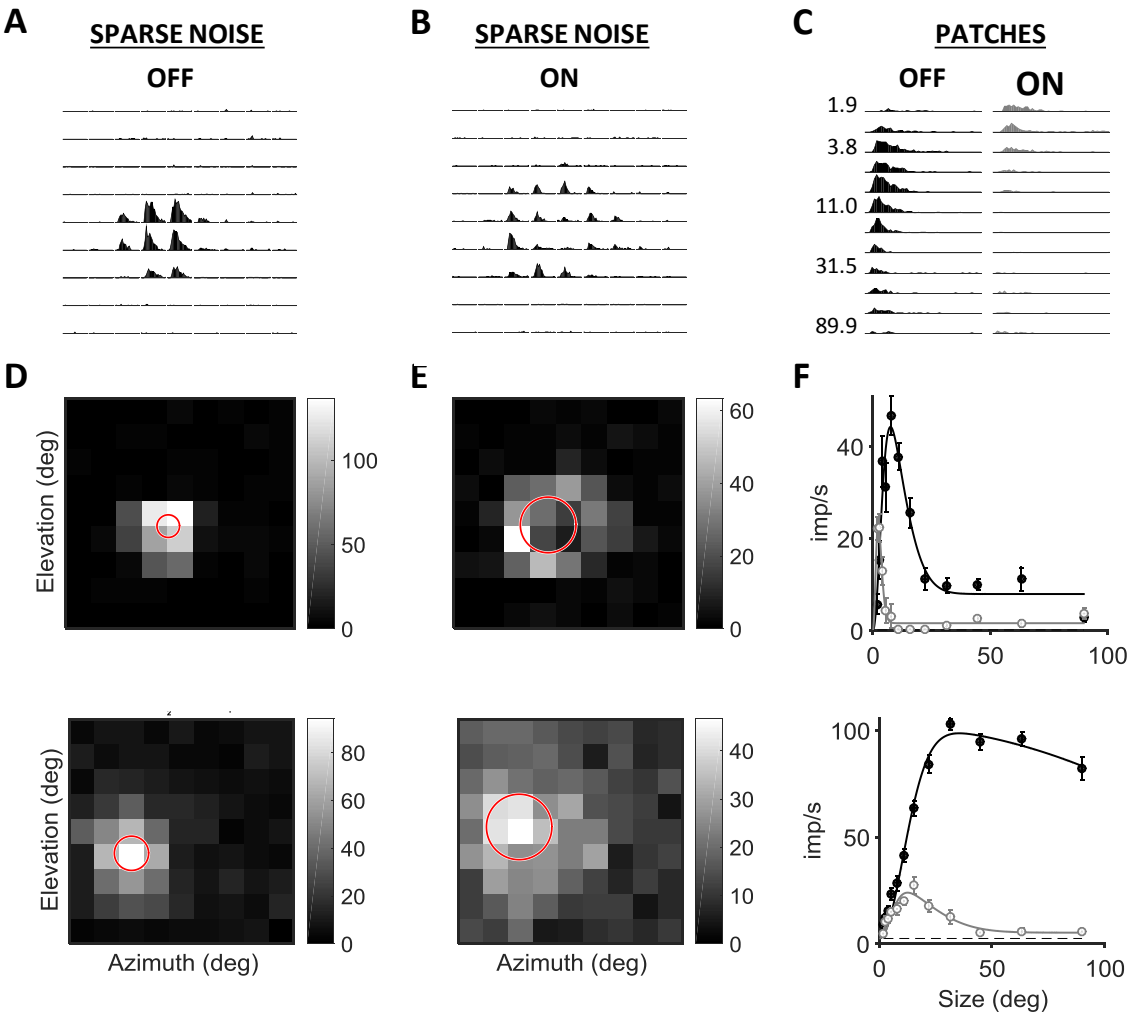

Figure 3.7. Example responses to small flashing squares and patches of different sizes. Each row shows example responses from the same neuron. *A* and *D* show responses to small black squares flashed in different locations. *B* and *E* show responses to small white squares flashed in different locations. *C* and *F* show responses to black (black histograms in *C* and black curves in *F*) and white (grey histograms in *C* and black curves in *F*) patches increasing in size. ***A.*** Example post stimulus time histograms (PSTHs) of one neuron in response to small black flashing spots at each stimulus location. X axis is 0.2 s. ***B***. As in *A*, in response to a white stimulus. ***C.*** PSTHs of an example neuron in response to black (left column) or white (right column) patches increasing in size. Numbers on the left of rows indicate stimulus diameter. X axis is 0.5 s. ***D-E.*** Each row shows a single neuron's OFF (D) and ON (E) responses to flashing spots. The first row shows responses for the same neuron shown in *A* and *B*. Grey scales indicate response magnitude (imp/sec). Red solid line represents best response fits of a two dimensional Gaussian convolved with the stimulus. ***F.*** Size tuning of example neurons in response to black (black) and white (grey) patches increasing in size. The first plot from the top depicts responses of the same neuron shown in *C*. Error bars indicate ±s.e.m. Solid lines represent best OFF (black) and ON (grey) response fits of a difference of Gaussians model.

Anaesthesia also had profound influence on response latency. To show this I measured responses to flashed, small black or white squares. I averaged measurements of response latency across all positions where response was significantly higher than the background activity. The average latency in response to white stimuli was 147±27 ms in anesthetized animals and 54±34 ms in awake animals; in response to black stimuli, latency was 134±22 ms in anesthetized animals and 49±27 ms in awake animals (Fig. 3.6c). Interestingly, while latency to white and black stimuli were similar in awake animals (Fig. 3.6d) in anesthetized responses to white stimuli were slower (Fig. 3.6e) ($p = 0.004$, Wilcoxon rank sum test).

The increase in response amplitude, and decrease in response latency in awake animals can also be seen in the average response to flashed black or white patches of optimal size (Fig. 3.6f,g). Scaling the PSTHs in response to black stimuli and aligning them to the peak (Fig. 3.6h) shows that the time it takes for responses to reach the peak, and to then fade, is similar in awake and anesthetized mice.

I conclude that brain state has a profound effect on responses of neurons in the mouse sSC. By decreasing both spontaneous and evoked firing rates and increasing response latency, anaesthesia is likely to alter how neurons integrate visual information. Our results are in agreement with previous studies performed in mouse LGN and V1 (Vaiceliunaite et al., 2013; Durand et al., 2016), suggesting that anaesthesia similarly affects the excitability of visual neurons in SC, LGN and V1.

3.3.2 Polarity preference and spatial organisation of receptive fields

Most neurons in sSC preferred black stimuli to white stimuli. In awake animals, 83.7% (185/221) of cells showed stronger response to the optimally positioned black stimulus (Fig. 3.8a. $p < 10^{-22}$, Wilcoxon signed rank test) and in anesthetized animals, 69.2% (45/65) of cells did (Fig. 3.8b. $p < 10^{-3}$). Additional measurements of response to black and white circular patches increasing in size (Fig. 3.8c,d) showed similar preference for black stimuli (awake animals, 40/46 cells, 87%; $p < 10^{-5}$; anesthetized animals 45/68 cells, 66.2%; $p = 0.004$). Thus, most neurons in sSC respond to both white and black stimuli, but responses to black stimuli are stronger in both anesthetized and awake animals.

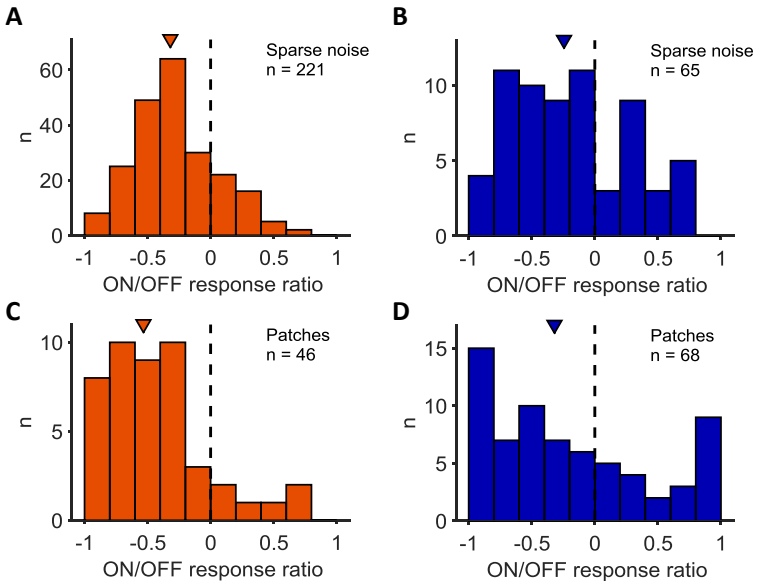

Figure 3.8. Response polarity of neurons in SC. Histograms of ratio of ON and OFF response amplitudes. Red lines indicate equal ON and OFF response amplitudes, bars on the left of the red bar indicate larger OFF response. Arrow heads represents median. Dashed vertical lines represent equal amplitudes of ON and OFF responses. ***A.*** ON/OFF ratio of responses to sparse noise stimulus in awake animals (n = 221; median -0.32, μ -0.28, s.d. 0.33). ***B.*** ON/OFF ratio of responses to sparse noise stimulus in anesthetized animals (n = 65; median -0.25, μ -0.17, s.d. 0.47). ***C.*** ON/OFF ratio if responses to patches in awake animals (n = 46; median -0.53, μ -43, s.d. 0.4). ***D.*** ON/OFF ratio if responses to sparse noise stimulus in awake animals (n = 68; median -0.32, μ -0.2, s.d. 0.62).

The preference of sSC neurons for black stimuli may arise if OFF subfields summated over a larger region of visual space, or had greater sensitivity compared to ON subfields. To compare the size of the OFF- and ON subfields, respectively, I characterised responses to black and white patches increasing in size (Fig. 3.7c,f). In each case I found the best predictions of a difference of Gaussians model, under the assumption that both ON and OFF subfields have center-surround receptive field organization (see Methods) (Enroth-Cugell and Robson, 1966;Croner and Kaplan, 1995). I included cells in which the best fitting prediction could explain at least 60% of variance in the data (Aw: OFF 39/46, 84.8%; ON: 29/46, 63%. An: OFF 54/68, 79.4%; ON: 47/68, 69.1%).

Summation area does not explain the stronger sensitivity to black stimuli. In awake animals, neurons generally showed similar preferred sizes for white and black stimuli ($p = 0.7$, Wilcoxon rank sum test), and in anesthetized mice neurons generally showed smaller preferred size for black patches ($p < 10^{-4}$) (Fig. 3.9a). Similarly, the receptive field centre size for ON and OFF

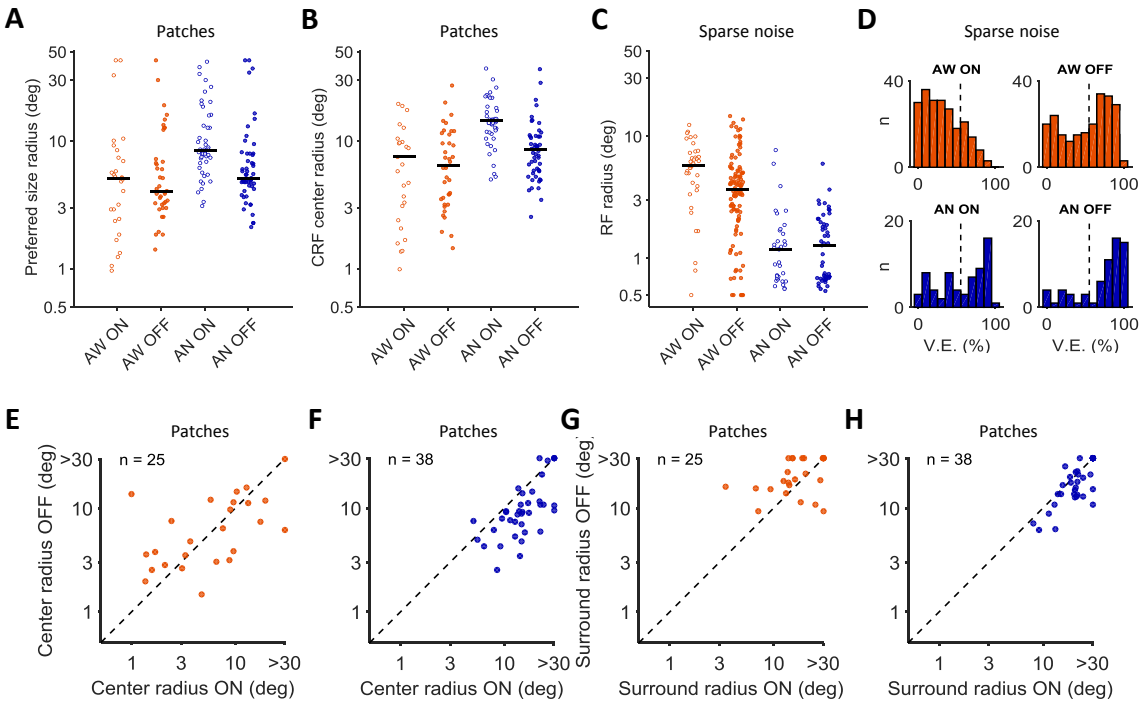

Figure 3.9. Size of ON and OFF subfields. ***A.*** Radius of preferred size for ON (empty) and OFF (filled) subfields in response to patches increasing in size, estimated from the response fits of a difference of Gaussians model (AW-ON: median 5.1, μ 4.7, s.d. 11.3, n = 29. AW-OFF: median 4, μ 5.2, s.d. 8.3, n = 39. AN-ON: median 8.5, μ 9.7, s.d. 9.2, n = 47. AN-OFF: median 5.1, μ 6.2, s.d. 9.4, n = 54). Horizontal bar represents median. ***B.*** Radius of classical receptive field center size for ON (empty) and OFF (filled) subfields in response to patches increasing in size, estimated from the response fits of a difference of Gaussians model (AW-ON: median 7.5, μ 6.8, s.d. 19.8, n = 29. AW-OFF: median 6.4, μ 6.4, s.d. 11.5, n = 39. AN-ON: median 14.5, μ 15.7, s.d. 15.3, n = 47. AN-OFF: median 8.5, μ 9.2, s.d. 15.29, n = 54). Horizontal bar represents median. ***C.*** Radius of ON (empty) and OFF (filled) subfields in response to sparse noise stimulus, estimated from the response fits of a two dimensional Gaussian convolved with the stimulus (AW-ON: median 5.8, μ 4.7, s.d. 3, n = 37. AW-OFF: median 3.7, μ 3.2, s.d. 3.1, n = 112. AN-ON: median 1.2, μ 1.2, s.d. 1.5, n = 34. AN-OFF: median 1.3, μ 1.2, s.d. 1, n = 49). ***D.*** Histograms depicting the distribution of variance in the data explained (V.E.) by the best fitting prediction of the Gaussian model fit to the responses to white (*left*, ON) and black (*right*, OFF) sparse noise stimulus, across the population of awake (*top*, orange) and anesthetized (*bottom*, blue) animals. Vertical dashed lines indicate threshold for inclusion in the analysis (60%): only neurons in which the model fit could explain at least 60% of variance in the data were included in subsequent analysis (AW-ON: 37/221, 16.7%. AW-OFF: 112/221, 50.7%. AN-ON: 34/65, 52.3%. AN-OFF: 49/65, 75.4%). ***E-F.*** Scatter plot of receptive field center radius for ON as a function of OFF subfields in awake *(E)* and anesthetized *(F)* animals, estimated from the fits of a difference of Gaussians model to responses to patches increasing in size. ***G-H.*** Scatter plot of receptive field surround radius for ON as a function of OFF subfields in awake *(G)* and anesthetized *(G)* animals, estimated from the fits of a difference of Gaussians model to responses to patches increasing in size.

subfields was similar in awake animals ($p = 0.94$) and under anaesthesia OFF subfields were smaller ($p < 10^{-5}$) (Fig. 3.9b,e,f). In counterpart analyses I estimated the radii of the ON and OFF subfields using the responses to flashing squares (Fig. 3.9c), for those cells where the fit could explain at least 60% of the variance in the data (Aw: OFF 112/221, 50.7%; ON 37/221, 16.7%. An: OFF 49/65, 75.4%; ON 34/65, 52.3%) (Fig. 3.9d). In awake animals, ON subfields were generally larger than OFF subfields ($p = 0.0014$, Wilcoxon rank sum test). In anesthetized animals the ON and OFF subfields were of similar size ($p = 0.69$, Wilcoxon rank sum test). Note that for many neurons in anesthetized animals the estimated radius was very small (the cluster of neurons with radius<1°, Fig. 3.9c). This is probably an artefact of the fitting procedure when neurons respond only to one or two of the tested positions. I note that the exclusion criteria exclude both neurons with little or no response and neurons with good responses but poorly fit by the Gaussian model, and so I may have excluded from the analysis neurons with particular patterns of activation. For example, some neurons responded well to individual positions in the sparse noise stimulus but did not display a unitary, clearly delimited receptive field, making it difficult for a Gaussian model to capture the variability in the data. The estimates of receptive field sizes reported here are therefore illustrative of the population of SC neurons that displayed spatially delimited receptive fields or conventional size tuning.

While estimates of subfield size obtained from sparse noise stimulus and patches were similar in awake animals, they clearly diverged in anesthetized mice, where estimated sizes were smaller for sparse noise. A simple explanation for the discrepancy may be a decrease in contrast sensitivity under anaesthesia: the small size of flashing spots away from the centre of the receptive field might not be sufficient to drive responses, while the use of patches of larger sizes would allow cells with low sensitivity to sum over larger portion of visual space and reach response threshold. A decrease in contrast sensitivity is in line with the larger portion of cells displaying pure ON or OFF responses in anesthetized animals, as illustrated by the proportion of cells having extreme values of ON/OFF response ratio (Fig. 3.8b,d).

In summary, I found that most neurons in mouse SC respond to both increases and decreases in luminance. The results are in agreement with previous studies of SC neurons in mouse (Wang et al. 2010), cat (McIlwain and Buser, 1968) and monkey (Schiller and Koerner, 1971). I also

conclude that neurons in the SC prefer decreases in luminance to increases in luminance, and this is because OFF subfields are more sensitive than ON subfields.

3.3.3 Linearity of spatial summation

The receptive fields of neurons throughout the visual pathways can be broadly classified as showing linear or non-linear spatial summation. In retina of cat, ganglion cells showing linear spatial summation (X cells) (Enroth-Cugell and Robson, 1966; Hochstein and Shapley, 1976a) can be distinguished from those showing clearly non-linear spatial summation (Y cells): these classes respectively correspond to beta- and alpha-like retinal ganglion cells defined morphologically (Boycott and Wassle, 1974). In visual cortex of cat, primate and mouse, a similar distinction can be made between simple-like and complex-like receptive fields (Hubel and Wiesel, 1962; Movshon et al., 1978; Durand et al., 2016). Previous work in SC of anesthetized and awake mice (Wang et al., 2010; Ito et al., 2017) has shown presence of some cells with linear or nearly linear spatial summation and others showing clearly non-linear spatial summation. Recent work in mouse LGN (Durand et al., 2016) has shown that while most receptive fields in anesthetized animals show linear spatial summation, non-linear spatial summation is more apparent in awake animals. Above I showed that, consistent with previous work, many neurons in SC respond to both black and white flashed stimuli, implying non-linear summation within receptive fields. In the following, I characterise the linearity of spatial summation in mouse SC neurons, in anesthetized and awake animals.

When a sinusoidal grating is drifted across the receptive field, it generates a sinusoidal flux in luminance at each point in the receptive field (Fig. 3.10a). The activity of a linear receptive field will be strongly modulated at the temporal frequency of the grating, while a non-linear cell will show elevation of the mean firing rate that is only weakly modulated at the grating temporal frequency (Fig. 3.10b). In the model of retinal Y-cell receptive fields proposed by Shapley and Hochstein, this is because the Y-cell receptive field includes multiple spatially overlapping subunits and the output of each subunit is rectified before summation within the receptive field. Similarly, cortical complex cells can be thought of as the summation of rectified subunits, like those found in cortical simple cells. Fourier analysis of the neuronal response to a drifting grating

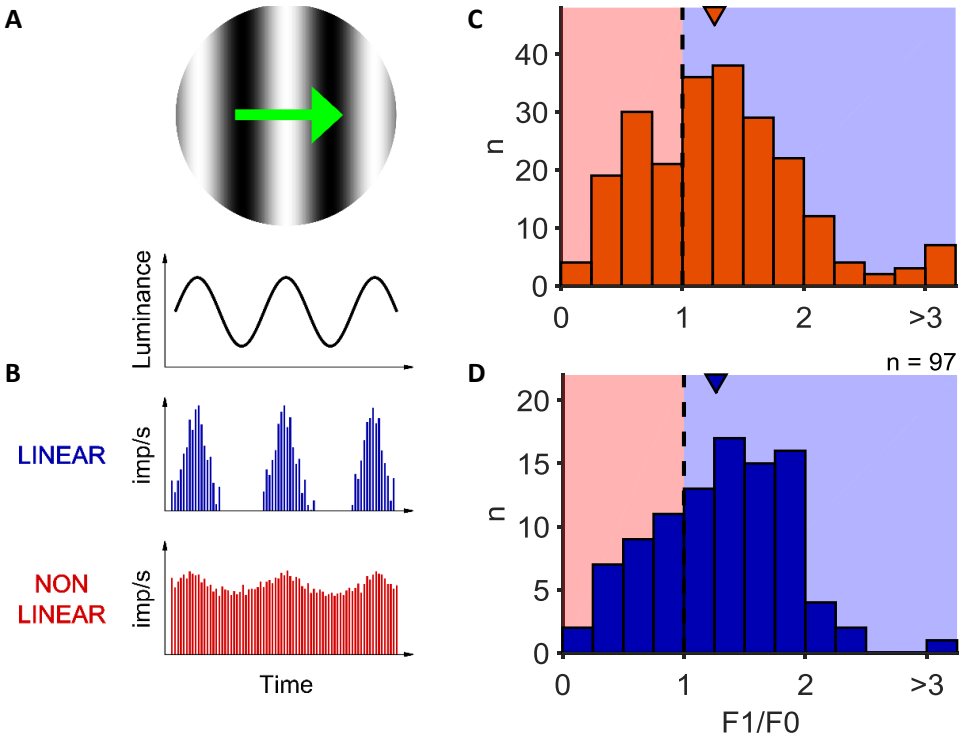

Figure 3.10. Linearity of spatial summation in response to drifting gratings. ***A-B.*** Schematic of linear and non-linear responses in the visual system. When a sinusoidally drifting grating is presented over a receptive field, the receptive field is subjected to luminance sinusoidally varying over time (*A*). Linear cells respond with a firing rate that is strongly modulated at the temporal frequency of the stimulus, while non-linear cells respond with an increased average firing rate weakly modulated at the stimulus temporal frequency (*B*). ***C-D***. Histogram of F1/F0 ratio of neurons in awake (*C*) and anesthetized (*D*) animals in response to a drifting sinusoidal grating of optimal spatial frequency. Red shaded areas indicates cells classified as non-linear (F1/F0 < 1). Blue shaded areas indicates cells classified as linear (F1/F0 ≥ 1). Arrow heads indicate medians (AW: 1.26; μ 1.31; s.d. 0.64. AN: 1.36; μ 1.3; s.d. 0.56).

Figure 3.11. Linearity of spatial summation in response to counterphase modulated gratings. ***A-D.*** *Left.* Raster plots of responses of four example neurons to counterphase modulated gratings. Each dot represents a spike. Each row represents a trial. I tested responses at 8 different phases (y-axis), each tested 4 to 10 times. Each colour represents different trials of equal phase. *Right*. Cycle-averaged post stimulus time histograms in response to each phase, colour coded as in (*left*). The spatial frequency of the grating was, in cyc/deg: *A*-0.05; *B*-0.02; *C*-0.05; *D*-0.07. The temporal frequency of the grating was, in cyc/sec: *A*-2; *B*-1.33; *C-2*; *D*-3. ***A-B.*** Example neurons recorded in awake (*A*) and anesthetized (*B*) mice displaying linear responses. Note that responses are mainly modulated at the temporal frequency of the stimulus (F1) showing one peak per cycle, while at the null phase the F2 dominates. Also note sporadic phase shifts of responses to equal phase in (*A)*, probably introduced by eye movements in awake animals. ***C-D.*** Example neurons recorded in awake (*C*) and anesthetized (*D*) mice displaying non-linear responses. Note that responses are modulated at twice the frequency of the stimulus (F1) and display similar responses at all phases. Also note that responses in (*C*) seem to be unaffected by eye movements. ***E-F.*** Scatter plot of F2/F1 ratios measured in awake (*E*) and anesthetized (*F*) animals in response to counterphase gratings, as a function of F1/F0 ratio measured in response to drifting sinusoidal gratings of

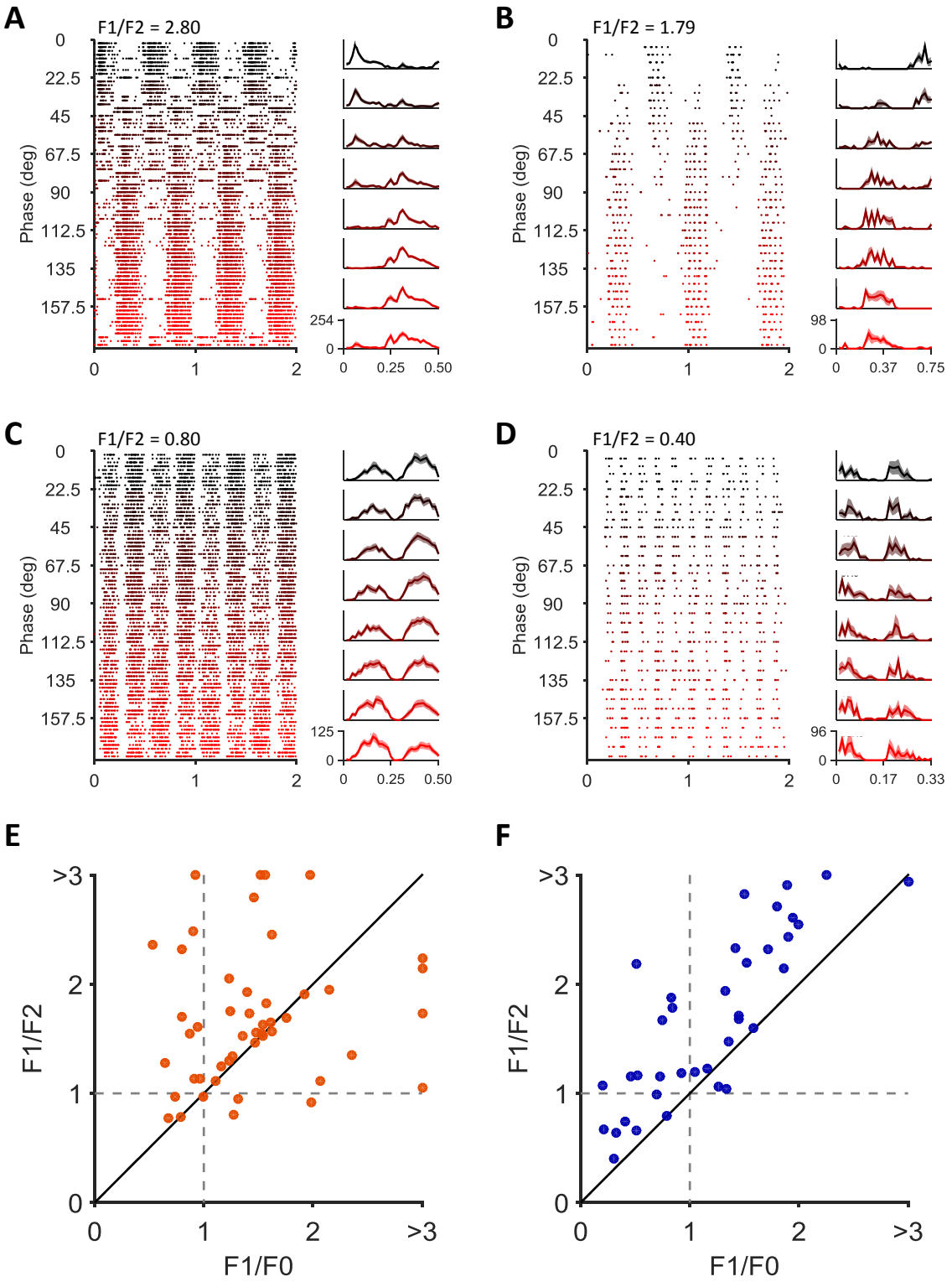
A
F1/F2 = 2.80
B
F1/F2 = 1.79
C
F1/F2 = 0.80
D
F1/F2 = 0.40
Phase (deg)
0
22.5
45
67.5
90
112.5
135
157.5
254
98
125
96
0.25
0.50
0.37
0.75
0.17
0.33
E
F
F1/F2
F1/F0
>3

enables comparison of the mean rate (average firing rate, or F0), and the amplitude of response at the temporal frequency of the stimulus (first harmonic, or F1). If the amplitude of the response modulated at the temporal frequency of the stimulus is larger than the average firing rate (F1/F0 ratio > 1), the cell is classified as linear or simple-like (Skottun et al., 1991). Cells with an F0 larger than the F1 are classified as non-linear or complex-like.

I derived F1/F0 ratios from responses to a large drifting grating of nearly optimal spatial frequency. F1 and F0 values were calculated separately for each trial and then averaged across trials. Figure 3.10 shows the distribution of F1/F0 ratio across the sample of SC cells in awake (Fig 3.10c) and anesthetized (Fig 3.10d) animals. In anesthetized animals the median F1/F0 ratio was 1.36 and 68/97 (70.1%) cells showed F1/F0 ≥ 1 (linear, or simple-like). The distribution of F1/F0 ratio in anesthetized animals was no different to that of awake animals (median 1.26. p = 0.59; Wilcoxon rank sum test), where 153/227cells (67.4%) were classified as being linear.

In a subset of units I further characterised spatial linearity using counterphase modulated sinusoidal gratings. In this experiment the grating is stationary but flickers with a sinusoidal temporal profile; I measured response at each of 8 spatial phases (Fig 3.11). Linear cells are again expected to show activity modulated at the temporal frequency of the stimulus (Fig. 3.11a,b). Non-linear units are expected to show modulation at twice that temporal frequency (the F2) because some subunits are responding at one temporal phase, and others are responding at the opposite temporal phase (Fig. 3.11c,d). In this case, linearity of spatial summation is captured by the ratio of the F1 response to the F2 response (with responses again calculated within trial and then averaged across trials). Fig 3.11e,f shows the distribution of this index across neurons in anesthetized and awake animals: in anesthetized animals the median F1/F2 ratio was 1.67 and 32/39 (82%) cells showed F1/F2 ratios ≥ 1 (linear, or simple-like). The distribution of F1/F2 ratio in anesthetized animals was no different to that of awake animals (p = 0.9; Wilcoxon rank sum test), where 41/48 neurons (85.4%) were classified as being linear. Comparison of this measurement and the F1/F0 ratio above in individual cells showed that classification of non-linear neurons is more conservative with counterphase gratings, and therefore the proportion of linear cells is higher using the F1/F2 ratio (Fig 3.11e,f).

3.3.4 Influence of eye movements on linear responses

Receptive fields early in the visual pathway are retinotopic, and when an awake animal moves its eyes, the portion of the external world that is imaged onto the receptive field also moves. Typical electrophysiological experiments average neural responses to several repetitions (trials) of each stimulus. This approach is not valid in awake animals if eye movements change the position of the receptive field with respect to the visual stimulus. For example, eye movements may cause trial-by-trial shifts in the spatial phase of a drifting grating relative to the receptive field, which will in turn result in a response phase shift between trials. Figure 3.12 shows schematically how eye movements can affect estimates of response linearity. Imagine a linear receptive field, 5° in diameter, sensitive to light increments, presented with a sinusoidal grating of 0.1 cyc/deg drifting at 1 cyc/sec. An eye movement of 5° shifts the position of the receptive field, with the result that the receptive field will 'see' opposite phases in the two trials (Fig. 3.12a-b. Blue, trial 1; green, trial 2). The response in each of the two trials will therefore have F1 components of opposite phases (Fig. 3.12c). Averaging across trials would therefore reduce the estimated amplitude of the F1 component of response, also reducing the estimate of spatial linearity (F1/F0). This effect will be strongest for high spatial frequencies, where

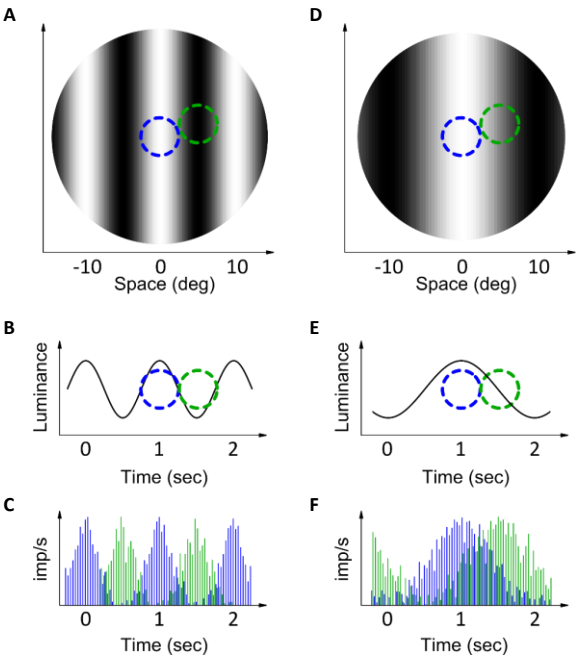

Figure 3.12. Schematic of interaction between eye movements and spatial frequency on the phase of linear responses. ***A.*** Blue and green circles represent the positions of a linear neuron's receptive field over a drifting sinusoidal grating in two trials with different eye positions, at the timestamp of 1 sec in *B*. ***B***. Given that the position of the receptive field is different between the blue and the green trials, the phase of luminance change over the receptive field will be shifted in time. ***C***. PSTHs of the linear neuron in the two trials. The different phase of the sinusoidal change in luminance results in phase shifted responses, in this case of opposite phase. ***D-E-F***. Same as A-B-C, but for a lower spatial frequency. When a lower spatial frequency is used, the shift in response phase due to eye movements is less pronounced.

relatively small eye movements can nevertheless cause large changes in response phase, while at low spatial frequencies the influence of eye movements on response phase will be correspondingly smaller (Fig. 3.12c-d-e).

Fig. 3.13 shows a real example of this phenomenon. During this experiment, I measured the response of a neuron to a vertical drifting grating of varying spatial frequency. The response to each spatial frequency was sampled 10 times (Fig. 3.13c) and the average eye position on each trial is plotted in Fig 3.13b. For demonstration purposes I split the trials into two groups, based on the eye's horizontal displacement (green and blue points). Fig. 3.13c shows the raster plot of all trials for each spatial frequency, with colour determined by eye position. Fig. 3.13d displays the raster plots of responses to each trial of one spatial frequency (0.075 cyc/deg), corresponding to the filled points in Fig. 3.13b. These raster plots show that response phase (spike timing) depends on eye position. This is clearer in Fig. 3.13e, which shows cycle-averaged PSTHs for trials in each group of eye positions. The PSTHs are of opposite phase, and the result is that PSTH averaged across all trials (Fig. 3.13e, black solid line) is less modulated than PSTHs for each eye position group. The impact of eye movements on estimates of receptive field properties is shown in Fig 3.13f, which compares the spatial frequency tuning of the F1 obtained after averaging spiking activity across trials (solid line), and F1 calculated from spiking activity within each trial and then averaged (dashed line). Averaging spiking activity (ie. constructing

Figure 3.13. Interaction of eye movements and spatial frequency on linear responses. ***A.*** *Left.* Snapshot of eye tracking during an experiment. *Right.* Same as in *A*, but thresholded to show pupil detection (red pixels). ***B***. Receptive field positions derived from eye tracking for an example linear neuron, during measurement of responses to a drifting sinusoidal grating of varying spatial frequencies. Each dot represents the average RF position during one trial. Colour code groups responses obtained from trials were the RF had similar horizontal position. ***C***. Each row shows the raster plot of responses in one trial (7 spatial frequencies, 10 trials each). ***D***. Enlarged raster plots of responses to 10 trials at 0.075 cyc/deg, colour coded as in *C,* and corresponding to the black filled points in *B*. Note the phase shift in responses to different receptive field positions. ***E***. Cycle-averaged PSTHs of responses shown in *D*. Shaded areas represent cycle averaged PSTHs of individual trials. Blue and green solid lines represent cycle-averaged PSTHs of blue and green responses from *D*, respectively. Note that the single and the averaged PSTHs have opposite phase due to horizontal displacement of RF position. Black solid line represents the cycle averaged PSTH across all trials in *D*. Note the lower F1 amplitude compared to the average PSTHs of responses with similar RF position. ***F***. Solid line shows F1 response amplitude at different spatial frequencies derived from responses averaged across all trials (as in *E*, black solid line). Dashed line shows the F1 response amplitudes at different spatial frequencies derived trial by trial and then averaged across trials. Note that the trial by trial F1 has a larger amplitude at higher spatial frequencies. Arrow head indicates spatial frequency of the stimulus for responses shown in D and E.

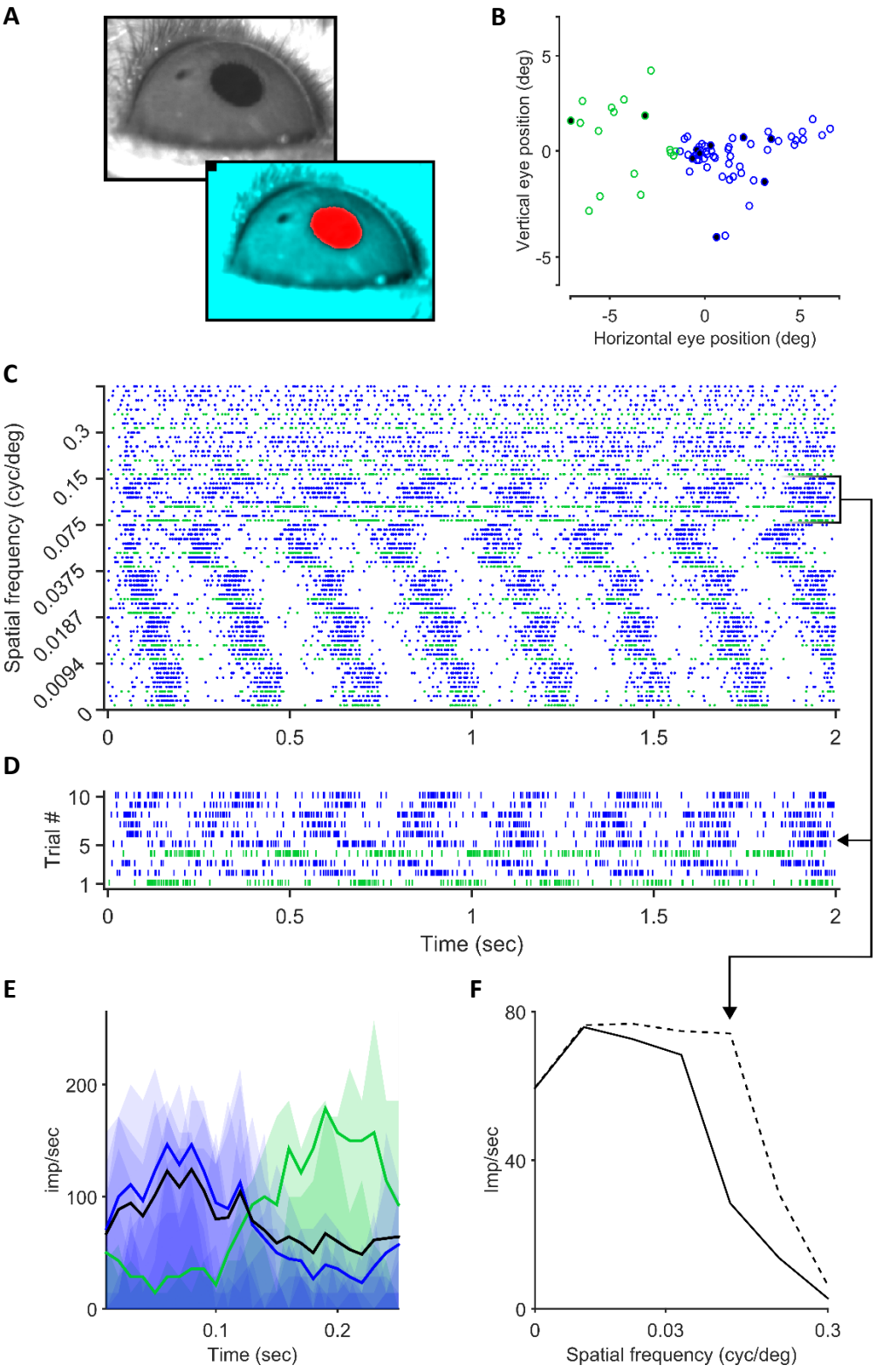
A
B
Vertical eye position (deg)
Horizontal eye position (deg)
C
Spatial frequency (cyc/deg)
D
Trial #
Time (sec)
E
imp/sec
Time (sec)
F
Imp/sec
Spatial frequency (cyc/deg)

PSTHs) across trials leads to an underestimation of spatial resolution, because the influence of eye movements on the temporal profile of average responses is strongest at high spatial frequencies.

Above, I classified cells as linear or non-linear based on the F1/F0 ratio at the optimal spatial frequency (Skottun et al., 1991). Fig 3.14 compares F1/F0 ratio derived from averaged responses (F1psth/F0) and trial-by-trial responses (F1/F0). As expected from the presence of eye movements, the difference in trial-by-trial and averaged F1/F0 is more prominent in awake animals than in anesthetized animals. In anesthetized animals 8/97 cells (8.1%) would have been misclassified as non-linear if I were to use trial-averaged PSTHs, while 40/227 (17.6%) cells would have been misclassified in awake animals. For all following analyses I therefore chose to use the trial-by-trial responses, and not averaged PSTHs, to characterize the response of all cells.

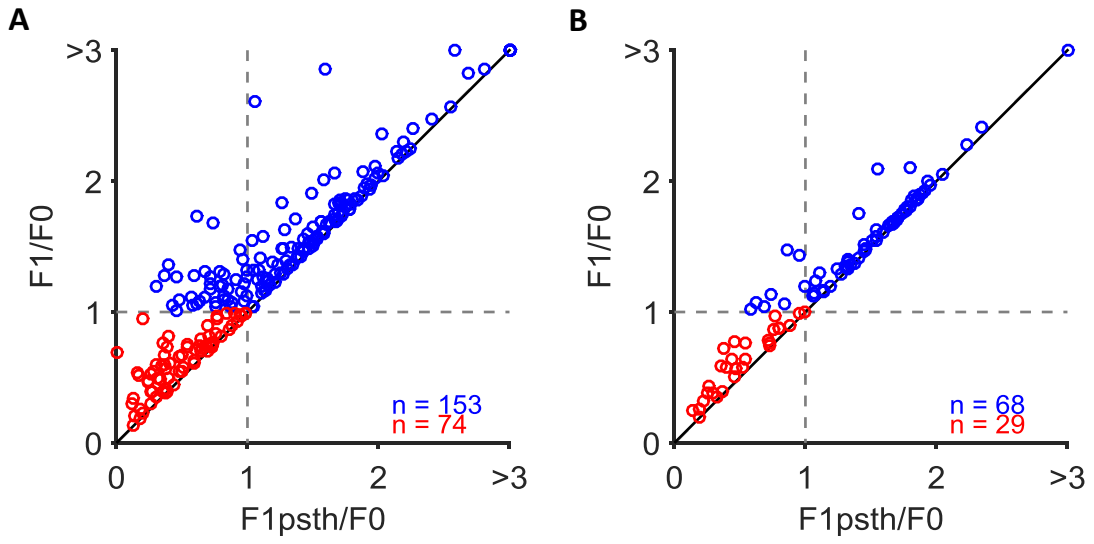

Figure 3.14. Eye movements and linearity of spatial summation. ***A-B.*** Comparison of F1/F0 ratio calculated deriving the F1 from the average PSTH across trials (F1psth/F0) rather than from the trial by trial responses (F1/F0), in response to a drifting sinusoidal grating of optimal spatial frequency. Vertical and horizontal dashed grey lines indicate threshold for cell classification as linear or non-linear for F1psth/F0 and F1/F0, respectively. Solid black line represents equality of the two ratios. Note that the F1psth/F0 underestimates the amplitude of the F1, causing underestimation of response linearity. Blue and red points indicate cells classified as linear and non-linear, respectively, using F1/F0. Neurons positioned on the left of the vertical dashed line and on top of the horizontal dashed line would have been misclassified as non-linear by using F1psth/F0. ***A***. Neurons recorded in awake animals (n=227). ***B***. Neurons recorded in anesthetized animals (n = 97).

3.3.5 Spatial resolution

The visual environment contains information at different spatial scales, from low (e.g. a clear sky) to high (e.g. blades of grass). Similarly the visual system contains neurons with receptive fields of different sizes, which allow analysis of information at various spatial scales. To gain insight into the spatial bandwidth of cells in mouse SC, I characterized their sensitivity to different spatial frequencies. To provide quantitative characterisation of spatial receptive fields I measured the response to large, high-contrast sinusoidal gratings drifting at the preferred orientation (where known) and at an average temporal frequency of 4.4± 3.4 Hz.

To show the envelope of spatial sensitivity, Fig 3.15b shows average spatial frequency tuning curves in awake and anesthetized animals. These average tuning curves indicate greater responsivity at high spatial frequencies in awake animals. The average tuning curves however mask wide variability in the shape of individual tuning curves (Fig. 3.15a), with some showing low-pass tuning, others highly bandpass tuning, and a broad variety of intermediate tuning widths. To provide a quantitative characterisation of tuning curves I found in each case the best predictions of a difference-of-Gaussians model of the spatial receptive field (Enroth-Cugell and Robson, 1966;Croner and Kaplan, 1995). I used these predictions to estimate the preferred spatial frequency, the size and sensitivity of the classical receptive field centre, and the amount of tuning (see Methods). The distribution of preferred spatial frequency was similar for awake and anesthetized animals (Fig. 3.15c, $p = 0.19$, Wilcoxon rank sum test), as was the distribution of receptive field centre sizes (Fig. 3.15d, $p = 0.13$, Wilcoxon rank sum test), and the index of the degree of spatial tuning (i.e. the roll off at low spatial frequencies; Fig 3.15e, $p = 0.5$, Wilcoxon rank sum test). I found a median spatial frequency resolution of 0.1 cyc/deg, with 10% of neurons resolving at least 0.32 cyc/deg in awake animals. In anesthetized animals the median was 0.09 cyc/deg and 10% of neurons resolved at least 0.17 cyc/deg. In both awake and anesthetized animals, I found strong quantitative differences between linear and non-linear cells: linear neurons tended to prefer lower spatial frequency while non-linear cells preferred higher spatial frequencies (AW: $p < 10^{-9}$, AN: $p < 10^{-5}$, Wilcoxon

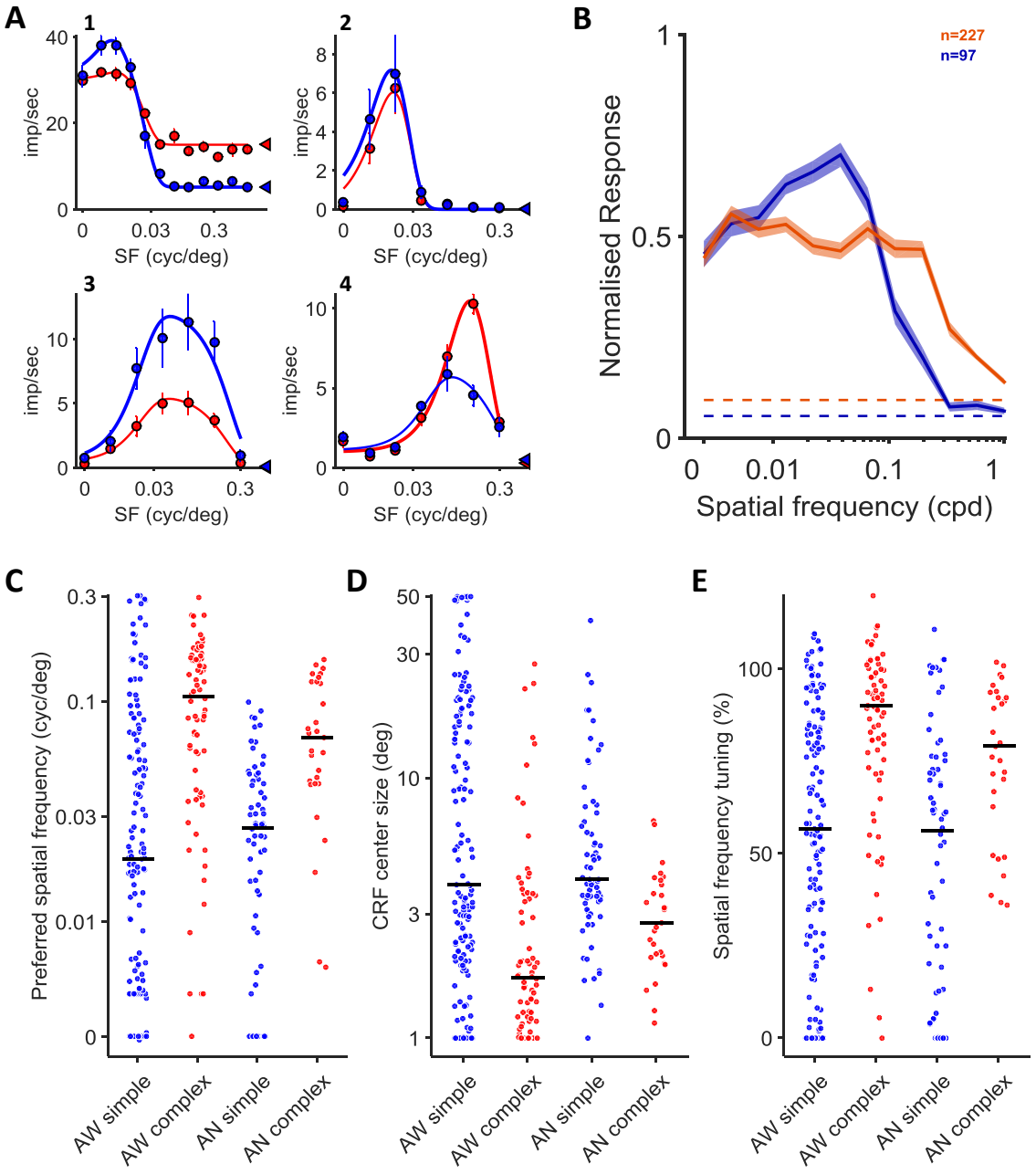

rank sum test). Similarly, the classical receptive field center size was smaller in non-linear cells (AW: $p < 10^{-7}$, AN: $p < 10^{-3}$, Wilcoxon rank sum test), and non-linear cells showed stronger tuning (AW: $p < 10^{-7}$, AN: $p < 10^{-3}$). Interestingly, anaesthesia significantly decreased the preferred spatial frequency, increased the receptive field centre size and decreased the tuning in non-linear neurons ($p = 0.04$, $p = 0.004$, $p = 0.046$, respectively. Wilcoxon rank sum test), while as a

Figure 3.15. Spatial frequency sensitivity of neurons in SC. I presented a large full contrast grating of fixed direction and temporal frequency, varying in spatial frequency. ***A*. 1-4.** Example responses of individual neurons to drifting sinusoidal gratings of varying spatial frequency. Points indicate response ± 1 s.e.m. Blue: F1 amplitude. Red: F0 amplitude. Please note that responses to a grating of spatial frequency 0 are plotted on the logarithmic x-axis at half of the first tested spatial frequency higher than 0. Arrow heads indicate spontaneous activity. Thicker blue or red solid lines indicate that the cell was classified as linear or non-linear, respectively. Solid lines show the best fit of a difference of Gaussians model. The optimal parameters for each cell were: **1)** K_c 0.067; K_s 0.001; r_c 13.6; r_s 3.36. **2)** K_c 0.037; K_s 0.018; r_c 15.7; r_s 0.1. **3)** K_c 2.05; K_s 0.016; r_c 1.38; r_s 7.76. **4)** K_c 2.74; K_s 0.59; r_c 1.52; r_s 1.5. ***B***. Population average spatial frequency tuning for awake (orange, n = 227) and anesthetized (blue, n=97) animals. Dashed lines indicate average normalized spontaneous activity. ***C***. Preferred spatial frequency for linear (blue) and non-linear (red) cells in awake (AW, left) and anesthetized (AN, right) animals, estimated from the response fits of a difference of Gaussians model (AW-lin: median 0.019, μ 0.051, s.d. 0.072, n = 153. AW-nlin: median 0.105, μ 0.107, s.d. 0.069, n = 74. AN-lin: median 0.027, μ 0.03, s.d. 0.025, n = 68. AN- nlin: median 0.067, μ 0.076, s.d. 0.045, n = 29). Horizontal bar represents median. ***D***. Size of CRF centre for linear (blue) and non-linear (red) cells in awake (AW, left) and anesthetized (AN, right) animals, estimated from the response fits of a difference of Gaussians model (AW-lin: median 3.83, μ 11.92, s.d. 14.46, n = 153. AW-nlin: median 1.7, μ 3.5, s.d. 5.04, n = 74. AN-lin: median 4.07, μ 6.46, s.d. 6.52, n = 68. AN- nlin: median 2.78, μ 3.07, s.d. 1.4, n = 29). Horizontal bar represents median. ***E.*** Spatial frequency tuning for linear (blue) and non-linear (red) cells in awake (AW, left) and anesthetized (AN, right) animals (AW-lin: median 56.58, μ 54.09, s.d. 36, n = 153. AW-nlin: median 89.94, μ 82.3, s.d. 25.08, n = 74. AN-lin: median 55.99, μ 47.84, s.d. 35.76, n = 68. AN- nlin: median 79.02, μ 74.98, s.d. 21.17, n = 29). Horizontal bar represents median.

population, linear cells showed no change. Hence, the increase in population averaged responses to high spatial frequency (Fig. 3.15b) was mainly due to the responses of non-linear cells.

3.3.6 Relation between classical receptive field sensitivity and size

The predictions of the difference-of-Gaussians model allow us to investigate the relation between sensitivity and size of receptive fields. Large receptive fields indicate that units receive (indirect) input from a larger number of photoreceptors, and therefore have a higher retinal flux (retinal illumination times area) (Enroth-Cugell and Shapley, 1973). It has been shown in cat that retinal ganglion cells with larger summating receptive fields undergo stronger light adaptation (Enroth-Cugell and Shapley, 1973). Functionally, this means that cells with large centres are less sensitive than neurons with small receptive fields, such that the integrated sensitivity, or volume (sensitivity times size) is independent of receptive field size (White et al., 2001). If sensitivity is inversely proportional to size then plotting the receptive field sizes against their sensitivities in a log-log scale should result in a regression line with a slope of -2. Similar to cat retinal ganglion

cells (Linsenmeier et al., 1982) and primate dLGN cells (Irvin et al., 1993; White et al., 2001) I found that for both anesthetized and awake animals the center sensitivity (K) was inversely correlated to size, with regression line slope of -2.2 in awake animals and -1.94 in anesthetized (Fig. 3.16a-b). The relationship between surround sensitivity and size was similar but slightly steeper, with a regression line slope of -2.53 in awake recordings and -2.57 in anesthetized, implicating that with increasing size the gain decreases more quickly for surrounds than it does for centres (Fig. 3.16c-d).

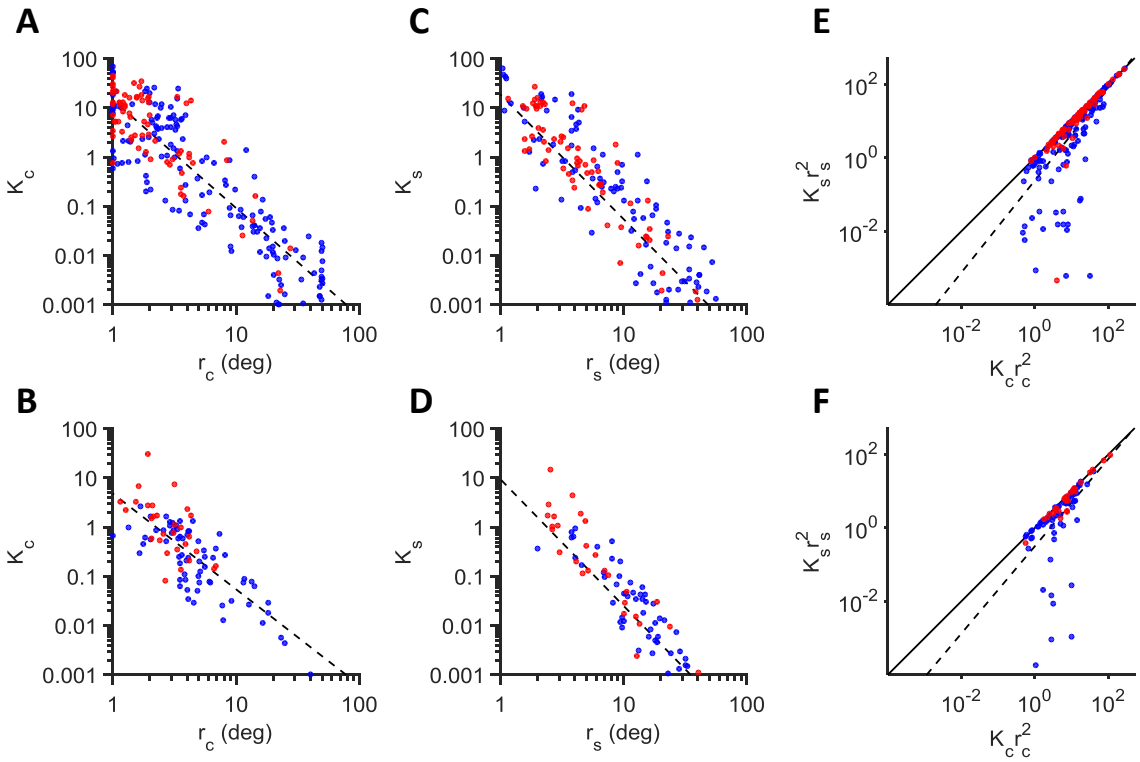

Figure 3.16. Relation between classical receptive field sensitivity and size. ***A.*** Scatter plot of classical receptive field center size (r_c) as a function of gain (K_c) in awake animals. The dashed regression line has the equation $K_c = 6.8\ r_c^{-2.2}$, $r^2 = -0.89$, $p<10^{-76}$. ***B.*** Scatter plot of classical receptive field center size (r_c) as a function of gain (K_c) in anesthetized animals. $K_c = 4.8\ r_c^{-1.94}$, $r^2 = -0.78$, $p<10^{-20}$. ***C.*** Scatter plot of classical receptive field surround size (r_s) as a function of gain (K_s) in awake animals. $K_s = 7.8\ r_s^{-2.53}$, $r^2 = -0.85$, $p<10^{-65}$. ***D.*** Scatter plot of classical receptive field surround size (r_s) as a function of gain (K_s) in anesthetized animals. $K_s = 9.5\ r_s^{-2.57}$, $r^2 = -0.77$, $p<10^{-76}$. ***E.*** Scatter plot of classical receptive field center volume ($K_c r_c^2$) as a function of surround volume ($K_c r_c^2$) in awake animals. $K_c r_c^2 = 0.29\ (K_s r_s^2)^{1.25}$, $r^2 = 0.73$, $p<10^{-39}$. $K_s r_s^2 / K_c r_c^2$: median 0.87, μ 0.71, s.d. 0.33. Solid line represents $K_c r_c^2 = K_s r_s^2$. ***F.*** Scatter plot of classical receptive field center volume ($K_c r_c^2$) as a function of surround volume ($K_s r_s^2$) in anesthetized animals. $K_c r_c^2 = 0.32\ (K_s r_s^2)^{1.19}$, $r^2 = 1$, $p=0$. $K_s r_s^2 / K_c r_c^2$: median 0.79, μ 0.7, s.d. 0.3. Solid line represents $K_c r_c^2 = K_s r_s^2$.

The integrated strength of the surround ($K_s\pi r_s^2$) relative to the center ($K_c\pi r_c^2$) determines the response of a center-surround receptive field to uniform illumination (Enroth-Cugell and Robson, 1966; Irvin et al., 1993) (Kr^2, Fig. 3.16e-f). Similar to primate dLGN cells (Irvin et al., 1993), I found that the integrated volume of the center and surround mechanisms in mouse SC is tightly balanced, with larger surround volumes associated with larger center volumes in both awake and anesthetized recordings. Cells generally showed slightly smaller surround volumes than center volumes, indicating weak but non-zero response to diffuse illumination. Interestingly, non-linear cells lie closer to the regression line, suggesting a tighter control of center and surround volumes (AW: $p < 10^{-7}$, AN: $p = 0.001$, Wilcoxon rank sum test). Cells lying further away from the regression line, in which the surround volume was much smaller than the center, were almost exclusively linear. This is in accord with the greater sensitivity of linear cells to low spatial frequencies.

In summary I found that for visual cells in the mouse SC, as for cat retinal ganglion cells (Linsenmeier et al., 1982) and primate dLGN neurons (Irvin et al., 1993; White et al., 2001), there is an inverse relation between receptive field gain and size with larger summation fields having lower sensitivity.

3.3.7 Temporal integration dynamics

The sensitivity to temporal frequency indicates how quickly a cell can integrate changes in luminance. These temporal dynamics are likely to be sensitive to anaesthesia, and in mouse LGN anaesthesia reduces sensitivity to high temporal frequencies. I therefore measured responses to large, high contrast sinusoidal gratings of preferred spatial frequency and orientation (if known), varying in temporal frequency.

Fig 3.17b shows the envelopes of temporal frequency responses in awake and anesthetized animals. The average tuning depends dramatically on anaesthesia, with a sharp increase in sensitivity to high temporal frequencies in awake animals. Neurons recorded in awake animals preferred temporal frequencies of 7 cyc/sec while during anesthetized recordings neurons preferred temporal frequencies around 2 cyc/sec (Fig. 3.17c). In both awake and anesthetized

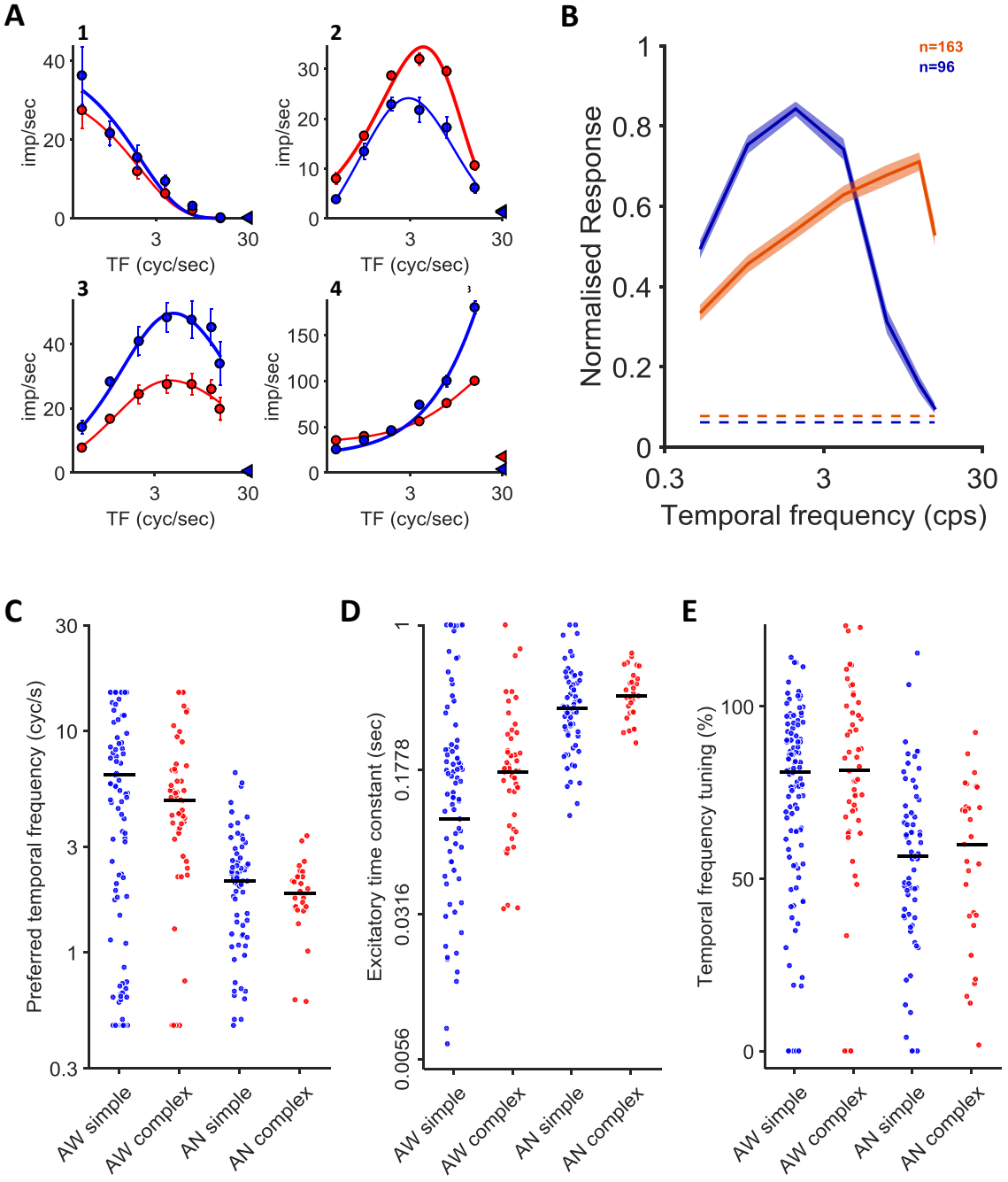

animals, however, individual cells displayed a wide variety of tuning curves, varying from low-pass to high-pass and with different degrees of tuning (Fig. 3.17a). To characterise these tuning curves I found the best predictions of a difference-of-exponentials (see Methods) (Derrington

Figure 3.17. Temporal frequency sensitivity of neurons in SC. I presented a large full contrast grating of fixed direction and spatial frequency, varying in temporal frequency. ***A*. 1-4.** Example responses of individual neurons to drifting sinusoidal gratings of varying temporal frequency. Points indicate response ± 1 s.e.m. Blue: F1 amplitude. Red: F0 amplitude. Arrow heads indicate spontaneous activity. Thicker blue or red solid lines indicate that the cell was classified as linear or non-linear, respectively. Solid lines show the best fit of a difference of exponentials model. The optimal parameters for each cell were: **1)** S_1 41.1; K_1 0.5; S_2 0.36; K_2 0.51. **2)** S_1 120.1; K_1 0.16; S_2 123.16; K_2 0.36. **3)** S_1 62.4; K_1 0.036; S_2 64.75; K_2 0.54. **4)** S_1 503.2; K_1 0.001; S_2 484.6; K_2 0.28. ***B***. Population average temporal frequency tuning for awake (orange, n = 163) and anesthetized (blue, n = 96) animals. Dashed lines indicate average normalized spontaneous activity. ***C***. Preferred temporal frequency for linear (blue) and non-linear (red) cells in awake (AW, left) and anesthetized (AN, right) animals, estimated from the response fits of a difference of exponentials model (AW-lin: median 6.4, μ 7.7, s.d. 5.8, n = 110. AW-nlin: median 4.9, μ 5.7, s.d. 4, n = 53. AN-lin: median 2.1, μ 2.2, s.d. 1.3, n = 67. AN-nlin: median 1.9, μ 1.9, s.d. 0.6, n = 29). Horizontal bar represents median. ***D***. Excitatory time constant for linear (blue) and non-linear (red) cells in awake (AW, left) and anesthetized (AN, right) animals, estimated from the response fits of a difference of exponentials model (AW-lin: median 0.099, μ 0.21, s.d. 0.3, n = 110. AW-nlin: median 0.17, μ 0.21, s.d. 0.19, n = 53. AN-lin: median 0.4, μ 0.4, s.d. 0.2, n = 67. AN-nlin: median 0.43, μ 0.45, s.d. 0.13, n = 29). Horizontal bar represents median. ***E.*** Temporal frequency tuning for linear (blue) and non-linear (red) cells in awake (AW, left) and anesthetized (AN, right) animals (AW-lin: median 81, μ 71.8, s.d. 29.6, n = 110. AW-nlin: median 31.4, μ 77.1, s.d. 31.8, n = 53. AN-lin: median 56.6, μ 54.6, s.d. 24.6, n = 67. AN-nlin: median 60, μ 54.3, s.d. 24.4, n = 29). Horizontal bar represents median.

and Lennie, 1984) from which I estimated the preferred temporal frequency, the excitatory time constant (indicating the temporal frequency resolution) and the amount of tuning (i.e. the roll off at low temporal frequencies).

Preferred temporal frequency was substantially reduced in anesthetized animals (Fig. 3.17c. $p < 10^{-12}$, Wilcoxon rank sum test). The excitatory time constant, an index of sensitivity to high temporal frequencies, was substantially shorter in awake recordings (Fig. 3.17e. $p < 10^{-17}$, Wilcoxon rank sum test). Similarly, the tuning index was stronger in awake than anesthetized animals (Fig. 3.17e. $p < 10^{-8}$, Wilcoxon rank sum test). In both awake and anesthetized animals, I found that linear neurons had a shorter excitatory time constant compared to non-linear cells (AW: $p = 0.03$, AN: $p = 0.04$, Wilcoxon rank sum test).

In summary I found that neurons in awake animals show substantially increased response to high temporal frequencies and more band-pass response. In addition, linear cells in both anesthetized and awake animals have higher resolution for high temporal frequencies than non-linear cells. Thus linear cells prefer lower spatial frequencies and have high temporal resolution, while non-linear cells have high spatial resolution and lower temporal resolution.

3.3.8 Speed tuning

The analyses above show how response of neurons in SC depends on the spatial- and temporal frequency of a drifting grating. These dimensions of the visual image are thought to be the building blocks for estimates of motion speed, which is important for a variety of tasks including prey capture, predator avoidance, depth perception and navigation through the world. While tuning for temporal frequency may indicate tuning for motion speed, speed (the ratio of temporal frequency/spatial frequency) varies with spatial and temporal frequency: patterns with higher spatial frequency move slower than patterns of the same temporal frequency but lower spatial frequency.

In anesthetized animals, some SC neurons have been shown to be sensitive to speed (Gale and Murphy, 2014). To ask if neurons in mouse SC are sensitive to speed, as well as spatial and temporal frequency, I measured their responses to a matrix of spatial and temporal frequencies spanning speeds varying from 1.5 to more than 800 deg/sec. Fig 3.13a shows responses of example cells to this matrix of temporal and spatial frequency. To characterise the speed tuning of each cell, I averaged the responses to combination of spatial- and temporal frequencies that produce similar speeds (that is, they lie on the positive diagonal of this matrix). I found diverse

Figure 3.18. Speed sensitivity of neurons in SC. I presented a large full contrast grating of fixed direction, varying in spatial and temporal frequency. ***A.*** *Left*. Matrix of example responses of individual neurons to drifting sinusoidal gratings of varying spatial (SF) and temporal frequency (TF). Grey scale indicates response amplitude in imp/sec. *Right.* Best fit of the speed tuning model for each cell shown on the left. The optimal parameters for each cell were: **1)** *A* 43.4; sf_{pref} 0.122; tf_0 3.71; σ_{sf} 0.92; σ_{tf} 1.75; ξ 0. **2)** *A* 97.8; sf_{pref} 0.064; tf_0 3.2; σ_{sf} 0.89; σ_{tf} 1.55; ξ 0.43. **3)** *A* 9; sf_{pref} 0.025; tf_0 5.23; σ_{sf} 0.92; σ_{tf} 0.75; ξ 0.67. ***B***. Population average of normalized responses to combinations of spatial and temporal frequency leading to similar speeds for awake (orange, n = 90) and anesthetized (blue, n = 63) animals. Dashed lines indicate average normalized spontaneous activity. ***C.*** Preferred speed for linear (blue) and non-linear (red) cells in awake (AW, left) and anesthetized (AN, right) animals, estimated from the response fits of the speed model (AW-lin: median 50.4, µ 213.5, s.d. 324.6, n = 26. AW-nlin: median 37, µ 51.4, s.d. 52.1, n = 14. AN-lin: median 51.9, µ 55.4, s.d. 27.1, n = 28. AN-nlin: median 45.5, µ 53.7, s.d. 40.4, n = 14). Horizontal bar represents median. ***D-E.*** Scatter plot of preferred speed as a function of preferred spatial frequency for awake (*D*) and anesthetized (*E*) animals, estimated from the response fits of the speed model. Blue and red points represent linear and non-linear cells, respectively. ***F-G.*** Scatter plot of preferred speed as a function of preferred temporal frequency for awake (*F*) and anesthetized (*G*) animals, estimated from the response fits the speed model. Blue and red points represent linear and non-linear cells, respectively.

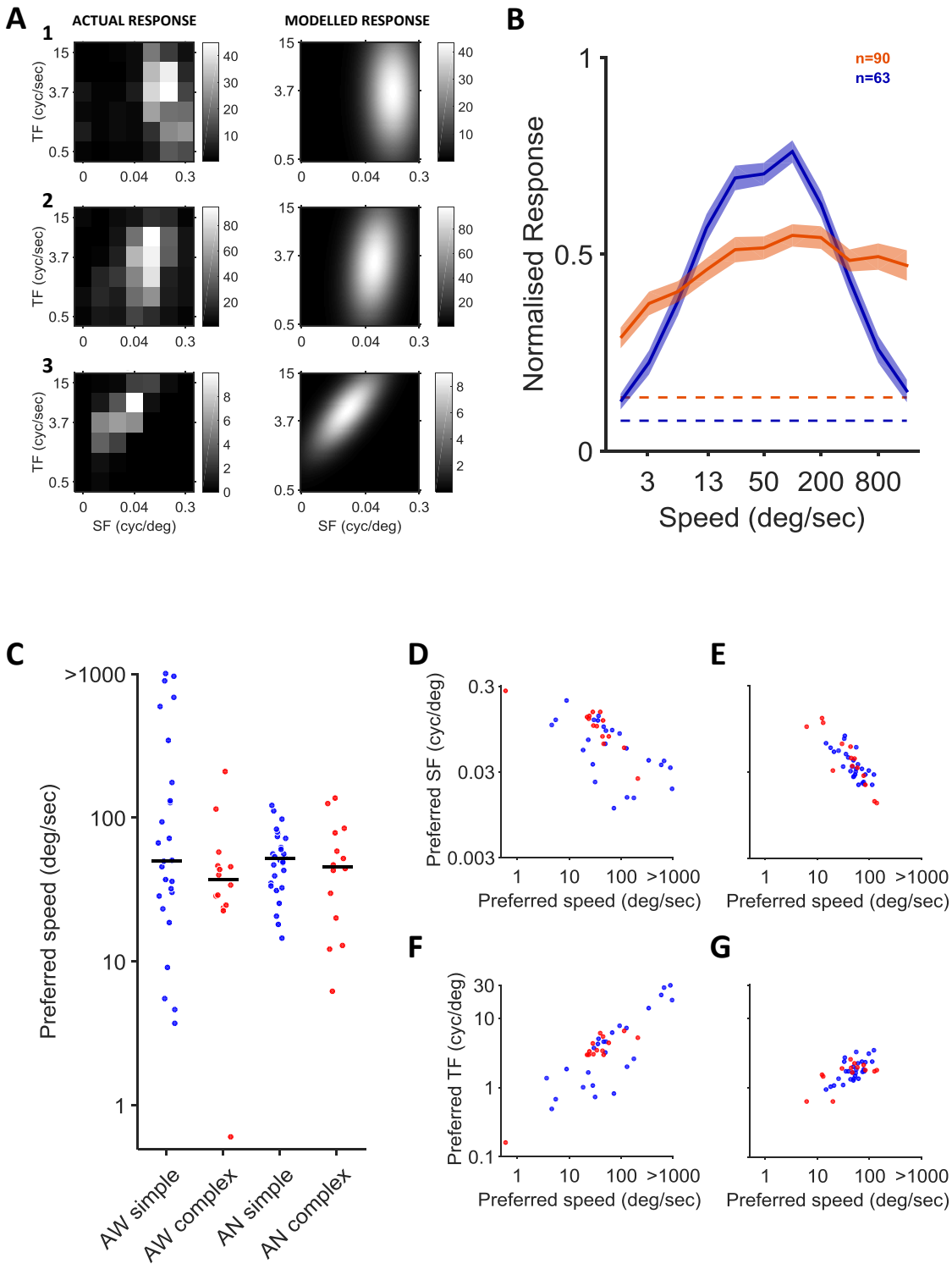
A
ACTUAL RESPONSE
MODELLED RESPONSE
1
2
3
TF (cyc/sec)
SF (cyc/deg)
15
3.7
0.5
0
0.04
0.3
B
Normalised Response
n=90
n=63
1
0.5
0
3
13
50
200
800
Speed (deg/sec)
C
Preferred speed (deg/sec)
>1000
100
10
1
AW simple
AW complex
AN simple
AN complex
D
E
Preferred SF (cyc/deg)
0.3
0.03
0.003
1
10
100
>1000
Preferred speed (deg/sec)
F
G
Preferred TF (cyc/deg)
30
10
1
0.1

responses, with some units showing low-pass and others showing high-pass tuning curves for speed, while other units showed weak or no tuning. The average speed tuning across the population of cells was broader in awake animals (Fig. 3.18b), as expected from the observation of broader envelopes for spatial and temporal frequency in awake animals. Preferred speed was similar in awake and anesthetized animals ($p = 0.86$, Wilcoxon rank sum test) and in linear and non-linear cells (AW: $p = 0.18$, AN: $p = 0.53$, Wilcoxon rank sum test) (Fig. 3.18c).

If a neuron is tuned for visual speed, a change in the spatial frequency of a drifting grating should induce a proportional change in its preferred temporal frequency. In other words, a speed tuned neuron will prefer the same speed despite changes in spatial frequency. Figure 3.19a-b shows the average temporal frequency tuning across the population measured at two spatial frequencies, 0.0094 cyc/deg (black) and 0.15 cyc/sec (red). In anesthetized animals the average temporal frequency tuning curve changed little with spatial frequency. Indeed, preferred temporal frequency did not depend strongly on test spatial frequency (Fig. 3.19b, inset). In awake animals the situation was different: the average tuning curve measured at high spatial frequency peaks at a higher temporal frequency, suggesting some degree of speed tuning in the population. Consistently, preferred temporal frequency in many neurons shifted to higher temporal frequency at higher spatial frequency (Fig. 3.19a, inset).

To quantify speed selectivity in awake and anesthetized animals I fit responses with an elliptical Gaussian (Fig. 3.18a, see Methods) (Priebe et al., 2003; Andermann et al., 2011; Gale and Murphy, 2014) from which I estimated the parameter ξ (speed-tuning index), the exponent of a power-law relationship between preferred temporal frequency and spatial frequency. The parameter ξ captures the degree of dependency of preferred temporal frequency on spatial frequency: values closer to 1 indicating shifting temporal frequency tuning curves at different spatial frequencies, so that the preferred temporal frequency is proportional to the spatial frequency and the preferred speed is stable (speed tuned cell); a value of 0 indicates a cell in which the preferred temporal frequency is independent of spatial frequency, so that the preferred speed varies with spatial frequency. For these analyses, I only include cells in which the model could explain at least 60% of the variance (Awake: 40/90 cells, 44.5%. Anesthetized: 42/63 cells, 66.7%). I observed speed tuning in both awake and anesthetized animals (Fig. 3.19c,

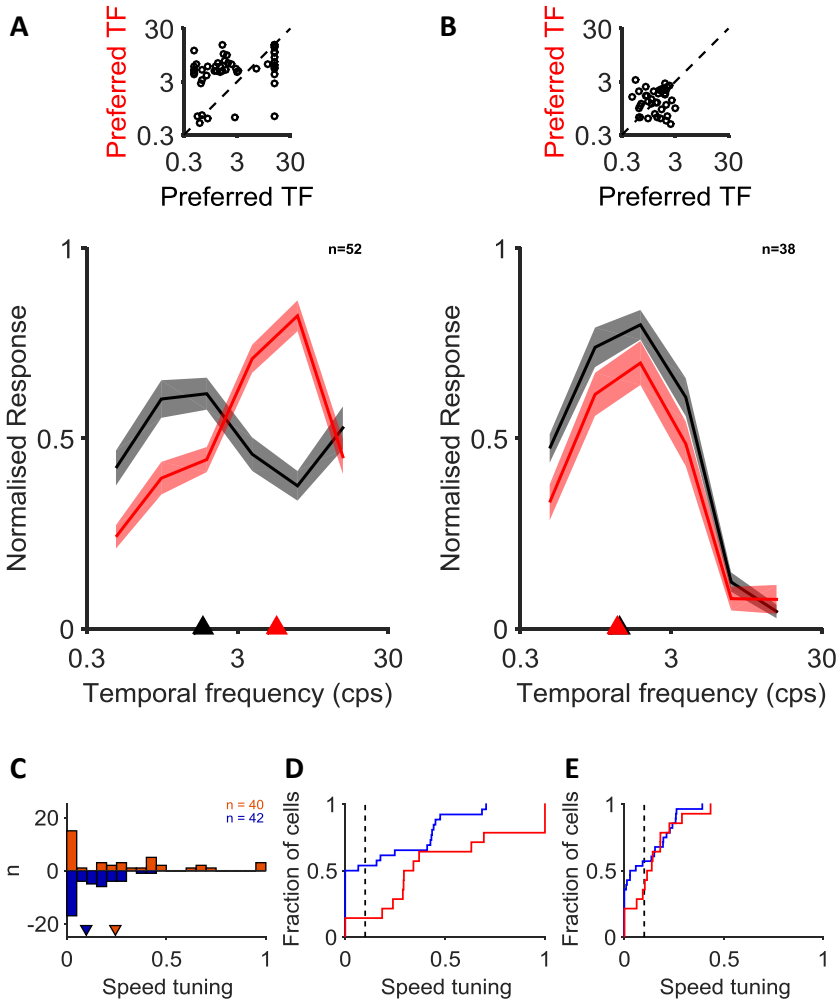

Figure 3.19. True speed sensitivity. A true speed sensitive cell should shift preferred temporal frequency when spatial frequency changes. ***A-B***. Population average of normalized responses to varying temporal frequency at a fixed spatial frequency of 0.0094 cyc/deg (black) or 0.15 cyc/deg (red), for awake (*A,* n = 52) and anesthetized (*B*, n = 38) animals. Arrow heads indicate average preferred temporal frequency. Only cells responsive at both spatial frequencies were included. Note that in awake animals the preferred temporal frequency depends on the spatial frequency of the stimulus and denotes speed selectivity, while in anesthetized the preferred temporal frequency is independent of spatial frequency. ***Insets.*** Scatter plot of single neurons' preferred temporal frequency at 0.0094 cyc/deg (x-axis) as a function of preferred temporal frequency at 0.15 cyc/deg (y-axis). Note that in awake animals (left) many cells increased their preferred temporal frequency at higher spatial frequency, while in anesthetized animals (right) the distribution was homogeneous around the dashed identity line. ***C.*** Histogram of speed tuning indices of neurons in awake (orange, n=40) and anesthetized animals (blue, n=42), estimated from the response fits of the speed model. Arrow heads indicate mean speed tuning indices (AW: 0.24; median 0.29; s.d. 0.31 imp/s. AN: 0.1; median 0.12; s.d. 0.12). ***D-E.*** Cumulative distributions of speed tuning indices shown in *C*, for awake (D) and anesthetized (E) animals. Blue and red lines represent linear and non-linear cells, respectively.

d,e. ξ>0.1. Aw: 24/40 cells, 60%. An: 21/42 cells, 50%), but the speed tuning of tuned neurons was significantly higher in awake mice (Aw: median, 0.43; mean, 0.47; s.d., 0.26; An: median, 0.2; mean, 0.26; s.d., 0.17. $p < 10^{-6}$; Wilcoxon rank sum test). Interestingly, non-linear cells showed higher speed tuning than linear cells in awake animals (Fig. 3.19d).

Similar to what has been observed in cortical areas of anesthetized mice (Andermann et al., 2011) I found a significant, although weaker, inverse correlation between speed tuning and preferred speed in awake animals (r = -0.37, p=0.019, Pearson's correlation coefficient of ξ and $\log_{10}$[preferred speed]). As expected, I found an inverse correlation between preferred speed and preferred spatial frequency (Fig. 3.19d,e. AW: r = -0.72, $p < 10^{-6}$. An: r = -0.84, $p < 10^{-11}$, Pearson's correlation coefficient), and a positive correlation between preferred speed and preferred temporal frequency (Fig. 3.18f,g. AW: r = 0.86, $p < 10^{-12}$. AN: r = 0.66, $p < 10^{-5}$, Pearson's correlation coefficient).

In summary, I found more speed tuned cells and broader speed sensitivity in awake animals. Similar to visual cortex (Andermann et al., 2011), the preferred speed was inversely correlated with preferred spatial frequency and positively correlated with preferred temporal frequency, and in awake animals the amount of tuning had a weak inverse correlation with preferred speed.

3.3.9 Direction and orientation tuning

Previous work has shown that a substantial proportion of neurons in SC of mouse display strong orientation or direction selectivity (Wang et al., 2010; Gale and Murphy, 2014; Inayat et al., 2015; Shi et al., 2017). This is similar to cats (Marchiafava and Pepeu, 1966; McIlwain and Buser, 1968; Sterling and Wickelgren, 1969), but in contrast with monkeys, where most SC receptive fields are insensitive to orientation or direction (Schiller and Koerner, 1971; Cynader and Berman, 1972; Goldberg and Wurtz, 1972a; Updyke, 1974; Marrocco and Li, 1977; Moors and Vendrik, 1979; Wurtz and Albano, 1980).

I therefore characterized the direction and orientation selectivity of the populations of neurons in the superior colliculus for drifting sinusoidal gratings. The direction of motion of a one-dimensional pattern like the gratings I used is ambiguous, because the same image is consistent with motion along an axis orthogonal to the patterns' orientation, or motion (at a

higher speed) along any other axis that is not parallel to the pattern orientation. Nevertheless I label motion direction as the motion orthogonal to the grating orientation, and I measured response to motion along both the possible directions for each orientation (eg. left and right movement for a vertical grating). Across the population I observed a wide range of tuning for orientation and direction (Fig. 3.20a). Some neurons displayed no preference for a particular orientation or direction, others responded preferentially to gratings drifting in the same orientation but in either direction, and others that were strongly selective for stimuli moving in a particular direction. Fig. 3.20b shows the average tuning curve for direction across the population of neurons, after shifting each of the tuning curves to the preferred direction.

To quantify the direction and orientation selectivity of individual neurons, I calculated both selectivity indices (DSI for direction and OSI for orientation) and the circular variance (global direction or orientation selectivity index, see Methods) (Fig. 3.20g-j). The global selectivity index (gDSI for direction and gOSI for orientation) is a better overall descriptor of selectivity (Mazurek et al., 2014), but many studies have reported only the selectivity index, and so I also report them (Wang et al., 2010; Andermann et al., 2011; Inayat et al., 2015 (also used gDSI); Niell and Stryker, 2008). In awake animals I found 41/155 cells (25.8%) displaying a DSI≥0.5 (a 3:1 ratio of the response to the preferred direction over its opposite), and 29/155 (18.7%) cells displaying a gDSI ≥0.25, indicating strong direction selectivity. In anesthetized animals, 5/86 (5.8%) neurons had a DSI≥0.5 or a gDSI ≥0.25. In agreement with previous studies (Wang et al., 2010) I found no evident bias for a particular motion direction (Fig. 3.21). In awake animals I found 30/155 cells (19.4%) with an OSI≥0.5, and 41/155 of the neurons (26.5%) had a gOSI ≥0.25. In anesthetized animals 8/86 (9.3%) of the neurons had an OSI≥0.5, and 11/86 neurons (12.8%) displayed a gOSI ≥ 0.25.

I found a significant increase in both DSI and gDSI in awake animals (DSI: $p<10^{-3}$, gDSI: p=0.008, Wilcoxon rank sum test), and a significant increase in gOSI but not OSI between anesthetized and awake animals (OSI: p=0.05, gOSI: $p<10^{-3}$, Wilcoxon rank sum test). I note that sometimes during the experiments a smaller grating was used to induce a robust response from the neuron under study. When a grating is viewed through a small window, this leads to blurring of the orientation spectrum of the stimulus, and in addition may exclude regions of the receptive

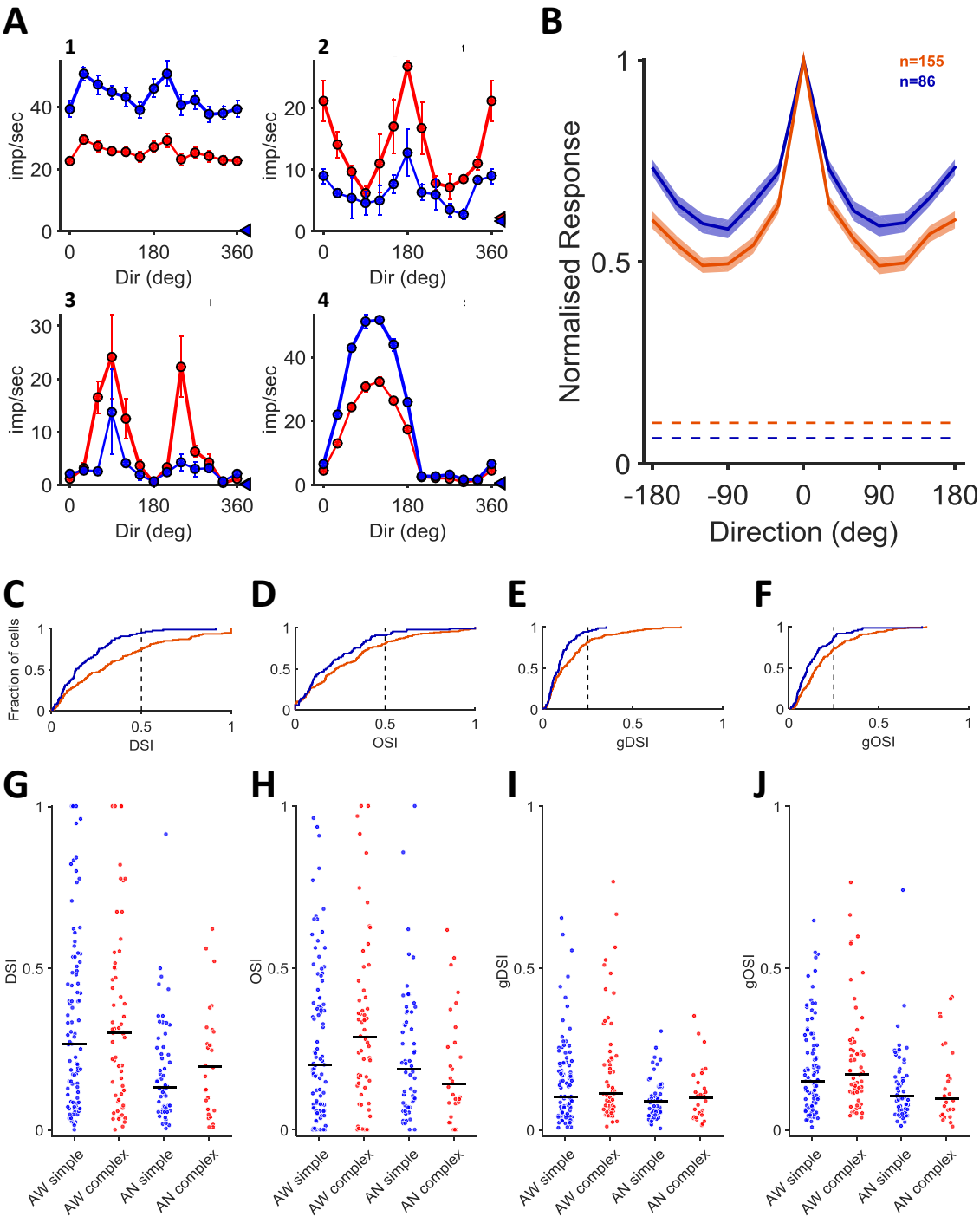
A
1
2
3
4
imp/sec
Dir (deg)
B
n=155
n=86
Normalised Response
Direction (deg)
C
D
E
F
Fraction of cells
DSI
OSI
gDSI
gOSI
G
H
I
J
AW simple
AW complex
AN simple
AN complex

Figure 3.20. Direction and orientation sensitivity of neurons in SC. I presented a large full contrast grating of fixed spatial and temporal frequency, varying in direction. ***A.* 1-4.** Example responses of individual neurons to drifting sinusoidal gratings of varying direction. Points indicate response ± 1 s.e.m. Blue: F1 amplitude. Red: F0 amplitude. Arrow heads indicate spontaneous activity. Thicker blue or red solid lines indicate that the cell was classified as linear or non-linear, respectively. The selectivity indices for each cell were: **1)** DSI 0.001; OSI 0.114; gDSI 0.029; gOSI 0.059. **2)** DSI 0.47; OSI 0.575; gDSI 0.107; gOSI 0.347. **3)** DSI 0.591; OSI 0.915; gDSI 0.243; gOSI 0.577. **4)** DSI 0.961; OSI 0.375; gDSI 0.656; gOSI 0.175. ***B***. Population average direction/orientation tuning for awake (orange, n = 163) and anesthetized (blue, n = 96) animals, where direction is relative to direction eliciting maximal response. Dashed lines indicate average normalized spontaneous activity. ***C-F.*** Cumulative distribution of awake (orange) and anesthetized (blue) animals for direction selectivity index (*C*), orientation selectivity index (*D*), global direction selectivity index (*E*) and global orientation selectivity index (*F*). ***G-J***. Distribution of parameters for linear (blue) and non-linear (red) cells in awake (AW, left) and anesthetized (AN, right) animals. Horizontal bar represents median. ***G.*** Direction selectivity index (AW: median 0.29, μ 0.34, s.d. 0.28, n = 155. AW-lin: median 0.27, μ 0.34, s.d. 0.28, n = 96. AW-nlin: median 0.3, μ 0.35, s.d. 0.28, n = 59. AN: median 0.14, μ 0.19, s.d. 0.16, n = 86. AN-lin: median 0.13, μ 0.18, s.d. 0.16, n = 58. AN-nlin: median 0.2, μ 0.21, s.d. 0.17, n = 28). ***H***. Orientation selectivity index (AW: median 0.23, μ 0.29, s.d. 0.25, n = 155. AW-lin: median 0.2, μ 0.27, s.d. 0.24, n = 96. AW-nlin: median 0.29, μ 0.33, s.d. 0.27, n = 59. AN: median 0.17, μ 0.22, s.d. 0.19, n = 86. AN-lin: median 0.19, μ 0.23, s.d. 0.2, n = 58. AN-nlin: median 0.14, μ 0.2, s.d. 0.17, n = 28). ***I.*** Global direction selectivity index (AW: median 0.11, μ 0.16, s.d. 0.15, n = 155. AW-lin: median 0.1, μ 0.15, s.d. 0.13, n = 96. AW-nlin: median 0.11, μ 0.18, s.d. 0.17, n = 59. AN: median 0.09, μ 0.1, s.d. 0.07, n = 86. AN-lin: median 0.09, μ 0.1, s.d. 0.06, n = 58. AN-nlin: median 0.1, μ 0.11, s.d. 0.09, n = 28). ***J.*** Global orientation selectivity index (AW: median 0.15, μ 0.2, s.d. 0.15, n = 155. AW-lin: median 0.15, μ 0.19, s.d. 0.14, n = 96. AW-nlin: median 0.17, μ 0.21, s.d. 0.16, n = 59. AN: median 0.1, μ 0.14, s.d. 0.12, n = 86. AN-lin: median 0.1, μ 0.14, s.d. 0.11, n = 58. AN-nlin: median 0.1, μ 0.14, s.d. 0.12, n = 28).

field that have an impact on the generation of orientation or direction selectivity. In anesthetized recordings I indeed observed a weak positive correlation between stimulus size and gDSI and gOSI that reached significance for the orientation tuning (gDSI: r=0.21, p=0.05; gOSI: r=0.37, p<0.001, Pearson's correlation coefficient), while in awake recordings this was not the case (gDSI: r=-0.02, p=0.8; gOSI: r=-0.007, p=0.38, Pearson's correlation coefficient). When I considered only neurons tested with gratings larger than 35° in diameter, only DSI appeared to differ between anesthetized and awake animals (gDSI: p=0.09, DSI: p=0.002, gOSI: p=0.15, OSI: p=0.67). Therefore, my measurements in anesthetized animals may underestimate the degree of orientation and direction selectivity.

In summary, I observed neurons with direction and/or orientation selectivity in mouse superior colliculus, consistent with previous work. Both direction and orientation tuning increased in awake animals, although the difference may have been due to the use of smaller

stimuli in a subset of cells cells or to undersampling of the most superficial layers of the SC in anesthetized mice. The increase in selectivity found in awake animals could alternatively reflect anaesthesia's modulation of the directionally selective retinal inputs and intracollicular connections present in SC (Shi et al., 2017), or rise from brain state differences in the activity of SC directionally selective GAD2+ neurons (Inayat et al., 2015).

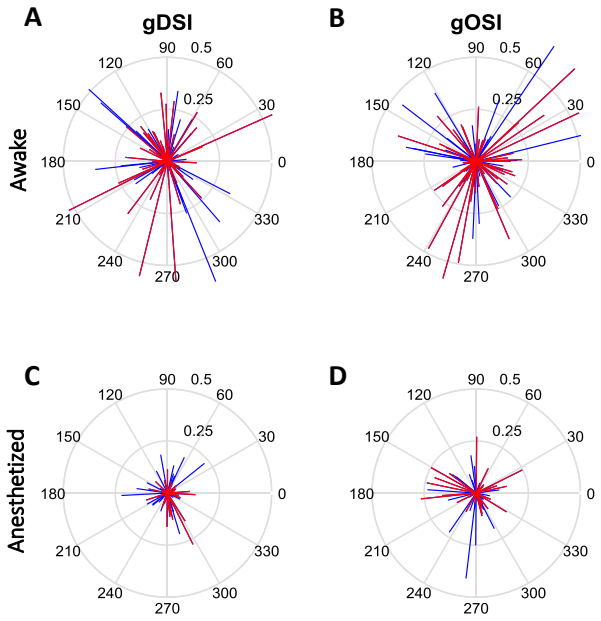

Figure 3.21. Direction and orientation preference. ***A-D.*** Polar plots of global direction selectivity index (*A,C*) and global orientation selectivity index (*B,D*) for awake (*A,B*, n = 155) and anesthetized (*C,D*, n = 86) animals. Blue and red points represent linear (*A*, n = 96; *C*, n = 58) and non-linear (*B*, n = 59; *D*, n = 28) cells, respectively. Radial displacement represents amplitude of selectivity index, from 0 in the center to 0.5 at the outer circle. Circular displacement indicates preferred direction (*A,C*) or orientation (*B,D*).

Figure 3.22. Contrast sensitivity of neurons in SC. I presented a large grating of fixed spatial frequency, temporal frequency, and direction, varying in contrast. ***A*. 1-4.** Example responses of individual neurons to drifting sinusoidal gratings of varying contrast. Points indicate response ± 1 s.e.m. Blue: F1 amplitude. Red: F0 amplitude. Arrow heads indicate spontaneous activity. Thicker blue or red solid lines indicate that the cell was classified as linear or non-linear, respectively. The selectivity indices for each cell were: **1)** R_{max} 1000, C_{50} 3, p 4. **2)** R_{max} 150.8, C_{50} 2.18, p 4.3. **3)** R_{max} 16, C_{50} 0.17, p 2.9. **4)** I did not use the model fits for supersaturating cells. ***B***. Population average to increasing contrast for awake (orange, n = 71) and anesthetized (blue, n = 70) animals. Dashed lines indicate average normalized spontaneous activity. ***C-E***. Distribution of parameters for linear (blue) and non-linear (red) cells in awake (AW, left) and anesthetized (AN, right) animals. Horizontal bar represents median. ***C.*** Semisaturation constant, or C_{50} (AW-lin: median 0.24, μ 0.44, s.d. 0.39, n = 40. AW-nlin: median 0.43, μ 0.51, s.d. 0.39, n = 16. AN-lin: median 0.79, μ 0.79, s.d. 0.22, n = 50. AN-nlin: median 0.73, μ 0.77, s.d. 0.17, n = 20). ***D.*** Exponent, or p (AW-lin: median 2.36, μ 2.43, s.d. 1.28, n = 40. AW-nlin: median 1.06, μ 1.68, s.d. 1.17, n = 16. AN-lin: median 3.36, μ 3.07, s.d. 0.99, n = 50. AN-nlin: median 3.12, μ 3, s.d. 0.77, n = 20). ***E.*** R_{max} / C_{50} (AW-lin: median 40.7, μ 52.1, s.d. 42.7, n = 40. AW-nlin: median 24, μ 41.1, s.d. 41, n = 16. AN-lin: median 9.6, μ 14.5, s.d. 16.7, n = 50. AN-nlin: median 15.1, μ 24.5, s.d. 24.9, n = 20). ***F-G***. Scatter plot of C_{50} as a function of R_{max} for linear (blue) and non-linear (red) cells in awake (F) and anesthetized (G) animals. ***F***. r = -0.39, p = 0.0028, Pearson's correlation coefficient. ***G***. r = -0.017, p = 0.89, Pearson's correlation coefficient.

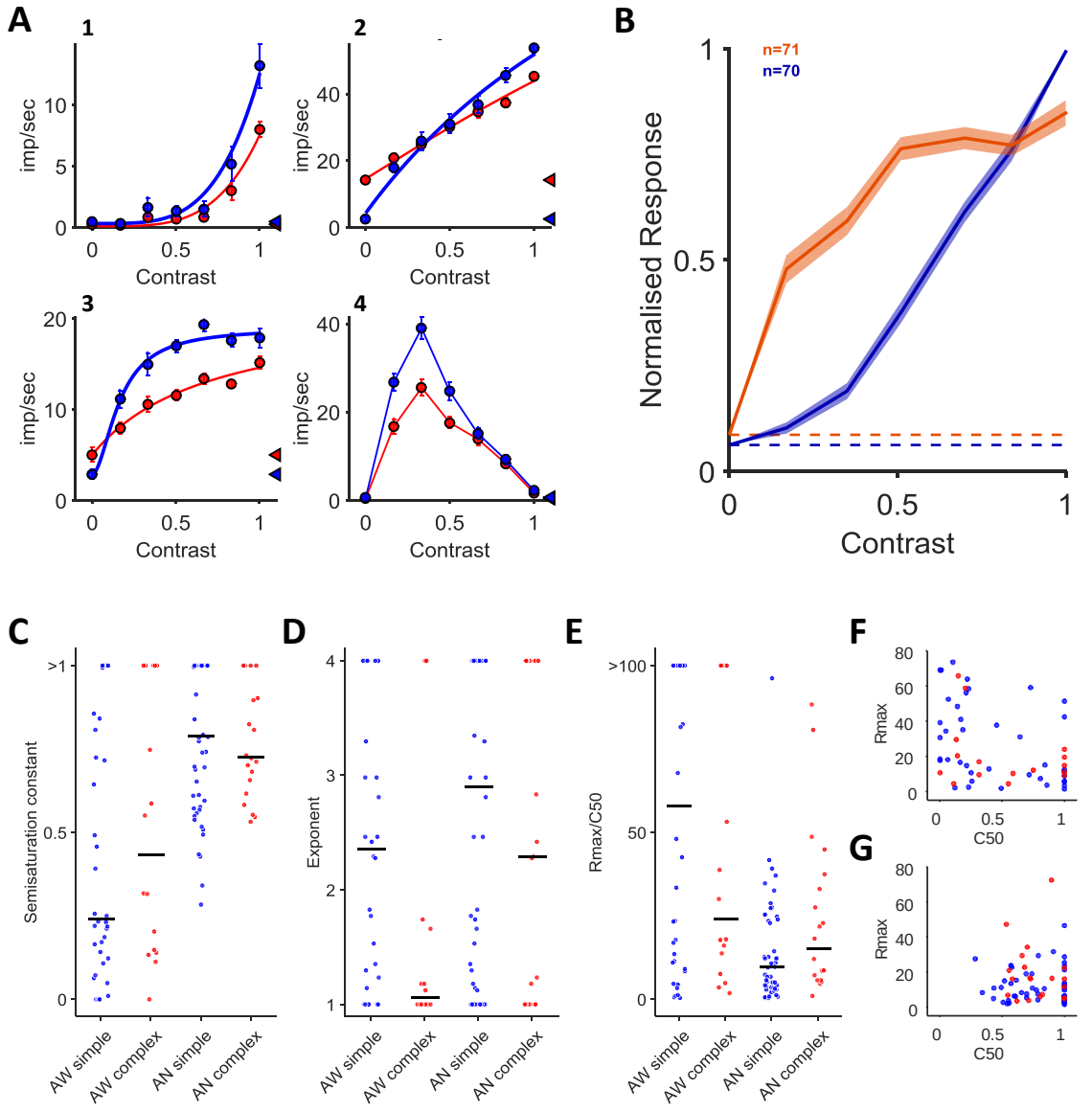

3.3.10 Contrast sensitivity

The sensitivity of neurons in the visual pathway can be characterised by the contrast response function, and in mouse primary visual cortex contrast sensitivity has been shown to be lower in anesthetized compared to awake animals (Vaiceliunaite et al., 2013). I therefore measured responses to large drifting sinusoidal gratings varying in contrast.

For each neuron I found the best predictions of a Naka-Rushton function (see Methods), from which I extracted the semi-saturation constant (C_{50}), the exponent and the maximal response. Contrast responses varied substantially, with some neurons showing response only to the highest contrasts, while others could even be bandpass, preferring intermediate contrast levels (Fig. 3.22a). These bandpass (or 'supersaturating') responses were found only in awake animals (15/71 cells, 21.1%). Since the estimate of semisaturation contrast is not well captured by a Naka-Rushton function in supersaturating cells, the subsequent analyses do not include these neurons. The supersaturation we observed in some of the neurons could reflect the activity of non-classical receptive field mechanisms, including normalization and surround suppression (see Chapter 4, Paragraph 4.3.1 and 4.3.2), which is known to increase with contrast (Sceniak et al., 1999; Solomon et al., 2006). If this was the case, supersaturating cells should display strong surround suppression. To test this, I compared the supersaturation index (1 - the ratio between the response at full contrast and the maximal response across all contrasts; an index > 0.25 indicates supersaturation) and the surround suppression index (see Chapter 4, Paragraph 4.3.1). Among the 18 units for which responses to gratings varying in both contrast and size were available, 6 showed supersaturation. Overall there was a slight positive correlation between supersaturation and suppression indices ($r = 0.53$, $p = 0.023$), indicating a tendency for supersaturating cells to have stronger surround suppression, but the numbers are small.

I observed a striking increase in contrast sensitivity from anesthetized to awake animals (Fig. 3.22b-c), with the average C_{50} across the population decreasing from a median 0.79 in anesthetized animals to 0.29 in awake animals ($p < 10^{-6}$, Wilcoxon rank sum test). Similarly, exponents were also lower in awake animals, implying less impact of threshold (Fig. 3.22d. $p < 10^{-4}$, Wilcoxon rank sum test). I found an inverse correlation between maximal firing rate and C50 in awake animals ($r = -0.39$, $p = 0.0027$) that was not present in anesthetized animals (Fig. 3.22f-g), probably because for responses linearly increasing with contrast the C50 and the maximal response are poorly defined. The difference arose from the appearance of cells with high firing rates and low semisaturation constant in awake animals. As a consequence, the distribution of the ratio between maximal response and C50, which characterises the overall

gain, shifted towards higher values in awake animals (Fig. 3.22e. $p < 10^{-4}$, Wilcoxon rank sum test). I found no differences between linear and non-linear cells (Wilcoxon rank sum test).

I conclude that SC neurons have high contrast sensitivity in awake mice, while anaesthesia profoundly decreases contrast sensitivity in SC. An analogous effect has been shown in mouse V1 (Vaiceliunaite et al., 2013), suggesting that anaesthesia is likely to similarly influence the contrast sensitivity of neurons across the visual system. Unlike V1 and LGN regions, where bandpass responses are found in both anesthetized and awake animals (Durand et al., 2016), we only encountered supersaturating neurons in awake mice.

3.4 DISCUSSION

These observations provide a comprehensive and quantitative analysis of visual receptive field properties in the superior colliculus of awake and anesthetized mice. I showed that neurons in mouse SC are highly sensitive and respond to both increases and decreases in luminance but prefer darkening stimuli, that they can have high spatial resolution and fast temporal integration, and can encode speed, direction and orientation of motion. Among these properties, contrast sensitivity and temporal integration dynamics were the most affected by anaesthesia. In the following, I first compare these observations with previous work, then compare the responses of neurons in awake and anesthetized animals.

3.4.1 Comparison with previous work in mouse SC

Previous quantitative work has generally described responses in anesthetized mice, and my observations in anesthetized animals are largely consistent with these: I find similar distribution of preferred sizes and preferred spatial and temporal frequency to Wang et al. (2010), and slightly fewer speed-tuned cells than (Gale and Murphy, 2014). Similar to Wang et al. (2010), I also found that most neurons display both ON and OFF responses, but I found a more pronounced preference for black stimuli. The discrepancy may be due to the fact that Wang et al. (2010) measured OFF responses from the offset of a white stimulus, while I measured them in response to the onset of a black stimulus.

My estimates of direction and orientation selectivity are similar to previous work that sampled across the superficial layers (Wang et al., 2010; Gale and Murphy, 2014). Recordings that instead concentrate on the uppermost layers of the SC find greater incidence of direction selectivity (Inayat et al., 2015; Shi et al., 2017). Direction selective retinal ganglion cells (DSRGCs) project to the upper portion of the superficial superior colliculus, while axons of retinal ganglion cells that do not display directional selectivity (alpha RGCs and ipRGCs) predominantly target the deeper layers (Huberman et al., 2008b; Kim et al., 2008; Huberman et al., 2009; Kim et al., 2010; Hong et al., 2011; Kay et al., 2011; Dhande and Huberman, 2014; Martersteck et al., 2017). Consistent with the anatomy there is a dorso-ventral gradient of direction selectivity in the superior colliculus, with lower direction selectivity with increasing depth (Inayat et al., 2015). In agreement with most recent studies (Wang et al., 2010; Gale and Murphy, 2014; Inayat et al., 2015; Shi et al., 2017) but in contrast with Drager and Hubel (1975) I found no particular bias in preferred direction.

One point of departure is that I found that ~70% of SC cells showed linear responses when measured with drifting or counterphase gratings. This appears to be a larger fraction than that reported for awake (Ito et al., 2017) and anesthetized animals (Wang et al., 2010), where the proportion of linear cells was ~40% and ~25%, respectively. A possible source of this discrepancy is the use of different electrodes, which is likely to bias neuronal sampling towards particular subpopulations of neurons. Some of the disagreement in awake animals (Ito et al., 2017) may also arise if analyses in that study constructed PSTHs across trials, and were thereby susceptible to eye movements (see below). However, the large fraction of linear-like neurons is also inconsistent with my own finding that most neurons in SC respond to both small white and black flashed spots, because these responses are inherently non-linear. Linear responses may nevertheless arise from ON and OFF subfields having imbalanced responses. If one subfield had stronger responses compared to the other, the summed activity would be mainly modulated in phase with the stronger subfield, resulting in nearly sinusoidal responses. Indeed, I found that SC neurons prefer black stimuli (Fig. 3.8). Additionally, SC neurons have been shown to have largely overlapping ON and OFF subfields (Wang et al., 2010); the stronger offset response to white compared to black stimuli (Fig. 3.6f,g) is therefore likely to have further strengthened the

response to black stimuli. Alternatively, as I will show in Chapter 4, responses of SC neurons are suppressed when the size of a grating is increased beyond the RF. If suppressive surrounds were particularly effective for one of the subfields, the response of the other would be more robust and dominate, linearizing the overall response. If this were the case, responses to small gratings should be more non-linear, but I found that linear cells showed F1/F0 ratio > 1 at all sizes (data not shown).

In anesthetized animals, it has been shown that the mouse superior colliculus is composed of at least four genetically, morphologically and functionally distinct neurons (Wang et al., 2010; Gale and Murphy, 2014). Horizontal cells, the prevalent class of GABAergic interneurons in the SC, are functionally distinct from narrow field, wide field and stellate neurons by means of their preferred speed (Gale and Murphy, 2014; 2016). Since most horizontal neurons prefer stimuli moving faster than 100 deg/sec and I rarely encountered neurons with such a preference, it is possible that I undersampled the population of horizontal neurons. It should nevertheless be noted that previous studies tested the velocity preference using small spots while I measured it using drifting gratings, and it is therefore likely that the discrepancy is due to the different stimuli. The functional properties observed in wide field, narrow field and stellate neurons are more overlapping, and similar to what I measured. In awake animals it remains an open question as to whether these anatomical subclasses also define functional subclasses, each of which representing certain features of the visual environment. If there are functional subclasses, and their responses were sufficiently different, it should be possible to define consistent subclasses of neurons by their responses across different stimulus sets, through for example principal component analysis (PCA). Initial attempts at PCA of response dimensions have not yet yielded clear functional subsets (not shown) but the response dimensions that should be included in the PCA are not *a priori* clear. For example, I have measured the correlation between spatial and temporal frequency preferences and found that the preferred spatial frequency is inversely correlated with the preferred temporal frequency in awake animals ($r = -0.37$, $p < 10^{-5}$, $n=157$), but not in anesthetized animals ($r = -0.16$, $p = 0.13$, $n = 92$). The inverse correlation found in awake animals is consistent with the differential preferences of linear and non-linear cells.

Linear cells preferred lower spatial frequencies and higher temporal frequencies, while non-linear cells preferred higher spatial frequencies and lower temporal frequencies.

3.4.2 Comparison with SC visual properties in other species

In rodents, the SC is a major visual centre in the brain, as demonstrated by the diverse visual deficits that follow its disruption (Schneider, 1969; Dean and Redgrave, 1984; Dean et al., 1989). In cat, a much more visual animal compared to rodents, the SC is still important for orienting behaviours towards novel or salient stimuli and for stimuli localization (Sprague and Meikle, 1965). In primates, the SC instead appears to be mainly concerned with the generation of targeted saccadic eye movements (McPeek and Keller, 2004; McPeek, 2008). Some differences between species (i.e. receptive field size, spatial frequency sensitivity) are expected from differences in their spatial acuity, which primarily reflect ganglion cell density – receptive fields are likely to be smallest in primate, larger in cat, and largest in rodents. The question that arises is if the expansion of visual cortex from rodent to cat to primate, is paralleled by a reduced functional role for the SC, and thus potentially a more specialised set of functional properties.

In cat, SC neurons similarly display ON and OFF responses and respond to a broad range of speeds (McIlwain and Buser, 1968). When compared with mouse SC, neurons in cat SC display smaller receptive fields, prefer higher spatial –and temporal frequency, and a high proportion of directionally selective neurons (McIlwain and Buser, 1968; Sterling and Wickelgren, 1969; Rosenquist and Palmer, 1971; Bisti and Sireteanu, 1976; Pinter and Harris, 1981; Waleszczyk et al., 2007; Markus et al., 2009). Neurons in the primate SC also show ON-OFF responses and are sensitive to a broad range of speeds (Schiller and Koerner, 1971; Wurtz and Albano, 1980). In contrast to mice but similar to cats, neurons in the primate SC have smaller receptive fields and prefer higher spatial –and temporal frequency compared to mice, while directional selectivity is sparser than in both cats' and mice's SC (Cynader and Berman, 1972; Tailby et al., 2012).

In conclusion, neurons in the SC of each species are more likely to show both ON and OFF responses than is observed in the retinal-thalamic pathway, and in rodent and cat direction selectivity appears more prominent than in primate. Whether this reflect different patterns of retinal input or central processing is unclear.

3.4.3 Comparison with other visual areas

Knowledge of how different areas and pathways are specialized for the analysis of certain visual features may help understanding of their functional role in visual perception. Information relative to some essential features is likely to be shared, while some others may be important for particular computations and therefore be present only in specific areas.

Neurons in the retina convey all the visual information available to the rest of the brain, and in mouse are likely to cluster in at least 30 functional output channels with distinct properties (Baden et al., 2016). In mouse, most retinal ganglion cells (RGC) project to the SC (Ellis et al., 2016). These include ON, OFF and ON-OFF RGCs. Surprisingly, the ON projections are more likely than OFF or ON-OFF (Ellis et al., 2016), and the larger response to black stimuli that I observe suggests that the gain of OFF inputs is selectively increased. The directional and speed sensitivity I found in SC is likely to be at least in part inherited from the retina: 40% of retinocollicular RGCs are directionally selective neurons (DS-RGCs) and sensitive to a broad range of speeds (Gauvain and Murphy, 2015). A number of genetically identified subpopulations of RGCs have been shown to project to the SC: the non-directional, ON-OFF W3 RGCs, and the directional OFF J-RGCs and ON-OFF BD-RGCs (Zhang et al., 2012; Kim et al., 2010). W3 cells have small ON-OFF receptive fields with high spatial resolution, are non-linear, and sensitive to moving stimuli (Zhang et al., 2012). The functional properties of non-linear cells in the SC resemble most of those in W3 RGCs, and are therefore likely to receive inputs from them. The broad range of visual properties available from RGCs make it likely that many of the functional properties I observed in SC neurons are inherited from the retina, and the role of biophysical properties in SC and/or intracollicular and intra-areal circuits remain to be determined.

RGCs that project to SC seem to prefer smaller stimuli, higher speeds and display more transient responses than those projecting to the dLGN (Ellis et al., 2016). Does the differential retinal input translate in different visual properties in SC and LGN? In line with retinal projections, neurons in the LGN seem to prefer slightly larger stimuli compared to SC (cf. Piscopo et al., 2013). Nevertheless, neurons in the two areas prefer similar spatial and temporal frequency, have similar orientation selectivity, and a substantial proportion of them is sensitive

to high speeds, while the level of directional selectivity in LGN is controversial (Piscopo et al., 2013; Durand et al., 2016). SC and LGN visual properties may therefore be more similar than would be expected from the differential retinal input. It is possible that the resemblance derives from colliculo-geniculate and/or cortico-collicular projections.

Are there clear differences between SC visual properties and those of visual cortex? The distribution of preferred spatial frequencies is similar between SC and primary visual cortex (cf. Andermann et al., 2011; Durand et al., 2016). Given the large variability in resolution encountered among neurons of either pathway, it is difficult to infer where fine-grained pattern analysis is computed. V1 has stronger orientation and direction selectivity than SC (Andermann et al., 2011; Durand et al., 2016), suggesting it may have a more prominent role in analysing these properties. In awake animals, V1 prefers lower temporal frequency and lower speeds than the SC, leading to the observation that subcortical structures (SC and LGN) respond better than primary visual cortex to fast stimuli (Andermann et al., 2011; Durand et al., 2016). Interestingly, SC lesions have shown that the SC does not influence the velocity tuning in V1, but do shape the velocity tuning of higher visual cortical areas, via area-specific subdivisions of the lateral posterior nucleus of the thalamus, making them sensitive to high speeds and recovering the loss of information about fast stimuli that occurs in V1 (Tohmi et al., 2014).

3.4.4 Influence of eye movements

Eye movements are an unavoidable feature of experiments in awake animals. Our measurements show that eye movements in mice are large enough to produce clear effects on visual response, and can confound some analyses. The response of a linear receptive field is by definition dependent on the position (equivalently, phase) of any stimulus, and eye movements shift the position of stimuli with respect to receptive fields. Our measurements show that the impact of eye movements can, to some degree, be mitigated by analysing individual trials where those trials have relatively short durations. Previous work has shown a bias to non-linear responses in V1 and LP of both anesthetized and awake mice, while in LGN neurons switched from being mainly linear in anesthetized animals to predominantly non-linear in awake animals (Durand et al., 2016). This discrepancy in LGN may arise if the authors averaged spiking activity

across trials before performing Fourier analyses, but the method is not stated. Because the receptive fields of LGN neurons are smaller than those in LP, and more linear than those in V1, their responses are more likely to be susceptible to eye movements. I note however that I also observe stronger responses to high spatial frequencies in SC in awake animals – and the neurons conveying high spatial frequency responses are likely to be non-linear cells. One possibility that arises is that anaesthesia selectively reduces the activity of non-linear neurons (or the non-linear components of their receptive fields).

The SC is important for sensorimotor integration, and may therefore help transform a retinal coordinate frame to one that is independent of eye position and thus more useful for behaviour. Indeed, in primates saccades originating from SC activity are known to be encoded in spatial rather than retinal coordinate frames (Mays and Sparks, 1980). Similarly, neurons in deeper layers of monkey SC shift their receptive fields towards a location predicted by an upcoming saccade, a phenomenon known as perisaccadic remapping and thought important in maintaining perceptual stability (Churan et al., 2012). In mouse eye movements are relatively small and do not appear to be goal directed, and the necessary translation between retinal and head-centred coordinate frames may therefore be negligible compared to monkeys. I have shown that eye movements shift the representation of the retinal image in SC. Whether neurons in mouse SC, like those in primate SC, help transform retinal to spatial coordinate frames may be a question worth pursuing.

3.4.5 Effect of anaesthetic state

Measurements from anesthetized animals reduce variability arising from, for example, motivational or emotional states. On the other hand, anaesthesia introduces other potential confounds by potentially modifying brain network dynamics and neurons' intrinsic biophysical properties. In agreement with previous work in LGN and V1 of mouse (Vaiceliunaite et al., 2013; Durand et al., 2016), I found anaesthesia-dependent changes in a variety of response properties. The most prominent difference is a marked increase in responsivity in awake animals, accompanied by a pronounced reduction in response latency. Anaesthesia mainly affected responses to high temporal frequency stimuli, similar to what has been observed in rat barrel

cortex (Devonshire et al., 2010), and I found more speed tuned cells in awake than in anesthetized animals. I note however that the reduced encounter rate of speed-tuned neurons in anesthetized animals may be confounded by the narrower sensitivity envelope for both spatial and temporal frequency in anesthetized mice.

I found larger receptive fields in awake animals when these fields were measured with small flashing stimuli. When stimulated with patches of increasing size, however, the preferred size and the CRF center size were smaller in awake animals. These observations are nevertheless consistent. Reduced sensitivity during anaesthesia may induce an "iceberg effect", mainly affecting the response from peripheral flanks of the receptive field when probed with flashing small squares. Increasing the size of a patch instead allows peripheral regions of the receptive field to still contribute to spatial summation.

I also found stronger direction and orientation selectivity in awake animals, almost twice that in anesthetized animals. This may partially reflect undersampling of the uppermost layers of SC in anesthetized animals. A more intriguing possibility is related to the fact that direction tuned cells receive directionally tuned input from the retina that is amplified by intracollicular excitatory connections between neurons with similar directional preferences (Shi et al., 2017). Anaesthesia may have an impact on either retinal or intracollicular mechanisms, for instance by reducing membrane conductances (Wang et al., 2014). The reduced conductance combined with a nonlinear threshold could reduce direction selectivity under anaesthesia. In addition, inhibitory intracollicular neurons are also likely to shape directional selectivity. In contrast to inhibitory neurons in primary visual cortex, which are less direction- or orientation selective than excitatory cells (Niell and Stryker, 2008), collicular $GAD2^{+}$ neurons show direction selectivity (Inayat et al., 2015). If, as is the case in primary visual cortex, wakefulness strongly increases inhibition (Haider et al., 2013), the increase in selectivity I observed could partly be due to increased role of inhibitory interneurons.

My observations do not specify the mechanisms that bring about the differences observed between awake and the anesthetized animals. However, anaesthesia may reduce the spontaneous and evoked firing rate of neurons by decreasing membrane conductance, thereby increasing the membrane time constant, and making it harder for the voltage to reach the

spiking threshold (Sceniak and Maciver, 2006; Haider et al., 2013; Wang et al., 2014). This would also increase response latency. Alternatively, anaesthesia may increase the conductance of specific background leak channels, implementing shunting inhibition: in rat cortical pyramidal neurons urethane causes Ba^{2+}-sensitive K^{+} channel to open, inducing a decrease in input resistance and a divisive change in firing rate (Sceniak and Maciver, 2006). In addition to changing the biophysical properties of SC neurons, anaesthesia is also likely to influence neurons sending the inputs to the SC. Reduced retinal activity cannot be ruled out. Feedback from primary visual cortex has also been shown to boost the gain of SC neurons (Zhao 2014), and the firing rate of V1 neurons decreases under anaesthesia (Vaiceliunaite et al., 2013).

3.5 CONCLUSION

The quantitative description of SC visual functional properties reported here provides a foundation for future studies aimed at uncovering the neural mechanisms underpinning these responses as well as intracollicular and inter-areal network dynamics.

Chapter 4

Neuronal correlates of visual saliency in mouse superior colliculus

4.1 INTRODUCTION

In Chapter 3 I presented the basic response properties of visual neurons in mouse superior colliculus (SC) in the framework of how receptive fields are generally described in the visual system, ignoring more modern concepts of receptive field organization such as non-classical receptive fields. Here, I will examine these functional properties of SC neurons, which may be important for the representation of salience. Attribution of salience to potential objects is essential for animals' survival, facilitating identification of potentially behaviourally important objects such as, for example, preys or predators. A stimulus is salient if it is dissimilar from its surroundings in either space or time. Possible neural mechanisms available in the brain for detecting salience may be non-classical receptive fields and adaptation.

The classical receptive field (CRF) is the portion of visual space from which activity can be elicited in a visual neuron (Hartline, 1940; Kuffler, 1953; Hubel and Wiesel, 1959). However, the CRF of most neurons is embedded in a larger non-classical receptive field (nCRF). This region can

have no effect on the spontaneous firing rate when stimulated alone, but modulates the response of the CRF when they are simultaneously stimulated (Allman et al., 1985b). The influence that the nCRF exerts over the CRF is usually suppressive, and has been shown to be stronger when the visual features over the nCRF match those over the CRF (Sillito et al., 1993; DeAngelis et al., 1994; Sillito et al., 1995; Levitt and Lund, 1997; Cavanaugh et al., 2002b; Muller et al., 2003; Girman and Lund, 2007; Ozeki et al., 2009; Shushruth et al., 2013; Self et al., 2014). As a consequence, suppression from nCRFs can trim neuronal responses, highlighting portions of the visual space that are different from the surroundings and making neurons sensitive to spatial context. The nCRF may therefore help the representation of salience through spatial competition. Surround suppression is a product of the nCRF known to be present in the retina, lateral geniculate nucleus, superior colliculus, primary visual cortex and higher cortical areas (Sterling and Wickelgren, 1969; Allman et al., 1985b; Jones et al., 2000; Solomon et al., 2002; Solomon et al., 2006; Vaiceliunaite et al., 2013; Self et al., 2014).

Through adaptation the response of neurons diminishes when stimuli are uniform over time, making them sensitive to recent stimulus history, more responsive to novel stimuli and therefore reducing the transmission of redundant information (Solomon and Kohn, 2014). Adaptation is a pervasive feature in visual coding and perception (Webster, 2015) and has also been observed throughout the visual system, from the retina (Smirnakis et al., 1997; Baccus and Meister, 2002), to the thalamus (Solomon et al., 2004) and superior colliculus (Boehnke et al., 2011), to the frontal eye fields (Mayo and Sommer, 2008). Adaptation can act on diverse timescales ranging from tens of milliseconds to hours (Baccus and Meister, 2002; Webster, 2015). Here I will concentrate on fast adaptation processes, within the first few hundreds milliseconds after stimulus onset.

The superior colliculus is a midbrain area that may be important in the representation of salience. It receives direct retinal input, primarily to the superficial layers, multisensory information in the intermediate layers, and provides descending motor outputs from the deep layers (Drager and Hubel, 1975; May, 2006; Gandhi and Katnani, 2011). The SC is important in controlling spatial attention and has been shown to be essential for the detection of a stimulus

among competing ones, guiding head and eye position towards interesting stimuli or away from threatening ones.

In mouse, the SC is the main target of retinal projections (Ellis et al., 2016), but little is known about the characteristics of nCRFs or adaptation mechanisms, particularly in awake animals. I establish this here, and find that most neurons in the mouse SC show nCRFs and are therefore modulated by spatial context. I characterise the visual selectivity of surround suppression and show that nCRFs are stronger when contrast, direction or temporal frequency surrounding the CRF match those over the CRF. In addition to the presence of nCRFs, I show that most neurons in the mouse SC also show strong adaptation, and that nCRF suppression and adaptation tend to be co-expressed, making neurons in the SC a suitable neural substrate for saliency detection in space and time. Finally, I show that the suppression provided by the nCRF, but not its tuning, adapts over time.

4.2 METHODS

All procedures were conducted in accordance with the UK Animals Scientific Procedures Act (1986). Experiments were performed at University College London under personal and project licenses released by the Home Office following appropriate ethics review.

4.2.1 Preparation

I performed acute extracellular neural recordings from anesthetized and awake mice, and chronic recordings from awake mice, in the superficial layers of the SC. For surgical, histological, visual stimulation and recording procedures, please refer to Chapter 3 (Section 3.2.1).

4.2.2 Visual stimuli

I first hand-mapped the receptive field position and adjusted the monitor location accordingly using a flexible arm to centre the receptive fields on the monitor. In those cases where the receptive field location was difficult to determine, I positioned the stimuli at the location of maximal activity in response to small flashing squares (see Chapter 3.2.2, *sparse noise stimulus*). Unless specified, stimuli lasted for 2 s with an interstimulus interval of 0.5 s. Each set

of stimuli included a blank condition (where the screen was held at the mean luminance) from which the spontaneous firing rates were estimated. Each set of stimuli was presented in pseudorandom order for 4-10 repetitions.

Size tuning. To measure the spatial summation properties of neurons, I used drifting sinusoidal gratings ranging in size from diameter 2° to 90° on a logarithmic scale. The parameters of the grating were chosen based on responses of isolated cells to the stimuli described in Chapter 3 (Sections 3.2.2, 3.2.3). I used the highest spatial frequency that could induce robust activity, to minimise the impact of the classical surround. In separate experiments, I presented large (80° outer diameter) annular gratings where the central part of the grating was obscured by a mean grey screen at each of 6 diameters (5°, 7.5°, 11.5°, 17.45°, 26.4°, 40°).

Central and annular drifting gratings. To investigate nCRF properties, I used combinations of a central grating surrounded by a large (80°) annular grating, as follows. The central patch was of fixed size, direction, spatial and temporal frequency. The parameters of the central grating were chosen as above. The annular grating had the same properties of the central patch unless specified, with a temporal frequency 0.5 Hz higher unless varied (see below). To measure the contrast sensitivity of nCRF and the interactions between contrast over the CRF and nCRF, I used a matrix of 5 contrasts for the central and the annular grating (0, 0.25, 0.5, 0.75, 1). In all other measurements, both the central and annular gratings were of contrast 1. To measure direction selectivity of nCRF I varied the annular grating in 8 directions, in 45° steps. To measure nCRF temporal frequency tuning I used annular gratings of 6 temporal frequencies (0.4688, 0.9375, 1.8751, 3.7502, 7.5, 15 cyc/sec). In each case, I also measured responses to the central gratings and key surrounding stimuli presented alone. It should be noted that although I focused on one unit in each recording to set the parameters of the visual stimuli, in most of the cases I recorded more than one neuron at the same time. Therefore, the stimulus properties may not be optimal for all units.

4.2.3 Data analysis

All offline analysis was performed using Matlab (MathWorks, Natick, MA, USA). Peristimulus time histograms (PSTHs) were constructed for each trial and subjected to Fourier analysis. I always extracted the mean firing rate (F0), and the modulation amplitude of response at the stimulus temporal frequency (first harmonic; F1). For further analysis, I used the F0 response for non-linear cells and the F1 response for linear cells (Skottun et al., 1991) (See Chapter 3, Section 3.3.3, *Linearity of spatial summation in response to drifting gratings*). When the spatial frequency tuning was not available, I used the F0 for all analyses. Unless stated, I refer to responses as stimulus evoked activity (F0 or F1 after subtraction of spontaneous firing rate). The optimal parameters for each model fitting were estimated using the Matlab function *lsqcurvefit*. In figures, statistical significance is indicated by **p<0.05*, ***p<0.01*, ****p<0.001*. Statistical tests are specified in the text. Unless stated, error bars indicate ± 1 S.E.M.

Size tuning. To characterise the dependence of response on the size of a grating patch I assumed that both the CRF and the nCRF could be described by concentric circular two-dimensional Gaussians (Solomon et al., 2006). The CRF excitatory activity (*Le*) to a grating of diameter *d* is proportional to the integrated volume of a Gaussian:

$$L_e(d) = \frac{2}{\sqrt{\pi}} \int_0^d e^{-(x/r_e)^2} dx \qquad \textit{(Eq. 4.1)}$$

where r_e is the CRF Gaussian envelope. A similar expression can be derived for the larger nCRF Gaussian (*Li*). I assumed that the nCRF has divisive influence on the activity of the CRF (Sceniak et al., 2001;Cavanaugh et al., 2002a), such that response is:

$$R(d) = \frac{K_e L_e(d)}{1 + K_i L_i(d)} \qquad \textit{(Eq. 4.2)}$$

where K_e and K_i are respectively the excitatory CRF and the suppressive nCRF gains. I estimated the preferred size from the model fit as the smallest size reaching 95% of the maximal response. To quantify the amount of suppression displayed by each cell, I calculated a suppression index (SI) as:

$$SI = 100 \times \frac{R_{opt} - R_{large}}{R_{opt}} \quad \textit{(Eq. 4.3)}$$

where R_{opt} is the response amplitude at the preferred size and R_{large} is the response amplitude at the largest tested size. I considered neurons as suppressed if SI > 10%.

Tuning of suppression. To characterise the tuning of the nCRF I computed a suppression index (SI):

$$SI = 100 \times \frac{R_{cent} - R_{test}}{R_{cent}} \quad \textit{(Eq. 4.4)}$$

where R_{cent} is the response amplitude to the central patch presented alone, and R_{test} is the response amplitude to the simultaneous presentation of the patch and the annulus. I used the SI to calculate a global direction selectivity index (gDSI) and a global orientation selectivity index as in Equations (3.12) and (3.13) respectively, substituting θ for the direction of the surrounding grating.

Adaptation index. I derived an adaptation index (AI) to characterise the change in response to a stimulus over time:

$$AI = 100 \times \frac{R_{transient} - R_{sustained}}{R_{transient}} \quad \textit{(Eq. 4.5)}$$

where $R_{transient}$ and $R_{sustained}$ are the average evoked activity during the first and last 0.5 s of stimulus presentation, respectively (stimuli lasted for 2 s, unless stated).

Time course of nCRF suppression tuning. To characterize how time affected nCRF suppression, I analyzed responses to the simultaneous presentation of a fixed central grating and a surrounding grating varying in either direction or temporal frequency. For each cell I calculated the average firing rate in response to all stimuli during the first 0.5 s and during the last 0.5 s of stimulus presentation, therefore using the F0 response. If the early or late responses to the center presented alone were not significantly larger than the spontaneous firing rate, or higher than the activity elicited by the surround presented alone (for details, see below), the

corresponding tuning curve was excluded from the analysis. Suppression indices were then independently calculated as discussed above.

4.2.4 Inclusion criteria

I considered neurons visually responsive if their maximal response was at least 1.4 spk/sec, and exceeded the mean maintained rate by at least 1.25 s.d. of that rate (anesthetized recordings) or 1.5 s.d. (awake recordings). In awake animals, where I often recorded from multiple units simultaneously, I included additional selection criteria: the estimated RF center needed to be within 10° of the stimulus center, and this was manually checked for each unit. In addition, I only included neurons in which the response to the center stimulus presented alone was larger than that to the surround stimulus presented alone.

4.3 RESULTS

In the following, I first show that non-classical receptive fields modulate the responses of most neurons in the SC of awake mice. I then describe nCRFs selectivity for contrast, pattern, and speed discontinuities in visual space, and report the effects induced by anaesthesia. The second part of the chapter investigates adaptation in the SC of awake animals and how it relates to nCRF suppression in single neurons, also comparing the measurements obtained in awake and anesthetized mice. The last section attempts to unveil the effect of adaptation on nCRF selectivity.

4.3.1 Non-classical receptive fields of neurons in superior colliculus of awake mouse

When the non-classical receptive field (nCRF) is larger than the classical receptive field (CRF) it is readily revealed by measuring the dependence of neuronal response on the size of a patch of drifting grating. Figure 4.1a (top) shows example cells. The firing rate first increases with stimulus size and then declines. The initial increase in response reflects the integration area of the CRF. Because I used relatively high spatial frequencies, this is primarily the centre mechanism of the CRF - the CRF surround is largely blind to these stimuli. The decrease in response for sizes

larger than the preferred reflects the suppression provided by the nCRF. I observed a variety of size tuning among SC neurons (Fig. 4.1a, top), but the majority of neurons showed surround suppression (Fig. 4.1b,c). Fig 4.1b shows average size tuning curves across the population of recorded neurons.

To characterise the size tuning curves, I found the best predictions of a ratio of Gaussian model (Fig. 4.1a, top) (Sceniak et al., 2001; Cavanaugh et al., 2002a), where the CRF and the nCRF are modelled as Gaussians and the nCRF divisively modulates the activity of the CRF (see Methods). From these model predictions I estimated the size and gain of the CRF and nCRF, the preferred grating size, and the suppression index (SI), which is the proportional reduction in response from the preferred to the largest size (neurons totally suppressed by large gratings would have an SI of 100%) (Fig.4c-f). I found a median SI of 65.2% (μ 57.6%, s.d. 32.8%), with 85/98 neurons (86.7%) displaying a SI > 10%. In most of the analyses below I include only units with SI greater than 10%. Neurons responded best to stimuli 11.8° in radius (μ 11.2°, s.d. 10.8°). The median estimated radius of the CRF was 18.7° (μ 15.8°, s.d. 19.1°), while the nCRF radius was on average 63° (μ 67.1°, s.d. 257.1°). The CRF gain was estimated to be on average 23.2 (μ 181.6, s.d. 332), while the nCRF gain was 22.8 (μ 195.8, s.d. 312.8).

To establish the contributions of CRF centre in response to gratings increasing in size, I stimulated the cells with an annular grating of increasing inner sizes (Fig. 4.1a, bottom). The use of a grating largely avoids the recruitment of the CRF surround, and therefore the response decreases sharply as the annulus inner edge extends towards the periphery of the CRF centre. Comparison with the size tuning curves (Fig. 4.1a, top) shows that in many cells nCRF suppression starts at sizes at which the CRF is still active, highlighting the spatial overlap between classical and non-classical receptive field activity.

I conclude that the CRF activity of most SC neurons is modulated by nCRFs implementing surround suppression and summating over a portion of visual space larger than the CRF centre. These results confirm previous studies showing that the presence of surround suppression is a common feature of SC neurons in many species (mouse: Wang et al., 2010; Gale and Murphy, 2014 rat: Girman and Lund, 2007; cat: Sterling and Wickelgren, 1969; monkey: Cynader and Berman, 1972; Goldberg and Wurtz, 1972a).

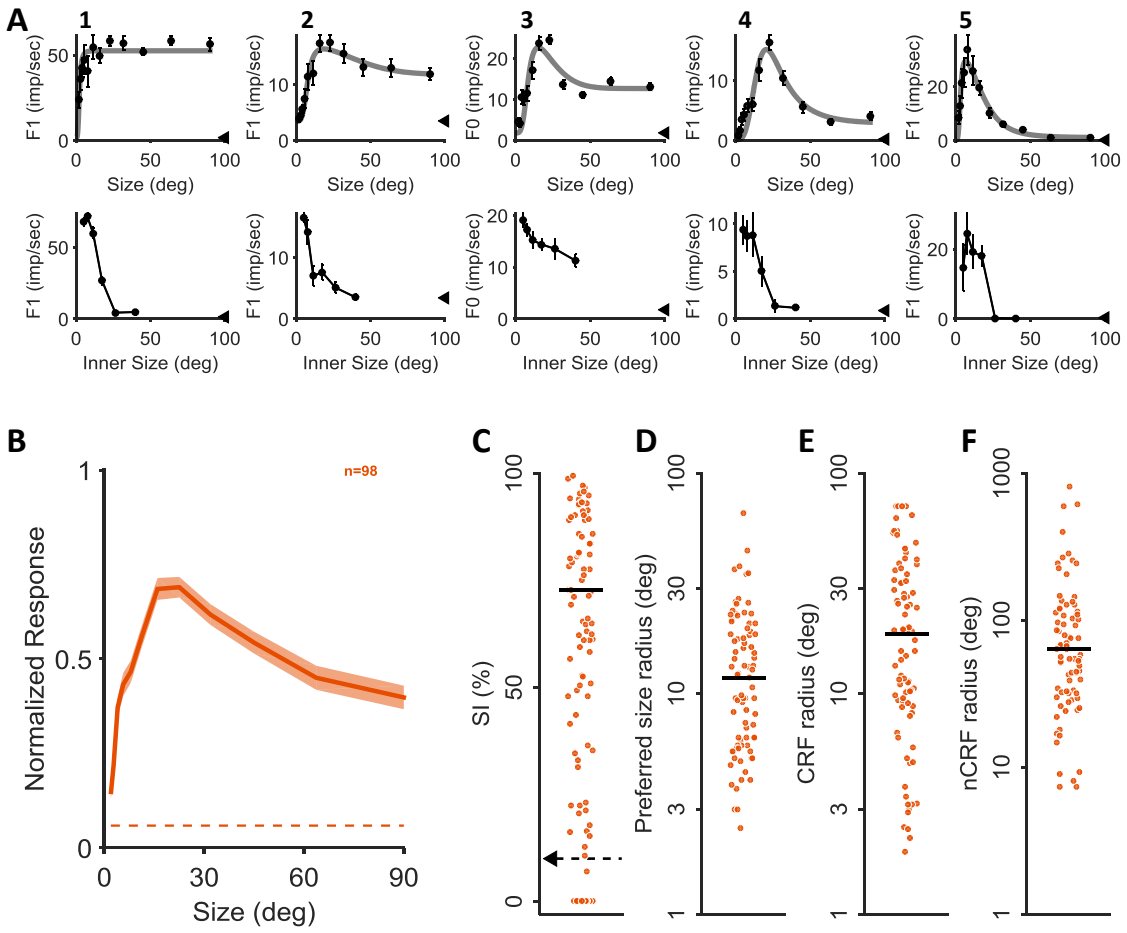

Figure 4.1. Spatial summation in SC cells of awake animals. I presented a patches of drifting sinusoidal gratings of fixed direction and temporal frequency, varying in size. ***A.* 1-5.** *Top.* Example responses of individual neurons to drifting sinusoidal gratings of varying size. F1 or F0 was used to characterize cells classified as linear or non-linear, respectively. Points indicate response ± 1 s.e.m. Arrow heads indicate spontaneous activity. Solid grey lines show the best fit of a ratio-of-Gaussians model. The optimal parameters for each cell were: **1)** K_e 44; K_i 6.1; r_e 4.2; r_i 4.2 **2)** K_e 77.7; K_i 26.9; r_e 27.7; r_i 31.6 **3)** K_e 29; K_i 8.7; r_e 15.7; r_i 20.1 **4)** K_e 4.5; K_i 2.5; r_e 9.3; r_i 36.4 **5)** K_e 196.6; K_i 202.2; r_e 14.9; r_i 36.6. The estimated SI was **1)** 0%, **2)** 35%, **3)** 48%, **4)** 81%, **5)** 97%. *Bottom.* Example responses of the neurons in *top* to annular drifting sinusoidal gratings of increasing inner size. Note that for cells 2, 3 and 5 surround suppression (top) starts at sizes in which the CRF is still summating. ***B***. Population average of normalized size tuning curves of neurons recorded in awake mice. Dashed lines indicate normalized average spontaneous activity. ***C***. Distribution of suppression indices across the population of neurons (SI. median 65.2%; mean 57.6%; s.d. 32.8%; n = 98). Arrow indicates SI = 10%. In subsequent plots, cells with SI≤10 were not included. ***D-F***. Distribution of estimated ratio-of-Gaussian parameters. Horizontal bars represent median. ***D***. Preferred sizes (median 11.8°; geomean 11.2°; s.d. 10.8°; n = 85). ***E***. Classical receptive field sizes (median 18.7°; geomean 15.8°; s.d. 19.1°; n = 85). ***F***. Non classical receptive field sizes (median 63.4°; geomean 67.1°; s.d. 2.57.1°; n = 85).

4.3.2 Selectivity of non-classical receptive fields

Above I showed that nCRFs allow neurons to integrate visual information over a region larger than their CRF. If nCRFs are a mechanism for salience, the modulation that they exert on the CRF activity should depend on the presence – or absence – of a visual discontinuity. That is, the action of the nCRF should highlight patterns that are different from their surroundings, and nCRFs should suppress responses to homogenous patterns. I therefore sought to determine if the action of nCRFs in SC is sensitive to visual discontinuities.

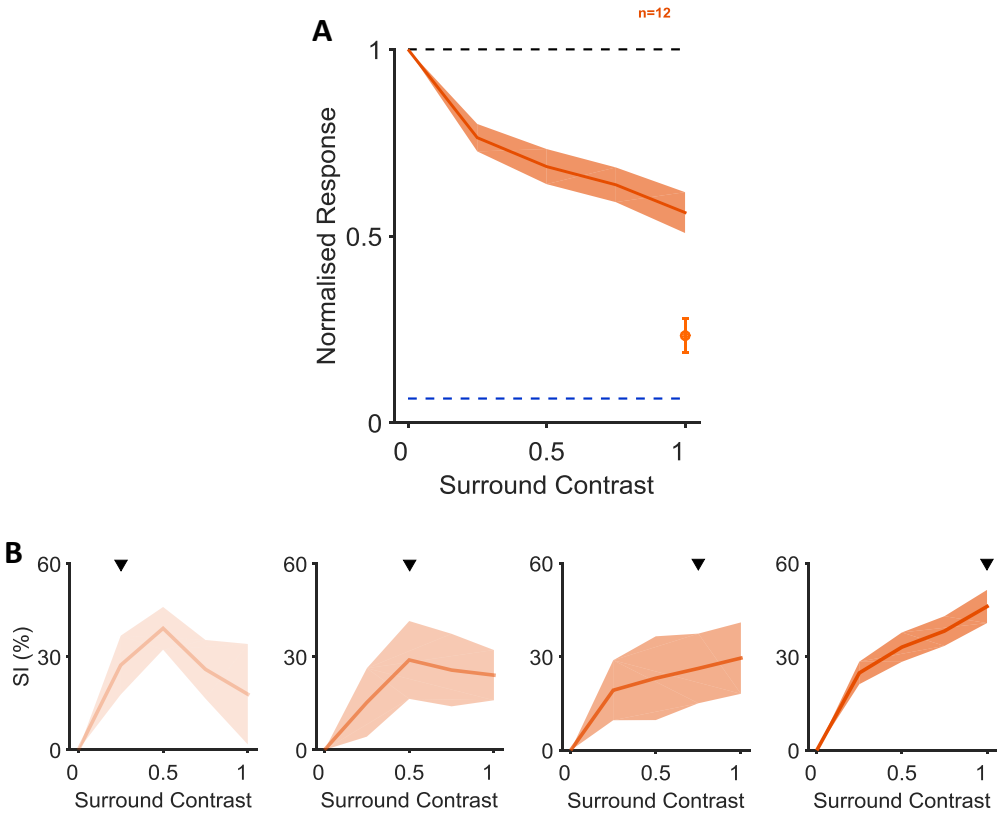

Figure 4.2. Non-classical receptive fields' sensitivity and selectivity to contrast in awake animals. ***A***. Population average of responses to simultaneous presentation of a central grating patch of fixed properties (size [diameter: μ 24.3°, s.d. 6.9] contrast, spatial frequency, temporal frequency, direction) and a surrounding grating varying in contrast (orange solid line), normalized to the response of a maximum contrast central patch presented alone (black dashed line). The bottom blue dashed line indicates the mean spontaneous activity. The isolated data point indicates the average response to maximal contrast annular grating presented alone. ***B***. Population average of suppression tuning curves in response to surrounds increasing in contrasts, using patches of different contrasts over the centre. Arrow heads indicate centre contrast (from left to right: 0.25, 0.5, 0.75, 1).

Contrast discontinuities

The simplest discontinuity in a pattern is a change in contrast. To characterise the contrast response of the nCRF, I measured the responses to a small grating patch centred over the CRF, while presenting annular patches of varying contrast (but otherwise identical). As expected, suppression generally increased with increased contrast of the annular grating (Fig. 4.2a). I next asked whether suppression from the nCRF depended on the contrast over the CRF. Fig. 4.2b shows the contrast tuning of annular suppression for each contrast of the central grating. Suppression saturated at low contrasts when the central grating was of low contrast; when the central grating was of higher contrast, annular suppression showed little saturation. In other words, surround suppression appeared tuned for the central patch contrast, being stronger when the contrast over the nCRF was similar to the contrast over the CRF.

Pattern discontinuities

Spatial discontinuities may also arise from a change in the spatial pattern. To characterise the sensitivity of nCRF suppression to pattern discontinuities I therefore varied the orientation (and motion direction) of the annular grating. I encountered many neurons in which suppression was strikingly dependent on the orientation of the annulus grating (Fig 4.3a). Fig 4.3c shows population average tuning after aligning to the orientation/direction that elicited maximal suppression. Suppression is clearly tuned for orientation and direction (Fig. 4.3c-f). To characterise the degree of orientation and direction selectivity of suppression in individual neurons, I used the vector sum (see Methods) to calculate global indices of orientation selectivity (gOSI) and direction selectivity (gDSI). On average, the gDSI was 0.23 (median, 0.13, s.d.; 0.21), with 24/64 units (37.5%) showing strong directional selectivity (gDSI ≥ 0.25). The average gOSI was 0.26 (median, 0.2; s.d. 0.2), with 25/64 cells (39%) showing strong orientation selectivity (gOSI ≥ 0.25).

Many SC neurons are selective for the direction or orientation of a moving grating and I therefore asked if tuned nCRF activity was more likely to be found in those units showing orientation or direction tuning for conventionally large, single patches of drifting grating. I found no correlation between nCRF tuning and conventional tuning for orientation or direction

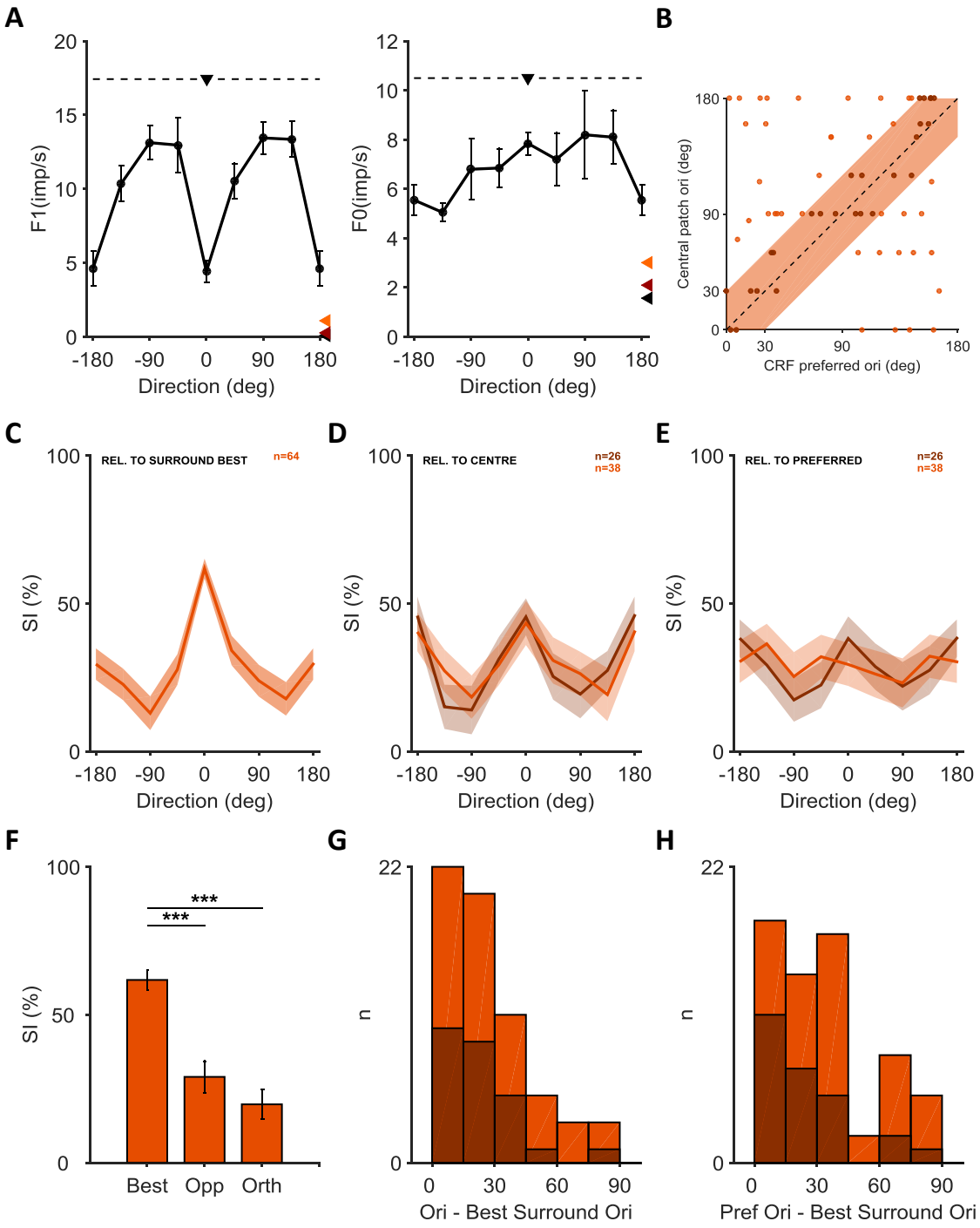
A
F1(imp/s)
Direction (deg)
F0(imp/s)
Direction (deg)
B
Central patch ori (deg)
CRF preferred ori (deg)
C
REL. TO SURROUND BEST
n=64
SI (%)
Direction (deg)
D
REL. TO CENTRE
n=26
n=38
SI (%)
Direction (deg)
E
REL. TO PREFERRED
n=26
n=38
SI (%)
Direction (deg)
F
***
***
SI (%)
Best
Opp
Orth
G
n
Ori - Best Surround Ori
H
n
Pref Ori - Best Surround Ori

(Fig. 4.4). Neurons displaying tuned responses to a grating were therefore not necessarily those ones showing tuned modulation from the surrounding spatial context.

To gain insight into the mechanisms that underpin nCRF selectivity, I asked whether the tuning of suppression depended on the stimulus preferred by the neuron or on the stimulus used for the central patch. If the tuning of suppression was similar to that preferred by the neuron, it would indicate that suppression arises in a fixed pool of activity from neurons with similar tuning preferences. If suppression was instead better predicted by the central stimulus, it would indicate a more flexible mechanism of pooling in the nCRF. I found that suppression was stronger for annular gratings of the same orientation as the central grating. This is shown by Fig 4.3d, which plots the population average tuning after aligning each curve to the central patch direction. Similarly, in most neurons the stimulus orientation presented to the centre was the orientation preferred by the nCRF (Fig. 4.3g). This remained the case if I only considered

Figure 4.3. Directional selectivity of suppressive fields in awake recordings. I presented a central grating patch of fixed properties (size [diameter: μ 30°, s.d. 12.3°], contrast, spatial frequency, temporal frequency, direction) surrounded by an annular grating of varying directions. ***A***. Amplitude of responses for two example units. Solid lines indicate the responses to simultaneous presentation of a central grating and annular grating of varying direction. The directions of the annular gratings are shifted so that 0 is the direction of the central grating. Top dashed lines indicate the response to the central grating presented alone. Downward arrow heads indicate centre direction. Leftward arrow heads indicate background activity (black) and response to parallel (red) and orthogonal (orange) surrounding stimuli presented alone. ***B***. Scatter plot of CRF preferred orientation and orientation used for the central patch (n=64). Dashed line is the unity line. Dashed area and dark dots indicate neurons in which the central patch orientation was within 30° form the CRF preferred orientation (n=26). ***C***. Population average of suppression in response to simultaneous presentation of a central and surrounding grating varying in direction. Individual tuning curves of suppression were shifted to make 0 the direction eliciting maximal suppression (n=64). ***D.*** Population averages of suppression in response to simultaneous presentation of a central and surrounding grating varying in direction. Individual tuning curves of suppression were shifted to make 0 the direction of the central grating. Dark and light orange lines indicate average tuning curve for cells in which the central patch orientation was or wasn't within 30° from the CRF preferred orientation, as in *B* (darker, n=26, lighter, n=38). ***E***. Population average of suppression in response to simultaneous presentation of a central and surrounding grating varying in direction. Individual tuning curves of suppression were shifted to make 0 the direction preferred by the CRF. Colour code as in *B-D.* ***F***. Average population suppression index at surround directions eliciting maximal suppression (Best dir, SI_{θ}) was significantly higher than at the opposite directions (Opposite dir, $SI_{\theta+\pi}$, $p < 10^{-11}$, Wilcoxon signed rank test) and averaged SIs at orthogonal directions (Orthogonal dir, $(SI_{(\theta+\pi/2)}+SI_{(\theta-\pi/2)})/2$, $p < 10^{-11}$, Wilcoxon signed rank test). ***G.*** Difference in orientation between center and surround eliciting maximal suppression (n=64). Dark bars indicate neurons in which the central patch orientation was within 30° form the CRF preferred orientation, as in *B,D* (n=26). ***H.*** Difference between CRF preferred orientation and surround orientation eliciting maximal suppression (n=64). Dark bars indicate neurons in which the central patch orientation was within 30° form the CRF preferred orientation, as in *B,E* (n=26).

neurons in which the central patch orientation was not within 30° of the preferred orientation (~60% of the tested neurons; Fig. 4.3b-d-g, lighter). The preferred orientation of the neuron did not explain the preferred orientation of the nCRF. This is shown by Fig 4.3e, which plots population average responses after aligning tuning curves to the preferred orientation of the neuron. Tuning is much less pronounced, and there is less relationship between preferred orientation and that preferred by the nCRF (Fig. 4.3h). The residual tuning is mainly due to those cells in which the direction used in the central patch was close to the CRF preferred (Fig. 4.3b-e-h, darker).

In summary, neurons in the SC of mouse can detect discontinuities in visual patterns. This appears to arise from a flexible mechanism that is sensitive to the statistics over both the CRF and the spatial context in which it is embedded. The sensitivity of surround suppression for pattern discontinuities has been observed in a variety of species in both SC (rat: Girman and Lund, 2007; cat: Sterling and Wickelgren, 1969) and other visual areas (Li and Li, 1994, Sillito et al., 1995; Ozeki et al., 2009; Self et al., 2014; Cavanaugh et al., 2002b), suggesting that nCRFs could be a common mechanism used to highlight salient stimuli throughout the visual system.

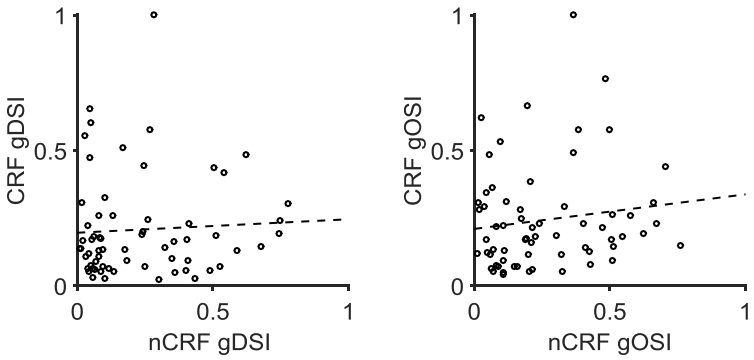

Figure 4.4. Relation of gDSI-gOSI between CRF and nCRF. Scatter plot of gDSI (left) and gOSI (right) of CRF as a function of selectivity of the nCRF in single neurons. Dashed lines represent the best fit regression line. gDSI: r=0.06, p=0.66, Pearson's correlation coefficient. gOSI: r=0.14, p=0.29, Pearson's correlation coefficient.

Speed discontinuities

Spatial discontinuities in speed may indicate presence of objects and potentially their depth. Objects that are closer to the viewer move across the visual field faster than those that are further from the viewer. To characterise speed selectivity of nCRF, I varied the temporal frequency of the annular grating. Some cells showed strong tuning, while others were broadly tuned (Fig. 4.5a), and on average, suppression was stronger at higher temporal frequencies (Fig. 4.5b). In individual neurons, suppression was stronger when the temporal frequency of

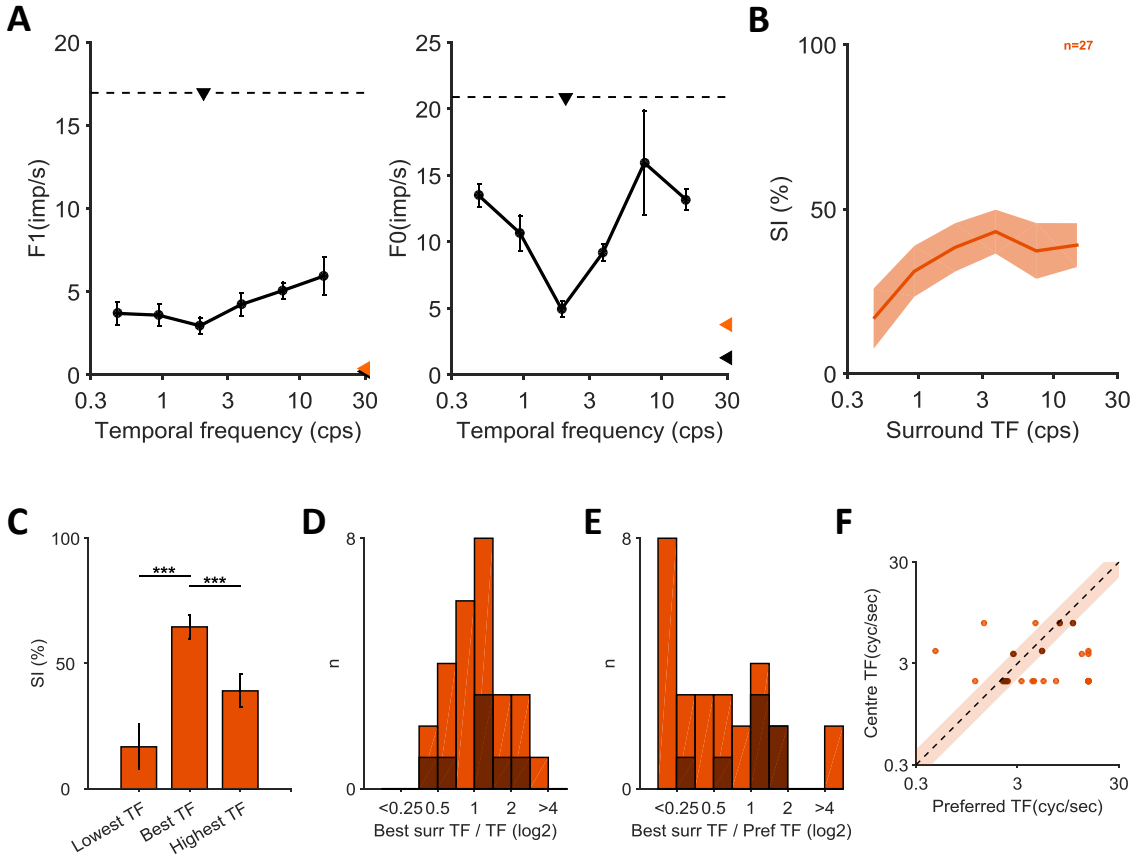

Figure 4.5. Temporal frequency selectivity of suppressive fields in awake recordings. I presented a central grating patch of fixed properties (size [diameter: μ 26.1°, s.d. 6.5°], contrast, spatial frequency, temporal frequency, direction) surrounded by an annular grating of varying temporal frequency. ***A***. Amplitude of responses for two example units. Top dashed lines indicate the response to the central grating presented alone. Downward arrow heads indicate centre temporal frequency. Leftward arrow heads indicate background activity (black) and response to surrounding stimuli presented alone (orange). ***B***. Population average suppression in response to simultaneous presentation of a central and surrounding grating varying in temporal frequency (n=27). ***C***. Average population suppression index at surround temporal frequency eliciting maximal suppression (Best TF) was significantly higher than at the lowest ($p<10^{-4}$, Wilcoxon signed rank test) and highest tested temporal frequencies (p =0.0002, Wilcoxon signed rank test), and suppression and the highest tested temporal frequency was significantly higher than suppression at the lowest tested temporal frequency (p=0.033, Wilcoxon signed rank test). ***D***. Logarithmic difference between centre temporal frequency and suppression center of mass temporal frequency (n=27). Dark bars indicate neurons in which the central patch temporal frequency was within half and twice the CRF preferred temporal frequency, as in *F* (n=7). ***E***. Logarithmic difference between CRF preferred temporal frequency and suppression center of mass temporal frequency (n=27). Dark bars indicate neurons in which the central patch temporal frequency was within half and twice the CRF preferred temporal frequency, as in *F* (n=7). ***F***. Scatter plot of CRF preferred temporal frequency and temporal frequency used for the central patch (n=27). Dashed line is the unity line. Dashed area and dark dots indicate neurons in which the central patch temporal frequency was within half and twice the CRF preferred temporal frequency (n=7).

the annular grating was close to the temporal frequency of the central grating (Fig 4.5d). By contrast, there was no clear bias of suppression towards temporal frequencies preferred by the neuron (Fig 4.5e), suggesting no relationship between the two. Non-classical receptive fields may therefore enable neurons to be sensitive to speed discontinuities.

The speed of a drifting grating, however, depends on both the spatial and temporal frequency of that grating. The speed (the ratio of temporal frequency/spatial frequency) of a low spatial frequency grating is higher than the speed of a grating with the same temporal frequency but higher spatial frequency. I therefore asked whether nCRFs are sensitive to speed, or to temporal frequency. In a subset of neurons I was able to measure the combined temporal and spatial frequency tuning of nCRFs. Fig. 4.6a shows the average temporal frequency tuning curves of nCRF suppression for annular gratings of increasing spatial frequency (from left to right). At low annular spatial frequencies, suppression was stronger at low temporal frequencies.

Figure 4.6. Speed selectivity of suppressive fields in awake recordings. I presented a central grating patch of fixed properties (size, contrast, spatial frequency, temporal frequency, direction) surrounded by an annular grating of varying temporal frequency and spatial frequency. ***A.*** Population average suppression in response to simultaneous presentation of a central and surrounding grating varying in temporal frequency (x-axis) and spatial frequency (panels from left to right, SF: 0.0187 cpd, n = 14; 0.0375 cpd, n = 14; 0.075 cpd, n = 15; 0.15 cpd, n = 14; 0.3 cpd, n = 13). Arrow heads indicate temporal frequency of the central grating. ***B.*** Population average suppression in response to simultaneous presentation of a central and surrounding grating varying in spatial frequency (x-axis) and temporal frequency (panels from left to right, TF: 0.47 Hz, n = 12; 0.94 Hz, n = 13; 1.88 Hz, n = 15; 3.75 Hz, n = 14; 7.5 Hz, n = 15; 15 Hz, n = 14). Arrow heads indicate spatial frequency of the central grating. ***C.*** nCRF preferred spatial frequency as a function of annular temporal frequency for single neurons (points and red lines) and average across the population (black solid curve). Horizontal line indicates spatial frequency of the central grating. Dashed line indicates the preferred nCRF spatial frequency predicted from the centre speed, if nCRFs were selective for speed. ***D.*** nCRF preferred temporal frequency as a function of annular spatial frequency for single neurons (points and red lines) and average across the population (black solid curve). Horizontal line indicates temporal frequency of the central grating. Dashed line indicates the preferred nCRF temporal frequency predicted from the centre speed, if nCRFs were selective for speed. ***C.*** nCRF preferred spatial frequency as a function of annular temporal frequency for single neurons (points and red lines) and average across the population (black solid curve). Horizontal line indicates spatial frequency of the central grating. Dashed line indicates the preferred nCRF spatial frequency predicted from the centre speed, if nCRFs were selective for speed. ***E.*** nCRF preferred speed as a function of annular temporal frequency for single neurons (points and red lines) and average across the population (black solid curve). Horizontal line indicates speed of the central grating. Dashed line indicates the preferred nCRF speed predicted from the centre spatial frequency, if nCRFs were selective for speed. ***F.*** nCRF preferred speed as a function of annular spatial frequency for single neurons (points and red lines) and average across the population (black solid curve). Horizontal line indicates speed of the central grating. Dashed line indicates the preferred nCRF speed predicted from the centre temporal frequency, if nCRFs were selective for speed.

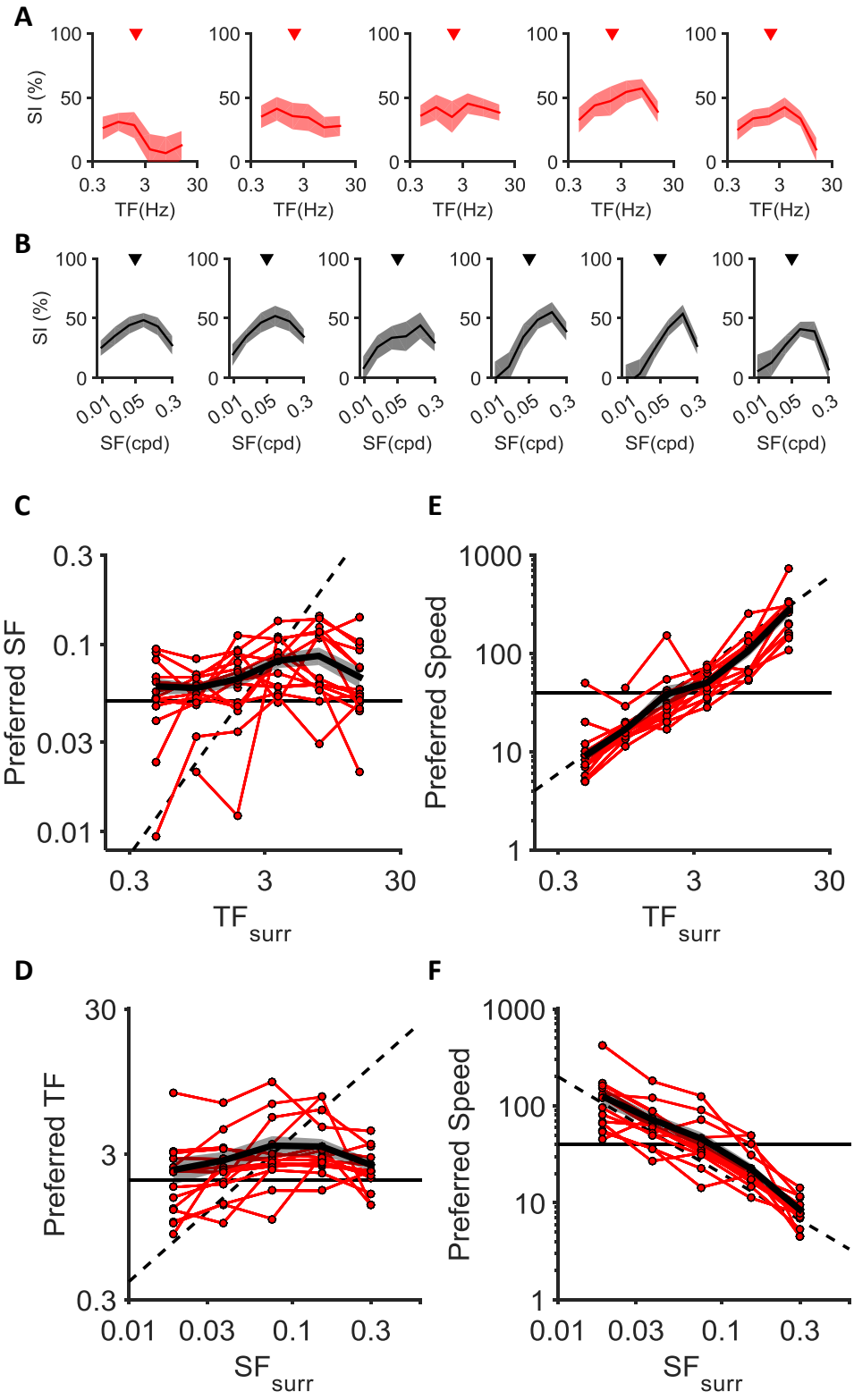
A
SI (%)
100
50
0
0.3
3
30
TF(Hz)
B
SI (%)
0.01
0.05
0.3
SF(cpd)
C
Preferred SF
0.3
0.1
0.03
0.01
TF surr
D
Preferred TF
30
3
0.3
SF surr
E
Preferred Speed
1000
100
10
1
F
Preferred Speed

Progressively increasing the annular spatial frequency resulted in shifts of suppression strength towards higher temporal frequency. Fig. 4.6b instead shows the average spatial frequency tuning curves of nCRF suppression, for annular gratings of increasing temporal frequency. The resulting tuning curves are similar at all temporal frequencies, with a slight tendency of suppression to increase with temporal frequency. The question that arises is if the amount of suppression is driven by the spatial frequency, temporal frequency, or speed over the centre. To gain more insight, I plotted the preferred spatial frequency of the nCRF as a function of annular temporal frequency (Fig. 4.6c), and found that the spatial frequency over the centre (horizontal black line) was a better predictor than centre grating speed (dashed line). Similarly, the temporal frequency over the centre (horizontal black line) was a better predictor than the centre speed (dashed line) for the preferred nCRF temporal frequency at different annular spatial frequency (Fig. 4.6d). I also plotted nCRF preferred speed as a function of annular temporal (Fig. 4.6e) or spatial (Fig. 4.6f) frequency. In line with Fig. 4.6c and 4.6d, the amount of suppression clearly depended more on the centre temporal or spatial frequency (dashed lines) rather than the centre speed (horizontal black line). Despite spatial and temporal frequency evidently influencing the strength of suppression, they do not explain it completely. It is therefore possible that surround suppression is weakly sensitive to speed.

I conclude that nCRFs in the mouse superior colliculus can help the detection of spatial and temporal frequency discontinuities, and display some interaction between the two that may reflect weak nCRF sensitivity to speed.

Independence of orientation and speed selectivity of nCRFs

I have shown that nCRFs in the mouse SC can be selective for orientation and temporal frequency. The SC receives visual input from both the retina and visual cortex, and it is well established that input from V1 modulates the gain of SC responses (Wang et al., 2010;Zhao et al., 2014), potentially by modulating the influence of the nCRF. To explore whether visual cortical activity may contribute to orientation tuning of nCRFs, I took advantage of the fact that neurons in mouse SC are more responsive to high temporal frequencies (higher speeds) than neurons in mouse V1 (Andermann et al., 2011;Durand et al., 2016). If SC neurons receiving nCRF suppression from visual cortex were distinct from those inheriting suppression from the retina

or from circuits within the SC, we would expect orientation selective suppression to be stronger in units where the nCRF is more sensitive to lower temporal frequencies. I therefore subdivided neurons into two groups based on the selectivity of the nCRF for temporal frequency, using the ratio of the average suppression at low (<3 cyc/sec) and high (>3 cyc/sec) temporal frequencies (Fig. 4.7a-c). Neurons with nCRFs that preferred higher temporal frequencies (black curves) showed similar nCRF orientation selectivity to those whose nCRF preferred lower temporal frequencies (red curves). Similarly, there was no correlation between preferred nCRF temporal frequency and nCRF global orientation selectivity index (gOSI) within cells (Fig. 4.7c. r = 0.007, p = 0.97, Pearson's correlation coefficient) [similar results were obtained when comparing preferred nCRF temporal frequency and nCRF gDSI]. The fact that nCRFs' responsiveness to high temporal frequencies is unrelated to their orientation tuning suggests that if the cortex is contributing to nCRF orientation selectivity in SC, its contribution is likely to be integrated with retinal or intracollicular nCRF mechanisms which are more sensitive to higher temporal frequencies. nCRFs in the superior colliculus are therefore probably built at different stages, inheriting some of their properties directly from the retina, computing others at a collicular level and possibly incorporating feedback information from the cortex.

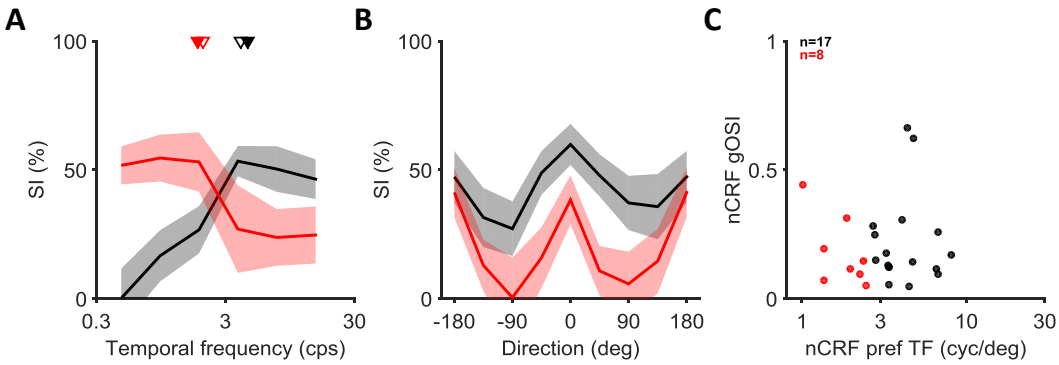

Figure 4.7. Independence of orientation and speed selectivity of nCRFs. I clustered cells based on nCRF suppression preference for high (> 3 cyc/sec, n = 17) or low (< 3 cyc/sec, n=8) temporal frequencies. Arrow heads indicate the average temporal frequency (A, B) or direction (C, D) used for the central patch. ***A***. Population average of suppression in response to simultaneous presentation of a central and surrounding grating varying in temporal frequency for cells with nCRF tuned for high (black) and low (red) temporal frequencies. ***B***. Population average of suppression in response to simultaneous presentation of a central and surrounding grating varying in direction for cells with nCRF tuned for high (black) and low (red) temporal frequencies. Surround directions are shifted so that 0 represents the centre direction. ***C***. Scatter plot of suppression center of mass temporal frequency and suppression global orientation selectivity index (r=0.007, p=0.97, Pearson's correlation coefficient).

Strength and selectivity of nCRF in anesthetized animals

Anaesthesia may have strong impact on nCRF properties. Indeed, in mouse primary visual cortex surround suppression is stronger in awake than anesthetized animals (Vaiceliunaite et al., 2013). I therefore made comparative measurements of surround suppression in the SC of anesthetized mice.

Similar to what has been observed in mouse primary visual cortex (Vaiceliunaite et al., 2013), I found that suppression was on average slightly stronger in awake than in anesthetized animals (Fig. 4.8a,c). I therefore compared the estimates of CRF and nCRF size and sensitivity obtained from the ratio-of-Gaussians model. These analyses showed that preferred size was similar (Fig. 4.8d), while size and sensitivity estimates of both CRFs and nCRFs were increased in awake animals (Fig. 4.8e-h). The difference between anesthetized and awake animals was greater for the nCRF than the CRF, suggesting that the nCRF is more disrupted by anaesthesia.

When I measured responses with annular gratings, I found that in awake animals responses persisted at larger annulus inner sizes (Fig. 4.8b). This may be consistent with generally increased contrast sensitivity in awake animals (Chapter 3, Fig. 3.22).

Suppression strength was particularly affected by anaesthesia at low contrasts (Fig. 4.9a), indicating that anaesthesia decreased nCRF contrast sensitivity. The tuning of suppression for centre contrast was less pronounced in anesthetized animals (Fig.4.9b), probably due to a decrease in nCRF contrast sensitivity.

nCRFs in anesthetized animals also displayed some direction and orientation tuning (Fig. 4.10a,d), but this selectivity was less pronounced than in awake animals. In anesthetized animals, I found that 10/50 units (20%) had a nCRF gDSI>0.25 (μ, 0.14; median, 0.08; s.d., 0.14), and 9/50 (18%) had a gOSI>0.25 (μ 0.16; median, 0.08; s.d., 0.17). The amount of nCRF tuning in single neurons was significantly lower in anesthetized animals for gOSI ($p<0.005$, Wilcoxon rank sum test), and gDSI ($p=0.014$, Wilcoxon rank sum test). In line with results obtained in awake animals, I found no correlation between classical and non-classical receptive field selectivity (Fig. 4.10g,h). Consistent with reduced selectivity, population average tuning curves aligned to the preferred direction of the surround, or to the stimulus used for the centre patch, are flatter than those obtained in awake animals (Fig. 4.10b,c). Despite the marked decrease in tuning, nCRFs

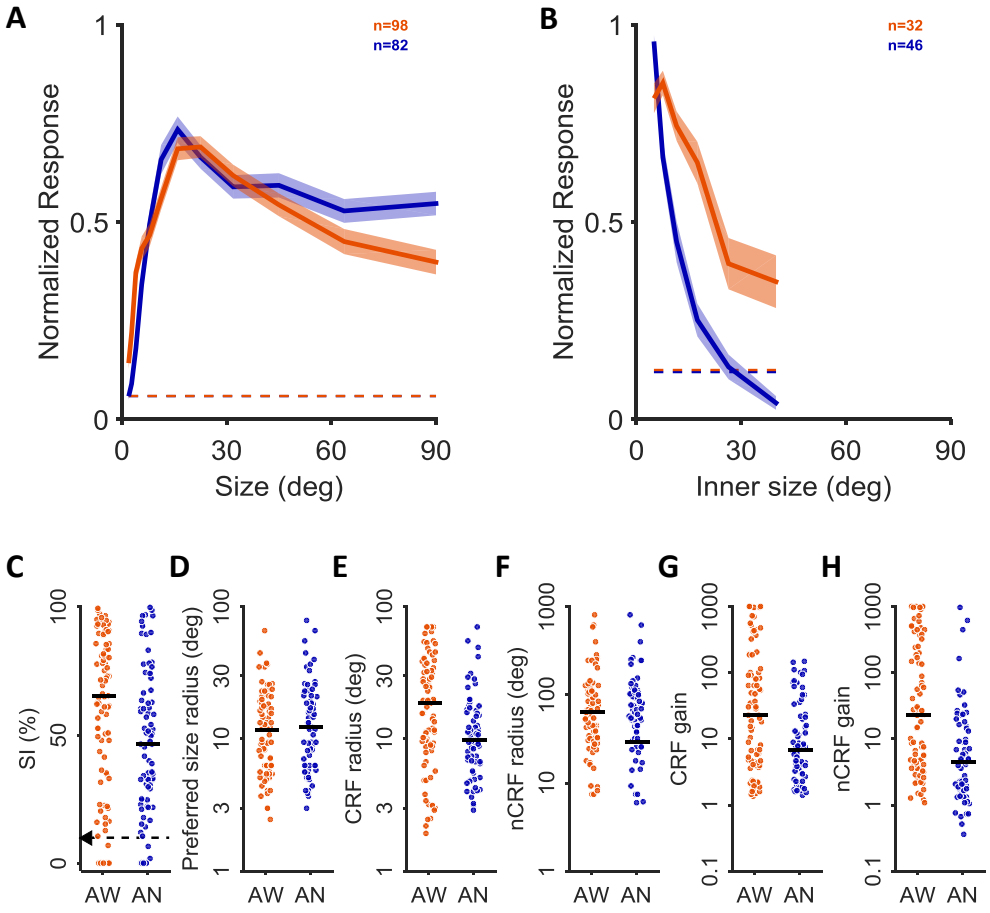

Figure 4.8. Spatial summation in SC cells. ***A.*** Population average of individual normalized size tuning curves of neurons recorded in awake (orange) and anesthetized (blue) mice. Dashed lines indicate normalized average spontaneous activity. ***B.*** Population average of normalized responses to annular gratings of increasing inner size of neurons recorded in awake (orange) and anesthetized (blue) mice. Dashed lines indicate normalized average spontaneous activity. ***C***. Distribution of suppression indices across the population of neurons recorded in awake (orange) and anesthetized (blue) mice (SI. AW: median 65.2%; mean 57.6%; s.d. 32.8%; n = 98. AN: median 46.5%; mean 46.2%; s.d. 28.6%; n = 82. p = 0.0088, Wilcoxon rank sum test). Arrow indicates SI = 10%. In subsequent plots, cells with SI ≤ 10 were not included. ***D-H***. Distribution of estimated ratio-of-Gaussian parameters for cells recorded in anesthetized (AN, blue) and awake (AW, orange) animals. Horizontal bars represent median. ***D***. Preferred sizes (AW: median 11.8°; geomean 11.2°; s.d. 10.8°; n = 85. AN: median 11.3°; geomean 12.6°; s.d. 9.8°; n = 73. p = 0.32, Wilcoxon rank sum test). ***E***. Classical receptive field sizes (AW: median 18.7°; geomean 15.8°; s.d. 19.1°; n = 85. An: median 9.8°; geomean 10.3°; s.d. 12°; n = 73. p = 0.001, Wilcoxon rank sum test). ***F.*** Non classical receptive field sizes (AW: median 63.4°; geomean 67.1°; s.d. 2.57.1°; n = 85. An: median 29.16°; geomean 36.8°; s.d. 211.1°; n = 73. $p < 10^{-5}$, Wilcoxon rank sum test). ***G***. Classical receptive field gains (AW: median 23.2; mean 181.6; s.d. 311.9; n = 85. An: median 6.8; mean 23.3; s.d. 35; n = 73. p = 0.001, Wilcoxon rank sum test). ***H***. Non classical receptive field gains (AW: median 22.7; mean 195.8; s.d. 312.8; n = 85. An: median 4.6; mean 38.6; s.d. 143.7; n = 73. $p < 10^{-5}$, Wilcoxon rank sum test).

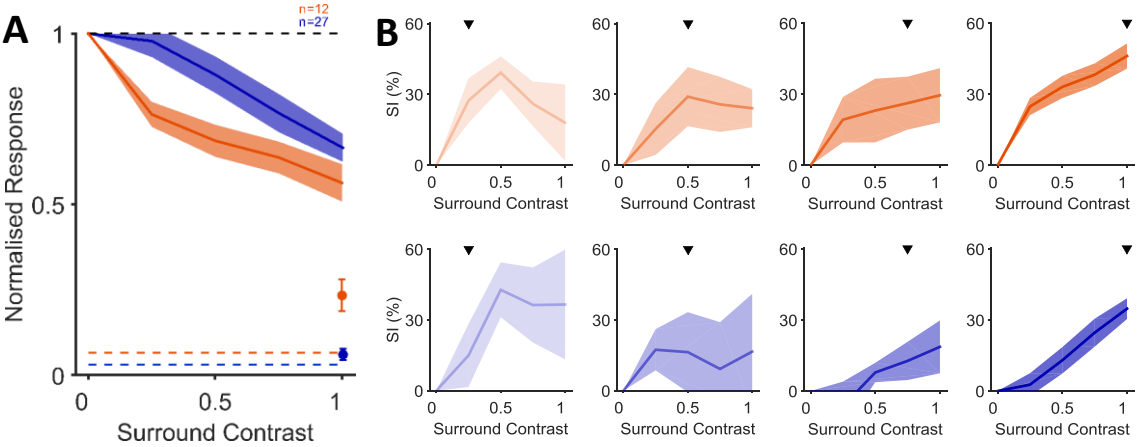

Figure 4.10. Non-classical receptive fields sensitivity and selectivity to contrast. ***A***. Population averages of responses in awake (*left*, orange, n = 12) and anesthetized (*right*, blue, n = 27) animals to simultaneous presentation of a central grating patch of fixed properties (size [AW diameter: μ 24.3°, s.d. 6.9; AN diameter: μ 21°, s.d. 13.2], contrast, spatial frequency, temporal frequency, direction) and surrounding grating varying in contrast, normalized to the response of a maximum contrast central patch presented alone. The top dashed line indicates the response to the maximum contrast central patch alone. The bottom dashed lines indicate the mean spontaneous activity. The isolated data points indicates the average responses to maximal contrast annular grating presented alone. The solid lines indicate average responses to the combination of central and surrounding grating of increasing surround contrast. ***B***. Population averaged suppression tuning curve in response to surrounds increasing in contrasts for awake (*top*, orange) and anesthetized (*bottom*, blue) animals, using patches of different contrasts over the centre. Arrow heads indicate contrast of the central grating (from left to right: 0.25, 0.5, 0.75, 1).

Figure 4.9. Directional selectivity of suppressive fields in anesthetized recordings. I presented a central grating patch of fixed properties (size [diameter: μ 19.9°, s.d. 13.6°], contrast, spatial frequency, temporal frequency, direction) surrounded by an annular grating of varying direction. ***A***. Population average of suppression in response to simultaneous presentation of a central and surrounding grating varying in direction. Individual tuning curves of suppression were shifted to make 0 the direction eliciting maximal suppression (n=50). ***B.*** Population averages of suppression after shifting individual tuning curves to make 0 the direction of the central grating. Dark and light blue lines indicate average tuning curves for cells in which the central patch orientation was or wasn't within 30° form the CRF preferred orientation, as in *I* (darker, n=17, lighter, n=33). ***C***. Population average of suppression after shifting individual tuning curves to make 0 the direction preferred by the CRF. Colour code as in *B,I.* ***D***. Average population suppression index at surround directions eliciting maximal suppression (Best dir, SI_{θ}) was significantly higher than at the opposite directions (Opposite dir, $SI_{\theta+\pi}$, $p < 10^{-11}$, Wilcoxon signed rank test) and averaged SIs at orthogonal directions (Orthogonal dir, $(SI_{(\theta+\pi/2)}+SI_{(\theta-\pi/2)})/2$, $p < 10^{-11}$, Wilcoxon signed rank test). ***E.*** Difference in orientation between center and surround eliciting maximal suppression (n=64). Colour code as in *B,H* (n=17). ***F.*** Difference between CRF preferred orientation and surround orientation eliciting maximal suppression (n=50). Colour code as in *B,C,I* (n=17). ***G-H.*** Scatter plot of gDSI (*G*) and gOSI (*H*) of CRF as a function of selectivity of the nCRF in single neurons. Dashed lines represent the best fit regression line. gDSI: r=0.24, p=0.09, Pearson's correlation coefficient. gOSI: r=0.04, p=0.79, Pearson's correlation coefficient. ***I.*** Scatter plot of CRF preferred orientation and orientation used for the central patch (n=50). Dashed line is the unity line. Dashed area and dark dots indicate neurons in which the central patch orientation was within 30° form the CRF preferred orientation (n=17).

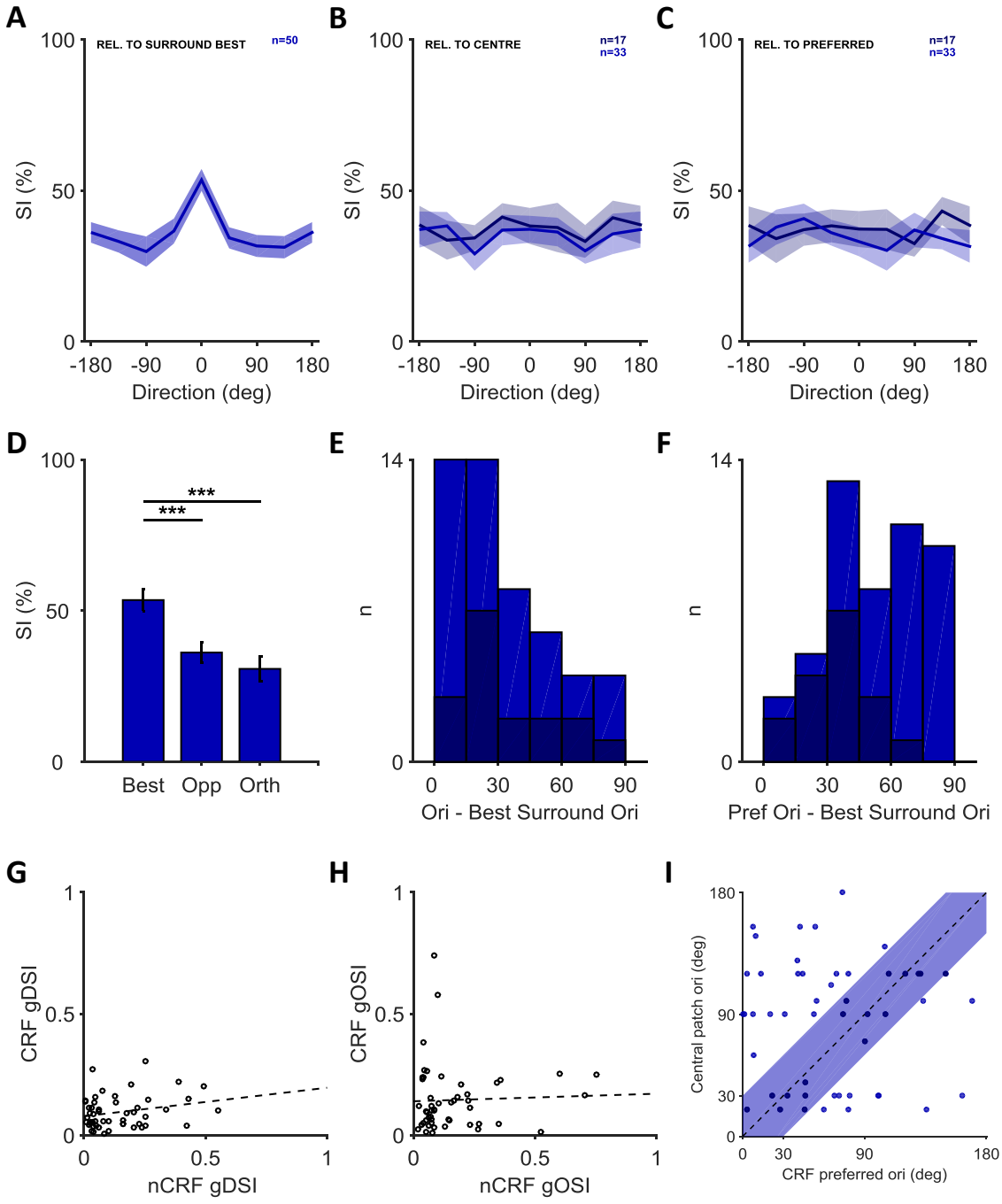
A
REL. TO SURROUND BEST
n=50
SI (%)
Direction (deg)
B
REL. TO CENTRE
n=17
n=33
C
REL. TO PREFERRED
D
***
***
Best Opp Orth
E
n
Ori - Best Surround Ori
F
Pref Ori - Best Surround Ori
G
CRF gDSI
nCRF gDSI
H
CRF gOSI
nCRF gOSI
I
Central patch ori (deg)
CRF preferred ori (deg)

were still stronger when the surround orientation matched the centre orientation (Fig. 4.10e,f). I therefore conclude that anaesthesia affects the magnitude of nCRF tuning but not their selectivity.

nCRFs in anesthetized animals showed some tuning for temporal frequency (Fig.4.11a,b). Interestingly, the bias of surround suppression for higher temporal frequency observed in awake animals was not present in anesthetized animals. Given the brain-state dependent increase in

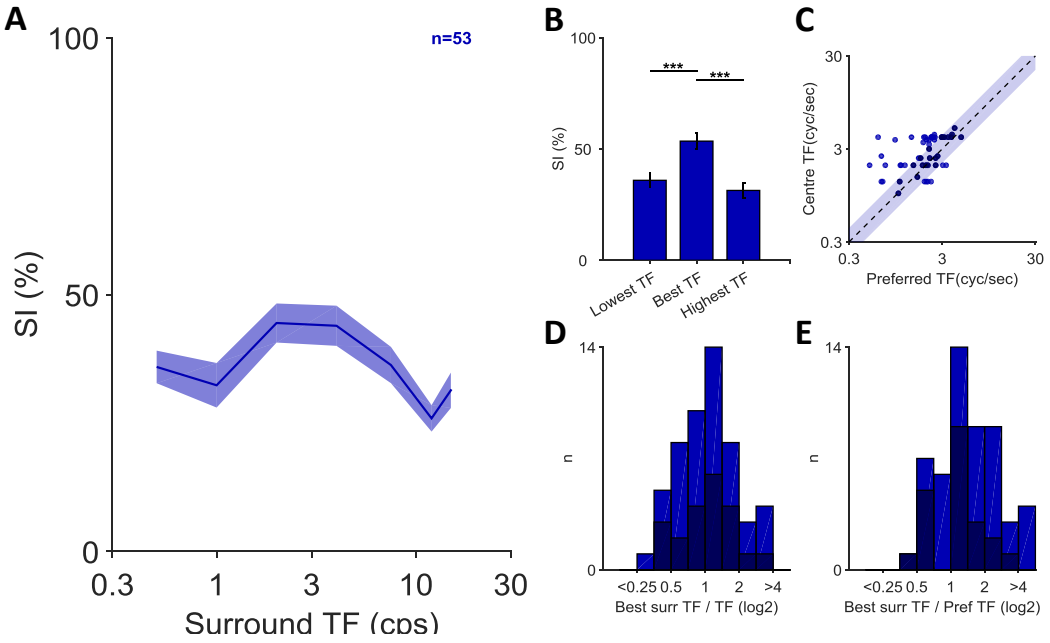

Figure 4.11. Temporal frequency selectivity of suppressive fields in anesthetized recordings. I presented a central grating patch of fixed properties (size [diameter: μ 21°, s.d. 14.9°], contrast, spatial frequency, temporal frequency, direction) surrounded by an annular grating of varying temporal frequency. ***A***. Population average suppression in response to simultaneous presentation of a central and surrounding grating varying in temporal frequency (n=53). ***B***. Average population suppression index at surround temporal frequency eliciting maximal suppression (Best TF) was significantly higher than at the lowest ($p<10^{-7}$, Wilcoxon signed rank test) and highest tested temporal frequencies ($p < 10^{-8}$, Wilcoxon signed rank test), and suppression and the highest tested temporal frequency was significantly higher than suppression at the lowest tested temporal frequency (p=0.048, Wilcoxon signed rank test). ***C***. Scatter plot of CRF preferred temporal frequency and temporal frequency used for the central patch (n=53). Dashed line is the unity line. Dashed area and dark dots indicate neurons in which the central patch temporal frequency was within half and twice the CRF preferred temporal frequency (n=21). ***D***. Logarithmic difference between centre temporal frequency and suppression center of mass temporal frequency (n=53). Dark bars indicate neurons in which the central patch temporal frequency was within half and twice the CRF preferred temporal frequency, as in *C* (n=21). ***F***. Logarithmic difference between CRF preferred temporal frequency and suppression center of mass temporal frequency (n=53). Dark bars indicate neurons in which the central patch temporal frequency was within half and twice the CRF preferred temporal frequency, as in *C* (n=21).

temporal frequency resolution in SC neurons of awake animals (Chapter 3, Section 3.3.7) that appears not to occur in V1 (Durand et al., 2016), this may be consistent with a role of intracollicular circuits in building nCRF. As observed for direction, nCRF temporal frequency tuning in anesthetized animals was less tuned compared to awake animals (Fig. 4.10a-b), but still selective for temporal frequencies close to that of the central patch (Fig. 4.10d,e). The effect supports the hypothesis that anaesthesia affects the strength of nCRFs tuning with less impact on its preferences.

4.3.3 Visual adaptation in mouse superior colliculus

The nCRF provides a mechanism for detecting and signalling visual spatial discontinuities. I therefore asked if counterpart mechanisms may enable detection of visual temporal discontinuities. Specifically, I asked how responses adapt over time to an unchanging visual stimulus.

Neurons in SC show variable time course of response to a drifting grating of optimal size. Some units show sustained response over the entire stimulus presentation (2 s), while others show only a transient response, strong in the first part of the stimulus presentation and then markedly diminished. Others showed intermediate behaviours (Fig. 4.12a). To quantify the change in response over time (i.e. adaptation), I calculated an adaptation index (AI) as the change in response from the first 0.5 s (transient response) to the last 0.5 s (sustained response). An AI of 100% would indicate that a unit does not respond at all in the latter time period. Most neurons showed moderate or strong adaptation, with 57/98 cells (58.2%) having an AI≥50%, and 88/98 cells (89.8%) with an AI≥10% (Fig. 4.12b). Neurons in the SC are therefore more likely to signal the appearance of objects rather than simply relaying the statistics of the visual scene.

To assess the robustness of adaptation effects, in a subset of neurons I also recorded responses to a small patch presented multiple times in rapid succession (sometimes called repetition suppression), and compared responses with those to drifting gratings (in this analysis, only responses to large gratings were available; Fig. 4.13). Neurons that displayed strong adaptation to drifting gratings also displayed strong adaptation to the repetition suppression experiment. For neurons with intermediate adaptation, the response to repeatedly appearing

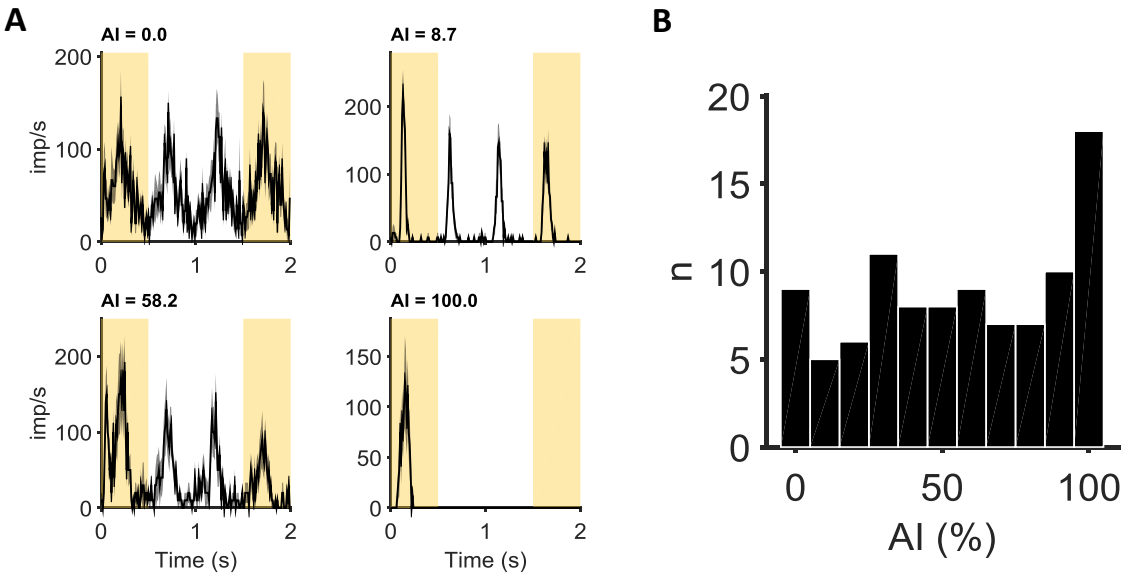

Figure 4.12. Short term adaptation in the SC. ***A.*** PSTHs in response to a drifting sinusoidal grating of optimal size for four example neurons. The adaptation index was 1) 0%, 2) 8.7%, 3) 58.2%, 4) 100%. ***B***. Distribution of adaptation indices in response to a drifting sinusoidal grating of optimal size across the population of neurons recorded in awake animals (μ, 56.2%; median, 59%; s.d., 33%).

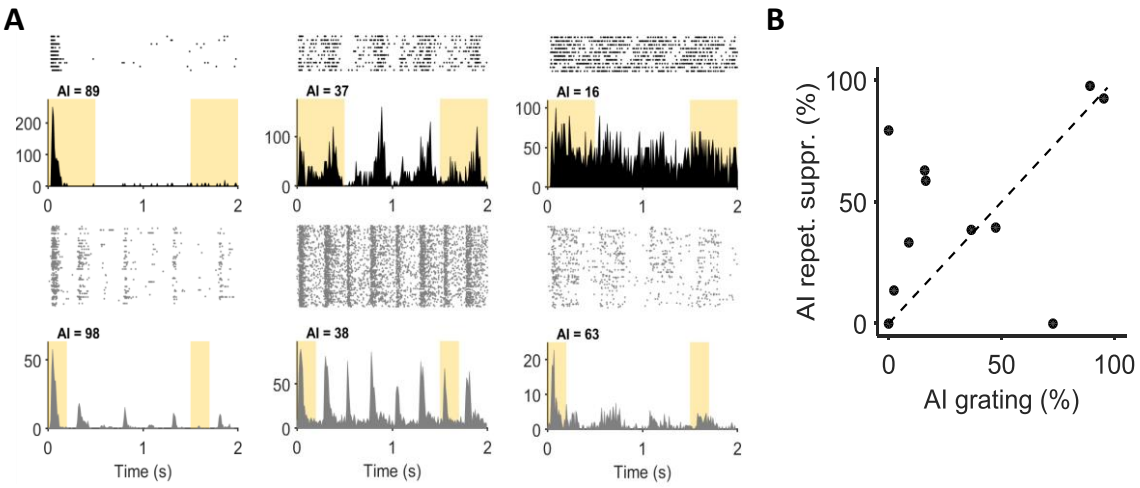

Figure 4.13. Comparison of adaptation in response to a large drifting sinusoidal grating of optimal spatial frequency and repetition suppression stimuli. ***A.*** Raster plots and PSTHs in response to a large drifting sinusoidal grating (black, top) or a small black spot (5-15°) appearing and disappearing at 2 Hz (grey, bottom). The stimulus was on for 250 ms with an insterstimulus interval of 250 ms for three example cells. Yellow areas indicate periods used to calculate adaptation indices (200 ms long). ***B***. Scatter plot of adaptation indices calculated from responses to a large drifting sinusoidal grating (as in *A*, black) and from responses to the repetition suppression paradigm (as in *A*, grey PSTHs) (n=11, r = 0.4, p=0.22, Pearson's

spots was more variable and did not necessarily correlate with adaptation in response to gratings (Fig.4.13b). The variance may reflect the different nature of the stimuli. In repetition suppression experiments, adaptation is estimated based on the response to the repeated onset of a stimulus, while when using gratings the onset of the stimulus only affects the first part of the response. The adaptation mechanisms measured with the two stimuli may therefore be slightly different.

4.3.4 Adaptation and suppression

The analyses above confirm the presence of visual adaptation in SC neurons, which may help neurons detect visual discontinuities. The question that arises is whether those neurons that show stronger adaptation also show stronger nCRFs.

I investigated the relation between adaptation and nCRFs in single neurons by comparing their adaptation and suppression indices. I observed that neurons with vigorous surround suppression also tended to show strong adaptation, while cells with less surround suppression also tended to adapt less (Fig. 4.14a). This produces a strong correlation between the indices of

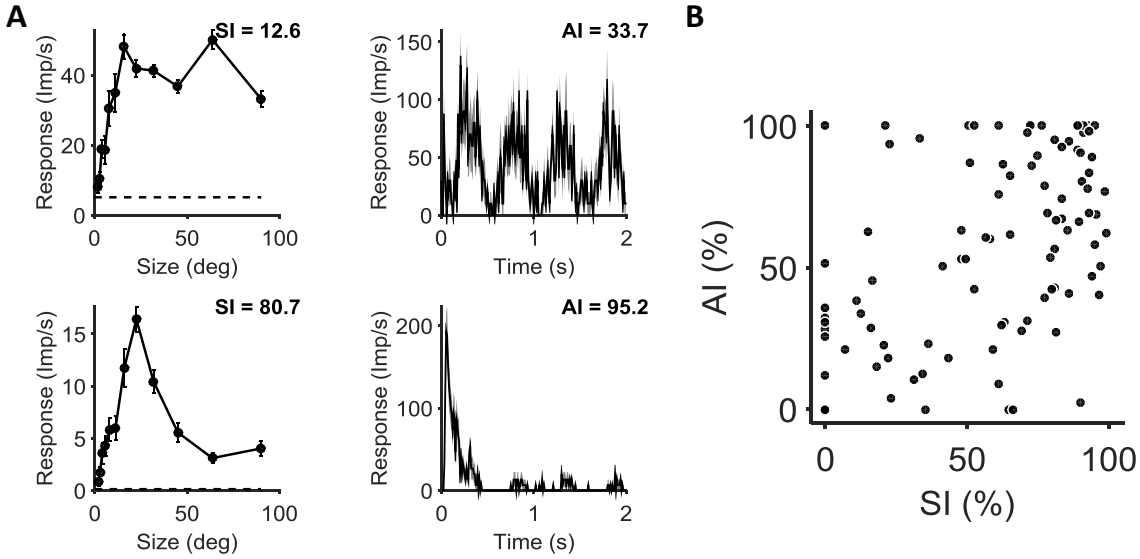

Figure 4.14. Relation between suppression and adaptation in awake animals. ***A.*** Size tuning curve (left) and PSTH in response to the stimulus of optimal size (right) for two example cells. *Top*: The cell had a suppression index of 12.6%, and an adaptation index of 33.7%. *Bottom*: The cell had a suppression index of 80.7%, and an adaptation index of 95.2%. ***B***. Scatter plot of suppression indices and adaptation indices in response to a grating of optimal size ($r=0.5$, $p<10^{-6}$, Pearson correlation coefficient, n=98).

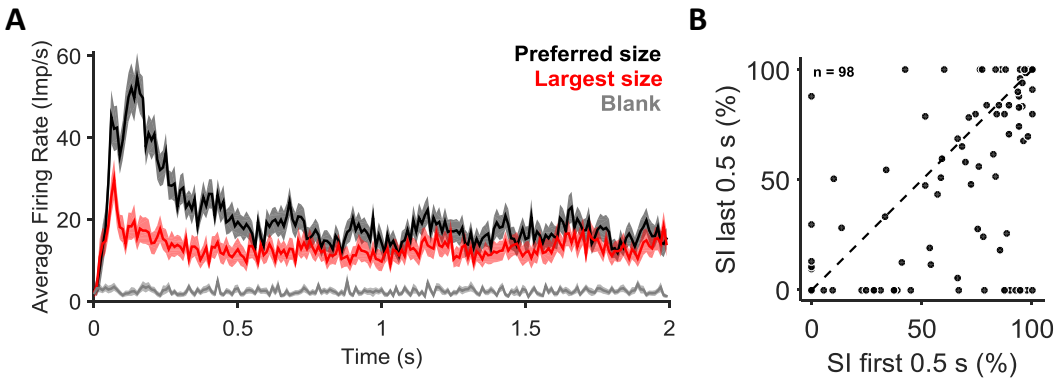

Figure 4.15. Time course of suppression. ***A.*** Average population PSTHs in response to a drifting sinusoidal grating of optimal size (black), to the largest tested size (red) and for spontaneous activity (grey). The difference between black and red PSTHs is due to surround suppression. ***B***. Scatter plot of suppression indices (SI) during the first 0.5 s of response as a function of SI during the last 0.5 s of response (n=98). Suppression is stronger in the first 0.5 s of stimulus presentation (μ 60.4%, median, 75%, s.d. 36.1%) compared to the last 0.5 s (μ, 44.8%, median 47.7%, 40.2%, $p<10^{-4}$, Wilcoxon signed rank test). Dashed line represents the unity line.

nCRF suppression and adaptation (Fig. 4.14b, r = 0.5, $p<10^{-6}$, Pearson correlation coefficient), indicating that cells able to detect visual discontinuities in spatial context were also more likely to be sensitive to contrast in temporal domain.

I next asked if there was any interaction between the mechanisms of suppression and adaptation. The population average PSTH shows that stimulus size has most impact on the initial transient response (Fig. 4.15a). To characterise individual neurons, I compared suppression indices in the first and last 0.5 s of response and found that the amount of suppression was higher in the first 0.5 s than in the last 0.5 s (Fig. 4.15b. $p < 10^{-4}$, Wilcoxon signed rank test). Thus suppression from the nCRF, like spiking activity, adapts over time.

In summary, visual adaptation covaries with strength of the nCRF in single cells, indicating that those cells sensitive to spatial context also tended to be sensitive to temporal context, and may therefore be able to detect saliency in multiple dimensions. My analysis also shows that suppression diminishes over time, suggesting that the nCRF is susceptible to adaptation. The co-occurrence of surround suppression and adaptation in individual neurons has not yet been investigated in any area. Despite this, in primate, RGCs that are part of the magnocellular pathway display more surround suppression and more adaptation than RCGs that are part of the parvocellular pathway (Solomon et al., 2004; Solomon et al., 2006). If such a segregation is

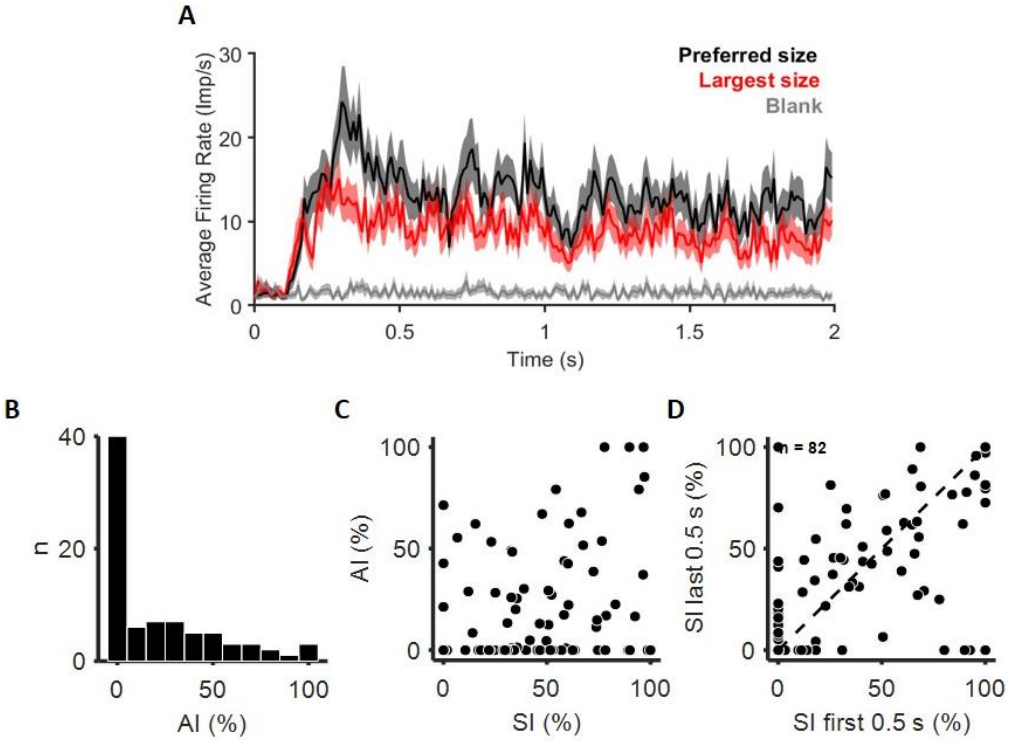

Figure 4.16. Relation between suppression and adaptation in anesthetized animals. ***A.*** Average population PSTHs in response to a drifting sinusoidal grating of optimal size (black), to the largest tested size (red) and for spontaneous activity (grey). The difference between black and red PSTHs is due to surround suppression. ***B.*** Distribution of adaptation indices in response to a drifting sinusoidal grating of optimal size across the population of neurons recorded in anesthetized animals (μ, 22.1%; median, 9.9%; s.d., 28.5%). ***C.*** Scatter plot of suppression indices and adaptation indices in response to a grating of optimal size (r=0.24, p=0.012, Pearson's correlation coefficient, n=82). ***D.*** Scatter plot of suppression indices (SI) during the first 0.5 s of response as a function of SI during the last 0.5 s of response (n=98). Suppression was similar during the first 0.5 (μ, 38%; median, 31.2%, s.d. 35.5%) and the last 0.5 s (μ, 38.6%; median, 35.8%, s.d. 33.5%, p=0.68, Wilcoxon signed rank test). Dashed line is the unity line.

present in the mouse retina, my results would suggest that the SC is likely to mainly receive inputs from "magnocellular-like" RCGs.

Adaptation and suppression in anesthetized recordings

Responses of neurons recorded in anesthetized animals were more sluggish than in awake, and the transient response was much less pronounced (Fig. 4.16a). Consistently, I found 15/82 neurons (18.3%) with an AI > 50%, and 41/82 units (50%) with an AI ≥ 10% (Fig. 4.16b), substantially lower than the corresponding fractions in awake animals ($p < 10^{-10}$, Wilcoxon rank sum test). Similarly, I observed reduced correlation between suppression and adaptation in

neurons recorded from anesthetized animals (Fig. 4.16c, r = 0.28, p = 0.012, Pearson's correlation coefficient), and found no difference between the amount of suppression in the first and last 0.5 s (Fig. 4.16d, p = 0.68, Wilcoxon signed rank test). I conclude that adaptation mechanisms are much weaker under anaesthesia. Similarly, while surround suppression is still potent in anesthetized animals, it appears less sensitive to adaptation.

4.3.5 Time course of non-classical receptive field suppression tuning

Above I showed that suppression from the nCRF is tuned for the visual properties of the stimulus presented over the CRF, and that suppression decreases over time. In this section, I ask if adaptation of surround suppression affects the selectivity of nCRF. To investigate the time course of suppression selectivity, I presented a small drifting grating over the CRF surrounded by an annular grating varying in direction or temporal frequency, and compared the amount of suppression during the first 0.5 s and the last 0.5 s of responses.

Suppression could be affected by adaptation in several ways (Fig. 4.17). In one scenario, the amount of suppression decreases over time independently of centre-surround feature contrast, resulting in a less suppressed but equally tuned late response (Fig. 4.17a). Alternatively, adaptation may have most impact on suppression from the preferred nCRF stimulus (thus resembling a divisive modulation of nCRF strength; Fig. 4.17c), or be affected in a mixed way (Fig. 4.17b). My observations show that the amount of suppression decreases over time at all directions and at all temporal frequencies (Fig. 4.18a and 4.18b). For surrounding gratings of different orientations/directions, the suppressive activity of nCRF diminished markedly, and

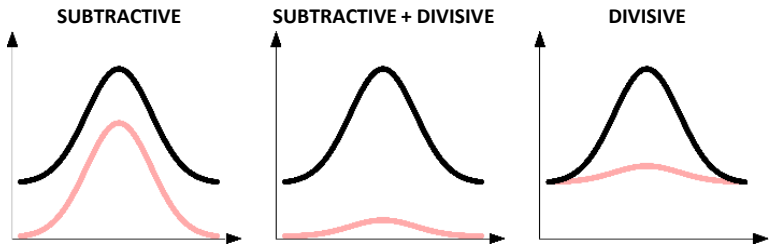

Figure 4.17. Effect of time over nCRF spatial tuning, models. Black lines represent the tuning of nCRF suppression during the initial part of responses. Red lines show how time might affect the tuning properties. Left: time linearly decreases suppression independently of tuning. Middle: time-dependent decrease in suppression has a linear and a divisive component. Right: time decreases suppression in a divisive fashion, resulting in a suppression decrement proportional to suppression strength.

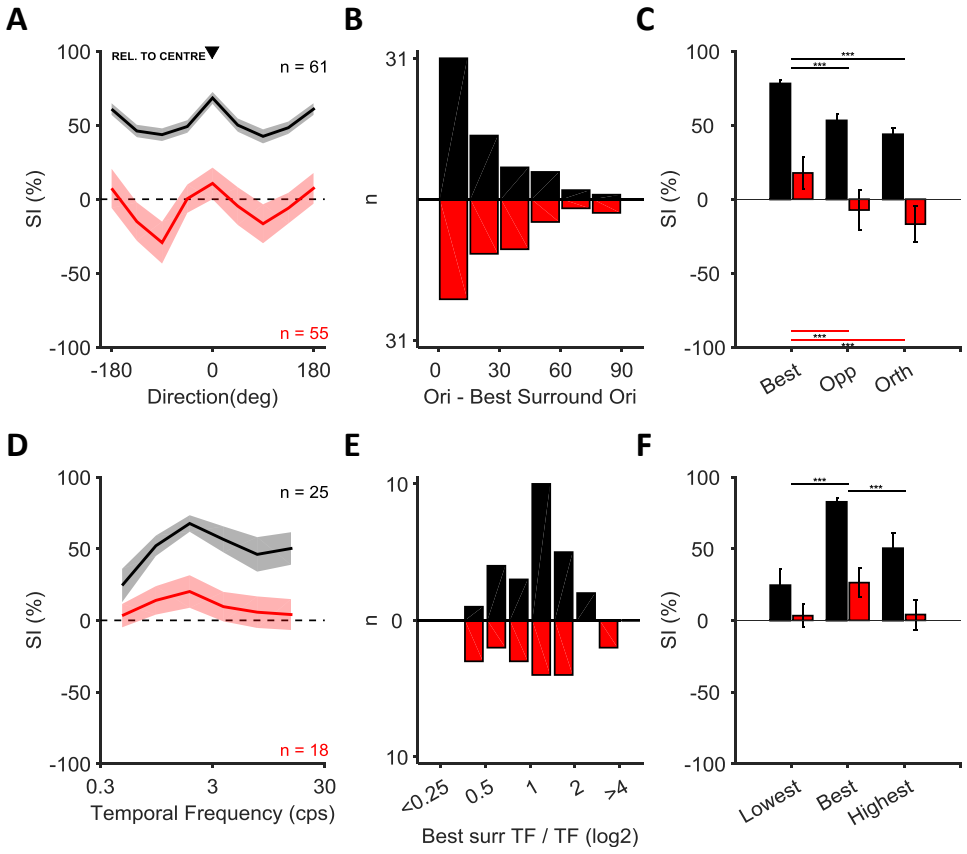

Figure 4.18. Effect of time over nCRF spatial tuning in awake recordings. I presented a central grating patch of fixed properties (size, contrast, spatial frequency, temporal frequency, direction) surrounded by an annular grating of varying direction (top) or temporal frequency (bottom) to compare the properties of nCRF suppression during the first (black) and last (red) half a second of stimulus presentation. ***A-B***. Population average of suppression during the first half a second (black) and last half a second (red) of response to simultaneous presentation of a central and surrounding grating varying in direction (*A*) or temporal frequency (*B*). In *A*, individual tuning curves of suppression were shifted to make 0 the direction of the central grating. ***C-D***. Difference in orientation (*C*) or logarithmic difference in temporal frequency (*D*) between center and surround eliciting maximal suppression during the first (black. *C*: n = 61. *D*: n = 25) and the last (red. *C*: n = 53. *D*: n = 18) half a second of response. ***E***: Average population suppression index at surround directions eliciting maximal suppression (Best dir, SI_{θ}) was significantly higher than at the opposite direction (Opposite dir, $SI_{\theta+\pi}$, $p<10^{-10}$, Wilcoxon signed rank test) and averaged SIs at orthogonal directions (Orthogonal dir, $(SI_{(\theta+\pi/2)}+SI_{(\theta-\pi/2)})/2$, $p<10^{-10}$, Wilcoxon signed rank test) during the first half a second of response (black). In the last half a second of response (red), the average population suppression index at surround directions eliciting maximal suppression was significantly higher than at the opposite direction ($p<0.001$, Wilcoxon signed rank test) and averaged SIs at orthogonal directions ($p<10^{-5}$, Wilcoxon signed rank test). ***F***. The population average of suppression during the first half a second of response (black) was larger at the temporal frequency eliciting maximal suppression than at the lowest ($p<0.001$, Wilcoxon signed rank test) and highest tested temporal frequencies ($p<10^{-4}$, Wilcoxon signed rank test). In the last half a second of suppression the difference in suppression was not significant (red. Lowest tested temporal frequency: $p = 0.09$. Highest tested temporal frequency: $p = 0.13$. Wilcoxon signed rank test).

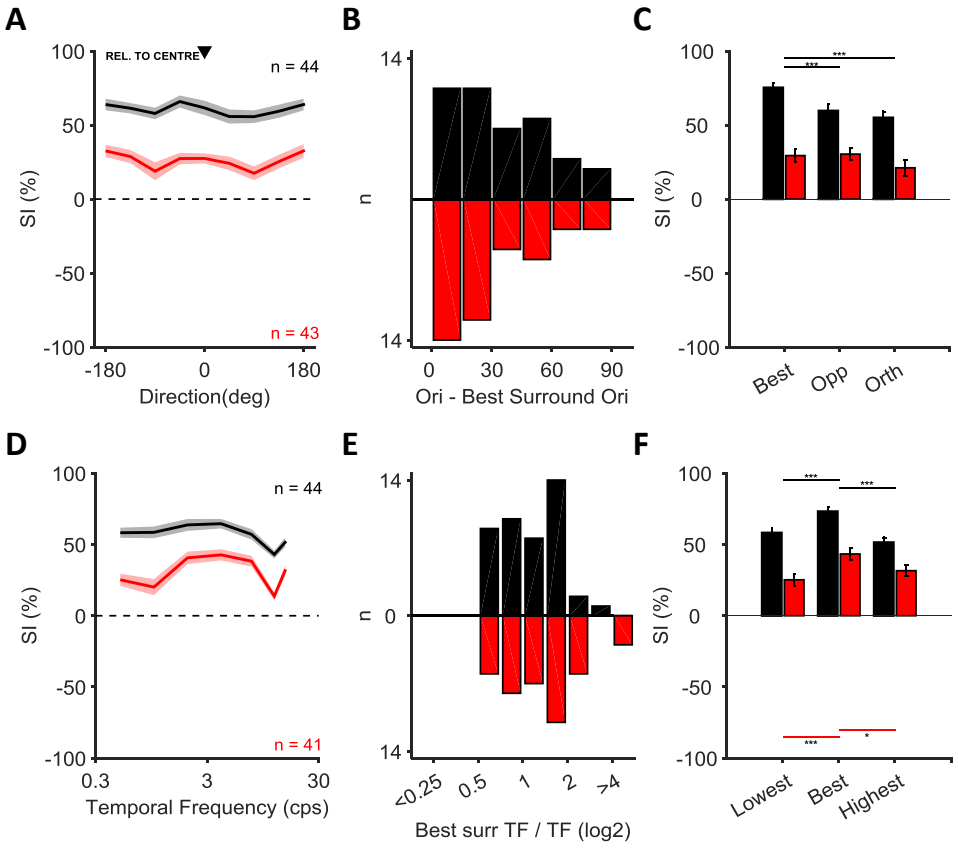

Figure 4.19. Effect of time over nCRF spatial tuning in anesthetized recordings. As in Fig. 4.18, for anesthetized animals. ***E***. Average population suppression index at surround directions eliciting maximal suppression (Best dir, SI_{θ}) was significantly higher than at the opposite direction (Opposite dir, $SI_{\theta+\pi}$, $p<10^{-7}$, Wilcoxon signed rank test) and averaged SIs at orthogonal directions (Orthogonal dir, $(SI_{(\theta+\pi/2)}+SI_{(\theta-\pi/2)})/2$, $p<10^{-7}$, Wilcoxon signed rank test) during the first half a second of response (black). In the last half a second of response (red), the average population suppression index at surround directions eliciting maximal suppression was not significantly higher than at the opposite direction (p=0.73, Wilcoxon signed rank test) or at orthogonal directions (p=0.15, Wilcoxon signed rank test). ***F.*** The population average of suppression during the first half a second of response (black) was larger at the temporal frequency eliciting maximal suppression than at the lowest ($p<10^{-6}$, Wilcoxon signed rank test) and highest tested temporal frequencies ($p<10^{-6}$, Wilcoxon signed rank test). In the last half a second of suppression the difference in suppression was also significant (red. Lowest tested temporal frequency: $p<10^{-4}$. Highest tested temporal frequency: p = 0.019. Wilcoxon signed rank test).

even became facilitatory at directions orthogonal to the centre (that is, SI<0). Suppression remained stronger when the properties of the surround matched the centre properties (Fig. 4.18c,d), although the phenomenon was more apparent for orientation than for temporal frequency (Fig. 4.18d). Similarly, the nCRF directional tuning was maintained in directional experiments while it decreased over time in temporal frequency experiments (Fig. 4.18e and 4.18f). My results therefore suggest that adaptation of surround suppression predominantly reflects reductions in untuned suppression, with smaller effects on tuned suppression.

Adaptation of nCRF suppression was less pronounced in anesthetized animals (Fig 4.19). This was somewhat surprising because in anesthetized animals I found no significant decrease in suppression in response to large gratings (Fig. 4.16d), and this was also the case if I just considered the neurons shown in Fig. 4.19. The cause of this discrepancy is unclear.

4.4 DISCUSSION

The results presented in this chapter describe two neural mechanisms that may be used for representing salience in mouse SC – surround suppression and adaptation. I showed that the responses of most SC neurons are modulated by both, with surround suppression making them sensitive to visual discontinuities and adaptation making them sensitive to novel stimuli. In addition, I also showed that the strength of surround suppression and adaptation covaries in single neurons and that surround suppression itself is susceptible to adaptation.

4.4.1 Non-classical receptive fields

Non-classical receptive fields have been described in the superior colliculus of many species (rat: Girman and Lund, 2007; cat: Sterling and Wickelgren, 1969; monkey: Cynader and Berman, 1972; Goldberg and Wurtz, 1972a; barn owl: Mysore et al., 2010; zebrafish: Del Bene et al., 2010), including mouse (Wang et al., 2010; Gale and Murphy, 2014). The observations here extend these by providing the spatiotemporal profile and feature selectivity of non-classical receptive fields in the mouse.

I have shown that the activity of most neurons is modulated by regions outside of the classical receptive field. This non-classical suppression makes neurons more selective for stimulus size.

My estimates of preferred size are slightly smaller than that of previous reports in anesthetized mice (Wang et al., 2010), which may be explained by increased non-classical suppression in awake animals: nCRF suppression was less contrast sensitive in anesthetized animals, similar to anaesthesia-induced reduction in sensitivity of CRF responses I showed in Chapter 3. Similar reduction of suppression under anaesthesia has been observed in mouse V1 (Vaiceliunaite et al., 2013), where anaesthesia has been proposed to exert an influence on surround suppression by influencing 'normalization signals' that are strongest for high contrast stimuli. Contrast is known to affect spatial summation (Sceniak et al., 1999; Solomon et al., 2002; Solomon et al., 2006; Carandini and Heeger, 2011; Ayaz et al., 2013; Vaiceliunaite et al., 2013), such that preferred size is larger, and surround suppression is reduced, at low contrast. My observations are in accordance with this, and suggest that anaesthesia's effect on normalization signals is not restricted to the visual cortex. I found no difference in preferred size between anesthetized and awake animals, but given the variability across the population, a comparison within neurons is necessary to unveil if anaesthesia increases the preferred size in SC.

In several brain areas and several species, the strength of surround suppression has been shown to depend on the similarity of stimuli shown to the CRF and the nCRF (Sillito et al., 1993; Sillito et al., 1995; Levitt and Lund, 1997; Cavanaugh et al., 2002b; Muller et al., 2003; Girman and Lund, 2007; Ozeki et al., 2009; Shushruth et al., 2013; Self et al., 2014), supporting the hypothesis that nCRFs make neurons sensitive to context and help the representation of salience. I have shown that the amount of non-classical suppression observed in individual SC neurons depends on the relative contrast over the CRF and the nCRFs, suggesting that surround suppression may be used by SC neurons to detect contrast discontinuities. Similarly, suppression depends on the relative direction and temporal frequency between the CRF and the surrounding region, being stronger when they are matched. nCRFs in the mouse superior colliculus are therefore sensitive to spatial discontinuities across multiple dimensions of the visual scene. Orientation selectivity of surround suppression has previously been taken to be a signature of surround suppression in primary visual cortex of mice, cats and monkeys (mouse: Self et al., 2014; cat: Nelson and Frost, 1978; DeAngelis et al., 1994; Ozeki et al., 2004; monkey: Sillito et al., 1995; Levitt and Lund, 1997; Cavanaugh et al., 2002b; Webb et al., 2005; Henry et al., 2013),

but my work and that of others proves that orientation selectivity is also a hallmark of surround suppression in the superior colliculus of rodents and cats (rat: Girman and Lund, 2007; cat: Sterling and Wickelgren, 1969). The degree of orientation selectivity of surround suppression in the LGN is controversial (Sillito et al., 1993; Solomon et al., 2002; Ozeki et al., 2004; Bonin et al., 2005; Naito et al., 2007) and currently unknown in mouse LGN. I observed stronger orientation tuning of suppression in awake animals, but because orientation tuning is generally diminished by anaesthesia in both SC (Chapter 3, Fig. 3.20) and V1 (Durand et al., 2016), the origin of orientation-tuned nCRFs in SC is unclear.

Less work has investigated the tuning of suppressive surrounds for speed or temporal frequency. In anesthetized cat LGN (Bonin et al., 2005) and macaque V1 (Webb et al., 2005) the nCRF is tuned towards high temporal frequencies, similar to my observations in SC of awake (but not anesthetized) mice. The overall increase in temporal frequency resolution that I observe in SC of awake mice (Chapter 3, Fig. 3.17) is not seen in V1 (Durand et al., 2016) and this may support the hypothesis that surround suppression in the mouse SC does not require cortical inputs, and is either inherited from the retina or computed in the SC.

In summary, I showed that suppression is stronger when the classical and the non-classical receptive fields are presented with similar contrast, direction and temporal frequency. Suppression is released in the presence of a discontinuity between the visual field over the CRF and over the nCRF.

4.4.2 Origin of surround suppression in the superior colliculus

The origin of surround suppression in the SC is unclear: it may be inherited from the retina, be computed by intracollicular circuits, or reflect feedback from the cortex. Given the high proportion of SC cells that are suppressed by surrounding stimuli, the first question to ask is if any retinal ganglion cells display similar properties. Most retinal ganglion cells send axonal terminals to the SC (Ellis et al., 2016) and it is likely that at least part of the functional properties found in the SC are directly inherited from the retina, as it has been shown to be the case for direction selectivity (Shi et al., 2017). While it remains unclear which specific RGC types project to the SC in mouse (Martersteck et al., 2017), there are some likely candidates and several

mouse RGC types are known to show suppression from regions surrounding their CRF. One type is the non-directionally selective, ON-OFF W3 cells (Zhang et al., 2012), thought to be a homolog of the "net convexity detector" cells in the frog retina (Lettvin et al., 1959) and the local edge detector (LED) cells first described in rabbit (Levick, 1967). Recent work also shows other RGCs with size sensitive responses that are ON-OFF and lacking directional selectivity (high definition retinal ganglion cells (HD) (Jacoby and Schwartz, 2017). J-RGCs and BD-RGCs also display size dependent receptive fields but, in contrast to W3 and HD-RGCs, are strongly directional selective, with J-RGCs having OFF responses and BD-RGGs having ON-OFF subfields. W3-RGCs, J-RGCs and BD-RGCs have been shown to project to the SC (Kim et al., 2010).

Surround suppression might also reflect computations within the SC. Intracollicular networks in the superficial SC have been shown to include inhibitory lateral interactions that suppress the activity of simultaneously activated neurons and are therefore suitable for the detection of salient stimuli (Phongphanphanee et al., 2014). We are still far from having a full description of neuronal subtypes and their functional properties in the SC, but recent genetic advances have revealed some of them. Inhibitory horizontal cells have been shown to respond to large stimuli (Gale and Murphy, 2014) and to help implement surround suppression on wide-field cells in mouse SC (Gale and Murphy, 2016). A similar mechanism for constructing size tuning is implemented by superficial interneurons in the zebrafish optic tectum (Del Bene et al., 2010) and by somatostatin interneurons in mouse primary visual cortex (Adesnik et al., 2012). Neurons in cat LGN have recently been shown to increase the amount of suppression inherited from upstream areas by dampening the effectiveness of retinal signals (Fisher et al., 2017); a similar process might take place in the SC.

The superior colliculus also receives massive input from primary visual cortex (May, 2006), that may therefore influence the responses of collicular neurons. Despite this, removal of cortico-collicular input seems to influence the gain of SC neurons without affecting their tuning properties (Wang et al., 2010;Zhao et al., 2014) suggesting a minor role of cortical feedback in the construction of visual selectivities of neurons in the SC.

4.4.3 Time course of SC responses

Adaptation is a neural mechanism that allows neurons to adjust their responses depending on the recent stimulus history. The reduction in response to a stimulus that is homogenous in time might be used by neurons to signal changes, and therefore saliency, in the time domain.

I have shown that most neurons in the mouse superior colliculus show adaptation: responses are characterized by an initial, large, transient response that decays quickly, even if the stimulus is moving (and thus not inducing light adaptation). In monkey, the amplitude of the initial transient response in SC is known to affect the nature and latency of orienting behaviours such as saccades (reviewed in Boehnke and Munoz, 2008). Given the likely importance of the initial transient for behavioural responses, it makes sense that the transient response should also be the main target of spatial contextual modulation brought in by the nCRF. I found that in mouse SC surround suppression had strong impact on the initial response, and that there was a strong correlation between the degree of adaptation and suppression within individual neurons. I therefore demonstrate that neurons characterized by a transient, adapting response are more likely to also be affected by spatial context and can therefore signal the presence of visually salient objects in both the spatial and the temporal domain. This may suggest the presence of a subpopulation of 'saliency' neurons within the SC that are simultaneously sensitive to discontinuities in diverse features of the visual field. Both surround suppression and adaptation were reduced under anaesthesia, but the impact on adaptation was stronger. The different impact of anaesthesia on adaptation and surround suppression suggests they reflect the activity of distinct neural mechanisms.

In primates, RGCs projecting to the magnocellular layers of the LGN, and LGN magnocellular cells themselves, are more likely to show surround suppression than ganglion cells and LGN cells that are part of the parvocellular pathway (Solomon et al., 2006). Interestingly, magnocellular pathway cells also show strong adaptation – mostly built in the retina – while parvocellular cells do not (Solomon et al., 2004). The co-occurrence of surround suppression and adaptation in the primate magnocellular pathway resembles my observations in the mouse SC, showing co-occurrence of surround suppression and adaptation in individual neurons. The magnocellular-

parvocellular segregation found in primates (and similar division of X- and Y cells in cat) is not at all clear in mouse (Piscopo et al., 2013), but if analogous pathways exist in this species it is likely that the SC mainly receives inputs from magnocellular-like retinal ganglion cells. Consistent with this hypothesis, mouse RGCs that show transient responses (like magnocellular cells in primate) preferentially target the SC and largely avoid the dLGN (Ellis et al., 2016).

Suppression was stronger during the initial response but less selective for the difference between a central stimulus and its surround. Non-selective suppression appeared to adapt more quickly than tuned suppression, and the consequence is that suppression is more sharply tuned in later activity. The effect of nCRF in the late phase of responses could even become facilitatory when the surround features were different from those over the CRF. This phenomenon raises the possibility that tuned nCRF activity may be constructed by two distinct neural mechanisms, a non-tuned adapting suppression and a tuned facilitation not affected by time. The possibility of adaptive nCRF suppression has already been raised in macaque V1 (Cavanaugh et al., 2002a). There, the reduction in suppression over time was attributed to decreases in the gain of both classical and non-classical mechanisms, but the gain of the nCRF adapted more quickly, hence reducing suppression over time. Similarly, my observations suggest that there is an untuned, adapting component of suppression in mouse SC. In V1 of mice and monkeys, untuned suppression is known to appear before tuned suppression, supporting the hypothesis that they could be implemented by distinct networks (Henry et al., 2013;Self et al., 2014). While these studies focused on the onset of suppression and did not investigate its decay over time, it is possible that tuned and untuned suppression in V1 might follow similar adaptive time courses to those I observed in SC. Whether the tuning of nCRFs is provided by tuned facilitation rather than tuned suppression is difficult to test using neuronal firing rate alone. Future experiments measuring the time course and selectivity of excitatory and inhibitory input currents would shed light on these mechanisms.

4.5 CONCLUSION

I have shown that nCRF suppression and adaptation robustly modulate the activity of most neurons in mouse SC. The presence of these mechanisms, likely to underpin the neuronal

representation of salience, supports the hypothesis that the superior colliculus is likely to be a key area for salience detection. Future experiments may elucidate the circuit mechanisms generating them, and reveal if they are used to organize the behavioural responses the SC is important for.

Chapter 5
Conclusion

The aim of this thesis was to expand our knowledge about how animals use information from the outside world to interact with it. The way an animal interacts with the environment determines its survival, and sensory systems have evolved so that organisms can gather appropriate information about the outside world and adjust their behaviour to it. The amount of information that the senses are able to provide is large, while behaviour is usually constrained to one or a few actions. In order to guide behaviour, the brain needs to filter and prioritise among available sensory information. The selection of information is crucial. Circumstances that require immediate action, such as the appearance of a predator, are likely to engage brain circuits that prioritize the event and the relevant information, ultimately disengaging other less important activities.

In this thesis, I first showed how mice respond to visual stimuli that simulate aerial predators. I proved that mice can use differences in visual information to guide behaviour, thereby also validating that the mouse is a suitable animal in which to study how visual information is prioritized. In order to shed light on how visual saliency may be encoded in the brain, I focused

on neural responses in the superior colliculus, an area thought to be important for the computation of saliency. I found that visual neurons in the superior colliculus are sensitive to a broad spectrum of visual features, which may allow it to represent saliency across many dimensions of the visual image. I then showed that the activity of neurons in the SC depends on spatial and temporal context, such that neural responses are diminished when the visual scene is homogenous in space and time and stronger when stimuli are novel or different from their background.

5.1 Defence behaviours in mice

In Chapter 2, I showed that mice can choose to execute freeze or flight – two distinct defensive behaviours – based on vision alone. Flight can be induced by a looming stimulus, simulating an approaching predator – mice should and do choose to escape from this imminent threat. I showed also that a small moving stimulus, simulating a potential but distal predator, triggers freezing – again this is rational, as freezing may reduce the likelihood of been detected by this potential threat. In addition during sweep-induced freezing sometimes mice sometimes choose to flee, suggesting that even while they are freezing these animals continue to evaluate among available defence strategies. In order to shed light on the visual properties that are more likely to induce freeze or flight, I manipulated the speed and the polarity of the sweep stimulus. I found that flight probability during sweeping stimuli increases with stimulus speed, suggesting that the neural system selecting flight is sensitive to stimulus velocity. In addition, I found that black and white sweeps trigger analogous responses. Previous work has shown that behavioural responses to a white looming stimulus are instead variable and trigger flight less reliably than do black looming stimuli (Yilmaz and Meister, 2013). Since those responses were obtained from a small number of animals, future experiments aimed at increasing the number of observations may be needed to determine how polarity sensitive both visually-guided behaviours are. If white looming stimuli indeed do not trigger flight behaviour, this may indicate fundamental differences in the selectivity of visual neurons subserving both behaviours.

The specific stimulus properties that mice use to distinguish sweeping from looming stimuli are not known, and it is of interest to discover if there is a particular visual feature that is

necessary and sufficient for each behaviour. Future experiments parametrically manipulating the various visual features of the stimuli (e.g. edges, contrast, trajectory, etc.) will be necessary to understand which – or which combination of – features is important. Discovering the visual features associated with the initiation of freeze or flight would not only help understanding the evolutionary drive behind those behaviours, but also help direct research aimed at understanding the brain circuits underpinning them. The superior colliculus is likely to have an important role in visually-driven defence behaviours, but it still not clear how much these behaviours rely on computations occurring within the SC. Similarly, it is not clear if and how visual cortex is involved, or if subcortical mechanisms alone are able to subserve the defensive behaviours I observed. To test if freeze and flight responses to visual stimuli depend on cortical or subcortical networks, or both, future experiments could investigate the behavioural response to sweep and loom stimuli while primary visual cortex is silenced through PV^+ interneurons optogenetic activation. Performing similar inactivation experiments in SC and other visual areas would shed light on which brain areas are critical for these defensive behaviours. If multiple areas are involved, this would open the possibility of perturbing specific feedforward and/or feedback connections among the relevant structures during the behavioural testing (e.g. disruption of V1 feedback projection to SC). Even after identification of the areas and inter-area connections critical for freeze and flight responses, it is likely that specific subpopulations of neurons in the identified areas play distinct roles in constructing these innate responses. It is known that flight responses can be triggered by a looming-sensitive, PV^+, glutamatergic population of neurons in SC (Shang et al., 2015), but it is not clear if these neurons are necessary for the flight in response to looming stimuli. Similarly, it has been shown that a subpopulation of glutamatergic neurons in SC can trigger freezing behaviour (Wei et al., 2015) and that a subset of SC neurons ('widefield cells') are selective for small stimuli moving across a large portion of the visual space (Gale and Murphy, 2014), but it is not known if the two populations are involved in freezing responses to a sweep stimulus. The necessity of these subpopulations for visually-induced freeze and flight could be tested by optogenetically inactivating them during the presentation of loom or sweep stimuli. Behavioural testing and recordings during disruption of

specific connections, neural subpopulations or areas would help unveil the circuits implicated in the categorical classification of sweep and loom.

Freeze and flight behaviours are very distinct responses, and therefore reflect a choice between conflicting motor plans. The fact that they appear evolutionarily conserved and rapidly engaged after stimulus presentation suggests that the circuits behind them may be tractable. The behavioural paradigm I have developed is therefore promising for studying perceptual decision making. Neural recordings from specific populations of neurons in the brain areas involved in these behaviours could shed light how visual signals are integrated and subsequently transformed into motor actions. For example, some neurons could carry information about the presence of a salient stimulus (as seen in Chapter 5 for the majority of neurons in SC), others could store increasing evidence for the identification of the stimulus in a certain category (sweep or loom), while others could signal the behavioural choice (freeze or flight). Once the subpopulations of neurons implicated in distinct portions of the decision process are identified, the neural circuit they are part of could be more easily tackeled. Understanding how visual information is integrated and transformed into behavioural outputs by relatively simple circuits is in turn likely to help understanding more complex processes of decision making.

Despite being a rapid and reproducible behaviour, I and others have shown that flight is not a simple reflex but involves consideration of a number of factors such as availability of refuge and, importantly, the refuge's location. Mice flee directly to refuge, suggesting that the brain may store a "homing vector" readily retrieved to guide escape when necessary, and quickly updated in case of environmental changes (Vale et al., 2017). How and where is the information about the refuge location stored in the brain? Is the homing vector stored and updated based on allocentric or egocentric cues? Is safety an important factor when a spatial representation of the environment is constructed? If safety is important, how and where is it encoded in the brain? How is information about refuge location used to guide motor response, and is that information combined with other contextual factors such as the trajectory of the predator? These questions require drawing the link between perceptual and cognitive representations in the brain, and answering them would shed light on brain mechanisms for visual perception, sensorimotor integration, decision-making, navigation, and memory. To start to answer some of these

questions, I would begin by repeating the sweep and loom tests described in this thesis while recording the activity of place cells and head-direction cells in the hippocampus and other brain regions involved in the representation of space (e.g. enthorinal cortex, retrosplinium). To investigate if safety is encoded in the spatial map of the environment, I would then establish if the nest position is particularly overrepresented compared to other regions of the arena. To shed light on how the information about safety is used during visually-triggered defensive behaviours, I would then look at how the activity of neurons encoding the nest position changes after the appearance of a threatening stimulus and during the animals' behavioural response.

5.2 Visual properties of SC neurons in mouse

In Chapter 3 I provided a description of the visual properties in neurons in the mouse superior colliculus, an area important for orienting behaviours in response to salient stimuli, in anesthetized and awake animals. My results are generally in agreement with previous studies performed in anesthetized animals, the main departure point being the proportion of neurons displaying linear responses, which was higher in our sample than reported in most previous work.

While surveying the properties of a large population of neurons, my experiments do not discriminate among different subpopulations of neurons in the SC, and in order to understand the computations taking place in the SC it would be important to have this information. Future experiments may be able to characterize the visual properties of different subpopulations of SC neurons in awake animals by performing recordings targeted to genetically identified neurons, as has been done in anesthetized animals (Gale and Murphy, 2014). Patch clamp recordings paired with optogenetic inactivation of the feedback coming from primary visual cortex could then help understanding the origin of eventual differences in visual preferences among the subpopulations, and suggest if different subclasses receive inputs from common or specific subpopulations of retinal ganglion cells, visual cortical cells etc. If the inputs were common to different subpopulations of SC neurons, this would open the question of how the observed differences are built within the SC.

I have shown that anaesthesia has a profound effect on the activity of SC neurons, mainly affecting their sensitivity to visual stimuli and their firing rates (both spontaneous and evoked), their response latency, and their sensitivity to rapidly moving stimuli. The question that arises is to what extent these changes are due to differences in retinal or cortical input, or to changes in the intrinsic biophysical properties of SC neurons. A comparison of the intracellular voltage in anesthetized and awake animals coupled with optogenetic manipulation of cortical feedback would shed light on some of the mechanisms giving rise to the anaesthesia-induced differences I observed.

5.3 nCRF and adaptation in mouse SC

Given the importance of the SC for orienting towards or away from salient stimuli, in Chapter 4 I investigated potential neural mechanisms for representing salience in space and time: surround suppression and adaptation. I showed that the majority of SC neurons show surround suppression, and that suppression is generally greatest when surrounding features match those over the CRF. Activity is therefore diminished for homogenous textures, while suppression is released in presence of a visual discontinuity. Most neurons in SC also show adaptation, and the magnitude of suppression and adaptation covaries in single neurons. These functional properties suggest that the SC is able to represent visual stimuli that are novel or that stand out from the rest of the visual scene, consistent with its role for orienting behaviours.

The origin of suppressive surrounds in the SC is unclear. In ‘wide-field’ SC cells, surround suppression is partly due to the activity of ‘horizontal’ cells (Gale and Murphy, 2016), but how the remaining suppression is implemented, and if this is true in other SC subpopulations that also display suppression (e.g. ‘narrow-field’ cells) is not known. Suppression may be inherited from the retina, built in the SC or reflect cortical input. In addition, the selectivity of suppressive surrounds for different visual properties over the CRF (direction, temporal frequency) may be implemented by distinct mechanisms. The use of intracellular and extracellular recordings combined with optogenetic approaches aimed at selectively disrupting the input from specific RGC populations, specific SC neurons, or cortical feedback, would help to determine the origin of surround suppression in the SC and in SC different subpopulations of neurons.

5.4 Conclusion

In summary, I have shown that mice use visual information to make behavioural choices, and that the mouse SC is endowed with neurons sensitive to large variety of visual features and apt to highlight visually salient stimuli. The SC is therefore a likely candidate for the implementation of a bottom-up representation of salience, particularly in rodents where it is a major hub of visually guided behaviour. The SC's capacity for representing salience is intriguingly complementary to its involvement in defensive behaviours, and makes it an appealing target brain area in which to further study the transformation of sensory information into behavioural outputs. The SC is unlikely to be the only area involved in the computation of salience and in the generation of defensive behaviours, but is likely to play a key role. It remains to be unveiled if the neural mechanisms I investigated here – surround suppression and adaptation – are those that enable salience encoding, and whether they help highlight the presence and level of threat of a potential predator.

Bibliography

Abrahamson, E.E., and Moore, R.Y. (2001). Suprachiasmatic nucleus in the mouse: retinal innervation, intrinsic organization and efferent projections. *Brain Res* 916**,** 172-191.

Adesnik, H., Bruns, W., Taniguchi, H., Huang, Z.J., and Scanziani, M. (2012). A neural circuit for spatial summation in visual cortex. *Nature* 490**,** 226-231.

Ahmadlou, M., Heimel, J.A. (2015). Preference for concentric orientations in the mouse superior colliculus. *Nat Commun* 6, 6773.

Albano, J.E., and Wurtz, R.H. (1982). Deficits in eye position following ablation of monkey superior colliculus, pretectum, and posterior-medial thalamus. *J Neurophysiol* 48**,** 318-337.

Allman, J., Miezin, F., and Mcguinness, E. (1985a). Direction- and velocity-specific responses from beyond the classical receptive field in the middle temporal visual area (MT). *Perception* 14**,** 105-126.

Allman, J., Miezin, F., and Mcguinness, E. (1985b). Stimulus specific responses from beyond the classical receptive field: neurophysiological mechanisms for local-global comparisons in visual neurons. *Annu Rev Neurosci* 8**,** 407-430.

Andermann, M.L., Kerlin, A.M., and Reid, R.C. (2010). Chronic cellular imaging of mouse visual cortex during operant behavior and passive viewing. *Front Cell Neurosci* 4**,** 3.

Andermann, M.L., Kerlin, A.M., Roumis, D.K., Glickfeld, L.L., and Reid, R.C. (2011). Functional specialization of mouse higher visual cortical areas. *Neuron* 72**,** 1025-1039.

Ayaz, A., Saleem, A.B., Scholvinck, M.L., and Carandini, M. (2013). Locomotion controls spatial integration in mouse visual cortex. *Curr Biol* 23**,** 890-894.

Baccus, S.A., and Meister, M. (2002). Fast and slow contrast adaptation in retinal circuitry. *Neuron* 36**,** 909-919.

Baden, T., Berens, P., Franke, K., Roman Roson, M., Bethge, M., and Euler, T. (2016). The functional diversity of retinal ganglion cells in the mouse. *Nature* 529**,** 345-350.

Baldauf, Z.B., Wang, X.P., Wang, S., and Bickford, M.E. (2003). Pretectotectal pathway: an ultrastructural quantitative analysis in cats. *J Comp Neurol* 464**,** 141-158.

Benevento, L.A., and Fallon, J.H. (1975). The ascending projections of the superior colliculus in the rhesus monkey (Macaca mulatta). *J Comp Neurol* 160**,** 339-361.

Bevins, R.A., and Besheer, J. (2006). Object recognition in rats and mice: a one-trial non-matching-to-sample learning task to study 'recognition memory'. *Nat Protoc* 1**,** 1306-1311.

Bickford, M.E., Zhou, N., Krahe, T.E., Govindaiah, G., and Guido, W. (2015). Retinal and Tectal "Driver-Like" Inputs Converge in the Shell of the Mouse Dorsal Lateral Geniculate Nucleus. *J Neurosci* 35**,** 10523-10534.

Billington, J., Wilkie, R.M., Field, D.T., and Wann, J.P. (2011). Neural processing of imminent collision in humans. *Proc Biol Sci* 278**,** 1476-1481.

Bisti, S., and Sireteanu, R.C. (1976). Sensitivity to spatial frequency and contrast of visual cells in the cat superior colliculus. *Vision Res* 16**,** 247-251.

Blanchard, D.C. (1997). Stimulus, environmental, and pharmacological control of defensive behaviors. 283-303.

Blasdel, G.G., and Salama, G. (1986). Voltage-sensitive dyes reveal a modular organization in monkey striate cortex. *Nature* 321**,** 579-585.

Boehnke, S.E., Berg, D.J., Marino, R.A., Baldi, P.F., Itti, L., and Munoz, D.P. (2011). Visual adaptation and novelty responses in the superior colliculus. *Eur J Neurosci* 34**,** 766-779.

Boehnke, S.E., and Munoz, D.P. (2008). On the importance of the transient visual response in the superior colliculus. *Curr Opin Neurobiol* 18**,** 544-551.

Bonin, V., Mante, V., and Carandini, M. (2005). The suppressive field of neurons in lateral geniculate nucleus. *J Neurosci* 25**,** 10844-10856.

Borji, A., and Itti, L. (2013). State-of-the-art in visual attention modeling. *IEEE Trans Pattern Anal Mach Intell* 35**,** 185-207.

Boycott, B.B., and Wassle, H. (1974). The morphological types of ganglion cells of the domestic cat's retina. *J Physiol* 240**,** 397-419.

Brandao, M.L., Cardoso, S.H., Melo, L.L., Motta, V., and Coimbra, N.C. (1994). Neural substrate of defensive behavior in the midbrain tectum. *Neurosci Biobehav Rev* 18**,** 339-346.

Bruce, C.J., Desimone, R., and Gross, C.G. (1986). Both striate cortex and superior colliculus contribute to visual properties of neurons in superior temporal polysensory area of macaque monkey. *J Neurophysiol* 55**,** 1057-1075.

Busse, L., Ayaz, A., Dhruv, N.T., Katzner, S., Saleem, A.B., Scholvinck, M.L., Zaharia, A.D., and Carandini, M. (2011). The detection of visual contrast in the behaving mouse. *J Neurosci* 31**,** 11351-11361.

Butter, C.M., Weinstein, C., Bender, D.B., and Gross, C.G. (1978). Localization and detection of visual stimuli following superior colliculus lesions in rhesus monkeys. *Brain Res* 156**,** 33-49.

Cang, J., and Feldheim, D.A. (2013). Developmental mechanisms of topographic map formation and alignment. *Annu Rev Neurosci* 36**,** 51-77.

Cannon, M.W., and Fullenkamp, S.C. (1991). Spatial interactions in apparent contrast: inhibitory effects among grating patterns of different spatial frequencies, spatial positions and orientations. *Vision Res* 31**,** 1985-1998.

Carandini, M., and Heeger, D.J. (2011). Normalization as a canonical neural computation. *Nat Rev Neurosci* 13**,** 51-62.

Card, G., and Dickinson, M.H. (2008). Visually mediated motor planning in the escape response of Drosophila. *Curr Biol* 18**,** 1300-1307.

Carello, C.D., and Krauzlis, R.J. (2004). Manipulating intent: evidence for a causal role of the superior colliculus in target selection. *Neuron* 43**,** 575-583.

Carman, L.S., and Schneider, G.E. (1992). Orienting behavior in hamsters with lesions of superior colliculus, pretectum, and visual cortex. *Exp Brain Res* 90**,** 79-91.

Carter-Dawson, L.D., and Lavail, M.M. (1979). Rods and cones in the mouse retina. I. Structural analysis using light and electron microscopy. *J Comp Neurol* 188**,** 245-262.

Casagrande, V.A., and Diamond, I.T. (1974). Ablation study of the superior colliculus in the tree shrew (Tupaia glis). *J Comp Neurol* 156**,** 207-237.

Cavanaugh, J., Alvarez, B.D., and Wurtz, R.H. (2006). Enhanced performance with brain stimulation: attentional shift or visual cue? *J Neurosci* 26**,** 11347-11358.

Cavanaugh, J., and Wurtz, R.H. (2004). Subcortical modulation of attention counters change blindness. *J Neurosci* 24**,** 11236-11243.

Cavanaugh, J.R., Bair, W., and Movshon, J.A. (2002a). Nature and interaction of signals from the receptive field center and surround in macaque V1 neurons. *J Neurophysiol* 88**,** 2530-2546.

Cavanaugh, J.R., Bair, W., and Movshon, J.A. (2002b). Selectivity and spatial distribution of signals from the receptive field surround in macaque V1 neurons. *J Neurophysiol* 88**,** 2547-2556.

Chalupa, L.M., and Thompson, I. (1980). Retinal ganglion cell projections to the superior colliculus of the hamster demonstrated by the horseradish peroxidase technique. *Neurosci Lett* 19**,** 13-19.

Cheong, S.K., Tailby, C., Solomon, S.G., and Martin, P.R. (2013). Cortical-like receptive fields in the lateral geniculate nucleus of marmoset monkeys. *J Neurosci* 33**,** 6864-6876.

Chubb, C., Sperling, G., and Solomon, J.A. (1989). Texture interactions determine perceived contrast. *Proc Natl Acad Sci U S A* 86**,** 9631-9635.

Churan, J., Guitton, D., and Pack, C.C. (2012). Perisaccadic remapping and rescaling of visual responses in macaque superior colliculus. *PLoS One* 7**,** e52195.

Clites, B.L., and Pierce, J.T. (2017). Identifying Cellular and Molecular Mechanisms for Magnetosensation. *Annu Rev Neurosci* 40**,** 231-250.

Comoli, E., Coizet, V., Boyes, J., Bolam, J.P., Canteras, N.S., Quirk, R.H., Overton, P.G., and Redgrave, P. (2003). A direct projection from superior colliculus to substantia nigra for detecting salient visual events. *Nat Neurosci* 6**,** 974-980.

Comoli, E., Das Neves Favaro, P., Vautrelle, N., Leriche, M., Overton, P.G., and Redgrave, P. (2012). Segregated anatomical input to sub-regions of the rodent superior colliculus associated with approach and defense. *Front Neuroanat* 6**,** 9.

Conley, M., and Friederich-Ecsy, B. (1993). Functional organization of the ventral lateral geniculate complex of the tree shrew (Tupaia belangeri): I. Nuclear subdivisions and retinal projections. *J Comp Neurol* 328**,** 1-20.

Cooper, W.E. (1997). Factors Affecting Risk and Cost of Escape by the Broad-Headed Skink (Eumeces laticeps): Predator Speed, Directness of Approach, and Female Presence. *Herpetologica* 53**,** 464-474.

Cosenza, R.M., and Moore, R.Y. (1984). Afferent connections of the ventral lateral geniculate nucleus in the rat: an HRP study. *Brain Res* 310**,** 367-370.

Croner, L.J., and Kaplan, E. (1995). Receptive fields of P and M ganglion cells across the primate retina. *Vision Res* 35**,** 7-24.

Crook, J.D., Peterson, B.B., Packer, O.S., Robinson, F.R., Troy, J.B., and Dacey, D.M. (2008). Y-cell receptive field and collicular projection of parasol ganglion cells in macaque monkey retina. *J Neurosci* 28**,** 11277-11291.

Cynader, M., and Berman, N. (1972). Receptive-field organization of monkey superior colliculus. *J Neurophysiol* 35**,** 187-201.

Davidson, R.M., and Bender, D.B. (1991). Selectivity for relative motion in the monkey superior colliculus. *J Neurophysiol* 65**,** 1115-1133.

De Vries, S.E., and Clandinin, T.R. (2012). Loom-sensitive neurons link computation to action in the Drosophila visual system. *Curr Biol* 22**,** 353-362.

Dean, P., and Redgrave, P. (1984). The superior colliculus and visual neglect in rat and hamster. I. Behavioural evidence. *Brain Res* 320**,** 129-141.

Dean, P., Redgrave, P., and Westby, G.W. (1989). Event or emergency? Two response systems in the mammalian superior colliculus. *Trends Neurosci* 12**,** 137-147.

Deangelis, G.C., Freeman, R.D., and Ohzawa, I. (1994). Length and width tuning of neurons in the cat's primary visual cortex. *J Neurophysiol* 71**,** 347-374.

Del Bene, F., Wyart, C., Robles, E., Tran, A., Looger, L., Scott, E.K., Isacoff, E.Y., and Baier, H. (2010). Filtering of visual information in the tectum by an identified neural circuit. *Science* 330**,** 669-673.

Derrington, A.M., and Lennie, P. (1984). Spatial and temporal contrast sensitivities of neurones in lateral geniculate nucleus of macaque. *J Physiol* 357**,** 219-240.

Desjardin, J.T., Holmes, A.L., Forcelli, P.A., Cole, C.E., Gale, J.T., Wellman, L.L., Gale, K., and Malkova, L. (2013). Defense-like behaviors evoked by pharmacological disinhibition of the superior colliculus in the primate. *J Neurosci* 33**,** 150-155.

Devonshire, I.M., Grandy, T.H., Dommett, E.J., and Greenfield, S.A. (2010). Effects of urethane anaesthesia on sensory processing in the rat barrel cortex revealed by combined optical imaging and electrophysiology. *Eur J Neurosci* 32**,** 786-797.

Dhande, O.S., and Huberman, A.D. (2014). Retinal ganglion cell maps in the brain: implications for visual processing. *Curr Opin Neurobiol* 24**,** 133-142.

Dhande, O.S., Stafford, B.K., Lim, J.A., and Huberman, A.D. (2015). Contributions of Retinal Ganglion Cells to Subcortical Visual Processing and Behaviors. *Annu Rev Vis Sci* 1**,** 291-328.

Doubell, T.P., Skaliora, I., Baron, J., and King, A.J. (2003). Functional connectivity between the superficial and deeper layers of the superior colliculus: an anatomical substrate for sensorimotor integration. *J Neurosci* 23**,** 6596-6607.

Drager, U.C., and Hubel, D.H. (1975). Responses to visual stimulation and relationship between visual, auditory, and somatosensory inputs in mouse superior colliculus. *J Neurophysiol* 38**,** 690-713.

Drager, U.C., and Hubel, D.H. (1976). Topography of visual and somatosensory projections to mouse superior colliculus. *J Neurophysiol* 39**,** 91-101.

Durand, S., Iyer, R., Mizuseki, K., De Vries, S., Mihalas, S., and Reid, R.C. (2016). A Comparison of Visual Response Properties in the Lateral Geniculate Nucleus and Primary Visual Cortex of Awake and Anesthetized Mice. *J Neurosci* 36**,** 12144-12156.

Dutta, A., and Gutfreund, Y. (2014). Saliency mapping in the optic tectum and its relationship to habituation. *Front Integr Neurosci* 8**,** 1.

Edwards, S.B., Rosenquist, A.C., and Palmer, L.A. (1974). An autoradiographic study of ventral lateral geniculate projections in the cat. *Brain Res* 72**,** 282-287.

Eilam, D. (2005). Die hard: a blend of freezing and fleeing as a dynamic defense--implications for the control of defensive behavior. *Neurosci Biobehav Rev* 29**,** 1181-1191.

Ellard, C.G. (1996). Laboratory studies of antipredator behavior in the Mongolian gerbil (Meriones unguiculatus): factors affecting response attenuation with repeated presentations. *J Comp Psychol* 110**,** 155-163.

Ellard, C.G., and Goodale, M.A. (1988). A functional analysis of the collicular output pathways: a dissociation of deficits following lesions of the dorsal tegmental

decussation and the ipsilateral collicular efferent bundle in the Mongolian gerbil. *Exp Brain Res* 71**,** 307-319.

Ellis, E.M., Gauvain, G., Sivyer, B., and Murphy, G.J. (2016). Shared and distinct retinal input to the mouse superior colliculus and dorsal lateral geniculate nucleus. *J Neurophysiol* 116**,** 602-610.

Endo, T., Yanagawa, Y., Obata, K., and Isa, T. (2003). Characteristics of GABAergic neurons in the superficial superior colliculus in mice. *Neuroscience Letters* 346**,** 81-84.

Ennaceur, A. (2010). One-trial object recognition in rats and mice: methodological and theoretical issues. *Behav Brain Res* 215**,** 244-254.

Enroth-Cugell, C., and Robson, J.G. (1966). The contrast sensitivity of retinal ganglion cells of the cat. *J Physiol* 187**,** 517-552.

Enroth-Cugell, C., and Shapley, R.M. (1973). Flux, not retinal illumination, is what cat retinal ganglion cells really care about. *J Physiol* 233**,** 311-326.

Fanselow, M.S. (1994). Neural organization of the defensive behavior system responsible for fear. *Psychon Bull Rev* 1**,** 429-438.

Fecteau, J.H., Bell, A.H., and Munoz, D.P. (2004). Neural correlates of the automatic and goal-driven biases in orienting spatial attention. *J Neurophysiol* 92**,** 1728-1737.

Fecteau, J.H., and Munoz, D.P. (2006). Salience, relevance, and firing: a priority map for target selection. *Trends Cogn Sci* 10**,** 382-390.

Feinberg, E.H., and Meister, M. (2015). Orientation columns in the mouse superior colliculus. *Nature* 519**,** 229-232.

Fitzpatrick, D., Conley, M., Luppino, G., Matelli, M., and Diamond, I.T. (1988). Cholinergic projections from the midbrain reticular formation and the parabigeminal nucleus to the lateral geniculate nucleus in the tree shrew. *J Comp Neurol* 272**,** 43-67.

Freedman, E.G., Stanford, T.R., and Sparks, D.L. (1996). Combined eye-head gaze shifts produced by electrical stimulation of the superior colliculus in rhesus monkeys. *J Neurophysiol* 76**,** 927-952.

Fukuda, Y., and Stone, J. (1974). Retinal distribution and central projections of Y-, X-, and W-cells of the cat's retina. *J Neurophysiol* 37**,** 749-772.

Gabbiani, F., Krapp, H.G., Koch, C., and Laurent, G. (2002). Multiplicative computation in a visual neuron sensitive to looming. *Nature* 420**,** 320-324.

Gale, S.D., and Murphy, G.J. (2014). Distinct representation and distribution of visual information by specific cell types in mouse superficial superior colliculus. *J Neurosci* 34**,** 13458-13471.

Gale, S.D., and Murphy, G.J. (2016). Active Dendritic Properties and Local Inhibitory Input Enable Selectivity for Object Motion in Mouse Superior Colliculus Neurons. *J Neurosci* 36**,** 9111-9123.

Gandhi, N.J., and Katnani, H.A. (2011). Motor functions of the superior colliculus. *Annu Rev Neurosci* 34**,** 205-231.

Gao, E., Deangelis, G.C., and Burkhalter, A. (2010). Parallel input channels to mouse primary visual cortex. *J Neurosci* 30**,** 5912-5926.

Gauvain, G., and Murphy, G.J. (2015). Projection-specific characteristics of retinal input to the brain. *J Neurosci* 35**,** 6575-6583.

Girman, S.V., and Lund, R.D. (2007). Most superficial sublamina of rat superior colliculus: neuronal response properties and correlates with perceptual figure-ground segregation. *J Neurophysiol* 98**,** 161-177.

Goldberg, M.E., and Wurtz, R.H. (1972a). Activity of superior colliculus in behaving monkey. I. Visual receptive fields of single neurons. *J Neurophysiol* 35**,** 542-559.

Goldberg, M.E., and Wurtz, R.H. (1972b). Activity of superior colliculus in behaving monkey. II. Effect of attention on neuronal responses. *J Neurophysiol* 35**,** 560-574.

Goodale, M.A., Foreman, N.P., and Milner, A.D. (1978). Visual orientation in the rat: a dissociation of deficits following cortical and collicular lesions. *Exp Brain Res* 31**,** 445-457.

Goodale, M.A., and Murison, R.C. (1975). The effects of lesions of the superior colliculus on locomotor orientation and the orienting reflex in the rat. *Brain Res* 88**,** 243-261.

Gottlieb, J. (2007). From thought to action: the parietal cortex as a bridge between perception, action, and cognition. *Neuron* 53**,** 9-16.

Graham, J. (1977). An autoradiographic study of the efferent connections of the superior colliculus in the cat. *J Comp Neurol* 173**,** 629-654.

Graybiel, A.M. (1978). A satellite system of the superior colliculus: the parabigeminal nucleus and its projections to the superficial collicular layers. *Brain Res* 145**,** 365-374.

Hafed, Z.M., and Chen, C.Y. (2016). Sharper, Stronger, Faster Upper Visual Field Representation in Primate Superior Colliculus. *Curr Biol* 26**,** 1647-1658.

Haider, B., Hausser, M., and Carandini, M. (2013). Inhibition dominates sensory responses in the awake cortex. *Nature* 493**,** 97-100.

Hall, W.C., and Lee, P. (1993). Interlaminar connections of the superior colliculus in the tree shrew. I. The superficial gray layer. *J Comp Neurol* 332**,** 213-223.

Harrington, M.E. (1997). The ventral lateral geniculate nucleus and the intergeniculate leaflet: interrelated structures in the visual and circadian systems. *Neurosci Biobehav Rev* 21**,** 705-727.

Harris, L.R. (1980). The superior colliculus and movements of the head and eyes in cats. *J Physiol* 300**,** 367-391.

Harting, J.K., Huerta, M.F., Hashikawa, T., and Van Lieshout, D.P. (1991). Projection of the mammalian superior colliculus upon the dorsal lateral geniculate nucleus: organization of tectogeniculate pathways in nineteen species. *J Comp Neurol* 304**,** 275-306.

Harting, J.K., Updyke, B.V., and Van Lieshout, D.P. (1992). Corticotectal projections in the cat: anterograde transport studies of twenty-five cortical areas. *J Comp Neurol* 324**,** 379-414.

Hartline, H.K. (1940). The receptive fields of optic nerve fibers. *American Journal of Physiology* 130**,** 690-699.

Hemmi, J.M., and Tomsic, D. (2012). The neuroethology of escape in crabs: from sensory ecology to neurons and back. *Curr Opin Neurobiol* 22**,** 194-200.

Hendry, S.H., and Reid, R.C. (2000). The koniocellular pathway in primate vision. *Annu Rev Neurosci* 23**,** 127-153.

Henry, C.A., Joshi, S., Xing, D., Shapley, R.M., and Hawken, M.J. (2013). Functional characterization of the extraclassical receptive field in macaque V1: contrast, orientation, and temporal dynamics. *J Neurosci* 33**,** 6230-6242.

Hochstein, S., and Shapley, R.M. (1976a). Linear and nonlinear spatial subunits in Y cat retinal ganglion cells. *J Physiol* 262**,** 265-284.

Hochstein, S., and Shapley, R.M. (1976b). Quantitative analysis of retinal ganglion cell classifications. *J Physiol* 262**,** 237-264.

Hofbauer, A., and Drager, U.C. (1985). Depth segregation of retinal ganglion cells projecting to mouse superior colliculus. *J Comp Neurol* 234**,** 465-474.

Hofbauer, A., and Hollander, H. (1986). Synaptic connections of cortical and retinal terminals in the superior colliculus of the rabbit: an electron microscopic double labelling study. *Exp Brain Res* 65**,** 145-155.

Hoffmann, K.P. (1973). Conduction velocity in pathways from retina to superior colliculus in the cat: a correlation with receptive-field properties. *J Neurophysiol* 36**,** 409-424.

Hong, Y.K., Kim, I.J., and Sanes, J.R. (2011). Stereotyped axonal arbors of retinal ganglion cell subsets in the mouse superior colliculus. *J Comp Neurol* 519**,** 1691-1711.

Hubel, D.H., and Wiesel, T.N. (1959). Receptive Fields of Single Neurones in the Cats Striate Cortex. *Journal of Physiology-London* 148**,** 574-591.

Hubel, D.H., and Wiesel, T.N. (1962). Receptive fields, binocular interaction and functional architecture in the cat's visual cortex. *J Physiol* 160**,** 106-154.

Hubel, D.H., and Wiesel, T.N. (1974). Sequence regularity and geometry of orientation columns in the monkey striate cortex. *J Comp Neurol* 158**,** 267-293.

Hubel, D.H., and Wiesel, T.N. (1979). Brain mechanisms of vision. *Sci Am* 241**,** 150-162.

Huberman, A.D., Feller, M.B., and Chapman, B. (2008a). Mechanisms underlying development of visual maps and receptive fields. *Annu Rev Neurosci* 31**,** 479-509.

Huberman, A.D., Manu, M., Koch, S.M., Susman, M.W., Lutz, A.B., Ullian, E.M., Baccus, S.A., and Barres, B.A. (2008b). Architecture and activity-mediated refinement of axonal projections from a mosaic of genetically identified retinal ganglion cells. *Neuron* 59**,** 425-438.

Huberman, A.D., and Niell, C.M. (2011). What can mice tell us about how vision works? *Trends Neurosci* 34**,** 464-473.

Huberman, A.D., Wei, W., Elstrott, J., Stafford, B.K., Feller, M.B., and Barres, B.A. (2009). Genetic identification of an On-Off direction-selective retinal ganglion cell subtype reveals a layer-specific subcortical map of posterior motion. *Neuron* 62**,** 327-334.

Inayat, S., Barchini, J., Chen, H., Feng, L., Liu, X., and Cang, J. (2015). Neurons in the most superficial lamina of the mouse superior colliculus are highly selective for stimulus direction. *J Neurosci* 35**,** 7992-8003.

Irvin, G.E., Casagrande, V.A., and Norton, T.T. (1993). Center/surround relationships of magnocellular, parvocellular, and koniocellular relay cells in primate lateral geniculate nucleus. *Vis Neurosci* 10**,** 363-373.

Ito, S., Feldheim, D.A., and Litke, A.M. (2017). Segregation of Visual Response Properties in the Mouse Superior Colliculus and Their Modulation during Locomotion. *J Neurosci* 37**,** 8428-8443.

Itti, L., and Koch, C. (2001). Computational modelling of visual attention. *Nat Rev Neurosci* 2**,** 194-203.

Itti, L., Koch, C., and Niebur, E. (1998). A model of saliency-based visual attention for rapid scene analysis. *IEEE Transactions on Pattern Analysis and Machine Intelligence* 20**,** 1254-1259.

Jacoby, J., and Schwartz, G.W. (2017). Three Small-Receptive-Field Ganglion Cells in the Mouse Retina Are Distinctly Tuned to Size, Speed, and Object Motion. *J Neurosci* 37**,** 610-625.

Jones, H.E., Andolina, I.M., Oakely, N.M., Murphy, P.C., and Sillito, A.M. (2000). Spatial summation in lateral geniculate nucleus and visual cortex. *Exp Brain Res* 135**,** 279-284.

Juavinett, A.L., and Callaway, E.M. (2015). Pattern and Component Motion Responses in Mouse Visual Cortical Areas. *Curr Biol* 25**,** 1759-1764.

Kaas, J.H., and Lyon, D.C. (2007). Pulvinar contributions to the dorsal and ventral streams of visual processing in primates. *Brain Res Rev* 55**,** 285-296.

Kasai, M., and Isa, T. (2016). Imaging population dynamics of surround suppression in the superior colliculus. *Eur J Neurosci* 44**,** 2543-2556.

Kaschube, M., Schnabel, M., Lowel, S., Coppola, D.M., White, L.E., and Wolf, F. (2010). Universality in the evolution of orientation columns in the visual cortex. *Science* 330**,** 1113-1116.

Kawamura, K., and Konno, T. (1979). Various types of corticotectal neurons of cats as demonstrated by means of retrograde axonal transport of horseradish peroxidase. *Exp Brain Res* 35**,** 161-175.

Kay, J.N., De La Huerta, I., Kim, I.J., Zhang, Y., Yamagata, M., Chu, M.W., Meister, M., and Sanes, J.R. (2011). Retinal ganglion cells with distinct directional preferences differ in molecular identity, structure, and central projections. *J Neurosci* 31**,** 7753-7762.

Kim, I.J., Zhang, Y., Meister, M., and Sanes, J.R. (2010). Laminar restriction of retinal ganglion cell dendrites and axons: subtype-specific developmental patterns revealed with transgenic markers. *J Neurosci* 30**,** 1452-1462.

Kim, I.J., Zhang, Y., Yamagata, M., Meister, M., and Sanes, J.R. (2008). Molecular identification of a retinal cell type that responds to upward motion. *Nature* 452**,** 478-482.

Kim, T., and Kerschensteiner, D. (2017). Inhibitory Control of Feature Selectivity in an Object Motion Sensitive Circuit of the Retina. *Cell Rep* 19**,** 1343-1350.

King, A.J. (2004). The superior colliculus. *Curr Biol* 14**,** R335-338.

King, J.G., Jr., Lettvin, J.Y., and Gruberg, E.D. (1999). Selective, unilateral, reversible loss of behavioral responses to looming stimuli after injection of tetrodotoxin of cadmium chloride into the frog optic nerve. *Brain Res* 841**,** 20-26.

Knudsen, E.I. (2011). Control from below: the role of a midbrain network in spatial attention. *Eur J Neurosci* 33**,** 1961-1972.

Knudsen, E.I., Schwarz, J.S., Knudsen, P.F., and Sridharan, D. (2017). Space-Specific Deficits in Visual Orientation Discrimination Caused by Lesions in the Midbrain Stimulus Selection Network. *Curr Biol* 27**,** 2053-2064 e2055.

Koch, C., and Ullman, S. (1985). Shifts in selective visual attention: towards the underlying neural circuitry. *Hum Neurobiol* 4**,** 219-227.

Kohn, A. (2007). Visual adaptation: physiology, mechanisms, and functional benefits. *J Neurophysiol* 97**,** 3155-3164.

Krauzlis, R., and Dill, N. (2002). Neural correlates of target choice for pursuit and saccades in the primate superior colliculus. *Neuron* 35**,** 355-363.

Krauzlis, R.J., Lovejoy, L.P., and Zenon, A. (2013). Superior colliculus and visual spatial attention. *Annu Rev Neurosci* 36**,** 165-182.

Kuffler, S.W. (1953). Discharge patterns and functional organization of mammalian retina. *J Neurophysiol* 16**,** 37-68.

Kustov, A.A., and Robinson, D.L. (1996). Shared neural control of attentional shifts and eye movements. *Nature* 384**,** 74-77.

Ledoux, J. (2012). Rethinking the emotional brain. *Neuron* 73**,** 653-676.

Lee, P.H., Schmidt, M., and Hall, W.C. (2001). Excitatory and inhibitory circuitry in the superficial gray layer of the superior colliculus. *J Neurosci* 21**,** 8145-8153.

Lettvin, J.Y., Maturana, H.R., Mcculloch, W.S., and Pitts, W.H. (1959). What the Frog's Eye Tells the Frog's Brain. *Proceedings of the IRE* 47**,** 1940-1951.

Leventhal, A.G., and Schall, J.D. (1983). Structural basis of orientation sensitivity of cat retinal ganglion cells. *J Comp Neurol* 220**,** 465-475.

Levick, W.R. (1967). Receptive fields and trigger features of ganglion cells in the visual streak of the rabbits retina. *J Physiol* 188**,** 285-307.

Levitt, J.B., and Lund, J.S. (1997). Contrast dependence of contextual effects in primate visual cortex. *Nature* 387**,** 73-76.

Li, C.Y., and Li, W. (1994). Extensive integration field beyond the classical receptive field of cat's striate cortical neurons--classification and tuning properties. *Vision Res* 34**,** 2337-2355.

Li, J., Levine, M.D., An, X., Xu, X., and He, H. (2013). Visual saliency based on scale-space analysis in the frequency domain. *IEEE Trans Pattern Anal Mach Intell* 35**,** 996-1010.

Li, Z. (2002). A saliency map in primary visual cortex. *Trends Cogn Sci* 6**,** 9-16.

Liang, F., Xiong, X.R., Zingg, B., Ji, X.Y., Zhang, L.I., and Tao, H.W. (2015). Sensory Cortical Control of a Visually Induced Arrest Behavior via Corticotectal Projections. *Neuron* 86**,** 755-767.

Linden, R., and Perry, V.H. (1983). Massive retinotectal projection in rats. *Brain Res* 272**,** 145-149.

Linsenmeier, R.A., Frishman, L.J., Jakiela, H.G., and Enroth-Cugell, C. (1982). Receptive field properties of x and y cells in the cat retina derived from contrast sensitivity measurements. *Vision Res* 22**,** 1173-1183.

Liu, Y.J., Wang, Q., and Li, B. (2011). Neuronal responses to looming objects in the superior colliculus of the cat. *Brain Behav Evol* 77**,** 193-205.

Livingstone, M., and Hubel, D. (1988a). Segregation of Form, Color, Movement, and Depth - Anatomy, Physiology, and Perception. *Science* 240**,** 740-749.

Livingstone, M., and Hubel, D. (1988b). Segregation of form, color, movement, and depth: anatomy, physiology, and perception. *Science* 240**,** 740-749.

Lock, T.M., Baizer, J.S., and Bender, D.B. (2003). Distribution of corticotectal cells in macaque. *Exp Brain Res* 151**,** 455-470.

Lovejoy, L.P., and Krauzlis, R.J. (2010). Inactivation of primate superior colliculus impairs covert selection of signals for perceptual judgments. *Nat Neurosci* 13**,** 261-266.

Malach, R., Amir, Y., Harel, M., and Grinvald, A. (1993). Relationship between intrinsic connections and functional architecture revealed by optical imaging and in vivo targeted biocytin injections in primate striate cortex. *Proc Natl Acad Sci U S A* 90**,** 10469-10473.

Marchiafava, P.L., and Pepeu, G. (1966). The responses of units in the superior colliculus of the cat to a moving visual stimulus. *Experientia* 22**,** 51-53.

Markus, Z., Berenyi, A., Paroczy, Z., Wypych, M., Waleszczyk, W.J., Benedek, G., and Nagy, A. (2009). Spatial and temporal visual properties of the neurons in the intermediate layers of the superior colliculus. *Neurosci Lett* 454**,** 76-80.

Marrocco, R.T., and Li, R.H. (1977). Monkey superior colliculus: properties of single cells and their afferent inputs. *J Neurophysiol* 40**,** 844-860.

Marshel, J.H., Garrett, M.E., Nauhaus, I., and Callaway, E.M. (2011). Functional specialization of seven mouse visual cortical areas. *Neuron* 72**,** 1040-1054.

Martersteck, E.M., Hirokawa, K.E., Evarts, M., Bernard, A., Duan, X., Li, Y., Ng, L., Oh, S.W., Ouellette, B., Royall, J.J., Stoecklin, M., Wang, Q., Zeng, H., Sanes, J.R., and Harris, J.A. (2017). Diverse Central Projection Patterns of Retinal Ganglion Cells. *Cell Rep* 18**,** 2058-2072.

Martin, P.R. (1986). The projection of different retinal ganglion cell classes to the dorsal lateral geniculate nucleus in the hooded rat. *Exp Brain Res* 62**,** 77-88.

Matute, C., and Streit, P. (1985). Selective retrograde labeling with D-[3H]-aspartate in afferents to the mammalian superior colliculus. *J Comp Neurol* 241**,** 34-49.

May, P.J. (2006). The mammalian superior colliculus: laminar structure and connections. 151**,** 321-378.

Mayo, J.P., and Sommer, M.A. (2008). Neuronal adaptation caused by sequential visual stimulation in the frontal eye field. *J Neurophysiol* 100**,** 1923-1935.

Mays, L.E., and Sparks, D.L. (1980). Saccades are spatially, not retinocentrically, coded. *Science* 208**,** 1163-1165.

Mazer, J.A., and Gallant, J.L. (2003). Goal-related activity in V4 during free viewing visual search. Evidence for a ventral stream visual salience map. *Neuron* 40**,** 1241-1250.

Mazurek, M., Kager, M., and Van Hooser, S.D. (2014). Robust quantification of orientation selectivity and direction selectivity. *Front Neural Circuits* 8**,** 92.

Mcilwain, J.T., and Buser, P. (1968). Receptive fields of single cells in the cat's superior colliculus. *Exp Brain Res* 5**,** 314-325.

Mcpeek, R.M. (2008). Reversal of a distractor effect on saccade target selection after superior colliculus inactivation. *J Neurophysiol* 99**,** 2694-2702.

Mcpeek, R.M., and Keller, E.L. (2002). Superior colliculus activity related to concurrent processing of saccade goals in a visual search task. *J Neurophysiol* 87**,** 1805-1815.

Mcpeek, R.M., and Keller, E.L. (2004). Deficits in saccade target selection after inactivation of superior colliculus. *Nat Neurosci* 7**,** 757-763.

Mohler, C.W., and Wurtz, R.H. (1977). Role of striate cortex and superior colliculus in visual guidance of saccadic eye movements in monkeys. *J Neurophysiol* 40**,** 74-94.

Moors, J., and Vendrik, A.J. (1979). Responses of single units in the monkey superior colliculus to moving stimuli. *Exp Brain Res* 35**,** 349-369.

Morin, L.P., and Studholme, K.M. (2014). Retinofugal projections in the mouse. *J Comp Neurol* 522**,** 3733-3753.

Movshon, J.A., Thompson, I.D., and Tolhurst, D.J. (1978). Spatial summation in the receptive fields of simple cells in the cat's striate cortex. *J Physiol* 283**,** 53-77.

Mufson, E.J., Martin, T.L., Mash, D.C., Wainer, B.H., and Mesulam, M.M. (1986). Cholinergic projections from the parabigeminal nucleus (Ch8) to the superior colliculus in the mouse: a combined analysis of horseradish peroxidase transport and choline acetyltransferase immunohistochemistry. *Brain Res* 370**,** 144-148.

Muller, J.R., Metha, A.B., Krauskopf, J., and Lennie, P. (2003). Local signals from beyond the receptive fields of striate cortical neurons. *J Neurophysiol* 90**,** 822-831.

Muller, J.R., Philiastides, M.G., and Newsome, W.T. (2005). Microstimulation of the superior colliculus focuses attention without moving the eyes. *Proc Natl Acad Sci U S A* 102**,** 524-529.

Mysore, S.P., Asadollahi, A., and Knudsen, E.I. (2010). Global inhibition and stimulus competition in the owl optic tectum. *J Neurosci* 30**,** 1727-1738.

Mysore, S.P., Asadollahi, A., and Knudsen, E.I. (2011). Signaling of the strongest stimulus in the owl optic tectum. *J Neurosci* 31**,** 5186-5196.

Naarendorp, F., Esdaille, T.M., Banden, S.M., Andrews-Labenski, J., Gross, O.P., and Pugh, E.N., Jr. (2010). Dark light, rod saturation, and the absolute and incremental sensitivity of mouse cone vision. *J Neurosci* 30**,** 12495-12507.

Naito, T., Sadakane, O., Okamoto, M., and Sato, H. (2007). Orientation tuning of surround suppression in lateral geniculate nucleus and primary visual cortex of cat. *Neuroscience* 149**,** 962-975.

Nelson, J.I., and Frost, B.J. (1978). Orientation-selective inhibition from beyond the classic visual receptive field. *Brain Res* 139**,** 359-365.

Niell, C.M., and Stryker, M.P. (2008). Highly selective receptive fields in mouse visual cortex. *J Neurosci* 28**,** 7520-7536.

Niell, C.M., and Stryker, M.P. (2010). Modulation of visual responses by behavioral state in mouse visual cortex. *Neuron* 65**,** 472-479.

Nummela, S.U., and Krauzlis, R.J. (2010). Inactivation of primate superior colliculus biases target choice for smooth pursuit, saccades, and button press responses. *J Neurophysiol* 104**,** 1538-1548.

Ogino, T., and Ohtsuka, K. (2000). Effects of superior colliculus inhibition on visual motion processing in the lateral suprasylvian visual area of the cat. *Invest Ophthalmol Vis Sci* 41**,** 955-960.

Oh, S.W., Harris, J.A., Ng, L., Winslow, B., Cain, N., Mihalas, S., Wang, Q., Lau, C., Kuan, L., Henry, A.M., Mortrud, M.T., Ouellette, B., Nguyen, T.N., Sorensen, S.A., Slaughterbeck, C.R., Wakeman, W., Li, Y., Feng, D., Ho, A., Nicholas, E., Hirokawa, K.E., Bohn, P., Joines, K.M., Peng, H., Hawrylycz, M.J., Phillips, J.W., Hohmann, J.G., Wohnoutka, P., Gerfen,

C.R., Koch, C., Bernard, A., Dang, C., Jones, A.R., and Zeng, H. (2014). A mesoscale connectome of the mouse brain. *Nature* 508**,** 207-214.

Oliva, D., Medan, V., and Tomsic, D. (2007). Escape behavior and neuronal responses to looming stimuli in the crab Chasmagnathus granulatus (Decapoda: Grapsidae). *J Exp Biol* 210**,** 865-880.

Ozeki, H., Finn, I.M., Schaffer, E.S., Miller, K.D., and Ferster, D. (2009). Inhibitory stabilization of the cortical network underlies visual surround suppression. *Neuron* 62**,** 578-592.

Ozeki, H., Sadakane, O., Akasaki, T., Naito, T., Shimegi, S., and Sato, H. (2004). Relationship between excitation and inhibition underlying size tuning and contextual response modulation in the cat primary visual cortex. *J Neurosci* 24**,** 1428-1438.

Perry, V.H., and Cowey, A. (1984). Retinal ganglion cells that project to the superior colliculus and pretectum in the macaque monkey. *Neuroscience* 12**,** 1125-1137.

Petrov, Y., Carandini, M., and Mckee, S. (2005). Two distinct mechanisms of suppression in human vision. *J Neurosci* 25**,** 8704-8707.

Pettit, D.L., Helms, M.C., Lee, P., Augustine, G.J., and Hall, W.C. (1999). Local excitatory circuits in the intermediate gray layer of the superior colliculus. *J Neurophysiol* 81**,** 1424-1427.

Phongphanphanee, P., Marino, R.A., Kaneda, K., Yanagawa, Y., Munoz, D.P., and Isa, T. (2014). Distinct local circuit properties of the superficial and intermediate layers of the rodent superior colliculus. *Eur J Neurosci* 40**,** 2329-2343.

Pietersen, A.N., Cheong, S.K., Solomon, S.G., Tailby, C., and Martin, P.R. (2014). Temporal response properties of koniocellular (blue-on and blue-off) cells in marmoset lateral geniculate nucleus. *J Neurophysiol* 112**,** 1421-1438.

Pinter, R.B., and Harris, L.R. (1981). Temporal and spatial response characteristics of the cat superior colliculus. *Brain Res* 207**,** 73-94.

Piscopo, D.M., El-Danaf, R.N., Huberman, A.D., and Niell, C.M. (2013). Diverse visual features encoded in mouse lateral geniculate nucleus. *J Neurosci* 33**,** 4642-4656.

Priebe, N.J., Cassanello, C.R., and Lisberger, S.G. (2003). The neural representation of speed in macaque area MT/V5. *J Neurosci* 23**,** 5650-5661.

Prusky, G.T., Alam, N.M., Beekman, S., and Douglas, R.M. (2004). Rapid quantification of adult and developing mouse spatial vision using a virtual optomotor system. *Invest Ophthalmol Vis Sci* 45**,** 4611-4616.

Prusky, G.T., and Douglas, R.M. (2004). Characterization of mouse cortical spatial vision. *Vision Res* 44**,** 3411-3418.

Prusky, G.T., West, P.W., and Douglas, R.M. (2000). Behavioral assessment of visual acuity in mice and rats. *Vision Res* 40**,** 2201-2209.

Purushothaman, G., Marion, R., Li, K., and Casagrande, V.A. (2012). Gating and control of primary visual cortex by pulvinar. *Nat Neurosci* 15**,** 905-912.

Reichardt, W. (1987). Evaluation of optical motion information by movement detectors. *J Comp Physiol A* 161**,** 533-547.

Rizzolatti, G., Camarda, R., Grupp, L.A., and Pisa, M. (1974). Inhibitory effect of remote visual stimuli on visual responses of cat superior colliculus: spatial and temporal factors. *J Neurophysiol* 37**,** 1262-1275.

Robinson, D.L., and Petersen, S.E. (1992). The pulvinar and visual salience. *Trends Neurosci* 15**,** 127-132.

Rodieck, R.W. (1965). Quantitative analysis of cat retinal ganglion cell response to visual stimuli. *Vision Res* 5**,** 583-601.

Rodman, H.R., Gross, C.G., and Albright, T.D. (1990). Afferent basis of visual response properties in area MT of the macaque. II. Effects of superior colliculus removal. *J Neurosci* 10**,** 1154-1164.

Rosenquist, A.C., and Palmer, L.A. (1971). Visual receptive field properties of cells of the superior colliculus after cortical lesions in the cat. *Exp Neurol* 33**,** 629-652.

Rossant, C., Kadir, S.N., Goodman, D.F.M., Schulman, J., Hunter, M.L.D., Saleem, A.B., Grosmark, A., Belluscio, M., Denfield, G.H., Ecker, A.S., Tolias, A.S., Solomon, S., Buzsaki, G., Carandini, M., and Harris, K.D. (2016). Spike sorting for large, dense electrode arrays. *Nat Neurosci* 19**,** 634-641.

Rowe, M.H., and Palmer, L.A. (1995). Spatio-temporal receptive-field structure of phasic W cells in the cat retina. *Vis Neurosci* 12**,** 117-139.

Sahibzada, N., Dean, P., and Redgrave, P. (1986). Movements resembling orientation or avoidance elicited by electrical stimulation of the superior colliculus in rats. *J Neurosci* 6**,** 723-733.

Sakatani, T., and Isa, T. (2004). PC-based high-speed video-oculography for measuring rapid eye movements in mice. *Neurosci Res* 49**,** 123-131.

Savage, M.A., Mcquade, R., and Thiele, A. (2017). Segregated fronto-cortical and midbrain connections in the mouse and their relation to approach and avoidance orienting behaviors. *J Comp Neurol* 525**,** 1980-1999.

Sceniak, M.P., Hawken, M.J., and Shapley, R. (2001). Visual spatial characterization of macaque V1 neurons. *J Neurophysiol* 85**,** 1873-1887.

Sceniak, M.P., and Maciver, M.B. (2006). Cellular actions of urethane on rat visual cortical neurons in vitro. *J Neurophysiol* 95**,** 3865-3874.

Sceniak, M.P., Ringach, D.L., Hawken, M.J., and Shapley, R. (1999). Contrast's effect on spatial summation by macaque V1 neurons. *Nat Neurosci* 2**,** 733-739.

Schaefer, K.P. (1970). Unit analysis and electrical stimulation in the optic tectum of rabbits and cats. *Brain Behav Evol* 3**,** 222-240.

Schiller, P.H., and Koerner, F. (1971). Discharge characteristics of single units in superior colliculus of the alert rhesus monkey. *J Neurophysiol* 34**,** 920-936.

Schiller, P.H., Stryker, M., Cynader, M., and Berman, N. (1974). Response characteristics of single cells in the monkey superior colliculus following ablation or cooling of visual cortex. *J Neurophysiol* 37**,** 181-194.

Schneider, G.E. (1969). Two visual systems. *Science* 163**,** 895-902.

Scholl, B., Tan, A.Y., Corey, J., and Priebe, N.J. (2013). Emergence of orientation selectivity in the Mammalian visual pathway. *J Neurosci* 33**,** 10616-10624.

Schwartz, O., Hsu, A., and Dayan, P. (2007). Space and time in visual context. *Nat Rev Neurosci* 8**,** 522-535.

Sefton, A.J., Mackay-Sim, A., Baur, L.A., and Cottee, L.J. (1981). Cortical projections to visual centres in the rat: an HRP study. *Brain Res* 215**,** 1-13.

Self, M.W., Lorteije, J.A., Vangeneugden, J., Van Beest, E.H., Grigore, M.E., Levelt, C.N., Heimel, J.A., and Roelfsema, P.R. (2014). Orientation-tuned surround suppression in mouse visual cortex. *J Neurosci* 34**,** 9290-9304.

Sengpiel, F., Sen, A., and Blakemore, C. (1997). Characteristics of surround inhibition in cat area 17. *Exp Brain Res* 116**,** 216-228.

Serrano-Pedraza, I., Grady, J.P., and Read, J.C. (2012). Spatial frequency bandwidth of surround suppression tuning curves. *J Vis* 12.

Shang, C., Liu, Z., Chen, Z., Shi, Y., Wang, Q., Liu, S., Li, D., and Cao, P. (2015). BRAIN CIRCUITS. A parvalbumin-positive excitatory visual pathway to trigger fear responses in mice. *Science* 348**,** 1472-1477.

Shapley, R.M., and Victor, J.D. (1978). The effect of contrast on the transfer properties of cat retinal ganglion cells. *J Physiol* 285**,** 275-298.

Sherk, H. (1979). A comparison of visual-response properties in cat's parabigeminal nucleus and superior colliculus. *J Neurophysiol* 42**,** 1640-1655.

Shi, X., Barchini, J., Ledesma, H.A., Koren, D., Jin, Y., Liu, X., Wei, W., and Cang, J. (2017). Retinal origin of direction selectivity in the superior colliculus. *Nat Neurosci* 20**,** 550-558.

Shushruth, S., Nurminen, L., Bijanzadeh, M., Ichida, J.M., Vanni, S., and Angelucci, A. (2013). Different orientation tuning of near- and far-surround suppression in macaque primary visual cortex mirrors their tuning in human perception. *J Neurosci* 33**,** 106-119.

Sillito, A.M., Cudeiro, J., and Murphy, P.C. (1993). Orientation sensitive elements in the corticofugal influence on centre-surround interactions in the dorsal lateral geniculate nucleus. *Exp Brain Res* 93**,** 6-16.

Sillito, A.M., Grieve, K.L., Jones, H.E., Cudeiro, J., and Davis, J. (1995). Visual Cortical Mechanisms Detecting Focal Orientation Discontinuities. *Nature* 378**,** 492-496.

Skottun, B.C., De Valois, R.L., Grosof, D.H., Movshon, J.A., Albrecht, D.G., and Bonds, A.B. (1991). Classifying simple and complex cells on the basis of response modulation. *Vision Res* 31**,** 1079-1086.

Smirnakis, S.M., Berry, M.J., Warland, D.K., Bialek, W., and Meister, M. (1997). Adaptation of retinal processing to image contrast and spatial scale. *Nature* 386**,** 69-73.

Smith, D.C., and Spear, P.D. (1979). Effects of superior colliculus removal on receptive-field properties of neurons in lateral suprasylvian visual area of the cat. *J Neurophysiol* 42**,** 57-75.

Solomon, S.G., and Kohn, A. (2014). Moving sensory adaptation beyond suppressive effects in single neurons. *Curr Biol* 24**,** R1012-1022.

Solomon, S.G., Lee, B.B., and Sun, H. (2006). Suppressive surrounds and contrast gain in magnocellular-pathway retinal ganglion cells of macaque. *J Neurosci* 26**,** 8715-8726.

Solomon, S.G., Peirce, J.W., Dhruv, N.T., and Lennie, P. (2004). Profound contrast adaptation early in the visual pathway. *Neuron* 42**,** 155-162.

Solomon, S.G., White, A.J., and Martin, P.R. (2002). Extraclassical receptive field properties of parvocellular, magnocellular, and koniocellular cells in the primate lateral geniculate nucleus. *J Neurosci* 22**,** 338-349.

Spear, P.D., Kim, C.B., Ahmad, A., and Tom, B.W. (1996). Relationship between numbers of retinal ganglion cells and lateral geniculate neurons in the rhesus monkey. *Vis Neurosci* 13**,** 199-203.

Sprague, J.M., and Meikle, T.H., Jr. (1965). The Role of the Superior Colliculus in Visually Guided Behavior. *Exp Neurol* 11**,** 115-146.

Stankowich, T., and Blumstein, D.T. (2005). Fear in animals: a meta-analysis and review of risk assessment. *Proc Biol Sci* 272**,** 2627-2634.

Stepniewska, I., Ql, H.X., and Kaas, J.H. (2000). Projections of the superior colliculus to subdivisions of the inferior pulvinar in New World and Old World monkeys. *Vis Neurosci* 17**,** 529-549.

Sterling, P., and Wickelgren, B.G. (1969). Visual receptive fields in the superior colliculus of the cat. *J Neurophysiol* 32**,** 1-15.

Sterling, P., and Wickelgren, B.G. (1970). Function of the projection from the visual cortex to the superior colliculus. *Brain Behav Evol* 3**,** 210-218.

Tafazoli, S., Safaai, H., De Franceschi, G., Rosselli, F.B., Vanzella, W., Riggi, M., Buffolo, F., Panzeri, S., and Zoccolan, D. (2017). Emergence of transformation-tolerant representations of visual objects in rat lateral extrastriate cortex. *Elife* 6.

Tailby, C., Cheong, S.K., Pietersen, A.N., Solomon, S.G., and Martin, P.R. (2012). Colour and pattern selectivity of receptive fields in superior colliculus of marmoset monkeys. *J Physiol* 590**,** 4061-4077.

Tang, J., Ardila Jimenez, S.C., Chakraborty, S., and Schultz, S.R. (2016). Visual Receptive Field Properties of Neurons in the Mouse Lateral Geniculate Nucleus. *PLoS One* 11**,** e0146017.

Taylor, A.M., Jeffery, G., and Lieberman, A.R. (1986). Subcortical afferent and efferent connections of the superior colliculus in the rat and comparisons between albino and pigmented strains. *Exp Brain Res* 62**,** 131-142.

Tehovnik, E.J. (1989). Head and body movements evoked electrically from the caudal superior colliculus of rats: pulse frequency effects. *Behav Brain Res* 34**,** 71-78.

Tinbergen, N. (1951). *The study of instinct.* New York, NY, US: Clarendon Press/Oxford University Press.

Tohmi, M., Meguro, R., Tsukano, H., Hishida, R., and Shibuki, K. (2014). The extrageniculate visual pathway generates distinct response properties in the higher visual areas of mice. *Curr Biol* 24**,** 587-597.

Tovee, M.J. (1995). Ultra-violet photoreceptors in the animal kingdom: their distribution and function. *Trends Ecol Evol* 10**,** 455-460.

Ungerleider, L.G., and Haxby, J.V. (1994). 'What' and 'where' in the human brain. *Curr Opin Neurobiol* 4**,** 157-165.

Updyke, B.V. (1974). Characteristics of unit responses in superior colliculus of the Cebus monkey. *J Neurophysiol* 37**,** 896-909.

Vaiceliunaite, A., Erisken, S., Franzen, F., Katzner, S., and Busse, L. (2013). Spatial integration in mouse primary visual cortex. *J Neurophysiol* 110**,** 964-972.

Vale, R., Evans, D.A., and Branco, T. (2017). Rapid Spatial Learning Controls Instinctive Defensive Behavior in Mice. *Curr Biol* 27**,** 1342-1349.

Van Hooser, S.D., Heimel, J.A., Chung, S., Nelson, S.B., and Toth, L.J. (2005). Orientation selectivity without orientation maps in visual cortex of a highly visual mammal. *J Neurosci* 25**,** 19-28.

Vaney, D.I., Peichl, L., Wassle, H., and Illing, R.B. (1981). Almost all ganglion cells in the rabbit retina project to the superior colliculus. *Brain Res* 212**,** 447-453.

Veale, R., Hafed, Z.M., and Yoshida, M. (2017). How is visual salience computed in the brain? Insights from behaviour, neurobiology and modelling. *Philos Trans R Soc Lond B Biol Sci* 372.

Vermaercke, B., Van Den Bergh, G., Gerich, F., and Op De Beeck, H. (2015). Neural discriminability in rat lateral extrastriate cortex and deep but not superficial primary visual cortex correlates with shape discriminability. *Front Neural Circuits* 9**,** 24.

Waleszczyk, W.J., Nagy, A., Wypych, M., Berenyi, A., Paroczy, Z., Eordegh, G., Ghazaryan, A., and Benedek, G. (2007). Spectral receptive field properties of neurons in the feline superior colliculus. *Exp Brain Res* 181**,** 87-98.

Wallace, D.J., Greenberg, D.S., Sawinski, J., Rulla, S., Notaro, G., and Kerr, J.N. (2013). Rats maintain an overhead binocular field at the expense of constant fusion. *Nature* 498**,** 65-69.

Wallace, M.T., and Stein, B.E. (1996). Sensory organization of the superior colliculus in cat and monkey. *Prog Brain Res* 112**,** 301-311.

Wang, L., Sarnaik, R., Rangarajan, K., Liu, X., and Cang, J. (2010). Visual receptive field properties of neurons in the superficial superior colliculus of the mouse. *J Neurosci* 30**,** 16573-16584.

Wang, Q., and Burkhalter, A. (2013). Stream-related preferences of inputs to the superior colliculus from areas of dorsal and ventral streams of mouse visual cortex. *J Neurosci* 33**,** 1696-1705.

Wang, Q., Sporns, O., and Burkhalter, A. (2012). Network analysis of corticocortical connections reveals ventral and dorsal processing streams in mouse visual cortex. *J Neurosci* 32**,** 4386-4399.

Wang, X.D., Chen, C., Zhang, D., and Yao, H. (2014). Cumulative latency advance underlies fast visual processing in desynchronized brain state. *Proc Natl Acad Sci U S A* 111**,** 515-520.

Wassle, H., and Illing, R.B. (1980). The retinal projection to the superior colliculus in the cat: a quantitative study with HRP. *J Comp Neurol* 190**,** 333-356.

Webb, B.S., Dhruv, N.T., Solomon, S.G., Tailby, C., and Lennie, P. (2005). Early and late mechanisms of surround suppression in striate cortex of macaque. *J Neurosci* 25**,** 11666-11675.

Webster, M.A. (2015). Visual Adaptation. *Annu Rev Vis Sci* 1**,** 547-567.

Wei, P., Liu, N., Zhang, Z., Liu, X., Tang, Y., He, X., Wu, B., Zhou, Z., Liu, Y., Li, J., Zhang, Y., Zhou, X., Xu, L., Chen, L., Bi, G., Hu, X., Xu, F., and Wang, L. (2015). Processing of visually evoked innate fear by a non-canonical thalamic pathway. *Nat Commun* 6**,** 6756.

Westby, G.W., Keay, K.A., Redgrave, P., Dean, P., and Bannister, M. (1990). Output pathways from the rat superior colliculus mediating approach and avoidance have different sensory properties. *Exp Brain Res* 81**,** 626-638.

White, A.J., Solomon, S.G., and Martin, P.R. (2001). Spatial properties of koniocellular cells in the lateral geniculate nucleus of the marmoset Callithrix jacchus. *J Physiol* 533**,** 519-535.

White, B.J., Berg, D.J., Kan, J.Y., Marino, R.A., Itti, L., and Munoz, D.P. (2017a). Superior colliculus neurons encode a visual saliency map during free viewing of natural dynamic video. *Nat Commun* 8**,** 14263.

White, B.J., Kan, J.Y., Levy, R., Itti, L., and Munoz, D.P. (2017b). Superior colliculus encodes visual saliency before the primary visual cortex. *Proc Natl Acad Sci U S A* 114**,** 9451-9456.

White, B.J., and Munoz, D.P. (2011). Separate visual signals for saccade initiation during target selection in the primate superior colliculus. *J Neurosci* 31**,** 1570-1578.

Wilz, K.J., and Bolton, R.L. (1971). Exploratory behavior in response to the spatial rearrangement of familiar stimuli. *Psychonomic Science* 24**,** 117-118.

Wong, A.A., and Brown, R.E. (2006). Visual detection, pattern discrimination and visual acuity in 14 strains of mice. *Genes Brain Behav* 5**,** 389-403.

Wurtz, R.H., and Albano, J.E. (1980). Visual-motor function of the primate superior colliculus. *Annu Rev Neurosci* 3**,** 189-226.

Wurtz, R.H., and Goldberg, M.E. (1972). Activity of superior colliculus in behaving monkey. IV. Effects of lesions on eye movements. *J Neurophysiol* 35**,** 587-596.

Xing, J., and Heeger, D.J. (2001). Measurement and modeling of center-surround suppression and enhancement. *Vision Res* 41**,** 571-583.

Yacoub, E., Harel, N., and Ugurbil, K. (2008). High-field fMRI unveils orientation columns in humans. *Proc Natl Acad Sci U S A* 105**,** 10607-10612.

Ydenberg, R.C., and Dill, L.M. (1986). The Economics of Fleeing from Predators. *Advances in the Study of Behavior* 16**,** 229-249.

Yilmaz, M., and Meister, M. (2013). Rapid innate defensive responses of mice to looming visual stimuli. *Curr Biol* 23**,** 2011-2015.

Yonehara, K., and Roska, B. (2013). Motion detection: neuronal circuit meets theory. *Cell* 154**,** 1188-1189.

Yoshida, M., Itti, L., Berg, D.J., Ikeda, T., Kato, R., Takaura, K., White, B.J., Munoz, D.P., and Isa, T. (2012a). Residual attention guidance in blindsight monkeys watching complex natural scenes. *Curr Biol* 22**,** 1429-1434.

Yoshida, T., Ozawa, K., and Tanaka, S. (2012b). Sensitivity profile for orientation selectivity in the visual cortex of goggle-reared mice. *PLoS One* 7**,** e40630.

Yu, C., Klein, S.A., and Levi, D.M. (2001). Surround modulation of perceived contrast and the role of brightness induction. *J Vis* 1**,** 18-31.

Zhang, Y., Kim, I.J., Sanes, J.R., and Meister, M. (2012). The most numerous ganglion cell type of the mouse retina is a selective feature detector. *Proc Natl Acad Sci U S A* 109**,** E2391-2398.

Zhao, X., Liu, M., and Cang, J. (2014). Visual cortex modulates the magnitude but not the selectivity of looming-evoked responses in the superior colliculus of awake mice. *Neuron* 84**,** 202-213.

Zhaoping, L. (2016). From the optic tectum to the primary visual cortex: migration through evolution of the saliency map for exogenous attentional guidance. *Curr Opin Neurobiol* 40**,** 94-102.

Zhou, N.A., Maire, P.S., Masterson, S.P., and Bickford, M.E. (2017). The mouse pulvinar nucleus: Organization of the tectorecipient zones. *Visual Neuroscience* 34.